# Mechanisms of ubiquitin signalling in cancer-related genome stability pathways




Kay Yi Chong
Trinity College
University of Oxford

A thesis submitted for the degree of
*Doctor of Philosophy*

October 2022

# Table of Contents

**Abstract** ..... i

**Acknowledgements** ..... ii

**List of Figures** ..... iii

**List of Tables** ..... vii

**List of Abbreviations** ..... viii

**1. Introduction** ..... 1

**1.1 DNA replication** ..... 2
1.1.1 Overview ..... 2
1.1.2 Proliferating cell nuclear antigen (PCNA) ..... 5

**1.2 Replication stress** ..... 8
1.2.1 Sources of replication stress and checkpoint activation ..... 8
1.2.2 DNA damage tolerance ..... 10
1.2.3 Replication fork remodelling ..... 12
1.2.4 Double-strand break repair ..... 15
1.2.5 Exploiting DNA replication stress in cancer therapy ..... 19

**1.3 Ubiquitylation** ..... 21
1.3.1 Ubiquitin ..... 21
1.3.2 Ubiquitylation cascade ..... 24
1.3.3 Ubiquitin modifications ..... 25
1.3.4 Ubiquitin-binding domains ..... 29

**1.4 Deubiquitylases (DUBs)** ..... 31
1.4.1 DUB classes ..... 31
1.4.2 Substrate recognition and linkage specificity ..... 32
1.4.3 Regulation of DUBs ..... 34

**1.5 Zinc Finger Containing Ubiquitin Peptidase 1 (ZUP1)** ..... 36
1.5.1 Discovery of ZUP1 as a novel DUB class ..... 36
1.5.2 Structure and ubiquitin chain specificity of ZUP1 ..... 37
1.5.3 Evidence for the roles of ZUP1 in DNA repair ..... 40

**1.6 Ubiquitin signalling at stressed replication forks** ..... 42
1.6.1 PCNA ubiquitylation ..... 42
1.6.2 RPA ubiquitylation ..... 43
1.6.3 FANCI–FANCD2 ubiquitylation ..... 44

**1.7 Overall aims and motivation** ..... 47

**2. Materials and Methods** ..... 48

**2.1 Materials** ..... 49
2.1.1 Buffers and additives ..... 49
2.1.2 Plasmids ..... 51
2.1.3 Oligonucleotides ..... 53
2.1.4 CRISPR sgRNA sequences ..... 54
2.1.5 Antibodies ..... 55
2.1.6 siRNAs ..... 56

**2.2 Cell culture** ..... 56
2.2.1 Maintenance of cell lines ..... 56
2.2.2 Generation of ZUP1 CRISPR-Cas9 knockout cells ..... 57
2.2.3 Generation of stable ZUP1 re-expressing rescue cell lines ..... 58
2.2.4 Drug treatment ..... 59

**2.3 Plasmid transfection** ..... 60

**2.4 siRNA transfection ..... 61**

**2.5 CRISPR-Cas9 analysis methods ..... 62**
2.5.1 Western blotting ..... 62
2.5.2 PCR genotyping ..... 62
2.5.3 Sanger sequencing and Inference of CRISPR Edits (ICE) analysis ..... 62

**2.6 Molecular biology techniques ..... 63**
2.6.1 Polymerase chain reaction (PCR) ..... 63
2.6.2 Site-directed mutagenesis ..... 64
2.6.3 Bacterial transformation and colony screening ..... 64
2.6.4 Plasmid purification ..... 65
2.6.5 CRISPR-Cas9 plasmid assembly ..... 65
2.6.6 Genomic DNA extraction ..... 65
2.6.7 Agarose gel electrophoresis ..... 66
2.6.8 Purification of DNA from agarose gels ..... 66
2.6.9 Measurement of DNA concentration ..... 66

**2.7 Clonogenic assay ..... 67**

**2.8 Cell cycle synchronisation by double thymidine block ..... 68**

**2.9 Flow cytometry ..... 68**
2.9.1 Assessing mCherry+ and GFP/Clover+ populations ..... 68
2.9.2 Cell cycle analysis ..... 69

**2.10 LMNA homology-directed repair assay ..... 70**

**2.11 Microscopy ..... 70**
2.11.1 Imaging of Clover localisation in cells ..... 70
2.11.2 Imaging of PCNA chromobody localisation in cells ..... 71

**2.12 Protein extraction and sample preparation ..... 71**
2.12.1 Cell lysis using Triton X-100 ..... 71
2.12.2 Cell lysis using denaturing buffers ..... 72
2.12.3 Protein concentration quantification ..... 73
2.12.4 Protein sample preparation ..... 73

**2.13 Western blotting ..... 74**

**2.14 Coomassie staining ..... 75**

**2.15 Immunoprecipitation ..... 75**
2.15.1 IP of FLAG ..... 75
2.15.2 IP of RFP ..... 76
2.15.3 IP of K63-linked ubiquitin ..... 76

**2.16 Deubiquitylase assay ..... 77**

**2.17 Affinity purification ..... 78**
2.17.1 Ni-NTA purification of His-ubiquitin ..... 78
2.17.2 Strep purification (Strep-tag system) ..... 79

**2.18 Statistical analysis ..... 80**

**3. Characterising ZUP1-Dependent DNA Repair Phenotypes ..... 81**

**3.1 Introduction ..... 82**

**3.2 Results ..... 85**
3.2.1 Consideration of ZUP1 splice isoforms ..... 85
3.2.2 CRISPR-Cas9 sgRNA design and strategy ..... 88
3.2.3 Validation of ZUP1 knockout in single cell-derived clones ..... 91
3.2.4 ZUP1 knockouts are sensitive to replication stress induced by genotoxic agents ..... 107
3.2.5 ZUP1 hypomorphs also exhibit sensitivity to genotoxic agents ..... 113

**3.3 Discussion ..... 116**
3.3.1 Challenges in the generation of CRISPR-Cas9 knockouts in cell lines with complex karyotypes . 116

3.3.2 Evaluation of knockout strategy to eliminate ZUP1 ..... 118
3.3.3 ZUP1 has a role in replication-coupled DNA repair ..... 119
3.3.4 The N-terminus of ZUP1 may be important for its DNA repair function ..... 121

**4. Defining the ZUP1 Complex in Cells ..... 123**

**4.1 Introduction ..... 124**

**4.2 Results ..... 128**
4.2.1 Defining the ZUP1 complex in cells ..... 128
4.2.2 ZUP1 interacts with another DUB, USP11 ..... 137
4.2.3 Dissecting USP11-ZUP1 and USP11-TCEAL1 interactions ..... 144

**4.3 Discussion ..... 154**
4.3.1 A novel interaction between two DUB classes ..... 154
4.3.2 Specificity of the second zinc finger of ZUP1 for binding USP11 ..... 156
4.3.3 USP11-TCEAL1 interaction mapping will aid future functional characterisation of TCEAL1 ..... 158
4.3.4 The ZUP1 interactome suggests a role for ZUP1 in ubiquitin signalling and DNA repair ..... 160

**5. Investigating the Roles of ZUP1 in DNA Repair ..... 163**

**5.1 Introduction ..... 164**

**5.2 Results ..... 168**
5.2.1 Optimising affinity purification and immunoprecipitation methods, and treatment conditions to detect ubiquitylated PCNA and RPA in cells ..... 168
5.2.2 ZUP1 loss is associated with elevated levels of PCNA polyubiquitylation during replication stress ..... 184
5.2.3 Attempts to rescue PCNA polyubiquitylation in ZUP1 knockout cells ..... 198
5.2.4 ZUP1 has a role in homologous recombination repair ..... 212

**5.3 Discussion ..... 219**
5.3.1 ZUP1 is a DUB that potentially reverses PCNA ubiquitylation ..... 219
5.3.2 ZUP1 may have an anti-HR role ..... 222

**6. Final Discussion and Concluding Remarks ..... 225**

**Appendices ..... 232**

**Appendix A (Supplemental information to Chapter 3) ..... 233**

**Appendix B (Supplemental information to Chapter 4) ..... 235**

**Appendix C (Supplemental information to Chapter 5) ..... 238**

**References ..... 241**

# Abstract

Ubiquitin signalling plays an integral role in orchestrating mammalian DNA repair pathways to promote genome stability. Ubiquitin signalling is regulated by deubiquitylating enzymes (DUBs) which catalyse the removal or trimming of ubiquitin from substrates. Zinc finger containing ubiquitin peptidase 1 (ZUP1) was recently discovered as a novel DUB class that cleaves K63-linked ubiquitin chains and has a putative role in genome stability. However, the mechanistic basis for ZUP1 function remains elusive. In this thesis, I have built upon these preliminary findings and investigated the cellular roles of ZUP1 in cancer-related genome stability mechanisms. In Chapter 3, I used CRISPR-Cas9 genetic approaches to generate isoform-specific ZUP1 knockout cells as tools to explore ZUP1-dependent DNA repair phenotypes. I discovered that ZUP1 knockout cells display hypersensitivity to mitomycin C (a DNA interstrand crosslinker), topotecan (a topoisomerase I inhibitor), PARP inhibitors, and an ATR inhibitor. These findings suggest that ZUP1 functions in specific replication-coupled DNA repair pathways that respond to lesions generated by these genotoxins. In Chapter 4, I sought to characterise the cellular ZUP1 complex and determine how various domains contribute to protein-protein interactions and complex assembly in cells. Importantly, I found that ZUP1 interacts with another DUB complex USP11/TCEAL1 through the ZUP1 second N-terminal zinc finger. I also characterised the interaction between USP11 and TCEAL1, allowing me to determine the interacting interfaces of the ZUP1-USP11-TCEAL1 complex. In Chapter 5, I extended the known substrates of ZUP1 and discovered that ZUP1 regulates PCNA polyubiquitylation during replication stress - the first example of a DUB that regulates PCNA polyubiquitylation. Furthermore, ZUP1 was found to have a potential role in homologous recombination repair. Collectively, the discoveries presented in this thesis provide novel insights into the cellular roles of ZUP1 in genome stability.

# Acknowledgements

Firstly, I would like to thank my DPhil supervisor, Dr. Ian Gibbs-Seymour for giving me the opportunity to work on this project and for his exceptional guidance, support, and understanding. This research would not have been possible without his extensive knowledge and invaluable input. I am also grateful to the Oxford Elizabeth Murphy Scholarship and its donor, Mr. Adrian Hohler for funding my DPhil.

I would like to thank Ben Foster, Martin Attwood and Matt Drake in the Gibbs-Seymour lab for their help, collaboration, useful discussions, and for sharing numerous reagents and cells. I would further like to thank Ben for going out of his way to help me multiple times and for reading this thesis. I would like to thank Luke Fulcher, Andreas Gerondopoulos and Tomoaki Sobajima from the Barr lab for their willingness to help with reagents and protocols. I am also thankful to Robert Hedley and Vasiliki Tsioligka from the Flow Cytometry facility at the Sir William Dunn School of Pathology for their technical assistance with my flow cytometry experiments.

A special thank you to my former mentor, Prof. Yang Yang-Hartwich who taught me how to conduct my first research experiment when I was an undergraduate student and has never stopped believing in me. I am also grateful to Trinity College for being a warm and friendly community. I would like to thank my College Senior Tutor, Prof. Valerie Worth and College Advisor, Prof. Paul Fairchild for their support and advice during challenging times. I am also thankful to Mo Carrami and Qinrui Wang for their invaluable advice on science and surviving the degree.

I am ever grateful to my parents and to Shawn and Mac for their relentless support and encouragement. I would like to thank the dear friends I have made in Oxford with special mention to Andrew, Amy, Debbie, Kome, Laura, Oleh, Otto, Rebecca, Salma, Spreeha and Sunny, for the beautiful friendships and memories. I am also thankful to Sukfun, Regina, Melody and Amanda for being there for me through the years.

# List of Figures

**Figure 1.1**: Major proteins present at the replication fork during the elongation step of eukaryotic DNA replication……..…….....4
**Figure 1.2**: Structure of human PCNA bound to DNA and examples of PIP box and APIM motif binding to PCNA……...……..…....…7
**Figure 1.3:** Summary of proposed models for fork reversal and restart following replication stress…….14
**Figure 1.4**: Key steps involved in homologous recombination repair of DSBs.....16
**Figure 1.5**: Ubiquitin structure and interaction surface patches…….....……22
**Figure 1.6**: Summary of the ubiquitylation cascade…….……..…....23
**Figure 1.7**: Examples of ubiquitin modifications……..…….…..27
**Figure 1.8**: Classes of human deubiquitylases and known members……..…..…31
**Figure 1.9**: Mechanisms of di-ubiquitin cleavage by deubiquitylases…….....…....33
**Figure 1.10**: Structure and domain architecture of ZUP1…….....39
**Figure 1.11**: Critical ubiquitylation platforms involved in the replication stress response……..……..……..46
**Figure 3.1**: ZUP1 domains, exons and reported splice isoforms……..……...86
**Figure 3.2**: CRISPR-Cas9 ZUP1 knockout strategies and outcomes…….....…90
**Figure 3.3**: Residual ZUP1 proteins were detected in cells edited using paired or single sgRNAs targeting exon 2……..…….....…93
**Figure 3.4**: Analysis of frameshift-inducing indel formation and ZUP1 protein loss in 293T clones edited at exon 2…….……..……..…....96
**Figure 3.5**: Editing outcomes in clones edited with sgRNA(s) targeting ZUP1 exon 6…….……..…….....…98
**Figure 3.6**: PCR genotyping of clones edited using paired intronic sgRNAs flanking exon 6…….……..……..…....102
**Figure 3.7**: Assessment of ZUP1 loss in single cell-derived clones generated by targeting exon 2 within ΔZUP1_Ex6 Clone 11…….……..…..106
**Figure 3.8**: Clonogenic survival assays in U2OS ZUP1 knockout clones…..……...….111
**Figure 3.9**: Clonogenic survival assays in U2OS ZUP1 hypomorphic clones.....115

**Figure 4.1**: Summary of the ZUP1 interactome previously identified by proteomics……..…...…127
**Figure 4.2**: Identification of ZUP1 domains involved in protein-protein interactions……..…...…131
**Figure 4.3**: Residual RPA binding to ZUP1 was observed when the α-2/3 region was deleted…….…….....….134
**Figure 4.4**: Assessing surface residues in the α-2/3 region of ZUP1 for their contribution to RPA interaction……..…….……....136
**Figure 4.5**: Identification of the ZUP1 zinc finger that mediates USP11 binding.....138
**Figure 4.6**: Comparison between USP11 UBL domains and ubiquitin, or ZUP1 zinc fingers and DNA polymerase eta (Pol η) UBZ domain…….……141
**Figure 4.7**: Glu43 and Met44 in ZUP1 ZnF2 are potential interacting residues that mediate USP11 binding……..…....143
**Figure 4.8**: Deletion of previously annotated USP11 domains or regions to identify potential sites involved in ZUP1 and TCEAL1 binding……..…....145
**Figure 4.9**: USP11 UBL2 domain and the disordered insert region may bind to TCEAL1 and ZUP1……...……148
**Figure 4.10:** Assessing the effects of deleting TCEAL1 α1 and α2 on USP11 and ZUP1 binding……..……..151
**Figure 4.11**: TCEAL1 binding to ZUP1 may be USP11-dependent, and TCEAL1 may have a regulatory role that influences USP11 protein abundance and binding to ZUP1……...……..….153
**Figure 4.12:** Summary of potential interacting domains of ZUP1, USP11 and TCEAL1 identified from mutagenesis studies in this chapter……160
**Figure 5.1**: Denaturing affinity purification and immunoprecipitation methods for detecting ubiquitylated RPA and PCNA in cells……..…….....……171
**Figure 5.2**: Sonication settings may have an impact on the detection of ubiquitylated PCNA by denaturing Strep pull-down……...…..……176
**Figure 5.3**: Optimisation of MMC treatment durations to analyse the effect of ZUP1 loss on PCNA and RPA ubiquitylation…….....…179
**Figure 5.4**: Synchronisation of 293T wild-type and ZUP1 knockout cells in S phase by double thymidine block……..……183

**Figure 5.5**: Polyubiquitylated PCNA is present at elevated levels and persists for at least 30 h in ZUP1 knockout cells treated with MMC……..……..186
**Figure 5.6**: ZUP1 loss is associated with elevated levels of polyubiquitylated PCNA in the presence of MMC……...…….…188
**Figure 5.7**: PCNA ubiquitylation in ZUP1 knockout cells may be dependent on RAD18……...……...…….190
**Figure 5.8**: Assessing the effects of RFWD3 knockdown on MMC-induced PCNA ubiquitylation in ZUP1 knockout cells…….……..….192
**Figure 5.9**: USP1 knockdown abolishes PCNA polyubiquitylation in ZUP1 knockout cells treated with MMC…….…...…….195
**Figure 5.10**: Denaturing pull-down of Strep-RPA32 to assess MMC induction of ubiquitylated RPA32……...……..197
**Figure 5.11**: Assessing the ability of transiently expressed FLAG-ZUP1 wild-type or C360R to rescue MMC-induced PCNA polyubiquitylation in ZUP1 knockout cells……..…..…….200
**Figure 5.12**: Assessing the effect of FLAG-ZUP1 wild-type on the recovery of MMC-induced PCNA polyubiquitylation in ZUP1 knockout cells……..…….…..202
**Figure 5.13**: Investigating the ZUP1 rescue effect of MMC-induced PCNA polyubiquitylation using stable ZUP1-complemented cell lines…….....….205
**Figure 5.14**: Immunoprecipitation of PCNA from ZUP1 knockout cells to assess the *in vitro* deubiquitylation of polyubiquitylated PCNA by recombinant ZUP1..……208
**Figure 5.15**: The effect of recombinant ZUP1 on the polyubiquitin chains in the immunoprecipitated PCNA fraction was reproduced in a different ZUP1 knockout clone…….……..….210
**Figure 5.16**: CRISPR-based Clover knock-in assay to assess the efficiency of homology-directed repair in cells…….……..……214
**Figure 5.17**: Optimisation of transfected plasmid ratios to maximise Cas9-mediated HDR and Clover knock-in……..……..…….215
**Figure 5.18**: ZUP1 knockouts exhibit enhanced HDR activity as indicated by the efficiency of Clover knock-in……..……..……217
**Figure 5.19**: The hyper-recombination phenotype in ZUP1 knockouts was confirmed when a transfection control was included in the LMNA HDR assay…..……..……..…….218
**Figure 6.1:** Model for the potential role of ZUP1 in DNA repair…….……..……..230

**Appendix A** (Supplemental information to Chapter 3) Figure 1 – 5……..…..…..…233
**Appendix B** (Supplemental information to Chapter 4) Figure 1 – 5……..…….....…235
**Appendix C** (Supplemental information to Chapter 5) Figure 1 – 5……..…….....238

# List of Tables

**Table 1.1**: Examples of known ubiquitin-binding domains……..……..…….28
**Table 2.1**: Buffers used in this thesis……..……..…..…..49
**Table 2.2**: Buffer additives used in this thesis……..……..….....50
**Table 2.3**: Plasmids used in this thesis……..……..…..…..51
**Table 2.4**: Oligonucleotides used for cloning or PCR…….....…...…….53
**Table 2.5**: Sequences of oligonucleotides used to clone the indicated sgRNA/Cas9 vectors……..……..……..54
**Table 2.6**: Antibodies used in this thesis…….....…55
**Table 2.7**: siRNAs used in this thesis……..……..……..56
**Table 2.8**: Cell lines used in this thesis……..……..…...57
**Table 5.1**: Comparison of experimental conditions used in denaturing pull-down or IP methods for the detection of ubiquitylated PCNA and RPA…….…….…….181

# List of Abbreviations

| | |
|---|---|
| 53BP1 | p53-binding protein 1 |
| AMC | 7-amino-4-methylcoumarin |
| APC | Adenomatous polyposis coli |
| APIM | AlkB homologue 2 PCNA-interacting motif |
| ATG4 | Autophagin |
| ATM | Ataxia-telangiectasia mutated |
| ATP | Adenosine triphosphate |
| ATR | Ataxia telangiectasia and Rad3-related |
| ATRi | ATR inhibitor |
| ATRIP | ATR-interacting protein |
| BARD1 | BRCA1-associated RING domain protein 1 |
| BIR | Break-induced replication |
| BRCA | Breast cancer gene |
| CDC | Cell division cycle protein |
| CDK | Cyclin-dependent kinase |
| CDT1 | Chromatin licensing and DNA replication factor 1 |
| CK2 | Casein kinase 2 |
| CMG | Cdc45-MCM-GINS |
| CPT | Camptothecin |
| CRISPR | Clustered Regularly Interspaced Short Palindromic Repeats |
| CRL | Cullin–RING E3 ubiquitin ligase |
| DDK | Dbf4-dependent kinase |
| DNA | Deoxyribonucleic acid |
| DNA-PKcs | DNA-dependent protein kinase catalytic subunit |
| dNTP | Deoxyribonucleoside triphosphate |
| DPC | DNA-protein crosslink |
| DSB | Double-strand break |
| dsDNA | Double-stranded DNA |
| DTT | Dithiothreitol |
| DUB | Deubiquitylase |
| DUSP | Domain present in ubiquitin-specific proteases |
| EDTA | Ethylenediaminetetraacetic acid |
| EME1 | Essential meiotic structure-specific endonuclease 1 |
| ESCRT0 | Endosomal sorting complex required for transport |
| ETAA1 | Ewing's tumor-associated antigen 1 |
| EV | Empty vector |
| Ex | Exon |
| EXO1 | Exonuclease 1 |
| FA | Fanconi anemia |
| FEN1 | Flap endonuclease 1 |
| FWD | Forward |

| | |
|---|---|
| gDNA | Genomic DNA |
| GFP | Green fluorescent protein |
| GST | Glutathione S-transferase |
| γH2AX | Phosphorylated histone H2AX |
| HDR | Homology-directed assay |
| HECT | Homologous to the E6-AP Carboxyl Terminus |
| HEK 293T | Human embryonic kidney 293T |
| HIRAN | HIP116, Rad5p N-terminal |
| HLTF | Helicase like transcription factor |
| HR | Homologous recombination |
| Hrs | Hepatocyte growth factor regulated tyrosine kinase substrate |
| HU | Hydroxyurea |
| ICE | Inference of CRISPR Edits |
| ICL | Interstrand crosslink |
| IDCL | Interdomain connector loop |
| JAMM | JAB1/MPN/MOV34 |
| LC-MS | Liquid chromatography mass spectrometry |
| LIG4 | DNA ligase 4 |
| LTGC | Long tract gene conversion |
| mAb | Monoclonal antibody |
| MCM | Minichromosome maintenance |
| MINDY | Motif interacting with Ub-containing novel DUB family |
| MIU | Motif interacting with ubiquitin |
| MMC | Mitomycin C |
| MRN | MRE11–RAD50–NBS1 |
| MS | Mass spectrometry |
| NEM | N-Ethylmaleimide |
| NF-κB | Nuclear factor kappa B |
| NHEJ | Non-homologous end joining |
| Ni-NTA | Nickel nitrilotriacetic acid |
| NMR | Nuclear magnetic resonance |
| ORC | Origin recognition complex |
| OTU | Ovarian tumor proteases |
| PA or Prg | Propargylated |
| pAb | Polyclonal antibody |
| PALB2 | Partner and localizer of BRCA2 |
| PAM | Protospacer adjacent motif |
| PARP | Poly [ADP-ribose] polymerase |
| PCNA | Proliferating cell nuclear antigen |
| PCR | Polymerase chain reaction |
| PDB | Protein Data Bank |
| PGK | Phosphoglycerate kinase |
| PIC | Protease inhibitor cocktail |
| PIKK | Phosphoinositide-3-kinase-related protein kinases |
| PIP | PCNA-interacting protein |
| Plk1 | Polo-like kinase 1 |
| Pol | Polymerase |

| | |
|---|---|
| PRC1 | Polycomb repressive complex 1 |
| PRP19 | Pre-mRNA processing factor 19 |
| RBR | RING-between-RING |
| REV | Reverse |
| RFC | Replication factor C |
| RFP | Red fluorescent protein |
| RFWD3 | Ring finger and WD repeat domain 3 |
| RING | Really Interesting New Gene |
| RNA | Ribonucleic acid |
| RNAi | RNA interference |
| RPA | Replication protein A |
| RPN13 | Regulatory particle subunit 13 |
| SDSA | Synthesis-dependent strand annealing |
| SDS-PAGE | Sodium dodecyl sulfate polyacrylamide gel electrophoresis |
| sgRNA | Single guide RNA |
| siRNA | Small interfering RNA |
| SLX | Structure-specific endonuclease subunit |
| SMARCAL1 | SWI/SNF related, matrix associated, actin dependent regulator of chromatin, subfamily a like 1 |
| SSB | Single-strand break |
| ssDNA | Single-stranded DNA |
| STAM | Signal transducing adaptor molecule |
| STUBL | SUMO-targeted ubiquitin ligases |
| TCEAL1 | Transcription elongation factor A protein-like 1 |
| TLS | Translesion synthesis |
| TOP1 | DNA topoisomerase I |
| TOPBP1 | DNA topoisomerase 2-binding protein 1 |
| TUBEs | Tandem ubiquitin binding entities |
| TXNIP | Thioredoxin interacting protein |
| Ub or Ubi | Ubiquitin |
| UbiCREST | Ubiquitin chain restriction |
| UBD | Ubiquitin-binding domain |
| Ubl or UBL | Ubiquitin-like |
| UBR5 | Ubiquitin protein ligase E3 component n-recognin 5 |
| UBZ | Ubiquitin-binding zinc finger |
| UCH | Ubiquitin carboxy-terminal hydrolases |
| UFM1 | Ubiquitin fold modifier 1 |
| UFSP | UFM1-specific protease |
| UIM | Ubiquitin-interacting motif |
| USP | Ubiquitin-specific protease |
| VPS | Vinyl pentynyl sulfone |
| ROS | Reactive oxygen species |
| WCE | Whole cell extracts |
| WRN | Werner syndrome ATP-dependent helicase |
| WT | Wild-type |
| XRCC | X-ray repair cross complementing 1 |
| ZHA | ZUP1 helical arm |

| | |
|---|---|
| ZnF | Zinc finger |
| ZRANB3 | Zinc finger RANBP2-type containing 3 |
| ZUP1 | Zinc finger containing ubiquitin peptidase 1 |

# 1

# Introduction

## Contents


**1.1 DNA replication……2**

1.1.1 Overview……2

1.1.2 Proliferating cell nuclear antigen (PCNA)……5

**1.2 Replication stress……8**

1.2.1 Sources of replication stress and checkpoint activation……8

1.2.2 DNA damage tolerance……10

1.2.3 Replication fork remodelling……12

1.2.4 Double-strand break repair……15

1.2.5 Exploiting DNA replication stress in cancer therapy……19

**1.3 Ubiquitylation……21**

1.3.1 Ubiquitin……21

1.3.2 Ubiquitylation cascade……24

1.3.3 Ubiquitin modifications……25

1.3.4 Ubiquitin-binding domains……29

**1.4 Deubiquitylases (DUBs)……31**

1.4.1 DUB classes……31

1.4.2 Substrate recognition and linkage specificity……32

1.4.3 Regulation of DUBs……34

**1.5 Zinc Finger Containing Ubiquitin Peptidase 1 (ZUP1)……36**

1.5.1 Discovery of ZUP1 as a novel DUB class……36

1.5.2 Structure and ubiquitin chain specificity of ZUP1……37

1.5.3 Evidence for the roles of ZUP1 in DNA repair……40

**1.6 Ubiquitin signalling at stressed replication forks……42**

1.6.1 PCNA ubiquitylation……42

1.6.2 RPA ubiquitylation……43

1.6.3 FANCI-FANCD2 ubiquitylation……44

**1.7 Overall aims and motivation……47**

## 1.1 DNA replication

### 1.1.1 Overview

DNA replication in eukaryotes is a complex and tightly regulated process that ensures the accurate and complete duplication of the genome during the cell cycle. DNA replication begins with the binding of the six-subunit origin recognition complex (ORC) to potential replication origins (Rivera-Mulia et al., 2016). During late mitosis or G1 phase, CDC6 and CDT1 are recruited to the replication origins which facilitate the loading of the double hexameric Mcm2-7 helicase complex (MCM), enabling it to encircle double-stranded DNA (dsDNA) in an inactive form (Blow and Dutta et al., 2005; Evrin et al., 2009).

In S phase, the activities of Dbf4-dependent kinase (DDK) and cyclin-dependent kinase (CDK) promote the recruitment of Cdc45 and the GINS hetero-tetramer which activate the helicase complex (Tanaka et al., 2006; Zegerman et al., 2006; Gambus et al., 2006; Tanaka et al., 2011; Costa et al., 2011). In budding yeast, the phosphorylation of MCM by DDK is essential for the recruitment of Sld3/7 and Cdc45, whereas CDK phosphorylation of Sld2 and Sld3 promotes their binding to Dpb11 and drives the recruitment of GINS (Heller et al., 2011; Yeeles et al., 2015). These kinases along with other firing factors, promote the remodelling of the double MCM hexamer into two active Cdc45-MCM-GINS (CMG) helicases (Deegan et al., 2016).

The CMG helicase encircles opposite single-stranded DNAs (ssDNAs) at the replication origin, and the unwinding of the parental dsDNA and helicase activation are mediated by Mcm10 and ATP hydrolysis (Douglas et al., 2018; Wasserman et al., 2019). The ssDNA strands that become exposed in the process are rapidly coated by the replication protein A (RPA) complex (Wold et al., 1997). The CMG helicase translocates 3’-5’ along the leading strand and directly interacts with Pol ε which is the primary DNA polymerase responsible for synthesising the leading strand in a continuous manner (Langston et al., 2014; Guilliam et al., 2020). The lagging strand

is synthesised in short Okazaki fragments, which is predominantly performed by Pol δ, and the Okazaki fragments are ligated to form a continuous DNA strand in a process known as 'maturation of Okazaki fragments' (Kunkel et al., 2008; Burgers et al., 2017). The Pol α-primase complex initiates strand synthesis by assembling RNA-DNA primers (Pellegrini, 2012). The unwinding of DNA and replication elongation result in supercoils, which are relaxed by type I and type II topoisomerases (Wang et al., 2002). The major players involved in the elongation step of DNA replication are presented in **Fig 1.1**.

One important determinant of the high fidelity of DNA replication is the intrinsic 3'-5' exonuclease activity of DNA polymerases (Ganai et al., 2016). Should a nucleotide be misincorporated, the nascent primer strand is transferred from the polymerase active site to the exonuclease active site that catalyses the removal of the nucleotide. This switching mechanism in Pol δ has been proposed to be mediated by a β-hairpin that extends from its exonuclease domain, while the P domain of Pol ε is thought to perform this role (Hogg et al., 2013; Attali et al., 2021). As described in the following section, Pol δ and Pol ε interact with proliferating cell nuclear antigen (PCNA) which enhances the processivity of the DNA polymerases (Chilkova et al., 2007; Guilliam et al., 2020). Unlike Pol ε, Pol δ is equipped to perform strand displacement synthesis at high efficiency which is key for Okazaki fragment maturation (Garg et al., 2004). Although Pol ε is the main polymerase for replicating leading strands, Pol δ is also recognised for its role in performing the initial extension of the leading strand (Yeeles et al., 2017; Guilliam et al., 2020).

DNA replication is terminated upon the convergence of two replication forks (Gambus et al., 2017; Dewar and Walter, 2017). During plasmid replication in *Xenopus* egg extracts, no detectable fork slowing was observed during fork convergence, suggesting that the converging CMG helicases approach one another on opposite strands (Dewar et al., 2015). A critical step during replication termination is the ubiquitylation of the Mcm7 subunit of CMG with K48-linked ubiquitin chains which is mediated by the E3 ligase, $SCF^{Dia2}$ in yeast (Maric et al., 2014). In higher eukaryotes, the E3 ligase $CUL2^{LRR1}$ promotes Mcm7 ubiquitylation within terminated CMGs

(Sonneville et al., 2017). Ubiquitylated CMG is recognised and disassembled by p97/VCP/Cdc48, a hexameric AAA+-type ATPase that binds and translocates ubiquitylated targets through its central pore, extracting them from cellular locations such as chromatin (Moreno et al., 2014; van den Boom et al., 2018). A mitotic pathway independent of $CUL2^{LRR1}$ was recently discovered, which triggers the unloading of terminated replisomes that remain associated with chromatin during mitotic entry. This pathway involves the E3 ligase TRAIP that mediates the ubiquitylation of Mcm7 prior to CMG disassembly, and requires p97/VCP activity (Moreno et al., 2019).

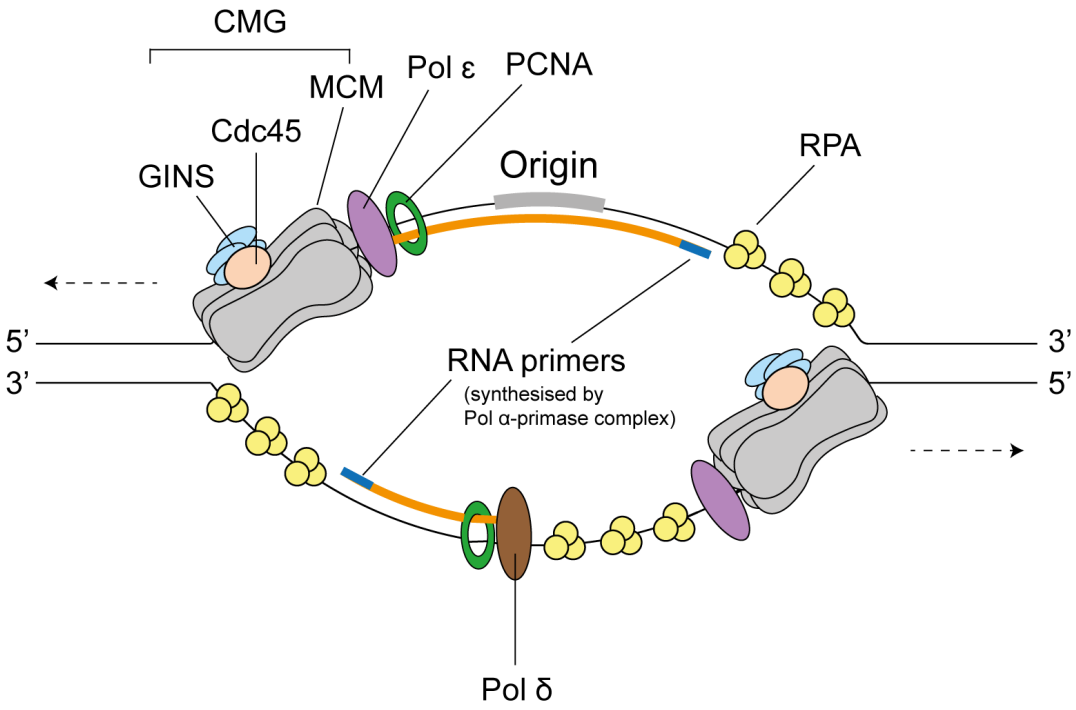



**Figure 1.1: Major proteins present at the replication fork during the elongation step of eukaryotic DNA replication.** Figure modified from Aria and Yeeles, 2019.

### 1.1.2 Proliferating cell nuclear antigen (PCNA)

DNA replication involves the dynamic recruitment and concerted action of DNA polymerases and numerous factors involved in leading and lagging strand synthesis. One crucial protein that coordinates the DNA replication machinery is PCNA, a ring-shaped homotrimer that encircles dsDNA and is referred to as the DNA sliding clamp (**Fig. 1.1**, **Fig. 1.2A**, Slade et al., 2018). The central channel of PCNA is lined with basic residues that form short-lived polar interactions with DNA phosphates that enable it to slide along the DNA (De March et al., 2017). Each PCNA monomer consists of two structurally similar domains that are bridged by a flexible interdomain connector loop. Many PCNA interacting partners bind to a hydrophobic pocket near this loop through PCNA-interacting protein (PIP)-box motifs or other binding modules such as the AlkB homologue 2 PCNA-interacting motif (APIM) (**Fig. 1.2B**; Gilljam et al., 2009; Boehm et al., 2016).

After replication initiation by the Pol α-primase complex, PCNA is loaded onto DNA at the primer-template junction by the replication factor C (RFC) complex which binds to ATP and facilitates the opening of the PCNA clamp (Kelch et al., 2011; Sakato et al., 2012). The PCNA ring closes around DNA upon ATP hydrolysis which leads to the dissociation of RFC from DNA-loaded PCNA. On the leading strand, one PCNA ring is loaded upon replication initiation, whereas the synthesis of each Okazaki fragment on the lagging strand involves the loading of one ring (Boehm et al., 2016). PCNA tethers Pol δ and Pol ε to replication forks and increases their processivity (Chilkova et al., 2007; Boehm et al., 2016). The greater binding affinity of Pol δ to PCNA is attributed to its low intrinsic processivity compared to Pol ε. Biochemical studies have shown that PCNA enhances the number of nucleotides incorporated by Pol δ and Pol ε in a single DNA-binding event, an effect that is particularly substantial for Pol δ (Chilkova et al., 2007). The unloading of PCNA is mediated by an RFC-like complex in which ATAD5 is present in place of the catalytic subunit RFC1 (Kubota et al., 2013; Lee et al., 2013).

PCNA coordinates the maturation of Okazaki fragments through its dynamic interactions with Pol δ, the flap endonuclease 1 (FEN1) and DNA ligase I (LIG1) (Burgers et al., 2017). Pol δ encounters and partly displaces the initiator primer of the previous Okazaki fragment into a 5'-flap structure (Balakrishnan et al., 2013). The flap is cleaved by FEN1 and the resulting nick is sealed by LIG1 to generate a continuous lagging strand DNA. Besides providing an interaction platform for these enzymes to function sequentially during Okazaki fragment maturation, PCNA has also been shown to stimulate FEN1-mediated cleavage and enhance the binding of FEN1 to the flap structure (Tom et al., 2000; Craggs et al., 2014).

The roles of PCNA are mainly executed through protein-protein interactions given the absence of intrinsic enzymatic activity. Post-translational modifications on PCNA significantly expand its functional capacity by serving as additional binding interfaces for interacting proteins (Mailand et al., 2013). Some PCNA-interacting proteins contain ubiquitin- or SUMO-binding motifs that bind ubiquitylated or SUMOylated PCNA respectively (Slade et al., 2018). As described later in this chapter, PCNA is ubiquitylated on lysine-164 in response to replication stress or DNA damage. The conjugation of a single ubiquitin on PCNA triggers 'polymerase switching' in which a specialised translesion synthesis (TLS) polymerase, equipped with a PIP-box and ubiquitin-binding domain, binds to modified PCNA and replaces the stalled replicative polymerase to bypass the DNA lesion (Kannouche et al., 2004; Bienko et al., 2005). In addition to recruiting such non-classical polymerases to stressed replication forks, PCNA also has a role in stimulating their catalytic activity (Haracska et al., 2002; Garg et al., 2005).

PCNA plays a central role not only in normal DNA replication, but also in DNA repair processes such as DNA damage tolerance, and chromatin assembly, through interactions with numerous partner proteins at replication forks (Boehm et al., 2016). While its protein interaction network has been extensively studied, it remains to be addressed how some of these crucial protein-protein interactions are regulated in a dynamic and highly coordinated manner (Slade et al., 2018).

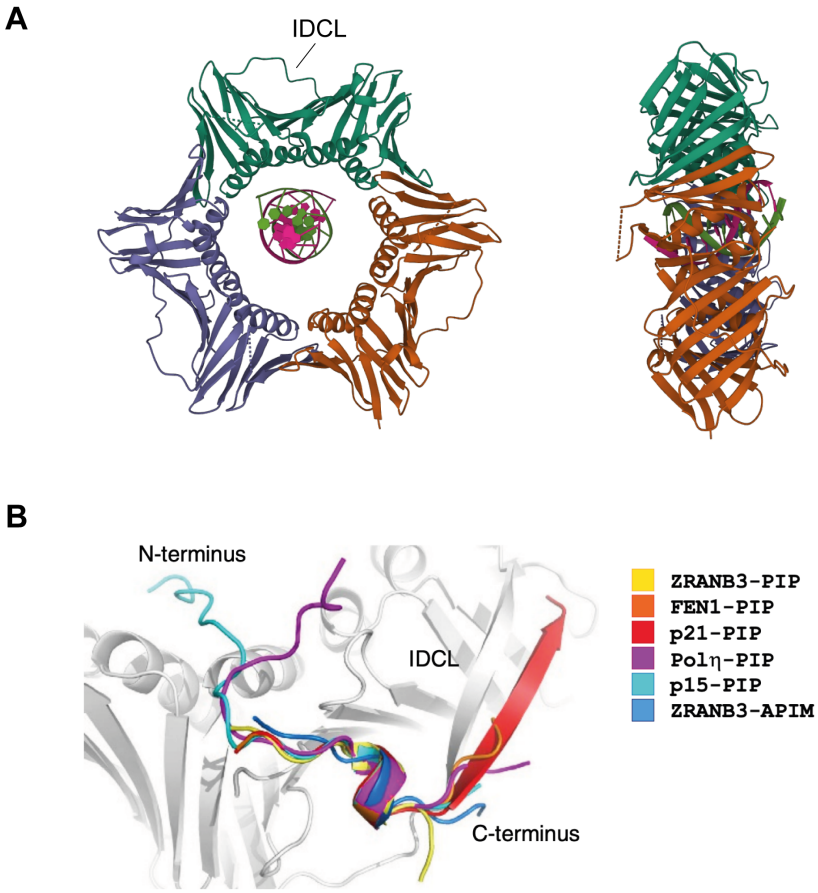



**Figure 1.2: Structure of human PCNA bound to DNA and examples of PIP box and APIM motif binding to PCNA.** A) Structure of human PCNA bound to DNA. The front (left) and side (right) views of PCNA bound to DNA (Protein Data Bank [PDB] code: 6GIS). The three PCNA subunits are coloured in green, blue and red. The interdomain connector loop (IDCL) for the PCNA subunit coloured in green is indicated. B) Superimposition of the indicated PCNA-bound PIP box and APIM motif peptides from different co-crystal structures. Yellow: ZRANB3-PIP$^{515–529}$ (PDB: 5MLO); orange: FEN1$^{336–348}$ (PDB: 1U7B), red: p21$^{143–160}$ (PDB: 1AXC); magenta: Pol η$^{694–713}$ (PDB: 2ZVK), cyan: p15$^{51–71}$ (PDB: 4D2G) and blue: ZRANB3-APIM$^{1065–1079}$ (PDB: 5MLW). Figure obtained from Sebesta et al., 2017.

## 1.2 Replication stress

### 1.2.1 Sources of replication stress and checkpoint activation

The DNA replication machinery faces the constant challenge of maintaining the fidelity of this process in the presence of DNA damage or obstacles arising from endogenous or exogenous sources (Saxena et al., 2022). Replication stress refers to the impaired progression of replication forks that compromises replication fidelity and genome stability. In response to replication stress, the appropriate checkpoint and repair mechanisms are activated to promote mechanisms that tolerate or repair the replication stressor(s), which are crucial to prevent the propagation of genome instability and diseases such as cancer (Zeman et al., 2014; Berti et al., 2020).

Replication stress can arise from naturally occurring secondary DNA structures such as hairpins and G-quadruplexes that physically obstruct the replication machinery (León-Ortiz et al., 2014). Certain forms of repetitive DNA sequences predispose to the formation of secondary structures which are typically resolved by helicases and nucleases to prevent their persistence at replication forks. Another natural source of replication stress is transcription-replication conflicts that frequently occur given that both machineries utilise the same DNA template (García-Muse et al., 2016; Lans et al., 2019; Bowry et al., 2021). Collisions occur when transcription and replication machineries approach one another in a head-on or co-directional orientation (García-Muse et al., 2016). R-loops, which are three-stranded nucleic acid structures characterised by an RNA-DNA hybrid and a displaced ssDNA strand, form during transcription and are thought to contribute to the deleterious effects of transcription-replication conflicts. R-loops have been shown to cause replication fork stalling and DNA damage and are prevented from accumulating to toxic levels by RNase H, helicases, and topoisomerase 1 (TOP1) which relaxes DNA supercoiling (Gan et al., 2011; Helmrich et al., 2011; Sollier et al., 2014; García-Muse et al., 2016; Promonet et al., 2020).

An imbalance of cellular deoxyribonucleoside triphosphate (dNTP) pools also leads to replication stress (Saxena et al., 2022). Low dNTP levels that result from excessive origin firing or the inhibition of ribonucleotide reductase by hydroxyurea, hamper DNA polymerase activities and result in fork stalling (Pai et al., 2017). Another source of replication stress is single-strand DNA breaks or 'nicks' that occur frequently in the genome and can be generated by free radicals. Nicks encountered by the CMG helicase have the potential to cause fork collapse and replisome dissociation (Vrtis et al., 2021). Other common lesions include ribonucleotides, base lesions and abasic sites (Mirsanaye et al., 2021). DNA interstrand crosslinks (ICLs) and DNA-protein crosslinks (DPCs) are widely studied toxic lesions that can be induced by chemotherapeutics. ICLs are generated from the covalent linkage between complementary DNA strands, and such lesions prevent the unwinding of DNA strands thereby inhibiting the progression of helicases and the replisome (Deans et al., 2011; Hashimoto et al., 2016). DPCs form bulky adducts when proteins in close proximity to DNA are trapped and form stable complexes with DNA (Kühbacher et al., 2020).

During replication stress, long ssDNA stretches may form as a result of the continued unwinding of DNA by the helicase while the polymerase is stalled (Zeman et al., 2014). The ssDNA is coated by the RPA complex (comprising RPA70, RPA32 and RPA14 subunits) which provides an interaction platform for the kinase ataxia telangiectasia and Rad3-related (ATR) and ATR-interacting protein (ATRIP) (Zou et al., 2003). ATR kinase activation is mediated by at least two proteins, TOBP1 and ETAA1 (Kumagai et al., 2006; Bass et al., 2016; Haahr et al., 2016). ATR phosphorylates checkpoint kinase 1 (CHK1), and the downstream effects constitute the replication or S phase checkpoint that arrests the cell cycle in S phase in response to replication stress (Saldivar et al., 2017). CHK1 in turn phosphorylates and inactivates CDC25 phosphatases including CDC25A which leads to CDK inhibition. The inhibition of CDK1 prevents entry into mitosis, while that of CDK2 inhibits origin firing (Toledo et al., 2017).

The ATR-CHK1 pathway prevents global origin firing whilst enabling the firing of local dormant origins within existing replication factories (Ge et al., 2010). This has been proposed to prevent further replication stress in unreplicated regions in the presence of genotoxic stress, while ensuring replication completion in the vicinity of stressed forks (Yekezare et al., 2013). The inhibition of global origin firing by ATR also delays the exhaustion of RPA which, if depleted to levels that can no longer support the accumulation of ssDNA, will result in fork collapse (Toledo et al., 2013). The ATR-CHK1 pathway also contributes to replication fork stabilisation to preserve their integrity during replication stress (Saldivar et al., 2017; Toledo et al., 2017). Checkpoint activation therefore minimises damage to replication forks while providing sufficient time for DNA repair before replication is resumed.

### 1.2.2 DNA damage tolerance

Cells are equipped with mismatch and excision repair pathways to remove DNA lesions such as base lesions, abasic sites and ribonucleotides (Mirsanaye et al., 2021). If DNA lesions are encountered by the replisome, a DNA damage tolerance pathway known as translesion synthesis (TLS) will be activated to enable the bypass of lesions and ensure uninterrupted fork progression while the lesions are removed post-replicatively (Branzei et al., 2016a).

TLS is activated by monoubiquitylated PCNA to which specialised TLS polymerases are recruited and bind with high affinity via their PIP-box and ubiquitin-binding domain motifs. The binding of a TLS polymerase to monoubiquitylated PCNA enables it to replace the stalled replicative polymerase and incorporate nucleotides opposite the lesion (Kannouche et al., 2004; Bienko et al., 2005). TLS polymerases include Y-family polymerases (Pol η, Pol ι, Pol κ and REV1), the B-family polymerase Pol ζ and A-family polymerases, each of which have preferences for specific lesions (Makridakis et al., 2012). Recently, PrimPol was reported as a TLS polymerase despite not directly interacting with PCNA, and is recruited to stalled forks through its binding to RPA (Guilliam et al., 2015; Guilliam et al., 2017). Many TLS polymerases

are inherently error-prone, owing to their active site architecture that enables them to accommodate bulky DNA lesions, thereby decreasing their ability to recognise incorrect incoming bases (Yang et al., 2007; Sale et al., 2013). The 3'-5' proofreading exonuclease domain is also absent in Y-family TLS polymerases (Sale et al., 2013). In UV-irradiated cells, USP1 was shown to undergo autocleavage which inactivates it and allows monoubiquitylated PCNA to accumulate (Huang et al., 2006). The expression of the active and non-degradable form of USP1 in human cells was found to inhibit UV-induced PCNA monoubiquitylation. From this, USP1 was proposed to reverse the signal on monoubiquitylated PCNA and prevent aberrant low-fidelity TLS activity.

While TLS is well characterised, relatively little is known about template switching, a recombination-mediated damage bypass mechanism (Leung et al., 2019). Template switching is thought to involve the formation of recombination-like intermediates and sister chromatid junctions (Branzei et al., 2008; Giannattasio et al., 2014; Lovett et al., 2017). In this process, the nascent strand temporarily utilises the newly synthesised undamaged sister chromatid strand as a template to replicate over the lesion (Branzei et al., 2016b). Template switching was proposed as an error-free, alternative pathway to TLS based on early studies in yeast showing a synergistic interaction between *MMS2* (encodes MMS2) and *REV3* (encodes the catalytic subunit of Pol ζ) (Broomfield et al., 1998). Further genetic characterisation revealed that homologous recombination genes act in the same pathway as *MMS2* (Ball et al., 2009). The UBC13–MMS2 complex together with RAD5 were shown in yeast to be required for polyubiquitylation of PCNA with K63-linked chains (Hoege et al., 2002). Collectively, these findings led to the model that the error-free pathway involves PCNA polyubiquitylation, homologous recombination factors, and template switching (Ball et al., 2009). However, the template switching mechanism (i.e., factors involved) and the specific role of polyubiquitylated PCNA in this process are not yet firmly established in vertebrates.

### 1.2.3 Replication fork remodelling

Stressed replication forks can undergo remodelling into transient structures prior to fork restart and replication re-initiation (Berti et al., 2020). Electron microscopy approaches have demonstrated the reversal of forks in response to a wide range of genotoxic insults (Zellweger et al., 2015). For example, it was observed in *Xenopus* egg extracts that one of the two replication forks that converge on ICL lesions undergoes reversal, which requires CMG unloading and precedes ICL unhooking (Amunugama et al., 2018). Fork reversal has been proposed to enable fork slowing, provide more time for repair and limit detrimental chromosomal breakage (Ahuja et al., 2016). To date, several DNA translocases have been identified as key regulators of fork reversal, each with distinct substrate preferences and interactions at stressed forks (Berti et al., 2020).

ZRANB3 promotes fork slowing and reversal upon replication stress induction through its DNA translocase activity and interaction with polyubiquitylated PCNA (Vujanovic et al., 2017). Another DNA translocase, SMARCAL1 is recruited to stalled forks through its direct binding to RPA which was shown to stimulate SMARCAL1-mediated regression of a damaged fork substrate containing a leading strand gap (Ciccia et al., 2009; Bétous et al., 2013). The ability of SMARCAL1 to catalyse branch migration of Holliday junctions and the reversal of replication fork substrates require the HARP2 and SNF2-like ATPase domains (Bétous et al., 2012). The Rad5-related DNA translocase, HLTF also promotes fork reversal and this requires its ATPase activity and HIRAN domain that binds specifically to the 3′-end of ssDNA (Kile et al., 2015). The translocases that mediate fork reversal are thought to have non-redundant roles in potentially different contexts of replication stress (Berti et al., 2020).

The RAD51 recombinase is required for effective fork reversal in human cells, however the details of how RAD51 promotes fork reversal is not currently known (Zellweger et al., 2015). RAD52 plays an important regulatory role in fork remodelling where it counteracts SMARCAL1-mediated fork reversal and maintains fork integrity by limiting MRE11-dependent degradation of the nascent strand after fork reversal

(Malacaria et al., 2019). Among the factors shown to facilitate fork restart is RECQ1 which utilises its ATPase and branch migration activities to promote branch migration of forks that have reversed following TOP1 inhibition, and enable replication fork restart (Berti et al., 2013). Reversed forks can also undergo nucleolytic processing by the DNA2 nuclease in conjunction with the WRN helicase prior to fork restart (Thangavel et al., 2015).

The precise mechanism by which fork reversal and restart occurs remains to be defined, and current models are illustrated in **Fig. 1.3** (Guilliam et al., 2021). Following fork uncoupling induced by a DNA lesion, the fork is reversed into a four-way structure while uncoupled CMG potentially traverses onto dsDNA ahead of the lesion (**Fig. 1.3A**). The nascent leading strand may undergo extension using the nascent lagging strand as a template, and subsequent branch migration catalysed by RECQ1 could lead to fork restart (**Fig. 1.3B**). CMG may re-engage ssDNA to restart replication once the fork is restored. Fork restart potentially occurs after the lesion is repaired. Degradation of the reversed fork mediated by DNA2-WRN may also precede fork restart (**Fig. 1.3C**). It has also been proposed that the parental dsDNA ahead of the lesion may unwind by the action of other helicases after fork reversal (**Fig. 1.3D**). According to the model in **Fig. 1.3D**, a new replication fork may be formed which could involve repriming of the leading strand, possibly through PrimPol, and the lesion may then undergo post-replicative repair followed by restoration of the reversed fork (Guilliam et al., 2021; Mourón et al., 2013).

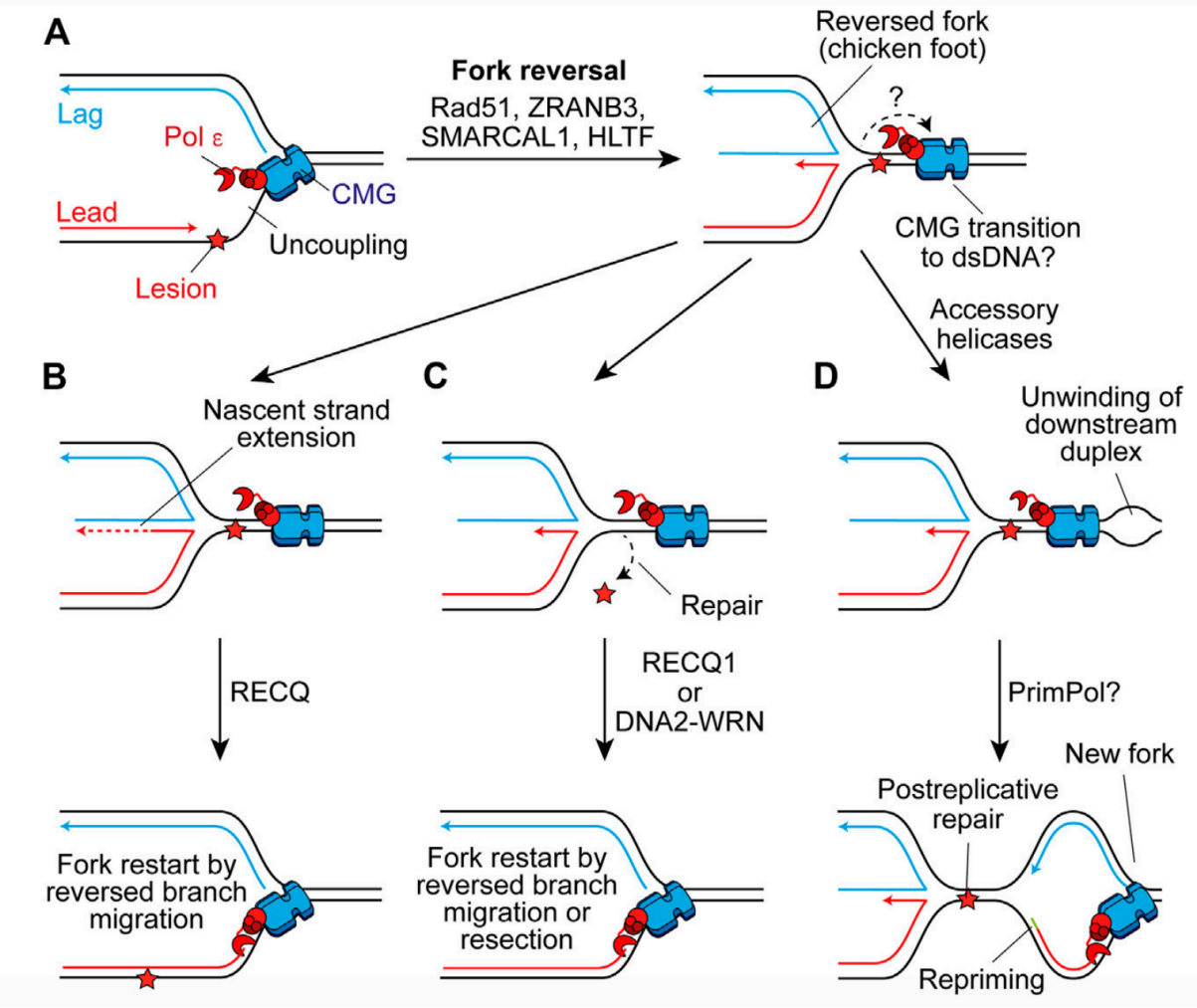



**Figure 1.3: Summary of proposed models for fork reversal and restart following replication stress.** A) As described in the text, fork reversal can occur on uncoupled forks in the presence of a DNA lesion, and is mediated by factors including RAD51, ZRANB3, SMARCAL1, and HLTF. CMG may engage duplex DNA ahead of the lesion. B) The nascent leading strand that has reversed may be extended using the nascent lagging strand as a template. Subsequent fork restart may occur by branch migration catalysed by RECQ1, while CMG may traverse back to ssDNA to restart replication. C) The DNA lesion may be repaired prior to RECQ1-mediated fork restart. Degradation of the reversed fork by DNA2-WRN may also occur prior to fork restart. D) The parental duplex ahead of the lesion may undergo unwinding to form a new replication fork which may involve repriming, while the reversed fork could be resolved once the lesion is removed post-replicatively. Figure obtained from Guilliam et al., 2021.

### 1.2.4 Double-strand break repair

Persistent replication stress can cause fork breakage or collapse that generates double-strand breaks (DSBs). The MRE11–RAD50–NBS1 (MRN) complex binds to DSBs and recruit the ATM kinase which, once activated, phosphorylates its targets including CHK2 and H2AX that trigger the DSB response (Lee et al., 2005; Alexander et al., 2016). Two main pathways that repair DSBs are homologous recombination (HR) and non-homologous end joining (NHEJ) (Scully et al., 2019).

The HR pathway can result in accurate repair outcomes by utilising homologous DNA sequences as the repair template. HR takes place in the S or G2 phases of the cell cycle when the sister chromatid is available (Mao et al., 2008). As illustrated in **Fig. 1.4**, the Ku70/80 heterodimer encircles broken DNA ends upon DSB formation. HR commences with DSB end resection performed by MRE11, and its endonuclease activity is promoted by CtIP. Subsequently, other nucleases such as EXO1, and DNA2 in conjunction with the BLM helicase, perform nucleolytic digestion which results in a 3' ssDNA overhang (Symington et al., 2014). This leads to the displacement of Ku70-Ku80 from DS ends. The RPA complex which coats the exposed ssDNA, is displaced by recombination factors such as BRCA2 to enable the loading of RAD51 which form RAD51 nucleoprotein filaments. The sequential phosphorylation of the RAD51 recombinase at S14 followed by T13 by Plk1 and CK2 respectively, was shown to promote RAD51 recruitment to sites of DNA damage by triggering its binding to the MRN component, NBS1 (Yata et al., 2012). The rapid polymerisation of RAD51 on flexible DNA was recently proposed to form the basis of its selective recognition of potentially more flexible ssDNA generated during DSB resection over ssDNA formed in normal conditions (Paoletti et al., 2020). RAD51 filaments perform homology search involving DNA strand invasion, where the invading strand pairs with complementary sequences within the template duplex DNA to allow repair synthesis (Scully et al., 2019). BRCA1-BARD1 facilitate multiple steps throughout HR including DNA end resection and RAD51 loading (Scully et al., 2019).

## DSB repair by homologous recombination

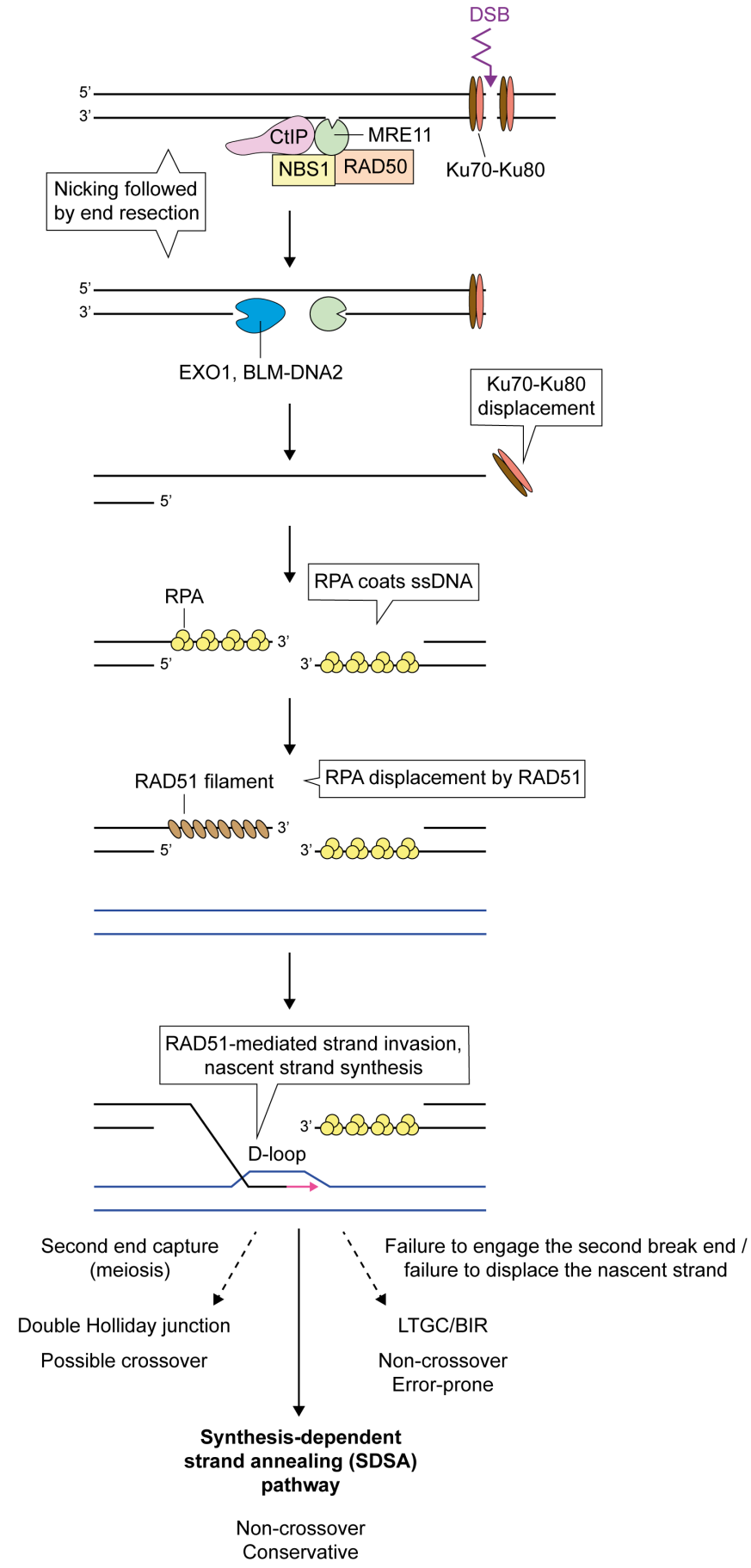


**Figure 1.4: Key steps involved in homologous recombination repair of DSBs.** As described in the text, DNA end resection is mediated by the endonuclease activity of the MRN complex, and the 5'-3' resection activities of EXO1 and DNA2-BLM. The RPA complex coats the exposed ssDNA regions and is rapidly displaced by RAD51 to form RAD51 nucleoprotein filaments. The non-crossover synthesis-dependent strand annealing (SDSA) pathway is the major repair pathway in somatic cells. In meiotic cells, a double Holliday junction intermediate can form and lead to possible crossover. In the absence of the second DNA end (e.g., one-ended DSBs) or if the nascent strand fails to be displaced, aberrant HR mechanisms can take place including long tract gene conversion (LTGC) and break-induced replication (BIR). Figure modified from Scully et al., 2019.

The major pathway for HR repair in somatic cells is the synthesis-dependent strand annealing (SDSA) pathway, which involves RAD51-mediated strand invasion of the template DNA, repair synthesis to extend the nascent strand, followed by its displacement (release) (**Fig. 1.4**; Scully et al., 2019). One-ended DSBs can arise when replication forks encounter a DNA lesion that causes fork stalling or collapse (Kramara et al., 2018). Without the engagement of a second DNA end, the high-fidelity SDSA pathway cannot take place. Instead, one-ended DSBs are repaired by break-induced replication (BIR) which involves strand invasion and extensive D-loop migration and is similar to long tract gene conversion (LTGC) where repair synthesis can extend to several kilobases (Kramara et al., 2018; Scully et al., 2019). BIR predisposes DNA to mutagenesis and chromosomal rearrangements (Elango et al., 2017). In the absence of functional HR, it is possible that one-ended DSBs will be joined to incompatible break ends by an alternative NHEJ pathway as described below, which can lead to rearrangements and genome instability (Ensminger et al., 2020).

In contrast to HR, NHEJ allows DNA ends to be ligated without utilising sequence homology, and can occur throughout the cell cycle including the S and G2 phases (Mao et al., 2008). The Ku heterodimer which binds to broken DNA ends, recruits the DNA-dependent protein kinase catalytic subunit (DNA-PKcs) which phosphorylate

numerous NHEJ factors including itself. DNA ends are ligated by the DNA ligase IV which forms a complex with XRCC4 (Stinson and Loparo et al., 2021). However, DNA ends are often complex and incompatible for immediate and precise ligation, including ends with damaged or adducted nucleotides. These ends can be modified by NHEJ end-processing enzymes including nucleases (e.g., Artemis) and polymerases (e.g., Pol μ, Pol λ) to convert termini into ligatable ends (Stinson and Loparo et al., 2021). An alternative NHEJ mechanism known as microhomology-mediated end-joining (MMEJ) aligns microhomologous sequences internal to the broken DNA ends prior to joining (Sfeir and Symington et al., 2015). MMEJ is a mutagenic process that is associated with insertions or deletions of nucleotides, and chromosomal rearrangements. Both MMEJ and HR are active in S phase and have a common initial end resection step to repair DSBs (Truong et al., 2013).

The failure of dedicated pathways to repair DSBs resulting from broken or collapsed forks will lead to irreversible, pan-nuclear DNA breakage and ultimately cell death. Toledo et al. referred to the lethal endpoint of replication stress as ‘replication catastrophe’. Replication catastrophe can be triggered by RPA exhaustion due to unrestrained origin firing and excessive ssDNA formation under conditions of replication stress and checkpoint failure or ATR inhibition (Toledo et al., 2013). The study reported that different sources of replication stress led to RPA depletion which inevitably resulted in fork breakage, and proposed that RPA levels are normally kept in excess to protect exposed ssDNA strands that arise from replication stress, and prevent irreversible collapse (Toledo et al., 2017).

### 1.2.5 Exploiting DNA replication stress in cancer therapy

Most cancers display persistent replication stress which is associated with genome instability and tumorigenic genetic alterations. Defective cell cycle checkpoints and DNA repair mechanisms are prevalent in cancers, therefore genome instability or mutations may not be efficiently prevented from propagating across cell divisions (Gaillard et al., 2015).

Therapeutic strategies that leverage the elevated replication stress levels in cancer either act to enhance these levels in cancer cells and induce cell death using DNA damaging chemotherapeutics or target specific vulnerabilities in cancer cells (Ubhi et al., 2019). One example of the latter is the synthetic lethal strategy used in the clinic for the treatment of BRCA1/BRCA2-mutant breast and ovarian cancers, which are hypersensitive to poly(ADP-ribose) polymerase (PARP) inhibitors (Lord and Ashworth, 2017). BRCA1 and BRCA2 have pivotal roles in HR repair of DSBs (Scully et al., 2019). Defective BRCA1 and BRCA2 in breast and ovarian cancers therefore cause HR deficiency. As described in Section 1.2.4, HR-defective cells may utilise lower-fidelity pathways such as alternative NHEJ to repair DSBs, and this can lead to mutagenesis or chromosomal translocations during the fusion of broken and incompatible DNA ends.

PARP enzymes (predominantly PARP1) participates in multiple DNA repair pathways including single-strand break (SSB) repair, and functions by PARylating itself and target proteins to regulate or mediate recruitment of DNA repair factors (Chaudhuri and Nussenzweig, 2017). During DNA replication, PARP detects unligated Okazaki fragments and is activated, resulting in recruitment of the SSB repair protein XRCC1 to promote repair (Hanzlikova et al., 2018). One model of PARP inhibitor toxicity was based on the report that in addition to their catalytic inhibition of PARP which can disrupt its DNA repair function, PARP inhibitors trap PARP onto DNA, forming cytotoxic lesions (Murai et al., 2012). It was later shown that PARP inhibitor treatment significantly accelerates replication fork elongation without stalling forks and induces replication stress (Maya-Mendoza et al., 2018). Recently, it was proposed that PARP

inhibitor synthetic lethality could be caused by the aberrant accumulation of exposed lagging strand ssDNA gaps resulting from defective Okazaki fragment processing in BRCA1-deficient cells treated with PARP inhibitors, which may exhaust RPA pools (Cong et al., 2021).

Other approved chemotherapeutics that target DNA replication in cancer include alkylating agents (e.g., cyclophosphamide, temozolamide) and platinum compounds (e.g., carboplatin, cisplatin) that form intra- and interstrand crosslinks between nucleotide bases, inhibitors of topoisomerase I (e.g., irinotecan and topotecan) and II (e.g., etoposide), and nucleoside analogues that inhibit DNA replication (e.g., gemcitabine). Some chemotherapeutics have shown potential for enhancing the sensitisation of tumours to radiation therapy by disrupting DNA repair pathways of cancer cells, such as inhibitors of DNA-PK, ATR, ATM, CHK1/2 and WEE1 (Biau et al., 2019). Therapeutic strategies that target the DNA damage response are currently limited by challenges such as drug resistance, therefore significant efforts are focused on identifying important novel players in DNA repair and improving our understanding of genome stability mechanisms.

## 1.3 Ubiquitylation

### 1.3.1 Ubiquitin

Ubiquitylation is a prevalent post-translational modification that regulates a vast range of proteins and cellular processes in a dynamic manner (Rape, 2017). The highly conserved 76-amino acid protein, ubiquitin, is central to the ubiquitylation machinery and is encoded by four genes (UBA52, RPS27A, UBB and UBC) either as a single ubiquitin fused to ribosomal proteins, or as polyubiquitin (Özkaynak et al., 1984; Finley et al., 1989). These ubiquitin precursors are processed into their mature form by deubiquitylases (DUBs) (Amerik et al., 2004).

Ubiquitin contains a β-grasp fold architecture and a flexible C-terminal tail (**Fig. 1.5A**; Vijay-Kumar et al., 1987). A hydrophobic surface which is referred to as the Ile44 patch, includes Leu8, Ile44, His68 and Val70, and serves as a binding interface for many ubiquitin-binding domains (UBDs) and the proteasome (**Fig. 1.5B**; Sloper-Mould et al., 2001; Dikic et al., 2009). As illustrated in **Fig. 1.5B**, other important interaction platforms include the Ile36 patch (comprising Ile36, Leu71 and Leu73), Phe4 patch (Gln2, Phe4 and Thr14), TEK box (Lys6, Lys11, Thr12, Thr14 and Glu34) and the Asp58 patch (Arg54, Thr55, Ser57 and Asp58) (Komander and Rape, 2012; Ronau et al., 2016). Some of these interaction surfaces display low sequence conservation with structurally similar ubiquitin-like (Ubl) modifiers, and have been suggested to contribute to the ability of DUBs to distinguish between ubiquitin and Ubl modifiers (Ye et al., 2011; Ronau et al., 2016).

Ubiquitin is conjugated to another protein through the formation of a covalent isopeptide bond between its C-terminal glycine and a residue on its substrate such as lysine, which is the most frequently reported acceptor residue. Ubiquitin can be conjugated to another ubiquitin protein on K6, K11, K27, K29, K33, K48 or K63, or on the N-terminal methionine which can generate M1-linked linear chains (**Fig. 1.5A**; Swatek and Komander, 2016). Ubiquitylation has also been shown to occur on serine,

threonine, and cysteine residues (McClellan et al., 2019). Ubiquitin can itself undergo modification by other post-translational modifications such as acetylation and phosphorylation, which regulates and diversifies ubiquitin signalling (Herhaus et al., 2015).

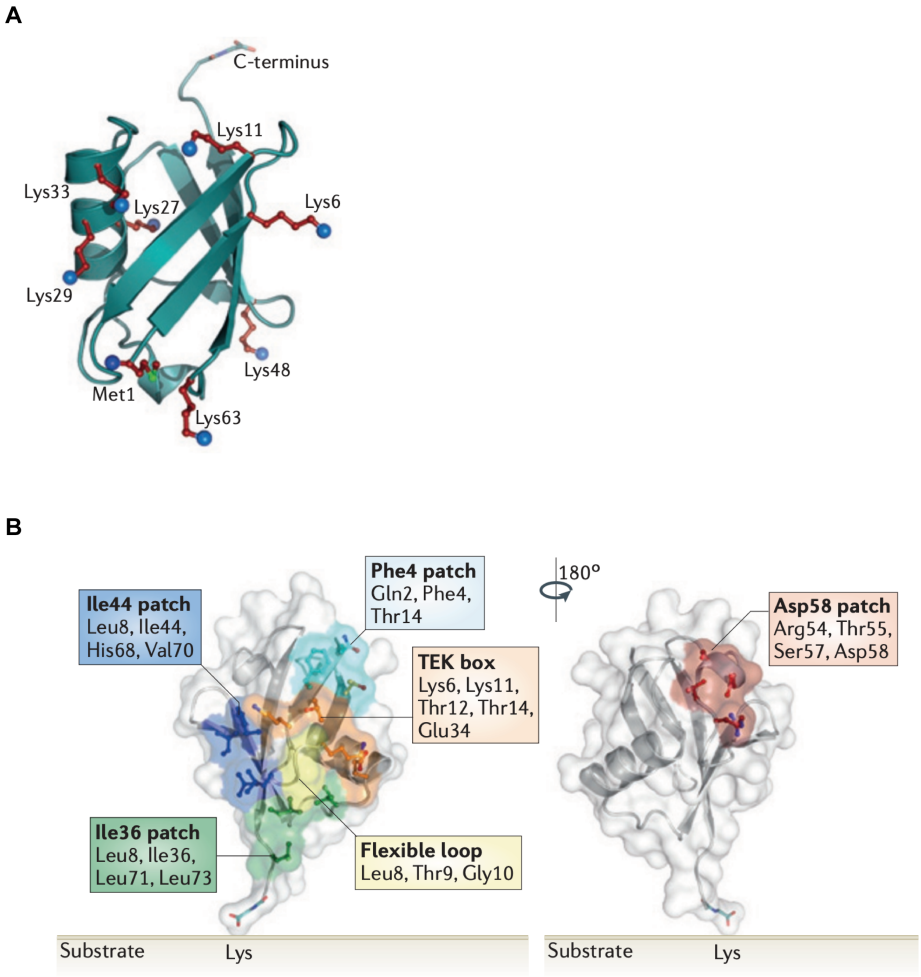



**Figure 1.5: Ubiquitin structure and interaction surface patches.** A) The seven Lys residues and N-terminal Met1 of human ubiquitin (PDB: 1UBQ) are shown as sticks. Amino groups that are modified during ubiquitin conjugation are denoted by blue spheres. The ubiquitin C-terminus is also shown. B) The structure and surface of ubiquitin showing the residues that form protein-protein interaction surface patches. As described in the main text, these include the Ile44 patch, Ile36 patch, Phe4 patch, Asp58 patch and the TEK box. Figure was obtained from Kulathu and Komander, 2012.

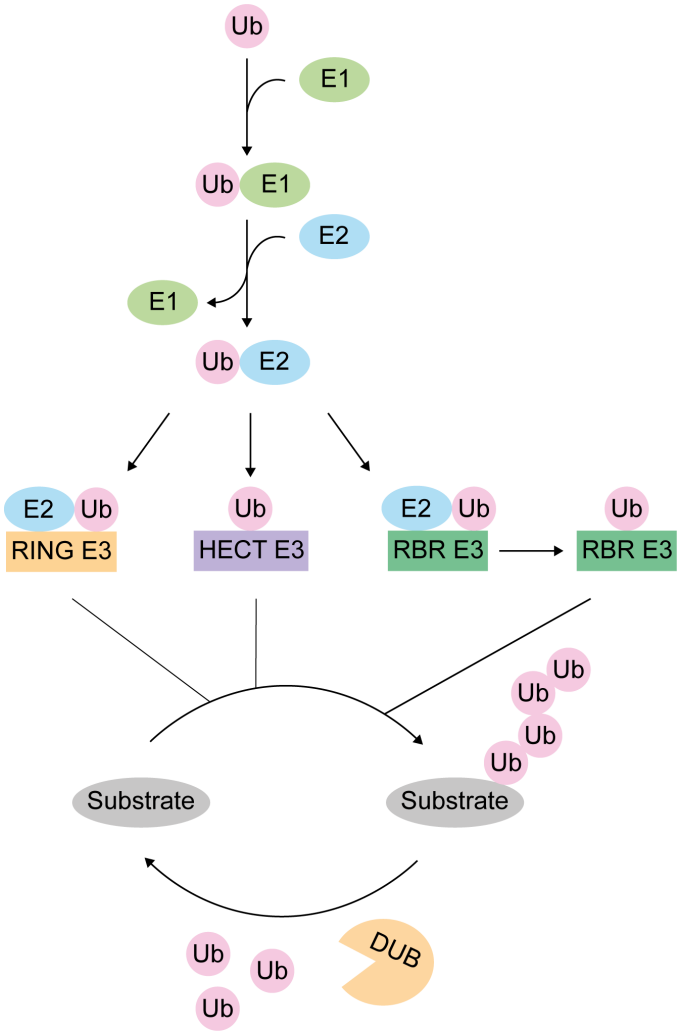



**Figure 1.6: Summary of the ubiquitylation cascade.** As described in the main text, ubiquitylation begins with the attachment of ubiquitin to an E1 enzyme, followed by the transfer of ubiquitin to an E2 enzyme. Ubiquitin can be transferred directly from the E2 to the acceptor residue of a substrate which is mediated by a RING E3 ligase, or first transferred from the E2 to a HECT E3 ligase with which ubiquitin forms a thioester intermediate before it is transferred to the substrate. Alternatively, an RBR E3 ligase may associate with the E2-ubiquitin complex before ubiquitin is transferred to the E3 Rcat domain, and subsequently to the substrate. Deubiquitylases (DUBs) remove ubiquitin modifications from substrates. Figure modified from Damgaard et al., 2021.

### 1.3.2 Ubiquitylation cascade

Ubiquitylation involves the coordinated and sequential actions of E1, E2 and E3 enzymes (**Fig. 1.6**). The C-terminus of ubiquitin is first adenylated by a ubiquitin-activating enzyme (E1), and a thioester bond is formed between ubiquitin and the catalytic cysteine of the E1 enzyme. Ubiquitin is then transferred onto the catalytic cysteine of a ubiquitin-conjugating enzyme (E2). After the E1-E2 thioester transfer, an E3 ubiquitin ligase mediates the transfer of ubiquitin from the E2 to the acceptor residue of a substrate protein. In the case of an acceptor lysine residue, this step leads to the formation of an isopeptide bond between the C-terminal glycine of ubiquitin and the ε-amino group of the substrate lysine (Passmore et al., 2004).

The mechanism of catalysis by E3 ligases in the final step of the cascade depends on the class of the E3 involved. RING E3 ligases, which constitute the largest class of E3 ligases, act as a scaffold by binding to the E2-ubiquitin complex via its RING domain and mediating the direct transfer of ubiquitin from the E2 to the substrate (Zheng et al., 2017). For reactions involving HECT E3 ligases, ubiquitin is first transferred from the E2 enzyme to the catalytic cysteine of the E3 with which ubiquitin forms a thioester intermediate, before it is transferred to the substrate (Metzger et al., 2012). The more recently characterised RING-between-RING (RBR) E3 ligases utilise similar mechanisms to both RING and HECT E3s, where it associates with the E2-ubiquitin complex via its RING1 domain, then transfers ubiquitin onto the catalytic cysteine of the Rcat domain of the RBR E3 ligase by transthiolation, before ubiquitin is transferred to the substrate (Spratt et al., 2014). Ubiquitin modifications and their resulting protein fates can be reversed by DUBs as described in Section 1.4 (Komander and Rape, 2012).

### 1.3.3 Ubiquitin modifications

Ubiquitin modifications regulate the fate of target proteins such as their activity, stability, localisation, or protein-protein interactions, and lead to distinct cellular signals depending on the type and topology of the modification as illustrated in **Fig. 1.7**. These outcomes are achieved by effector proteins that recognise ubiquitin modifications via one or more ubiquitin-binding domains (UBDs). Monoubiquitylation refers to the conjugation of a single ubiquitin onto the target protein. This modification can also occur on multiple residues of the substrate, and is termed multi-monoubiquitylation (Yau and Rape, 2016). Monoubiquitylation has been frequently reported to mediate protein-protein interactions. For example, monoubiquitylation of PCNA on K164 in response to replication stress promotes its interaction with TLS polymerases, whereas monoubiquitylation of the transcription factor SMAD4 inhibits its binding to phospho-SMAD2 (Hoege et al., 2002; Bienko et al., 2005; Dupont et al., 2009).

Ubiquitin proteins can be conjugated to each other to form polyubiquitin chains on target proteins. Polyubiquitin chains exist in distinct topologies depending on the linkage type and present unique interaction surfaces (Scott et al., 2015). The length, linkage type and conformation of the chains therefore allow recognition by distinct effector proteins that lead to diverse signalling outcomes (Yau and Rape, 2016). Some linkage types are assembled by linkage-specific enzymes, for example the E2 enzyme Ube2S is specific for generating K11-linked chains and has been shown to cooperate with the E3 APC/C to form these chains (Yau and Rape, 2016).

Among the best characterised homotypic polyubiquitin chains (i.e, containing a single linkage type) are K48-linked chains, the predominant linkage type in cells (Swatek and Komander, 2016). K48-linked chains serve as the primary signal that direct ubiquitylated substrates to the 26S proteasome where they are degraded. Both open and closed conformations of unbound K48-linked chains have been reported, however K48-linked diubiquitin chains in complex with their ligands have been shown to primarily adopt open conformations (Varadan et al., 2002; Varadan et al., 2005;

Zhang et al., 2009; Békés et al., 2016; Rahighi et al., 2016). Recently, monoubiquitylation was also suggested to provide a signal for the proteasomal degradation of substrates (Braten et al., 2016).

Another extensively studied homotypic polyubiquitin chain type is K63-linked chains that mediate signal transduction, DNA repair, innate immune responses and protein sorting during endocytosis, amongst others (Yau and Rape, 2016; Rape, 2017). K63-linked chains exist in both open and closed conformations in the absence of a ligand and in complex with target proteins (Komander et al., 2009; Sato et al., 2009; Sekiyama et al., 2012; Liu et al., 2015). The binding of ESCRT0, STAM and Hrs to K63-linked chains were suggested to inhibit their association with the proteasome (Nathan et al., 2013).

M1-linked (linear) chains are well-established to regulate NF-κB signaling and immune signalling (Yau and Rape, 2016). K11-linked polyubiquitin chains have been suggested as an alternative trigger of proteasomal degradation, which may rely on their cooperation with other linkage types in a branched chain configuration (Grice et al., 2015). K29-linked chains have been implicated in neurodegenerative disorders and Wnt/β-catenin signaling (Tracz et al., 2021). The roles of other homotypic chain types are not as clear, and some have been observed in combination with other linkage types in mixed or branched chains (Swatek and Komander, 2016).

Mixed or branched chains expand the diversity of ubiquitylation signals by forming different combinations of ubiquitin chain linkages and topologies (Yau and Rape, 2016). In mixed chains, each ubiquitin monomer is modified by a single ubiquitin at varying residues, whereas branched chains are generated when a ubiquitin monomer is modified with two or more ubiquitin proteins at different residues. Branched chains with associated cellular roles include K11/K48, K29/K48 and K48/K63 linkages (Meyer et al., 2014; Ohtake et al., 2016; Yau et al., 2017; Ohtake et al., 2018; Oh et al., 2020). Branched chains can be synthesised by pairs of E3 enzymes with distinct linkage specificities, and their sequential action is thought to allow the spatiotemporal regulation of the different ubiquitylation signals (French et al., 2021). For example, the

pro-apoptotic regulator TXNIP is first modified with K63-linked chains by the E3 ITCH before being modified with K48-linked chains by UBR5, resulting in branched K48/K63 chains and the proteasomal degradation of TXNIP (Ohtake et al., 2018). Branched chains can also be formed by a single E3 that assembles different linkages on its own, or in collaboration with multiple E2s with different linkage specificities (French et al., 2021).

Further contributing to the diversity of ubiquitin signals, ubiquitin is itself subject to post-translational modifications such as acetylation and phosphorylation (Herhaus et al., 2015). In addition, ubiquitin chains may include distinct ubiquitin-like modifiers such as SUMO. SUMO-targeted ubiquitin ligases (STUBLs) can assemble ubiquitin chains on proteins that were previously modified with SUMO (Prudden et al., 2007).

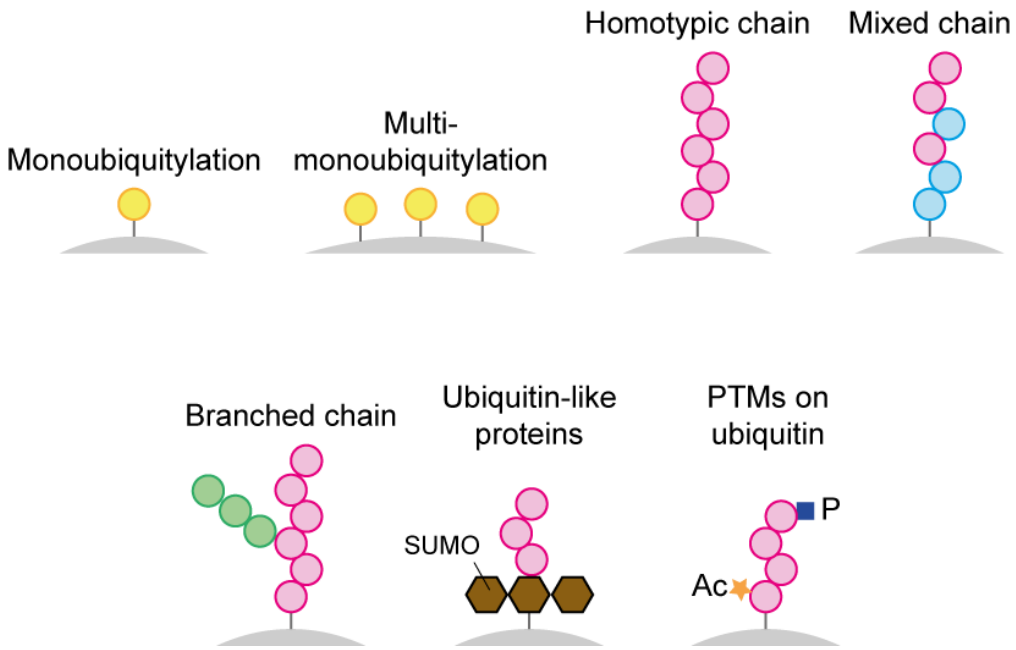



**Figure 1.7: Examples of ubiquitin modifications.** The modification of protein substrates by ubiquitin monomers on a single or on multiple acceptor sites are referred to as monoubiquitylation and multi-monoubiquitylation, respectively. Homotypic chains involve ubiquitin proteins linked through the same acceptor residue, e.g K63-linked chains. Mixed chains are generated by ubiquitin subunits that are modified on a single acceptor residue, and this residue varies between the subunits as indicated by the different colours. Branched chains form when at least

one ubiquitin subunit contains modifications on multiple acceptor residues. Ubiquitin chains may contain Ub-like modifiers such as SUMO. Ubiquitin can also be modified by other PTMs as indicated. Figure modified from French et al., 2021 and Damgaard et al., 2021.

| Domains | UBD abbreviations | Name | Examples of proteins | References |
|---|---|---|---|---|
| Helical | UIM | Ubiquitin-interacting motif | Ataxin-3, RAP80 | Burnett et al., 2003; Sato et al., 2009 |
| | MIU | Motif interacting with ubiquitin | MINDY-1, Rabex-5 | Abdul Rehman et al., 2016; Penengo et al., 2006 |
| | UMI | UIM- and MIU-related UBD | RNF168 | Pinato et al., 2011 |
| | DUIM | Double-sided UIM | HRS | Hirano et al., 2006 |
| | UBA | Ubiquitin-associated domain | Cezanne-1/2, UBC1 | Wu et al., 2019; Girard et al., 2015 |
| | CUE | Coupling of ubiquitin to ER degradation domain | Cue2, Vps9 | Kang et al., 2003; Prag et al., 2003 |
| | GAT | GGA and TOM1 domain | TOM1, GGA3 | Akutsu et al., 2005; Kawasaki et al., 2005 |
| | UBAN | Ubiquitin-binding domain in ABINs and NEMO | ABIN1/2/3, NEMO | Wagner et al., 2008; Yoshikawa et al., 2009 |
| | VHS | VPS27, HRS and STA domain | STAM, GGA3 | Hong et al., 2009; Puertollano et al., 2004 |
| | UBM | Ubiquitin-binding motif | Polymerase iota (Pol ι), REV1 | Bomar et al., 2010 |
| | MyUb | Myosin VI UBD | Myosin VI | He et al., 2016 |
| | AnkUBD | Ankyrin (Ank) repeat UBD | TRABID | Licchesi et al., 2011 |
| Zinc finger (ZnF) | UBZ | Ubiquitin-binding ZnF domain | Polymerase eta (Pol η), ZUP1 | Bienko et al., 2005; Kwasna et al., 2018 |
| | NZF | NPL4 ZnF domain | TRABID, NPL4 | Kristariyanto et al., 2015; Wang et al., 2003 |
| | ZnF A20 | ZnF of A20 domain | A20, Rabex-5 | Wertz et al., 2004; Mattera et al., 2006 |
| | ZnF UBP | ZnF of ubiquitin-specific processing protease domain | USP5, HDAC6 | Reyes-Turcu et al., 2006; Boyault et al., 2006 |
| Ubiquitin-conjugating-like | UBC | Ubiquitin-conjugating domain | UbcH5c | Brzovic et al., 2006 |
| | UEV | Ubiquitin E2 variant domain | TSG101, Mms2 | Sundquist et al., 2004; Tsui et al., 2005 |
| Pleckstrin-homology (PH) | GLUE | GRAM-like ubiquitin-binding in EAP45 domain | EAP45 | Alam et al., 2006 |
| | PRU | Pleckstrin-like receptor for ubiquitin | Rpn13 | Husnjak et al., 2008 |
| Others | Jab1/MPN domain | Jab1/MPN domain | Prp8p | Bellare et al., 2006 |
| | PFU | PLAA family UBD | PLAA | Fu et al., 2009 |
| | SH3 | Src homology | Sla1 | He et al., 2007 |
| | WD40 repeat β-propeller | WD40 repeat β-propeller | PLAA | Pashkova et al., 2010 |
| | DC-UbP_N | DC-UbP_N | DC-UbP/UBTD2 | Song et al., 2010 |
| | MDA-9 UBD | MDA-9 UBD | MDA-9 | Okumura et al., 2011 |

**Table 1.1: Examples of known ubiquitin-binding domains.** Table modified from Kliza et al., 2020.

### 1.3.4 Ubiquitin-binding domains

Ubiquitin modifications are recognised by ubiquitin-binding domains (UBDs) within effector proteins, and these domains form non-covalent interactions with the ubiquitin signals (Husnjak et al., 2012). At least 25 different types of UBDs have been identified in humans which vary in structure, size, and mode of ubiquitin recognition, some of which are summarised in **Table 1.1** (Zhou et al., 2018; Radley et al., 2019; Kliza et al., 2020). The UBDs described below are those composed of α-helices or zinc fingers.

UBDs with α-helical structures interact with the Ile44 hydrophobic patch of ubiquitin (Hurley et al., 2006). The ubiquitin-interacting motif (UIM) and motif interacting with ubiquitin or inverted UIM (MIU) are single helix domains that interact with ubiquitin. The UIM and MIU are the smallest UBDs characterised by a consensus sequence with approximately 20 residues and have been shown to bind monoubiquitin with relatively weak affinities (Hurley et al., 2006; Penengo et al., 2006; Lee et al., 2006). UIM and MIU motifs are often arranged in tandem to enable proteins to interact with polyubiquitin chains that may be of specific linkage types. For example, the DUB MINDY-1 contains a tandem MIU repeat that is highly specific for binding K48-linked polyubiquitin chains (Kristariyanto et al., 2017). The study demonstrated that multiple binding sites on the second MIU (MIU2) were involved in binding all three ubiquitin moieties in a K48-linked polyubiquitin chain, while the first MIU (MIU1) enhances these interactions. The distance between two binding sites within MIU2 was also shown to be important for polyubiquitin binding. Other helical UBDs include the ubiquitin binding in ABIN and NEMO (UBAN) motif that adopts a parallel coiled-coil dimer structure presenting two binding sites for M1-linked di-ubiquitin chains and has also been observed to bind chains of the K63 linkage (Yoshikawa et al., 2009; Herhaus et al., 2019).

Zinc finger UBDs constitute a large proportion of UBDs and exhibit unique ubiquitin binding modes and affinities (Hurley et al., 2006). Zinc finger structures are maintained by the coordination between $Zn^{2+}$ and well-conserved Cys and His residues

(Cassandri et al., 2017; Kluska et al., 2018). Ubiquitin-binding ZnF (UBZ) domains which comprise ~30 residues are present in Y-family TLS polymerases such as Pol η and mediate their interaction with monoubiquitylated PCNA to initiate translesion synthesis (Bienko et al., 2005). UBZ domains fold into the classical C2H2 zinc-finger structure composed of the typical ββα fold, and the exposed region of its C-terminal α-helix interacts with the hydrophobic patch of ubiquitin (Bomar et al., 2007). Other zinc finger UBDs include the ZnF UBP which comprises ~130 residues and is found in many DUBs (Hurley et al., 2006). The ZnF UBP domain contains a deep cavity into which the C-terminal diglycine of ubiquitin is inserted to form extensive interactions with the domain (Reyes-Turcu et al., 2006).

## 1.4 Deubiquitylases (DUBs)

### 1.4.1 DUB classes

To date, around 100 DUBs have been identified in humans, which can be divided into two groups based on their catalytic mechanisms and further subclassified into 7 structurally distinct families (Basar et al., 2020; **Fig. 1.8**). The zinc-dependent metalloprotease DUBs are the JAB1/MPN/MOV34 (JAMM) family DUBs (at least 12 human members) while cysteine protease DUBs comprise six families: ubiquitin-specific proteases (USPs, 56 members), ovarian tumor proteases (OTUs, 17 members), ubiquitin carboxy-terminal hydrolases (UCHs, 4 members), the motif interacting with ubiquitin-containing novel DUB family (MINDYs, 5 members), the Josephin family (4 members) and the most recently discovered zinc finger containing ubiquitin peptidase 1 family (ZUP1, 1 member).

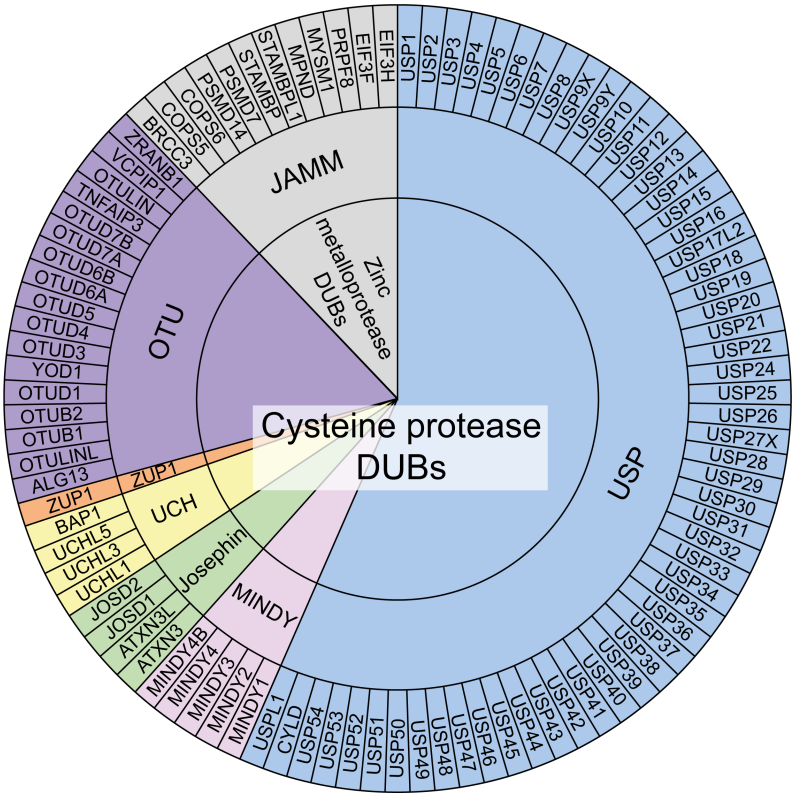



**Figure 1.8: Classes of human deubiquitylases and known members.** Figure modified from Elu et al., 2022.

### 1.4.2 Substrate recognition and linkage specificity

DUBs contain at least one ubiquitin-binding site, the S1 site, that orients the ubiquitin C-terminus and scissile bond across the active site for hydrolysis. For DUBs that cleave ubiquitin polymers, the S1 site binds the distal ubiquitin within the chain, which has its C-terminus positioned across the catalytic center and contains the carboxylate of the hydrolysed isopeptide bond. The S1' site is occupied by the proximal ubiquitin which is conjugated to the C-terminus of the distal ubiquitin, and contains the amine of the hydrolysed peptide bond (Mevissen and Komander, 2017). Some DUBs have additional ubiquitin-binding sites that bind long ubiquitin chains and may contribute to their linkage preference (Reyes-Turcu et al., 2009; Mevissen and Komander, 2017).

Cysteine protease DUBs typically contain a catalytic triad that includes the catalytic cysteine involved in nucleophilic attack, an adjacent basic histidine, and often an acidic residue. As illustrated in **Fig. 1.9**, once the catalytic cysteine is deprotonated, the cysteine attacks the isopeptide bond to generate a tetrahedral intermediate which is stabilised by an oxyanion hole. The proximal ubiquitin is released, an acyl intermediate is formed, and a water molecule mediates deacylation which generates a second tetrahedral intermediate. This intermediate destabilises and releases the distal ubiquitin (Mevissen and Komander, 2017). A few exceptions of cysteine protease DUBs are known to utilise non-canonical catalytic mechanisms (Lange et al., 2022). In contrast to cysteine protease DUBs, metalloproteases DUBs harbour a zinc ion in its active site that is coordinated by catalytic residues and a water molecule. The activated water molecule carries out a nucleophilic attack that results in a tetrahedral intermediate and the cleavage of the isopeptide bond, which releases ubiquitin (**Fig. 1.9**; Mevissen and Komander, 2017).

DUBs either bind to the modified protein and cleaves ubiquitin from it or interact with the ubiquitin modification itself (Mevissen and Komander, 2017). This is mediated by interaction domains within DUBs that recognise the protein that they deubiquitylate, and/or UBDs that bind ubiquitin. An example of a DUB that displays specific binding

to the ubiquitylated substrate is USP22 (Ubp8 in yeast) that make contacts with both histone H2B and the conjugated monoubiquitin (Morgan et al., 2016). Some DUBs target ubiquitin chains of specific linkage types, such as MINDY DUBs which are specific for cleaving K48-linked chains, and most JAMM metalloproteases which are K63-specific. Other DUBs such as the USP family show little or no linkage preference, with a few exceptions including CYLD which preferentially cleaves K63- and M1-linked chains, and USP30 that exhibits specificity for K6-linked chains (Mevissen and Komander, 2017).

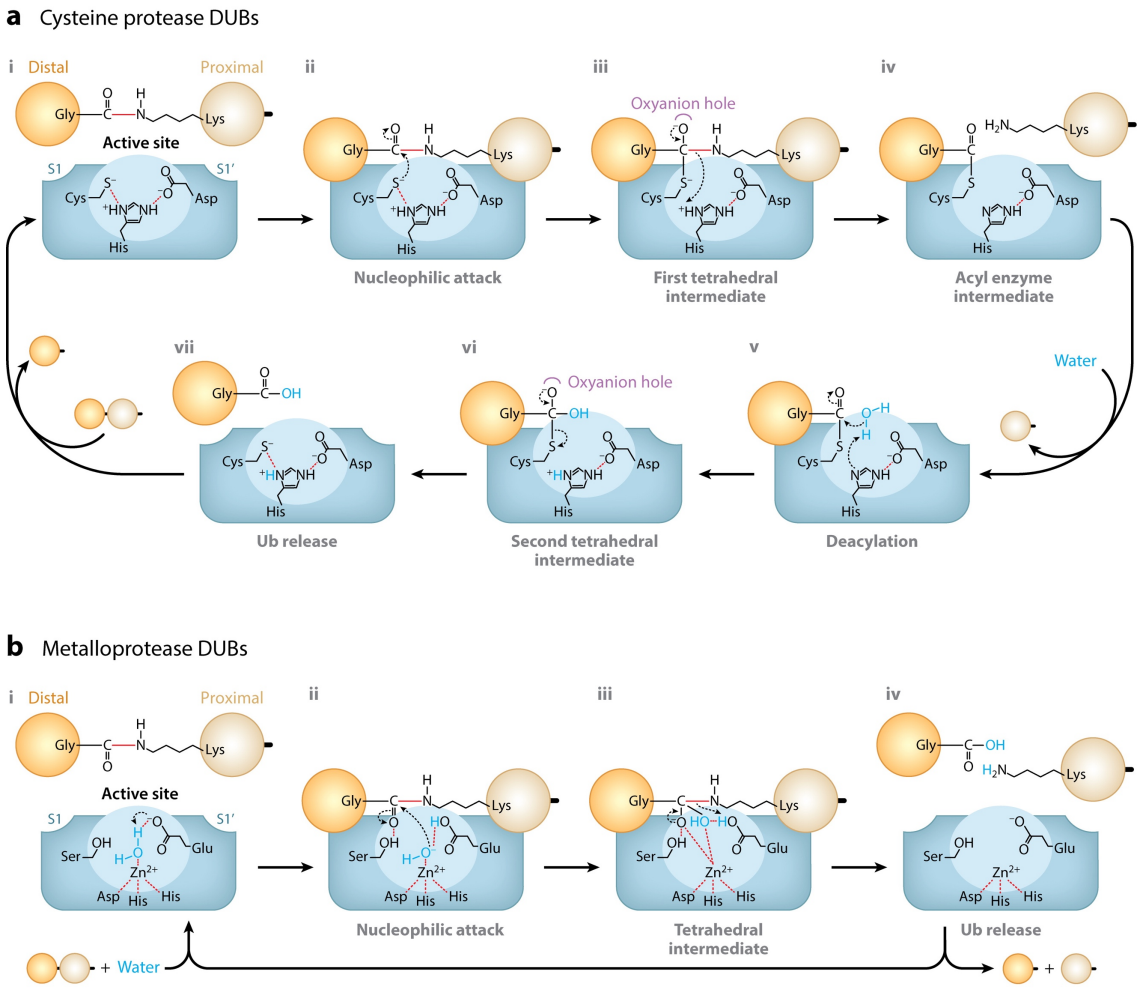



**Figure 1.9: Mechanisms of di-ubiquitin cleavage by deubiquitylases.** The catalytic mechanisms of cysteine protease DUBs and metalloprotease DUBs are summarised in the main text. Figure obtained from Mevissen and Komander et al., 2017.

Some DUBs possess endo-cleavage activity where they preferentially cleave ubiquitin chains from the middle (Mevissen and Komander, 2017). The released unanchored chain would undergo further processing to regenerate single ubiquitin moieties. Other DUBs show exo-cleavage activity where they process chains from the distal end which directly generates monoubiquitin. Endo-cleavage activity is apparent in most OTU DUBs, while MINDY-1 is an example of a DUB that displays exo-cleavage activity when it cleaves long K48-linked polyubiquitin chains (Mevissen et al., 2013; Abdul Rehman et al., 2016). Some DUBs cleave monoubiquitin from specific protein targets (e.g., histone-directed DUBs), and others are known to remove ubiquitin chains from protein substrates en bloc (e.g., proteasomal DUBs) (Clague et al., 2019).

### 1.4.3 Regulation of DUBs

To regulate ubiquitin signals in a dynamic and accurate manner, DUBs are themselves tightly regulated to ensure their appropriate localisation, abundance, and catalytic activity (Sahtoe and Sixma, 2015). Many regulatory mechanisms are performed through post-translational modifications of DUBs. For example, the phosphorylation of USP10 by the ATM kinase promotes its nuclear translocation where it deubiquitylates p53 (Yuan et al., 2010). The monoubiquitylation of ATXN3 was shown to trigger a conformational change that leads to its activation (Todi et al., 2009; Todi et al., 2010).

Many DUBs have misaligned active sites that must be rearranged to enable substrates to bind the active site (Reyes-Turcu et al., 2009). In a process known as substrate-assisted catalysis, the binding of ubiquitin to DUBs including OTULIN and USP7 triggers the realignment of the catalytic residues to allow catalysis (Hu et al., 2002; Keusekotten et al., 2013). Some DUBs rely on accessory domains or binding partners for the allosteric modulation of their activity. This mode of regulation is illustrated by the UCH-L5 DUB which binds the proteasome regulatory particle

component, RPN13. The RPN13 DEUBAD domain allosterically activates UCH-L5 upon binding and promotes substrate binding and DUB activity (Sahtoe et al., 2015).

DUBs may also be regulated by intramolecular interactions via internal domains. The N-terminal ZnF-UBP (nUBP) of USP5 significantly enhances its own catalytic activity in an allosteric manner (Avvakumov et al., 2012). This domain binds tightly to the catalytic core, and its removal was found to markedly decrease the catalytic activity of USP5. In USP7, the HUBL domain interacts with a ‘switching’ loop in the catalytic domain which enhances ubiquitin binding and catalysis (Faesen et al., 2011).

## 1.5 Zinc Finger Containing Ubiquitin Peptidase 1 (ZUP1)

### 1.5.1 Discovery of ZUP1 as a novel DUB class

In 2018, ZUP1 was discovered by four independent groups as the founding member of a novel DUB class with no homology to other known DUBs, and its catalytic domain has a unique architecture compared with other classes (Kwasna et al., 2018; Haahr et al., 2018; Hermanns et al., 2018; Hewings et al., 2018). Kwasna et al. utilised the active-site directed probe, propargylated ubiquitin (Ub-Prg or Ub-PA) to isolate cysteine protease DUBs from cell extracts and identified ZUP1 as one of the recovered DUBs (Kwasna et al., 2018). The alkyne moiety of Ub-Prg, propargylamine which is present at the C-terminus of ubiquitin, potently and selectively reacts with the catalytic cysteine residue of DUBs over other cysteine proteases and forms a vinyl thioether linkage (Ekkebus et al., 2013). The catalytic domain of ZUP1 was shown to be modified by Ub-Prg and not UFM1-Prg, a ubiquitin-like modifier (UBL), which motivated subsequent efforts to characterise the structure and DUB activity of ZUP1 (Section 1.5.2). Hewings et al. used Ub vinyl pentynyl sulfone (Ub-VPS) which contains a HA tag, ubiquitin, a cysteine-reactive electrophile, and a C-terminal alkyne that attaches to a cleavable biotin-azide (Hewings et al., 2018). This probe significantly enriched for ZUP1 from HEK 293T cell lysates, and ZUP1 was confirmed to react with ubiquitin activity-based probes *in vitro*, which was abolished by the mutation of the ZUP1 catalytic cysteine (C360A).

The investigation of ZUP1 as a DUB by Haahr et al. and Hermanns et al. was initiated by sequence analyses that revealed conserved UBDs within ZUP1 (Haahr et al., 2018; Hermanns et al., 2018). This was followed by assays to assess its DUB activity based on the reactivity of ZUP1 with Ub-vinyl sulfone, Ub-Rhodamine, Ub-PA and its ability to liberate the fluorophore AMC (7-amino-4-methylcoumarin) from a ubiquitin-AMC fusion. The ability of ZUP1 to react with the ubiquitin probes motivated further efforts to characterise ZUP1 as a DUB (Section 1.5.2). From sequence analyses, ZUP1 is distantly related to the UFM1-specific protease (UFSP) and autophagin (ATG4)

families of cysteine proteases (Hermanns et al., 2018). ZUP1 uses a different catalytic histidine to UFSP and ATG4, and its active site architecture is nearly a mirror image of the active sites of UFSP and ATG4. Hermanns et al. further showed that while ZUP1 is highly reactive toward Ub-PA, it was unable to react with propargylated UFM1 (UFM1-PA) or the propargylated Atg8 homolog (LC3B-PA), suggesting that ZUP1 is likely to be a DUB rather than a UFM1- or LC3-specific protease (Hermanns et al., 2018).

### 1.5.2 Structure and ubiquitin chain specificity of ZUP1

ZUP1 comprises 578 amino acids with four C2H2-type zinc fingers at its N-terminus, where the second and third zinc fingers are separated by a long disordered linker (**Fig. 1.10**). The zinc fingers are followed by a MIU motif, a ubiquitin-binding ZUP1 helical arm (ZHA), and a protruding α-2/3 helix-turn-helix region as revealed by the crystal structures (Kwasna et al., 2018; Hermanns et al., 2018). The catalytic domain spans residues 294 to 578 at the C-terminus.

Crystal structures of ZUP1 were obtained from the MIU onwards in complex with Ub-Prg (residues 232 to 578) (**Fig. 1.10**; Kwasna et al., Hermanns et al., 2018). Two prominent helical extensions are formed by the hairpin-like helix-turn-helix structure annotated as α-2/3, and the ZHA that are perpendicular to one another. The ZHA forms the distal (S1) binding site that interacts with the Ile44 patch of ubiquitin, and *in vitro* DUB assays revealed that the fourth zinc finger is primarily responsible for binding polyubiquitin and is a UBZ domain. The UBZ was proposed by Kwasna et al. to provide the proximal ubiquitin binding site. An alternative model is that the UBZ may bind to the S3 ubiquitin which is supported by the AlphaFold prediction of ZUP1 structure (Jumper et al., 2021). The catalytic core forms a globular compact structure, and the catalytic triad is composed of C360, H491 and D512. Hydrophobic and ionic interactions primarily exist between ubiquitin and the ZHA, whereas the binding between ubiquitin and the catalytic core mainly involves ionic interactions (Kwasna et al., 2018).

From *in vitro* DUB assays utilising recombinant proteins, the groups showed that ZUP1 is highly specific for cleaving long K63-linked polyubiquitin chains which was confirmed to be dependent on its catalytic activity. ZUP1 displays endo-cleavage activity (Kwasna et al., 2018; Hewings et al., 2018; Haahr et al., 2018; Hermanns et al., 2018). Kwasna et al. demonstrated that the addition of the UBZ domain to the catalytic domain of ZUP1, which does not cleave polyubiquitin in isolation, led to the activation of ZUP1 and the selective cleavage of K63-linked polyubiquitin, but no activity was shown towards other linkage types. The authors also reported the weak binding of ZUP1 to tetraubiquitin composed of M1, K48 and K6 linkages. Nuclear magnetic resonance (NMR) studies performed by Hewings et al. revealed the interaction of ZUP1 with K63-linked and K48-linked di-ubiquitin, despite lacking DUB activity towards K48-linked chains.

GFP-ZUP1 was expressed in and immunopurified from human HEK293 cells, and its interaction with recombinant ubiquitin $K63_{1-7}$ chains was found to be impaired by point mutations within the MIU or UBZ domains (Haahr et al., 2018). Mutations within the UBZ that disrupt ubiquitin binding were shown to impair the DUB activity of ZUP1 (Kwasna et al., 2018). Kwasna et al. further showed that alanine substitutions of residues within the ZHA impaired DUB activity, which highlights the importance of the ZHA and UBZ for binding and potentially positioning polyubiquitin chains for catalysis.

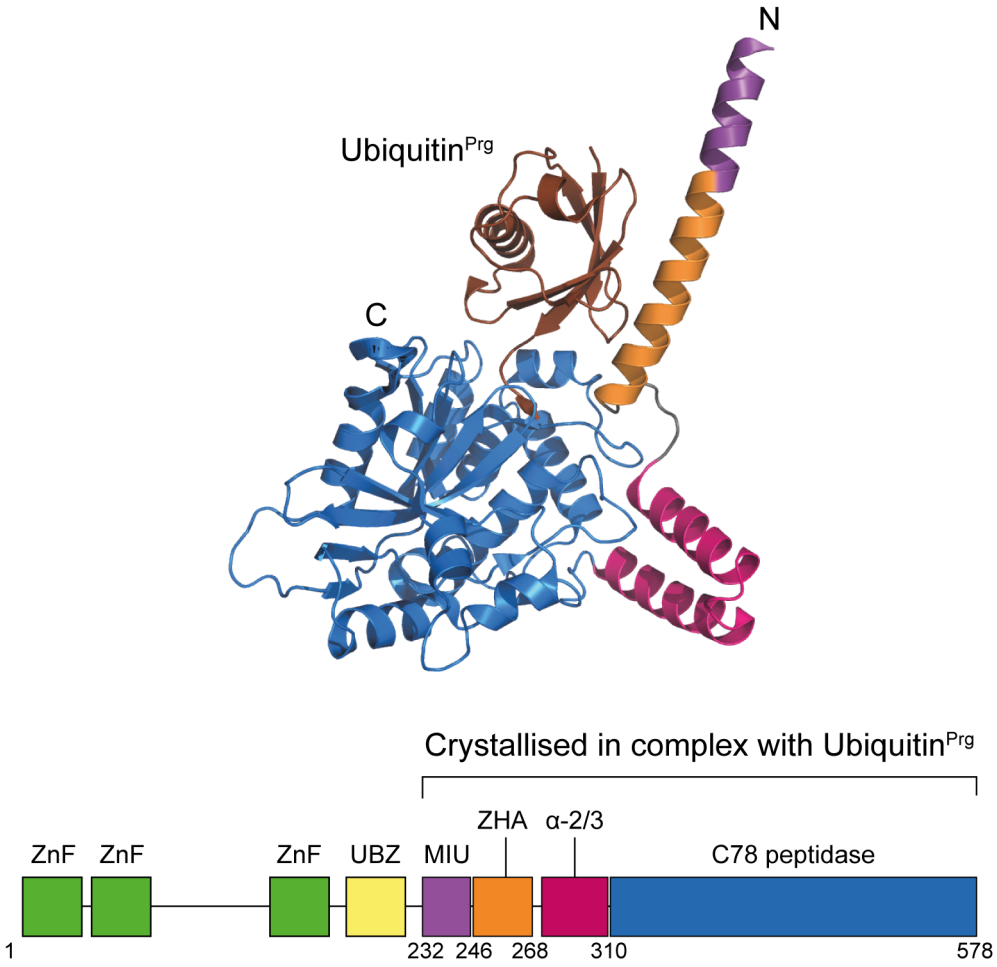



**Figure 1.10: Structure and domain architecture of ZUP1.** Top: Crystal structure of ZUP1 (residues 232–578) in complex with ubiquitin-Prg (PDB code: 6FGE). The colours of the structure correspond to the protein domains (bottom). Ubiquitin-Prg is coloured in brown. Figure was prepared in Pymol.

### 1.5.3 Evidence for the roles of ZUP1 in DNA repair

The identification of several DNA replication and repair factors in the ZUP1 interactome by proteomic studies provided a motivation for investigating the role of ZUP1 in DNA repair (Kwasna et al. 2018; Hewings et al., 2018; Hermanns et al., 2018). The studies identified the RPA complex as a highly enriched interacting partner of ZUP1. As described in the earlier sections, RPA has an important role in protecting exposed ssDNA from nucleolytic degradation and destabilisation or fork collapse (Dueva et al., 2020). Another important DNA replication and repair protein identified as a ZUP1 interacting partner is PCNA (Gibbs-Seymour lab, unpublished). The third ZUP1 interacting protein with well-established roles in DNA repair is USP11, which regulates critical factors involved in homologous recombination repair (Orthwein et al., 2015; Yu et al., 2016).

Kwasna et al. reported that the depletion of ZUP1 in U2OS cells by RNA interference (RNAi) led to the accumulation of DNA damage markers such as chromatin-bound 53BP1 and γH2AX in unstressed conditions, suggesting endogenous DNA damage in the absence of ZUP1. To assess if ZUP1 is important in maintaining genome stability in the presence of exogenous DNA damage, Haahr and colleagues treated ZUP1-depleted cells with DNA damaging agents and observed the accumulation of RPA32 foci (upon camptothecin treatment) and micronuclei (following camptothecin, aphidicolin or hydroxyurea treatment). YFP-tagged ZUP1 was also shown to be recruited to DNA damage sites in cell nuclei damaged by laser micro-irradiation (Kwasna et al., 2018). Mutational analyses by Haahr et al. revealed that the recruitment of GFP-ZUP1 to localised DNA lesions generated by laser micro-irradiation or the FokI nuclease, was dependent on the MIU, UBZ and the three N-terminal zinc fingers, although the deletion of the latter spanned a considerably large region.

ZUP1-depleted cells were also found to be hypersensitive to ionising radiation and a topoisomerase I inhibitor, camptothecin (Kwasna et al., 2018). As ZUP1 depletion led to elevated K63-linked polyubiquitin levels after the induction of fork stalling at the

Lac repressor (LacR)-bound *LacO* array, ZUP1 was proposed to regulate K63-linked ubiquitylation of proteins at damaged forks (Haahr et al., 2018).

Many aspects of ZUP1 function remain unclear, such as the mechanisms by which ZUP1 is recruited to sites of DNA damage, and the specific DNA repair pathway in which it functions. The *bona fide* cellular substrate(s) of ZUP1 are also yet to be identified, and although a previous report has shown that siRNA-mediated knockdown of ZUP1 leads to increased levels of endogenous RPA70 and RPA32 modified by K63-linked polyubiquitin chains following hydroxyurea treatment, this awaits validation in permanent gene disruption systems such as CRISPR-Cas9 knockouts (Hewings et al., 2018). Additionally, the binding partners of ZUP1 and the significance of these interactions in the context of genome stability are another crucial facet of ZUP1 function that needs to be clarified. It is also not known how the proteins or cellular processes regulated by the K63-selectivity and endo-DUB activity of ZUP1 lead to the preservation of genome stability during replication stress as proposed by the preliminary reports. ZUP1 has not been implicated in human disease, however further investigation of its DNA repair role could reveal novel mechanisms or druggable targets for cancer therapy that targets DNA replication (Section 1.2.5).

## 1.6 Ubiquitin signalling at stressed replication forks

### 1.6.1 PCNA ubiquitylation

As described in Section 1.2, DNA replication may still proceed in the presence of polymerase-blocking lesions due to the translesion synthesis pathway that facilitates replication across the lesion. The lesion may also trigger fork remodelling processes that lead to fork restart. Central to these DNA damage tolerance pathways is ubiquitylated PCNA which provides a binding and signalling platform to maintain genome stability following replication stress.

Replication stress triggers PCNA monoubiquitylation at K164, which is mediated by the E3 ligase RAD18 in conjunction with the E2 enzyme, RAD6 (Hoege et al., 2002). Monoubiquitylated PCNA recruits TLS polymerases that possess both PCNA-interacting motifs and UBDs, unlike replicative DNA polymerases that only contain PCNA-interacting motifs. These interaction sites allow TLS polymerases to bind with high affinity to monoubiquitylated PCNA (Slade et al., 2018). The requirement of PCNA monoubiquitylation for TLS activity has been debated, however PCNA monoubiquitylation has been shown to play a significant role in enhancing the efficiency of TLS (Hendel et al., 2011). In the absence of exogenous damage, the E3 ligase $CRL4^{Cdt2}$ was shown to promote PCNA monoubiquitylation which leads to TLS, possibly to prevent spontaneous replication stress (Terai et al., 2010).

Monoubiquitylated PCNA was shown in UV-irradiated cells to be negatively regulated by USP1 based on the finding that UV induces the autocleavage and inactivation of USP1, which correlates with the accumulation of monoubiquitylated PCNA (Huang et al., 2006). Hydroxyurea-induced monoubiquitylated PCNA was also shown to correspond to a decrease in USP1 (Lim et al., 2018). Niimi et al. reported that monoubiquitylated PCNA accumulates following UV, MMS or MMC treatment, but noted that only UV-stimulated monoubiquitylated PCNA was accompanied by a loss of USP1 (Niimi et al., 2008). It is currently unclear whether the autocleavage of USP1

to regulate PCNA monoubiquitylation occurs in response to DNA lesions apart from UV, or whether USP1 also targets polyubiquitylated PCNA.

PCNA can also be polyubiquitylated with K63-linked polyubiquitin chains at K164 (Slade et al., 2018). The mechanism and regulation of this modification are poorly understood. PCNA polyubiquitylation has been suggested to promote template switching based on studies in yeast (Section 1.2.2). The ZRANB3 translocase, which facilitates fork reversal and restart, is recruited to polyubiquitylated PCNA during replication stress via the presence of both PCNA-interacting motifs and UBDs (Ciccia et al., 2012). SHPRH and HLTF have been proposed as E3 ligases for PCNA polyubiquitylation (Unk et al., 2006; Motegi et al., 2006; Unk et al., 2008; Masuda et al., 2018). More recently, RFWD3 was suggested to have a role in promoting PCNA mono- and polyubiquitylation through RAD18 (Gallina et al., 2021).

### 1.6.2 RPA ubiquitylation

Replication stress results in the generation of extended ssDNA regions that are rapidly coated by the RPA complex (Maréchal and Zou, 2015). RPA-ssDNA serves as a recruitment platform for the ATR kinase that coordinates replication checkpoint (Section 1.2.1). All three RPA subunits were shown to be ubiquitylated following UV exposure, and robust ubiquitylation of RPA70 and RPA32 were also detected upon treatment with hydroxyurea, camptothecin or aphidicolin (Elia et al., 2015). The ubiquitin linkage type(s) formed on RPA are not clear and have been suggested to involve K63-linked chains (Maréchal et al., 2014; Elia et al., 2015).

The E3 ligases PRP19 and RFWD3 were proposed to promote RPA ubiquitylation, and the silencing of these genes, or mutations that impair their binding to RPA, resulted in a decrease in damage-induced RPA ubiquitylation (Maréchal et al., 2014; Elia et al., 2015; Inano et al., 2017; Dubois et al., 2017; de Moura et al., 2018). PRP19 was suggested to mediate the recruitment of ATRIP, the regulatory partner of ATR to sites of DNA damage, and the E3 ligase activity and RPA binding of PRP19 are

potentially important for ATR activation (Maréchal et al., 2014). The recruitment of PRP19 and ubiquitylation of RPA were suggested to depend on PIKK-mediated RPA32 phosphorylation. This dynamic ubiquitylation and phosphorylation machinery on RPA was proposed to promote homologous recombination although the mechanisms remain elusive (Maréchal et al., 2014; Dubois et al., 2017). It was also shown that RPA-mediated RFWD3 recruitment to stalled forks may be important for ICL repair (Feeney et al., 2017).

### 1.6.3 FANCI–FANCD2 ubiquitylation

A major pathway that repairs ICLs involves the Fanconi anemia (FA) pathway which is coupled to DNA replication (Semlow and Walter, 2021). In *Xenopus* egg extracts, it was shown that the initiation of ICL repair requires the convergence of two DNA replication forks on the ICL (Zhang et al., 2015). In the FA pathway, the multi-component FA core E3 ligase complex is activated to monoubiquitylate the FANCI–FANCD2 (Fanconi anemia group I protein–Fanconi anemia group D2 protein) (ID2) heterodimer, by functioning together with the E2 enzyme UBE2T (Lemonidis et al., 2022). This results in the formation of ID2 nuclear foci to which FA proteins localise and mediate DNA repair, including BRCA2 (FANCD1), BRIP1 (FANCJ), PALB2 (FANCN), RAD51C (FANCO), SLX4 (FANCP), XPF (FANCQ), RAD51 (FANCR), BRCA1 (FANCS), XRCC2 (FANCU), REV7 (FANCV), and RFWD3 (FANCW) (Renaudin et al., 2020). The nuclease incision complex composed of XPF and SLX4 is thought to mediate incisions on either side of the ICL to enable lesion unhooking and bypass (Douwel et al., 2014).

Recent cryo-EM studies have revealed that the monoubiquitylation of ID2 stabilises the complex on DNA (Alcón et al., 2020; Wang et al., 2020). However, the Ile44 patch of the conjugated ubiquitin becomes more inaccessible to protein-protein interactions in this conformation, which challenges the view that the ID2 complex recruits the incision complex through UBDs. Deubiquitylation of the ID2 complex is catalysed by USP1 which forms a complex with UAF1 (Nijman et al., 2005;

Oestergaard et al., 2007; Cohn et al., 2007). A recent study revealed an extensive interaction interface between UAF1 and FANCI that is critical for USP1-mediated deubiquitylation of monoubiquitylated ID2 (Rennie et al., 2021). Unlike PCNA, it was shown that FANCD2 monoubiquitylation is not modulated by USP1 autocleavage (Oestergaard et al., 2007).

Another ICL repair pathway that acts on a subset of ICLs (psoralen-ICLs and AP-ICLs) is the NEIL3 pathway which involves cleavage of the crosslink by the NEIL3 glycosylase (Semlow and Walter, 2021). Cisplatin-ICLs are not cleaved by NEIL3 and instead require the FA pathway. Following fork convergence on the ICL, ubiquitylation of CMG by TRAIP with short ubiquitin chains recruit NEIL3 to cleave the crosslink. If TRAIP further extends the ubiquitin chains on CMG, this triggers p97-dependent CMG unloading and enables the FA pathway (Wu et al., 2019).

**Fig 1.11** summarises the key factors involved in the ubiquitylation of RPA, PCNA, and FANCI-FANCD2 during replication stress.

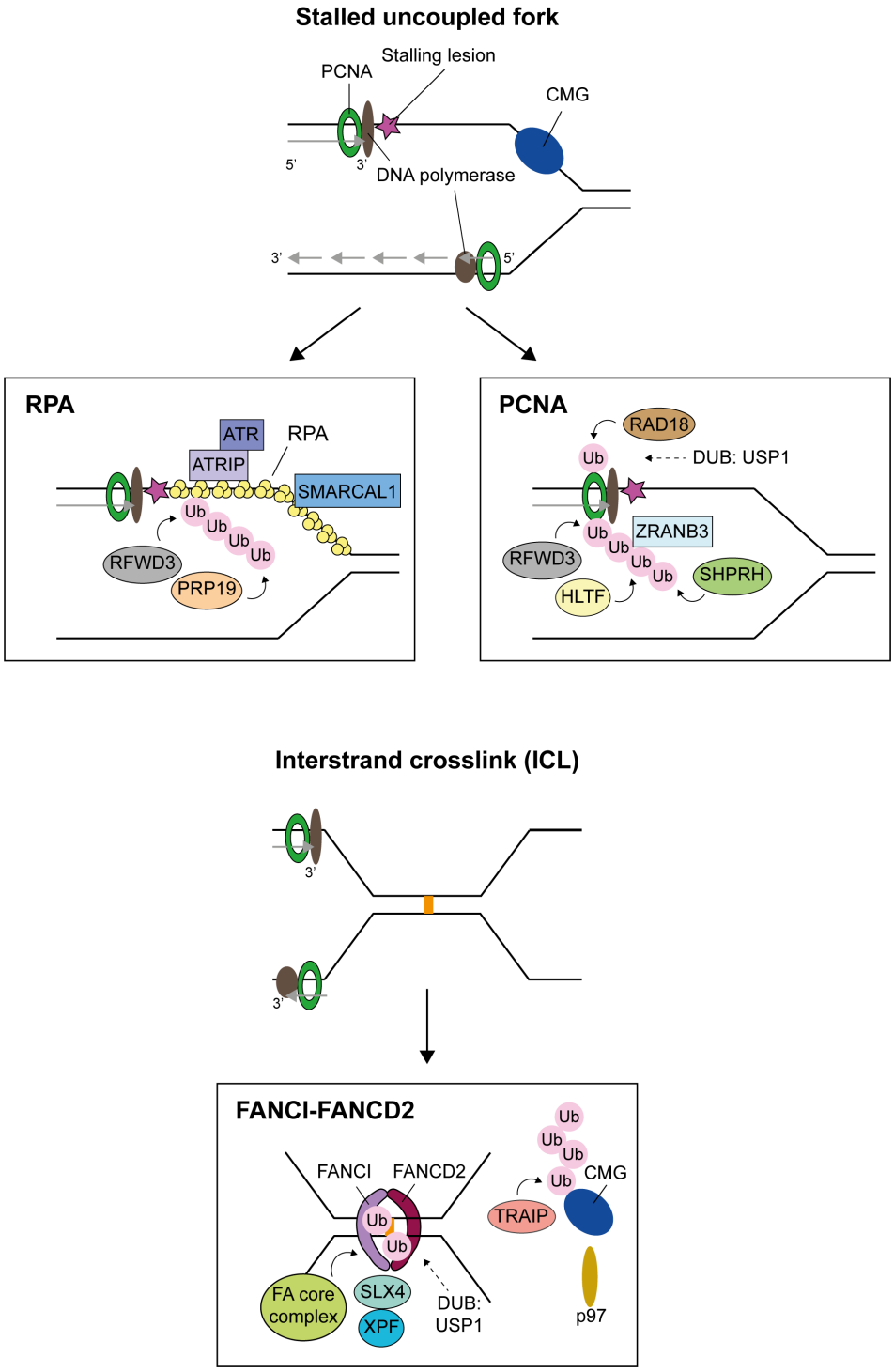



**Figure 1.11: Critical ubiquitylation platforms involved in the replication stress response.** Key factors involved in the ubiquitylation of RPA, PCNA, and FANCI-FANCD2 are shown, including the E3 ligases (activity indicated by the curved arrows), DUBs (activity indicated by the dotted arrows), and DNA repair factors that mediate the repair process as described in the main text. Figure modified from Mirsanaye et al., 2021.

## 1.7 Overall aims and motivation

As outlined so far, replication stress is a common characteristic of cancer. Numerous chemotherapeutics have been developed to target DNA replication in cancer, or specific vulnerabilities in the cancer cell response to replication stress (Section 1.2.5). Ubiquitin signalling is being investigated for pharmacological targeting in cancer therapy, where the proteasome and DUBs are examples of targets that have been assessed (D'Arcy et al., 2015). The proteasome inhibitor, bortezomib is an approved drug for the treatment of multiple myeloma and mantle cell lymphoma (Chen et al., 2011). Small-molecule inhibitors of USP7 are being developed as potential anti-cancer drugs given the key roles of USP7 in regulating p53 stability where it deubiquitinates and stabilises MDM2 (Qi et al., 2020).

ZUP1 is a novel DUB that has been suggested to play an important role in maintaining genome stability, however our understanding of various aspects of ZUP1 function remains in its infancy. This includes the specific DNA repair pathway in which ZUP1 functions, its cellular substrate(s), the significance of the interactions with its binding partners, and the mechanisms of its recruitment to sites of DNA damage. Defining ZUP1 function in DNA repair will lead to a more complete understanding of genome stability pathways, which could potentially inform current cancer therapies that target DNA replication and repair, or lead to future therapeutic strategies.

To this end, this work set out to address the following aims:

- To determine the specific DNA repair pathway(s) that ZUP1 functions within.
- To define the components of the cellular ZUP1 complex.
- To identify novel substrate(s) for ZUP1.

# 2

# Materials and Methods

## Contents


2.1 Materials……49
2.2 Cell culture……56
2.3 Plasmid transfection……60
2.4 siRNA transfection……61
2.5 CRISPR-Cas9 analysis methods……62
2.6 Molecular biology techniques……63
2.7 Clonogenic assay……67
2.8 Cell cycle synchronisation by double thymidine block……68
2.9 Flow cytometry……68
2.10 LMNA homology-directed repair assay……70
2.11 Microscopy……70
2.12 Protein extraction and sample preparation……71
2.13 Western blotting……74
2.14 Coomassie staining……75
2.15 Immunoprecipitation……75
2.16 Deubiquitylase assay……77
2.17 Affinity purification……78
2.18 Statistical analysis……80

## 2.1 Materials

### 2.1.1 Buffers and additives

The buffers used in this thesis are listed in **Table 2.1**. The indicated components were dissolved in MilliQ water.

**Table 2.1: Buffers used in this thesis.**

| Buffer | Composition |
|---|---|
| Mammalian cell lysis | |
| Triton X-100 buffer | 100 mM NaCl, 1% Triton X-100, 50 mM Tris-HCl pH 8 |
| Denaturing affinity purification or immunoprecipitation | |
| Buffer A (Ni-NTA) | 6 M Guanidine HCl, 100 mM $NaH_2PO_4/Na_2HPO_4$, 15 mM imidazole, adjusted to pH 8.0 |
| TI buffer (Ni-NTA) | 25 mM Tris, 20 mM imidazole, adjusted to pH 6.8 |
| 1:3 buffer (Ni-NTA) | 1 volume of Buffer A : 3 volumes of TI buffer |
| Urea lysis buffer (IP K63) | 6 M urea, 20 mM Tris pH 8.0, 2.5 mM $MgCl_2$, 100 mM NaCl, 0.1% Triton X-100 |
| IP lysis buffer (IP K63) | 4 M urea, 20 mM Tris pH 7.5, 135 mM NaCl, 1.5 mM $MgCl_2$, 1% Triton X-100, 1 mM EDTA, 10% glycerol, 50 mM NaF |
| Wash buffer (IP K63) | 20 mM Tris pH 7.5, 135 mM NaCl, 1.5 mM $MgCl_2$, 1% Triton X-100, 1 mM EDTA, 10% glycerol, 50 mM NaF |
| Denaturing buffer (Strep-tag) | 20 mM Tris-HCl pH 7.5, 50 mM NaCl, 0.5% sodium deoxycholate, 0.5% IGEPAL CA-630, 0.5% SDS, 1 mM EDTA |
| Agarose gel electrophoresis, SDS-PAGE, immunoblotting | |
| TAE buffer | Diluted to 1X from 50X 1L stock (Biochemistry media kitchen): 242 g Tris base, 57.1 ml acetic acid, 18.6 g EDTA disodium salt dihydrate, adjusted to pH 8.3, autoclaved |
| MES running buffer | Diluted to 1X from 20X stock (Thermo Fisher Scientific) |
| MOPS running buffer | Diluted to 1X from 20X stock (Thermo Fisher Scientific) |
| TBST | 1X TBS, 0.1% Tween-20 |
| Blocking buffer | 5% milk in 1X TBST |
| Deubiquitylase assay | |
| DUB reaction buffer | 20 mM Tris pH 7.5, 100 mM NaCl |

The buffer additives used in this thesis are listed in **Table 2.2**. The buffers to which the additives were added are specified in **Section 2.12**.

**Table 2.2: Buffer additives used in this thesis.**

| Additive | Final molarity in relevant buffers | Source | Identifier |
|---|---|---|---|
| NEM (N-Ethylmaleimide) | 5 mM (or 2 mM in Ni-NTA Buffer A; or 10 mM in urea lysis buffer [IP K63] and IP lysis buffer [IP K63]) | Sigma-Aldrich | Cat# E1271 |
| DTT (dithiothreitol) | 1 mM (or 5 mM in DUB reaction buffer) | Thermo Fisher Scientific | Cat# R0862 |
| PIC (protease inhibitor cocktail) | 1X (from 1000X stock containing 2 mM AEBSF, 0.3 µM Aprotinin, 116 µM Bestatin, 14 µM E-64, 1 µM Leupeptin and 1 mM EDTA) | Sigma-Aldrich | Cat# P2714 |
| NaF | 1 mM | Sigma-Aldrich | Cat# 201154 |
| β-glycerophosphate | 10 mM | Sigma-Aldrich | Cat# G9422 |
| Sodium orthovanadate | 0.1 mM | Sigma-Aldrich | Cat# S6508 |
| PR-619 (2,6-diamino-5-thiocyanatopyridin-3-yl thiocyanate) | 100 µM | Apex Bio | Cat# A8212 |
| 1,10-Phenanthroline | 5 mM | Sigma-Aldrich | Cat# 131377 |
| MG-132 | 10 µM (or 25 µM in urea lysis buffer [IP K63] and IP lysis buffer [IP K63]) | Selleck | Cat# S2619 |

### 2.1.2 Plasmids

The plasmids used in this thesis are listed in **Table 2.3**.

**Table 2.3: Plasmids used in this thesis (continued on the following page).**

| Plasmid | Application | Source |
|---|---|---|
| pSpCas9(BB)-2A-Puro (PX459) V2.0 | Backbone vector for sgRNA/Cas9 constructs | Addgene #62988 |
| PX459 ZUP1 (#33 exon 2) | CRISPR-Cas9 targeting of ZUP1 exon 2 | Cloned in-house |
| PX459 ZUP1 (#11 exon 2) | CRISPR-Cas9 targeting of ZUP1 exon 2 | Cloned in-house |
| PX459 ZUP1 (#23 exon 2) | CRISPR-Cas9 targeting of ZUP1 exon 2 | Cloned in-house |
| PX459 ZUP1 (#8 exon 6) | CRISPR-Cas9 targeting of ZUP1 exon 6 | Cloned in-house |
| PX459 ZUP1 (#71 exon 6) | CRISPR-Cas9 targeting of ZUP1 exon 6 | Cloned in-house |
| PX459 ZUP1 (#2 exon 6) | CRISPR-Cas9 targeting of ZUP1 exon 6 | Cloned in-house |
| PX459 ZUP1 (#3 exon 6) | CRISPR-Cas9 targeting of ZUP1 exon 6 | Cloned in-house |
| pcDNA5/FRT/TO/FLAG (N-terminal) | Backbone vector for FLAG constructs (N-terminal tagging) | Kind gift from Francis Barr lab |
| FLAG-ZUP1 | Note: Contains 3x GGGGS linker after the FLAG tag as with all other FLAG constructs | Cloned in-house |
| FLAG-ZUP1 146-578 | Mutagenesis scan for protein binding | Cloned in-house |
| FLAG-ZUP1 186-578 | Mutagenesis scan for protein binding | Cloned in-house |
| FLAG-ZUP1 231-578 | Mutagenesis scan for protein binding | Cloned in-house |
| FLAG-ZUP1 272-578 | Mutagenesis scan for protein binding | Cloned in-house |
| FLAG-ZUP1 311-578 | Mutagenesis scan for protein binding | Cloned in-house |
| FLAG-ZUP1 Δα2/3 (Δ275-310) | Mutagenesis scan for protein binding | Cloned in-house |
| FLAG-ZUP1 Δα2/3 (Δ275-310) + GSG | Mutagenesis scan for protein binding | Cloned in-house |
| FLAG-ZUP1 E286Q | Mutagenesis scan for protein binding | Cloned in-house |
| FLAG-ZUP1 N288A | Mutagenesis scan for protein binding | Cloned in-house |
| FLAG-ZUP1 S295A | Mutagenesis scan for protein binding | Cloned in-house |
| FLAG-ZUP1 H298A | Mutagenesis scan for protein binding | Cloned in-house |
| FLAG-ZUP1 K301S | Mutagenesis scan for protein binding | Cloned in-house |
| FLAG-ZUP1 D303N | Mutagenesis scan for protein binding | Cloned in-house |
| FLAG-ZUP1 M305A | Mutagenesis scan for protein binding | Cloned in-house |
| FLAG-ZUP1 E306Q | Mutagenesis scan for protein binding | Cloned in-house |
| FLAG-ZUP1 ΔZnF1 (Δ1-25) | Mutagenesis scan for protein binding | Cloned in-house |
| FLAG-ZUP1 ΔZnF2 (Δ31-52) | Mutagenesis scan for protein binding | Cloned in-house |
| FLAG-ZUP1 ΔZnF1+2 (Δ1-52) | Mutagenesis scan for protein binding | Cloned in-house |

## Table 2.3 (continued): Plasmids used in this thesis.

| Plasmid | Application | Source |
|---|---|---|
| FLAG-ZUP1 ZnF1 D16A/M17A | Mutagenesis scan for protein binding | Cloned in-house |
| FLAG-ZUP1 ZnF2 E43A/M44A | Mutagenesis scan for protein binding | Cloned in-house |
| FLAG-ZUP1 ZnF3 D168A/M169A | Mutagenesis scan for protein binding | Cloned in-house |
| FLAG-ZUP1 ZnF4 I207A/L208A | Mutagenesis scan for protein binding | Cloned in-house |
| FLAG-USP11 | Mutagenesis scan for protein binding | Cloned in-house |
| FLAG-USP11 67-963 | Mutagenesis scan for protein binding | Cloned in-house |
| FLAG-USP11 186-963 | Mutagenesis scan for protein binding | Cloned in-house |
| FLAG-USP11 288-963 | Mutagenesis scan for protein binding | Cloned in-house |
| FLAG-USP11 Δ489-778 | Mutagenesis scan for protein binding | Cloned in-house |
| pDEST-YFP-ZUP1 | Mutagenesis scan for protein binding | Cloned in-house |
| FLAG-USP11 ΔUBL2 only (Δ493-574) | Mutagenesis scan for protein binding | Cloned in-house |
| FLAG-USP11 ΔInsert only (Δ575-775) | Mutagenesis scan for protein binding | Cloned in-house |
| FLAG-TCEAL1 | Mutagenesis scan for protein binding | Cloned in-house |
| FLAG-TCEAL1 Δα1 (Δ102-109) | Mutagenesis scan for protein binding | Cloned in-house |
| FLAG-TCEAL1 Δα2 (Δ124-153) | Mutagenesis scan for protein binding | Cloned in-house |
| pDEST12.2 | Backbone vector for ubiquitin constructs | Kind gift from Ivan Ahel lab |
| pDEST12.2-FLAG-linker-His-linker-ubiquitin | Denaturing pull-down (Ni-NTA) | Cloned in-house |
| pDEST12.2-TwinStreptag-ubiquitin | Denaturing pull-down (Strep-tag®) | Cloned in-house (Twin-Strep-tag® sequence obtained from IBA Lifesciences) |
| pcDNA5/FRT/TO/TwinStrep-RPA2 | Denaturing pull-down (Strep-tag®) | Cloned in-house |
| FLAG-RPA1 | Co-expressed with Strep-RPA2 | Cloned in-house |
| FLAG-RPA3 | Co-expressed with Strep-RPA2 | Cloned in-house |
| FLAG-ZUP1 C360R | Rescue experiments in ZUP1 knockouts | Cloned in-house |
| pcDNA5/FRT/TO-mCherry | Empty vector control for mCherry expression | Kind gift from Francis Barr lab |
| pCCC-TagRFP | PCNA chromobody | Chromotek #ccr |
| pSpCas9(BB) (PX330) | Backbone vector for PX330 LMNA sgRNA/Cas9 | Addgene via Benoit Kornmann's lab (kind gift) |
| PX330 LMNA sgRNA/Cas9 | CRISPR-Cas9 targeting of LMNA | Graham Dellaire (Dalhousie University), Pinder et al., 2015 |
| pCR2.1 Clover-LMNA donor | Homology repair donor template for Clover knock-in | Graham Dellaire (Dalhousie University), Pinder et al., 2015 |
| pcDNA5/FRT/TO-GFP | Empty vector control for GFP expression | Kind gift from Francis Barr lab |

### 2.1.3 Oligonucleotides

**Table 2.4** lists the oligonucleotides used by myself for generating the indicated plasmids, based on the oligonucleotide sequences determined by NEBaseChanger. PCR primers are also listed in this Table. Other in-house plasmids indicated in **Table 2.3** that are not mentioned here were cloned by others in the Gibbs-Seymour lab.

**Table 2.4: Oligonucleotides used for cloning or PCR.**

| Description | Sequence (5'-3') |
|---|---|
| Primers for the generation of FLAG-ZUP1 ΔZnF1 (Δ1-25) | F: GAAAGTGAAATTATATGTCCATTTTGCAAGTTGTCAGG<br>R: GGATCCACCGCCACCGGA |
| Primers for the generation of FLAG-ZUP1 ΔZnF2 (Δ31-52) | F: TTTGAGCAGAATACACTTG<br>R: TATAATTTCACTTTCCATGTG |
| Primers for the generation of FLAG-ZUP1 ΔZnF1+2 (Δ1-52) | F: TTTGAGCAGAATACACTTGAAAGAAACTTTGAGAGG<br>R: GGATCCACCGCCACCGGA |
| Primers for the generation of FLAG-ZUP1 ZnF1 D16A/M17A | F: CTCAGAACCAGCCGCGAAAGCTCACC<br>R: GTTACTGTTTCACCACAAATATTAC |
| Primers for the generation of FLAG-ZUP1 ZnF2 E43A/M44A | F: GAATTATGATGCAGCGTGTTTTCATATCGAAACAGCTC<br>R: ACACCTGACAACTTGCAAAATG |
| Primers for the generation of FLAG-ZUP1 ZnF3 D168A/M169A | F: GCACAGTGAAGCTGCGGAAACTCATG<br>R: TCCTCTATTTTTCCACAG |
| Primers for the generation of FLAG-USP11 ΔUBL2 only (Δ493-574) + GSGSGSG | F: CGGCTCCGGCTCAGGTCGCATTGAGGCC<br>R: GAGCCGGAGCCGTGGCTGATAGGCAGTGG |
| Primers for the generation of FLAG-USP11 ΔInsert only (Δ575-775) + GSGSGSG | F: CGGCTCCGGCAAGGCTCCCGTGCGGCTG<br>R: GAGCCGGAGCCCACCTCATAGACGAAGATATCATCACGGTC |
| Primers for the generation of FLAG-TCEAL1 Δα1 (Δ102-109) | F: CGCCCGCAATTTAGAGGG<br>R: GCTTCCTTCTTCAAGCTTATGTTTTC |
| Primers for the generation of FLAG-TCEAL1 Δα2 (Δ124-153) | F: AGCCGTCCTTATCCTATTTAAG<br>R: GCTTAAATTTCTGCCATGTATG |
| Primers for the generation of FLAG-ZUP1 C360R | F: AGGTTGGGGTCGTGGTTACAG<br>R: TTGTCGCCTAAAGATGAATG |
| PCR primer 'FWD' (ZUP1 exon 6) | ATTGGGAGCAAATTGATTAAGACTG |
| PCR primer 'REV1' (ZUP1 exon 6) | GCCCCCTGAGGATCAAAAC |
| PCR primer 'REV2' (ZUP1 exon 6) | CAGATGACAAGTTCAGAGTACTAG |
| PCR primer for amplifying ZUP1 exon 2: Forward | AATCCAGCGTTAAAGACCAAGT |
| PCR primer for amplifying ZUP1 exon 2: Reverse | GAGTCCAGGACAGTCCAGATGC |

### 2.1.4 CRISPR sgRNA sequences

**Table 2.5** outlines the oligonucleotides that contain ZUP1-targeting sgRNA sequences. The oligonucleotide pairs were phosphorylated, annealed and ligated to generate the indicated sgRNA/Cas9 vectors as described in **Section 2.6.5**. These vectors contain a U6 promoter-driven sgRNA cassette and encodes wild-type *S. pyogenes* Cas9 (SpCas9) (Ran et al., 2013a). sgRNAs targeting ZUP1 exon 2 were previously designed in the lab using the computational design tool, CHOPCHOP (Labun et al., 2019). sgRNAs targeting ZUP1 exon 6 were designed using CRISPOR and CHOPCHOP (Concordet et al., 2018; Labun et al., 2019). The scores for each sgRNA targeting ZUP1 exon 6 are presented in **Appendix A: Fig. 2**.

**Table 2.5: Sequences of oligonucleotides used to clone the indicated sgRNA/Cas9 vectors.**

| sgRNA/Cas9 plasmid | Target | Sequence (5'-3') |
|---|---|---|
| PX459 ZUP1 (#33 exon 2) | ZUP1 exon 2 | F: CACCGTCCAGCCTGACCGAAATAAA<br>R: AAACTTTATTTCGGTCAGGCTGGAC |
| PX459 ZUP1 (#11 exon 2) | ZUP1 exon 2 | F: CACCGCAGATCCTTTTATTTCGGTC<br>R: AAACGACCGAAATAAAAGGATCTGC |
| PX459 ZUP1 (#23 exon 2) | ZUP1 exon 2 | F: CACCGAGCTCACCTAATTGTTCACA<br>R: AAACTGTGAACAATTAGGTGAGCTC |
| PX459 ZUP1 (#2 exon 6) | ZUP1 exon 6 | F: CACCGGATTTAGGTATGGTGCGTGA<br>R: AAACTCACGCACCATACCTAAATCC |
| PX459 ZUP1 (#3 exon 6) | ZUP1 exon 6 | F: CACCGTATGTACTCGGGGAACTTTA<br>R: AAACTAAAGTTCCCCGAGTACATAC |
| PX459 ZUP1 (#8 exon 6) | ZUP1 exon 6 | F: CACCGCATCTTTAGGCGACAAAGGT<br>R: AAACACCTTTGTCGCCTAAAGATGC |
| PX459 ZUP1 (#71 exon 6) | ZUP1 exon 6 | F: CACCGGGCGACAAAGGTTGGGGTTG<br>R: AAACCAACCCCAACCTTTGTCGCCC |

### 2.1.5 Antibodies

The antibodies used in this thesis are listed in **Table 2.6**.

**Table 2.6: Antibodies used in this thesis.**

| Antigen | Antibody type | Dilution | Source | Identifier |
|---|---|---|---|---|
| ZUP1 | Mouse pAb | 1:1000 | DC Biosciences | Custom |
| ZUP1 | Mouse mAb | 1:1000 | DC Biosciences | Custom |
| ZUP1 | Rabbit pAb | 1:1000 | Sigma-Aldrich | Cat# HPA044426 |
| Vinculin | Mouse mAb | 1:5000 | Santa Cruz Biotechnology | Cat# sc-73614 |
| FLAG | Mouse mAb | 1:10000 | Sigma-Aldrich | Cat# A8592 |
| RPA70 | Rabbit mAb | 1:4000 | Abcam | Cat# ab79398 |
| RPA32 (Chapter 4) | Rabbit mAb | 1:4000 | Abcam | Cat# ab76420 |
| RPA32 (Chapter 5) | Rabbit pAb | 1:5000 | Bethyl | Cat# A300-244A |
| RPA14 | Rabbit pAb | 1:4000 | Novus Biologicals | Cat# NBP1-87141 |
| USP11 | Rabbit pAb | 1:2000 | Bethyl | Cat# A301-613A |
| TCEAL1 | Rabbit pAb | 1:1000 | Sigma-Aldrich | Cat# HPA060384 |
| UBR5 | Rabbit mAb | 1:4000 | Cell Signaling Technology | Cat# 65344 |
| PCNA | Rabbit pAb | 1:1000 | Abcam | Cat# ab18197 |
| p-RPA32 (S4/8) | Rabbit pAb | 1:5000 | Bethyl | Cat# A300-245A |
| p-RPA32 (T21) | Rabbit mAb | 1:2500 | Abcam | Cat# ab109394 |
| p-RPA32 (S33) | Rabbit pAb | 1:2500 | Bethyl | Cat# A300-246A |
| Total ubiquitin | Mouse mAb | 1:5000 | Thermo Fisher Scientific | Cat# 14-6078-82 |
| K63-linked polyubiquitin | Mouse mAb | 1:500 | Thermo Fisher Scientific | Cat# 14-6077-82 |
| K63-linked polyubiquitin (IP) | Rabbit mAb | 2 µg Ab per mg total protein | Sigma-Aldrich | Cat# 05-1308 |
| Twin-Strep-tag® | Mouse mAb | 1:10000 | IBA Lifesciences | Cat# 2-1509-001 |
| Ubiquitylated PCNA (K164) | Rabbit mAb | 1:1000 | Cell Signaling Technology | Cat# 13439 |
| RAD18 | Rabbit pAb | 1:5000 | Bethyl | Cat# A301-340A |
| RFWD3 | Rabbit pAb | 1:5000 | Bethyl | Cat# A301-397A |
| USP1 | Rabbit mAb | 1:1000 | Cell Signaling Technology | Cat# 8033 |
| RFP | Rabbit pAb | 1:5000 | Abcam | Cat# ab290 |
| CtIP | Mouse mAb | 1:1000 | Active Motif | Cat# 61142 |
| Mouse (secondary antibody) | Donkey pAb | 1:2000 | Jackson ImmunoResearch | Cat# 715-035-150 |
| Rabbit (secondary antibody) | Donkey pAb | 1:2000 | Jackson ImmunoResearch | Cat# 711-035-152 |

### 2.1.6 siRNAs

The siRNAs used in this thesis are listed in **Table 2.7**.

**Table 2.7: siRNAs used in this thesis.**

| siRNA | Source | Identifier |
|---|---|---|
| siControl (ON-TARGETplus Non-targeting Control Pool) | Horizon Discovery | Cat# D-001810-10-20 |
| siZUP1 (ON-TARGETplus SMARTpool) | Horizon Discovery | Cat# L-015894-02-0005 |
| siUSP11 (ON-TARGETplus SMARTpool) | Horizon Discovery | Cat# L-006063-00-0005 |
| siTCEAL1 (ON-TARGETplus SMARTpool) | Horizon Discovery | Cat# L-019850-00-0005 |
| siRAD18 (ON-TARGETplus SMARTpool) | Horizon Discovery | Cat# L-004591-00-0005 |
| siRFWD3 (ON-TARGETplus SMARTpool) | Horizon Discovery | Cat# L-017095-00-0005 |
| siUSP1 (ON-TARGETplus SMARTpool) | Horizon Discovery | Cat# L-006061-00-0005 |
| siCtIP | Eurofins | Sequence: GCUAAAACAGGAACGAAUC (Sartori et al., 2007) |

## 2.2 Cell culture

### 2.2.1 Maintenance of cell lines

The cell lines used in this thesis are outlined in **Table 2.8**. Cells were maintained in Dulbecco's Modified Eagle Medium (DMEM) containing high glucose, GlutaMAX™ supplement and pyruvate (Thermo Fisher Scientific), supplemented with 10% fetal bovine serum (FBS) (Thermo Fisher Scientific). Stably transduced cell lines expressing the hygromycin resistance gene were cultured in the presence of 100 µg/ml hygromycin B (Thermo Fisher Scientific), which was excluded during experiments. Cells were cultured at 37°C in a humidified incubator with 5% $CO_2$. Cells were used during passages p6-p13 for all experiments in this study.

Cells were passaged by aspirating the media, washing once with sterile PBS (Thermo Fisher Scientific) then adding TrypLE Express (Thermo Fisher Scientific) to dissociate cells from culture dishes. Culture dishes containing TrypLE were placed in the incubator for 2 minutes (min). Once detached, TrypLE was inactivated by adding DMEM + 10% FBS, and cells were transferred to a sterile tube for centrifugation at

300 x g for 5 min. The supernatant was aspirated and cells were resuspended in DMEM + 10% FBS for subsequent passaging or plating. Cell counts were performed using the DeNovix CellDrop automated cell counter with settings that had been optimised for counting 293T or U2OS cells.

**Table 2.8: Cell lines used in this thesis.**

| Cell line | Description | Source | Ploidy and karyotype | Derivatives |
|---|---|---|---|---|
| 293T | Derivative of human embryonic kidney 293 cells and expresses the SV40 T-antigen | ATCC (CRL-3216) | • Hypertriploid, with alterations including: der (1) t (1;5) (p10;q10); der (1) t (1;15) (q42;q13)x2; dup (13)q14q34); der (22) t (17;22) (q21;q13) (Perpiñá et al., 2020)<br><br>• Modal chromosome number of its parental 293 line is 64 in 30% of cells (ATCC) | • 293T ΔZUP1_Ex2 clones<br>• 293T ΔZUP1_Ex6 clones<br>• 293T ΔZUP1_Ex6/2 clones<br>• 293T WT pLenti-PGK-Hygro EV Pool<br>• 293T WT pLenti-PGK-Hygro ZUP1 WT Pool<br>• 293T ΔZUP1_Ex6/2 Clone 4 pLenti-PGK-Hygro EV Pool<br>• 293T ΔZUP1_Ex6/2 Clone 4 pLenti-PGK-Hygro ZUP1 WT Pool<br>• 293T ΔZUP1_Ex6/2 Clone 4 pLenti-PGK-Hygro ZUP1 C360R Pool |
| U2OS | Human osteosarcoma cell line | ATCC (HTB-96) | • 69–80 chromosomes (Raftopoulou et al., 2020)<br><br>• Very few normal chromosomes are present. Composed of whole or partial chromosome gains or losses, unbalanced translocations, deletions, multicentric chromosome formations (Raftopoulou et al., 2020) | • U2OS ΔZUP1_Ex2 clones<br>• U2OS ΔZUP1_Ex2/6 clones |

### 2.2.2 Generation of ZUP1 CRISPR-Cas9 knockout cells

293T cells were plated in 60 mm dishes such that they were 80% confluent the next day. Approximately 24 hours (h) after plating, cells were transfected with PX459 sgRNA/Cas9 vectors that target specific ZUP1 exons (**Table 2.5**, **Fig. 3.2**). The transfection was performed using the TransIT-LT1 transfection reagent (Mirus Bio) as outlined in **Section 2.3**. For the strategy involving two sgRNAs, the vectors were co-transfected at a 1:1 ratio (**Fig. 3.2**). 24 h post-transfection, cells were transferred to 15 cm dishes. The next day, cells were selected with 3 µg/ml puromycin for 24 h, after which puromycin was removed and cells were allowed to recover in complete growth medium for at least 48h. Puromycin-resistant cell pools were counted and diluted to distribute 50 cells among the wells of a 96-well plate. Each cell pool was

plated in four 96-well plates. The next day, wells containing a single cell were identified using an inverted microscope and topped up with complete medium.

At least 6 days later, single cells that had grown into 60-70% confluent colonies were trypsinised and distributed into two matching wells in separate 24-well plates. Clones were harvested from one plate to check for ZUP1 knockout by Western blotting, and the potential knockout clones were then expanded from the matching 24-well plate. The knockout was validated further by PCR genotyping, Sanger sequencing and ICE analysis as described in **Section 2.5**.

For the generation of 293T ΔZUP1_Ex6/2 clones, two separate rounds of editing and clonal expansion were performed, where ΔZUP1_Ex6 single cell-derived clones were first generated using exon 6-targeting sgRNAs. 293T ΔZUP1_Ex6 Clone 11 was transfected with a sgRNA/Cas9 vector targeting exon 2 and the single cell cloning procedure was repeated to derive 293T ΔZUP1_Ex6/2 clones (**Chapter 3**, **Fig. 3.2**).

### 2.2.3 Generation of stable ZUP1 re-expressing rescue cell lines

Lentiviruses that contain ZUP1 wild-type, ZUP1 C360R or the empty vector in their genome, along with the hygromycin resistance gene, were generated and collected by Matt Drake in the Gibbs-Seymour lab. The lentiviral vectors from which the lentiviruses were generated also contain the phosphoglycerate kinase (PGK) promoter and are named as follows: pLenti-PGK-Hygro EV, pLenti-PGK-Hygro ZUP1 WT, pLenti-PGK-Hygro ZUP1 C360R.

293T WT and ΔZUP1_Ex6/2 Clone 4 were plated in 6-well plates and transduced with different volumes of EV, ZUP1 WT or ZUP1 C360R lentiviral supernatants. 24 h later, the lentivirus was removed, wells were washed once with medium then replaced with complete growth medium. Cells were selected with 500 µg/ml hygromycin B (Thermo Fisher Scientific) which was replenished every 3 days until they were nearly confluent. Cells were passaged in the presence of 500 µg/ml hygromycin B for at least 2

passages before reducing the concentration to 100 µg/ml for maintenance in culture. The hygromycin-resistant cell pools were validated for ZUP1 expression by Western blotting. Hygromycin was excluded from the growth media during experiments. The cell pools were named based on the lentiviral vectors from which the lentiviruses were generated, for example 293T ΔZUP1_Ex6/2 Clone 4 pLenti-PGK-Hygro ZUP1 WT Pool.

### 2.2.4 Drug treatment

**Mitomycin C (MMC)**: MMC (Sigma-Aldrich) was dissolved in DMSO to a 1 mM stock solution and aliquots were frozen in -20°C. The aliquots were thawed in the dark before use. For clonogenic assays (described in **Section 2.7**), MMC solution was further diluted in DMSO to 100 µM before adding to complete growth medium in tubes to prepare a final concentration range of 10 to 100 nM. For other assays, MMC was diluted in complete medium to treat cells at the indicated concentrations and durations. As with all drug treatments, an identical volume of diluted drug was added to each tube.

**Olaparib**: Olaparib (Enzo Life Sciences) was dissolved in DMSO to a 10 mM stock solution and aliquots were frozen in -20°C. The aliquots were thawed in the dark before use. For clonogenic assays, olaparib solution was either added directly to the complete medium in tubes or diluted further in DMSO to 100 µM before addition to the medium to prepare a final concentration range of 10 to 1000 nM.

**Talazoparib**: Talazoparib (Selleck) was dissolved in DMSO to a 10 mM stock solution and aliquots were frozen in -20°C. The aliquots were thawed in the dark before use. For clonogenic assays, talazoparib solution was diluted further in DMSO to 10 µM or 0.1 µM before addition to the complete medium in tubes to prepare a final concentration range of 0.01 to 10 nM.

**Topotecan**: Topotecan hydrochloride (Tocris Bioscience) was dissolved in sterile $H_2O$ to a 10 mM stock solution and aliquots were frozen in -20°C. The aliquots were thawed in the dark before use. For clonogenic assays, topotecan solution was diluted further in $H_2O$ to 100 µM or 10 µM before addition to the complete medium in tubes to prepare a final concentration range of 1 to 100 nM.

**AZD6738**: AZD6738 (ApexBio) was dissolved in DMSO to a 10 mM stock solution and aliquots were frozen in -20°C. The aliquots were thawed in the dark before use. For clonogenic assays, AZD6738 solution was diluted further in DMSO to 1 mM before addition to the complete medium in tubes to prepare a final concentration range of 100 to 800 nM.

**Hydroxyurea**: Hydroxyurea (Sigma-Aldrich) was dissolved in sterile $H_2O$ to a 1 M stock solution and aliquots were frozen in -20°C. The aliquots were thawed in the dark before use. For clonogenic assays, hydroxyurea solution was diluted in growth medium in tubes to prepare a final concentration range of 1 to 30 mM. For other assays, hydroxyurea was diluted in complete medium to treat cells at the indicated concentrations and durations.

## 2.3 Plasmid transfection

The transfection reagent used for plasmid transfection was either the TransIT-LT1 transfection reagent (Mirus Bio) or PEI MAX solution (Polysciences). A 10 cm dish of cells containing 10 ml growth media was transfected with the following volumes: 1.5 ml Opti-MEM supplemented with GlutaMAX (Thermo Fisher Scientific), 7.5 µl DNA from 1 µg/µl stock and 22.5 µl transfection reagent. If multiple plasmids were co-transfected, they were added from 1 µg/µl stocks to give a total DNA volume of 7.5 µl. Depending on the duration of the experiment, cells were plated at least 16 h prior to transfection at a density such that cells were ≤90% confluent on the day of harvest. Plasmid DNA was first added to Opti-MEM and mixed by pipetting. The transfection

reagent was then added and mixed by pipetting. The tube was incubated at room temperature for 25 min. The transfection complexes were mixed before adding drop-wise to the culture vessel, which was then rocked gently to distribute the complexes evenly. For co-transfection of multiple plasmids, one plasmid was mixed with Opti-MEM before the addition of the next plasmid. For co-immunoprecipitation assays described in **Section 2.15.1**, the growth medium was replaced with fresh medium 24 h after transfection.

## 2.4 siRNA transfection

Reverse siRNA transfection was performed using Lipofectamine RNAiMAX (Thermo Fisher Scientific) where cells were transfected in suspension during plating. For a 10 cm dish of cells, 1 x $10^6$ cells were added to a tube containing complete growth medium to give a total volume of 8 ml. Two mastermixes were prepared in separate tubes. Mastermix 1 contains 20 µl RNAiMAX mixed with 1 ml Opti-MEM, while mastermix 2 contains the appropriate volume of siRNA added to 1 ml Opti-MEM. The mastermixes were combined and incubated for 15 min at room temperature. After incubation, the transfection mix was mixed with the cells in the tube, followed by a 5-min incubation at room temperature before plating in a 10 cm dish. The growth medium was replaced 24 h post-transfection with fresh media. Cells were harvested at least 48 h post-transfection for downstream analyses.

The final siRNA molarities used in this thesis were matched by the siControl: siZUP1 (50 nM), siUSP11 (10 nM), siTCEAL1 (10 nM), siRAD18 (20 nM), siUSP1 (20 nM), siRFWD3 (5 nM), siCtIP (20 nM). The siRNA product information is listed in **Table 2.7**.

## 2.5 CRISPR-Cas9 analysis methods

### 2.5.1 Western blotting

The first method of screening single cell-derived clones for ZUP1 knockout involved lysing the clones in Triton X-100 buffer and preparing protein samples for Western blotting as detailed in **Sections 2.12** and **2.13**. ZUP1 expression was determined using an in-house ZUP1-specific mouse antibody. Potential knockout clones were validated further by PCR genotyping, Sanger sequencing and ICE analysis as described below.

### 2.5.2 PCR genotyping

Clones that had been CRISPR-edited using paired sgRNAs flanking exon 6 were assessed for exon 6 deletion by PCR. The genomic DNA (gDNA) extraction, PCR and agarose gel electrophoresis protocols are described in **Section 2.6**. Two fragments spanning exon 6 were amplified by PCR using two pairs of primers, FWD and REV1, or FWD and REV2 (**Fig. 3.6, Table 2.4**). The band sizes were visualised by agarose gel electrophoresis to determine the homo- or heterozygosity of the edits, and some bands were purified from the gel to examine the edited sequence by Sanger sequencing.

### 2.5.3 Sanger sequencing and Inference of CRISPR Edits (ICE) analysis

Clones that had been CRISPR-edited using sgRNA #33 that targets exon 2 (**Table 2.5**) were assessed for frameshift indels within exon 2. The gDNA was extracted and a region spanning exon 2 was amplified by PCR using a pair of primers flanking the region (**Table 2.4**). The amplicon was sent for Sanger sequencing and the traces were analysed by the ICE software (https://ice.synthego.com/) using the sequence of the

wild-type amplicon as a control. The ICE software identifies the type and percentage of alleles that have been modified with indels, and calculates the overall editing efficiency and knockout score (Hsiau et al., 2019). The ICE algorithm and definition of each scoring matrix are described by Hsiau et al. and the Synthego website.

## 2.6 Molecular biology techniques

### 2.6.1 Polymerase chain reaction (PCR)

To amplify a ZUP1 region in the CRISPR-edited clones, PCR was performed in 25 µl reaction volumes containing 12.5 µl Q5 High-Fidelity 2X Master Mix (NEB), 1.25 µl each of 10 µM forward and reverse primer, 100 ng of template DNA and nuclease-free $H_2O$ to make up the remaining volume. The reaction was performed using the ProFlex PCR thermal cycler (Thermo Fisher Scientific) and the following cycling conditions: 30 seconds (s) at 98°C for initial denaturation; 35 cycles of 98°C for 10 s, 64°C for 30 s, 72°C for 30 s per kb; followed by the final extension for 2 min at 72°C. PCR cleanup was performed using the PCR purification kit (Qiagen).

For site-directed mutagenesis reactions, PCR was performed in 25 µl reaction volumes containing 12.5 µl Q5 High-Fidelity 2X Master Mix (NEB), 1.25 µl each of 10 µM forward and reverse primer, 25 ng of template DNA and nuclease-free $H_2O$ to make up the remaining volume. The reaction was performed using the ProFlex PCR thermal cycler (Thermo Fisher Scientific) and the following cycling conditions: 30 s at 98°C for initial denaturation; 25 cycles of 98°C for 10 s, 50-72°C* for 30 s, 72°C for 30 s per kb; followed by the final extension for 2 min at 72°C. *The annealing temperature is recommended by NEBaseChanger based on the mutagenic primers used. After the PCR, a kinase, ligase and DpnI (KLD) treatment was performed by assembling the following components provided in the Q5 site-directed mutagenesis kit (NEB): 1 µl PCR product, 5 µl 2X KLD reaction buffer, 1 µl 10X KLD enzyme mix and 3 µl nuclease-free $H_2O$. The reagents were mixed by pipetting several times and incubated at room temperature for 15 min.

### 2.6.2 Site-directed mutagenesis

Primers for site-directed mutagenesis were designed using NEBaseChanger (https://nebasechanger.neb.com). The DNA template is typically the wild-type protein construct. The PCR and KLD reactions were performed as described above. After the KLD reaction, 5 µl of the KLD mix was transformed into 50 µl chemically competent 5-alpha *E. coli* cells previously prepared from the stock: NEB 5-alpha Competent *E. coli* (High Efficiency) (NEB). The bacterial colonies were screened for the desired vectors as described below.

### 2.6.3 Bacterial transformation and colony screening

Chemically competent 5-alpha *E. coli* cells were thawed on ice. 1-2 µl of DNA (1 to 100 ng) was added to 50 µl of competent cells. The tube was flicked gently and incubated on ice for 30 min. The heat shock was performed at 42°C for 30 s in a water bath, after which the tube was returned to ice for 2 min. 300 µl of pre-warmed SOC was added to the tube and mixed in a ThemoMixer (Eppendorf ThermoMixer C) at 1000 rpm for 1 h at 37°C. The bacteria was plated on LB agar plates supplemented with the appropriate antibiotic and left to grow for 16 h at 37°C. For pDEST12.2 vectors, One Shot ccdB Survival 2 T1$^{R}$ Competent Cells (Thermo Fisher Scientific) were used instead.

The next day, approximately 16 h later, plates were removed from 37°C and kept at 4°C until further use. Three single bacterial colonies were chosen to inoculate separate tubes containing 3 ml of LB medium supplemented with the appropriate antibiotic. The bacterial cultures were left to grow for 16 h at 37°C with shaking. Plasmid DNA was purified by miniprep as described below. The DNA size was verified by restriction digestion and agarose gel electrophoresis, and the sequence was determined by Sanger sequencing.

### 2.6.4 Plasmid purification

Plasmids from 3 ml bacterial cultures were purified using the QIAprep Spin Miniprep Kit (Qiagen) according to the manufacturer's protocol. Plasmids from 200 ml bacterial cultures were purified using the PureLink HiPure Plasmid Filter Maxiprep Kit (Thermo Fisher Scientific) according to the manufacturer's protocol. The concentration and purity of the purified plasmids were determined using a spectrophotometer as described in **Section 2.6.9**.

### 2.6.5 CRISPR-Cas9 plasmid assembly

The PX459 vector was digested with FastDigest BpiI (Thermo Fisher Scientific) according to the manufacturer's instructions. The digested vector was run on an agarose gel and purified from the gel as described in **Section 2.6.7** and **2.6.8**. The sgRNA oligonucleotide pair was phosphorylated using T4 Polynucleotide Kinase (NEB) according to the manufacturer's protocol then annealed using the ProFlex PCR thermal cycler (Thermo Fisher Scientific) and the following conditions: 37°C for 30 min, 95°C for 5 min, then cooled to 25°C at 5°C/min. The ligation reaction was performed using the Quick Ligation kit (NEB) according to the manufacturer's instructions. The ligation product was transformed into competent cells and this was followed by colony screening and plasmid purification.

### 2.6.6 Genomic DNA extraction

CRISPR-edited clones that were grown in 60 mm dishes were lysed in 500 µl QuickExtract DNA Extraction Solution (Lucigen). The lysates were transferred to tubes which were vortexed for 15 s, placed on a 65°C heat block for 6 min, vortexed for 15 s, and finally placed on a 98°C heat block for 2 min. The DNA concentration was measured as described in **Section 2.6.9** and diluted in nuclease-free $H_2O$.

### 2.6.7 Agarose gel electrophoresis

DNA was run on 0.8% or 1.2% agarose gels depending on its size. The gel was prepared by dissolving UltraPure Agarose (Thermo Fisher Scientific) in 1X TAE buffer, then adding 5 µl SYBR Safe DNA Gel Stain (Thermo Fisher Scientific) to 100 ml of the dissolved agarose. The gel was left to polymerise in the gel mold tray. 6X Gel Loading Dye (NEB) was mixed with the DNA samples to give a final concentration of 1X prior to loading. The Quick-Load Purple 1 kb DNA Ladder (NEB) or 1kb Plus DNA Ladder was loaded alongside the samples. The gel tank was filled with 1X TAE buffer and the gel was run at 100 V for at least 45 min. Gels were imaged using the GelDoc imager (BioRad).

### 2.6.8 Purification of DNA from agarose gels

After agarose gel electrophoresis, DNA fragments were visualised with UV. A clean razor blade was used to slice the desired DNA band from the gel. The gel was weighed in a tube to determine the volume of buffer to add during the DNA purification, which was performed using the QIAquick Gel Extraction Kit (Qiagen) according to the manufacturer's instructions.

### 2.6.9 Measurement of DNA concentration

The purity and concentration of DNA were determined using the NanoDrop Lite spectrophotometer (Thermo Fisher Scientific). DNA concentration was measured at 260 nm. The DNA purity was determined using the absorbance ratio of $A_{260}/A_{280}$, where a value of ~1.8 was considered to be of sufficient purity.

## 2.7 Clonogenic assay

Clonogenic assays were performed as previously described (Franken et al., 2006). The previously optimised drug dose range was prepared by serial dilution in complete growth medium (**Section 2.2.4**). U2OS wild-type or ZUP1 knockout clones were counted and cells were added to tubes containing the drug at densities that had been optimised based on their plating efficiencies. Cells were plated in technical triplicates for each dose in 6-well plates at the following densities: U2OS WT (188 cells/well), U2OS ΔZUP1_Ex2/6 Clone 38 (249 cells/well), U2OS ΔZUP1_Ex2/6 Clone 62 (310 cells/well), U2OS ΔZUP1_Ex2/6 Clone 69 (276 cells/well), U2OS ΔZUP1_Ex2 Clone P2B2 (184 cells/well). The 6-well plates were kept in the incubator from Day 0 to Day 12. For 24 h drug treatments of MMC, topotecan and hydroxyurea, the wells were washed once with medium 24 h after the addition of the drug, and replaced with complete growth medium before returning to the incubator until Day 12, when colonies were stained. For chronic drug treatments of olaparib, talazoparib and AZD6738, the drug was replenished on Days 3, 6 and 9 and colonies were stained on Day 12.

On Day 12, the media was discarded and wells were washed twice with PBS. After removing residual PBS, 3 ml of crystal violet solution was added to each well. The plates were left to stain at room temperature for at least 30 min before removing the crystal violet solution and rinsing the plates in $ddH_2O$. After drying the plates, presumed colonies were marked using a Counter-Pen (VWR) before counting true colonies (comprising ≥ 50 cells) under an inverted microscope. The surviving fraction at each dose was calculated by dividing the mean number of colonies at the particular dose by that formed by the DMSO control (or $H_2O$ in the case of topotecan and hydroxyurea), and values were averaged from three biological replicates.

## 2.8 Cell cycle synchronisation by double thymidine block

Synchronisation of cells in S phase by double thymidine block has been described previously (Whitfield et al., 2002). The protocol outlined here is summarised in **Fig. 5.4A**. Cells were plated at a density such that cells were 25-30% confluent the next day. Approximately 24 h later, the growth medium was removed and cells were treated with 2 mM thymidine (Sigma-Aldrich) dissolved in growth medium. 18 h later, thymidine was removed, dishes were washed once with medium and replaced with fresh medium. After 9 h of thymidine release, the medium was removed and cells were treated with 2 mM thymidine. 17 h later, thymidine was removed, dishes were washed once with medium and replaced with fresh medium which may include MMC/DMSO at the indicated concentration and durations. Cells were either harvested for cell cycle analysis by flow cytometry, or for Western blotting or denaturing Strep pull-downs as described below. For denaturing Strep pull-downs, the Strep-ubiquitin transfection was performed during the first 9 h release from thymidine. In siRNA depletion experiments, the siRNA reverse transfection was performed during the plating of cells.

## 2.9 Flow cytometry

### 2.9.1 Assessing mCherry+ and GFP/Clover+ populations

Cells were dissociated from 60 mm dishes by trypsinisation and PBS + 1% FBS was added to the dishes. Cells were collected in tubes, pelleted by centrifugation at 500 x g for 5 min then resuspended in 900 µl PBS + 1% FBS. Tubes were placed on ice and protected from light, and cells were analysed on the BD LSRFortessa X-20 flow cytometer (BD Biosciences). Cells were first gated using side scatter (SSC-A) versus forward scatter (FSC-A) plots to exclude dead cells and debris. Doublets were excluded using SSC-height versus SSC-width plots. Transfected cells were designated as the cell population expressing the transfection control, mCherry, using SSC-A versus mCherry-A plots. Transfected cells were then gated for Clover+ cells

using SSC-A versus Clover-A plots. 10,000 events were acquired for each reading, and 3 technical readings were taken for each biological replicate. The percentages of mCherry+ Clover+ cells were analysed using FlowJo v10.8.1 Software (BD Life Sciences).

### 2.9.2 Cell cycle analysis

Cells were dissociated from 60 mm dishes by trypsinisation and pelleted by centrifugation. The cell pellet was resuspended in 300 µl cold PBS. The tube was vortexed for at least 15 s while adding 700 µl cold methanol to fix cells. Fixed cells were stored in -20°C overnight. Cells were pelleted by centrifugation at 300 x g for 10 min at 4°C and the methanol was removed. Cells were washed twice in cold PBS, and the washed cell pellet was resuspended in 200 µl PI/RNAse staining buffer (BD Biosciences). Cells were incubated for 15 min at room temperature in the dark before analysis on the BD LSRFortessa X-20 flow cytometer (BD Biosciences). The gating of cells was performed as described above to exclude dead cells, debris and doublets. The DNA content of cells was determined using count versus PI plots and the proportions of cells in different cell cycle stages were analysed using FlowJo v10.8.1 Software (BD Life Sciences). 10,000 events were acquired for each reading.

## 2.10 LMNA homology-directed repair assay

The LMNA HDR assay has been described previously (Pinder et al., 2015). Cells were plated in 60 mm dishes such that they were ~70% confluent the next day. 24 h later, cells were co-transfected with mCherry empty vector, PX330 LMNA sgRNA/Cas9 and pCR2.1 Clover-LMNA donor at an optimised ratio of 1 : 1.5 : 7.5, using the TransIT-LT1 transfection reagent (Mirus Bio) as described in **Section 2.3**. As the control, the PX330 empty vector was transfected in place of LMNA sgRNA/Cas9. 24 h post-transfection, cells were trypsinised and half were re-plated in new 60 mm dishes. 72 h post-transfection, cells were harvested for flow cytometry and analysed for mCherry+ and Clover+ populations as described in **Section 2.9.1**. For siRNA depletion experiments, the siRNA reverse transfection was performed during cell plating.

## 2.11 Microscopy

### 2.11.1 Imaging of Clover localisation in cells

Cells that were prepared for the LMNA HDR assay described above were plated in an additional set of 60 mm dishes containing coverslips. 72 h post-transfection, the growth medium was removed and 1X DPBS (Thermo Fisher Scientific) was added gently to the walls of the dishes using a Pasteur pipette to wash. After 2 DPBS washes, 4% formaldehyde was added to fix cells at room temperature for 15 min. After fixation, dishes were washed 3 times in DPBS. Cells were permeabilised by incubating coverslips with 0.2% Triton X-100 for 5 min, after which dishes were washed once in DPBS. After removing DPBS, DAPI (Thermo Fisher Scientific) that was diluted 1:5000 in 1X DPBS was added to the coverslips and left to stain for 5 min. DAPI was removed and dishes were washed twice in DPBS, then twice in $ddH_2O$. Dried coverslips were mounted on glass slides in Mowiol 4-88 (Sigma-Aldrich) and imaged using a 40X objective on an Olympus BX61 upright microscope equipped

with filter sets for DAPI, GFP/Alexa Fluor 488, 555, 568, and 647 (Chroma Technology Corp.), and a Photometrics Prime camera. Images were converted to TIFF files using the MetaMorph imaging software (Molecular Dynamics Inc). Images in the DAPI and GFP channels were merged using Fiji (Schindelin et al., 2012) and cropped in Adobe Photoshop.

### 2.11.2 Imaging of PCNA chromobody localisation in cells

Cells that were transfected with the PCNA chromobody (pCCC-TagRFP, Chromotek) or the mCherry empty vector control for RFP IP as described in **Section 2.15.2**, were imaged prior to the IP to visualise the localisation of the chromobody in cells. Images were acquired using the ZOE Fluorescent Cell Imager (Bio-Rad) and the red fluorescence (excitation: 556/20 nm; emission: 615/61 nm) and brightfield channels. Images were exported as TIFF files, merged using Fiji (Schindelin et al., 2012) and cropped in Adobe Photoshop.

## 2.12 Protein extraction and sample preparation

### 2.12.1 Cell lysis using Triton X-100

The volume of Triton X-100 buffer used to lyse one 60 mm dish of cells of ~80% confluence is 350 µl. The following additives were added to the Triton X-100 buffer just before use at the concentrations outlined in **Table 2.2**: NEM, DTT, PIC, NaF, β-glycerophosphate and sodium orthovanadate. For FLAG co-immunoprecipitation experiments, benzonase nuclease (Sigma-Aldrich) was also included in the buffer at a 1:500 concentration, along with 2 mM $MgCl_2$. Dishes were washed 3 times with cold PBS by gentle addition to the wall of the dishes. Cold Triton X-100 buffer was added to cells, and cells were immediately scraped on ice using a cell scraper. Cell lysates were transferred to pre-chilled tubes which were rotated at 4°C for 30 – 45

min, then centrifuged at 13,000 x g at 4°C for 10 min. The supernatants were transferred to fresh tubes and the protein concentration was measured using the Bio-Rad protein assay dye and Bradford protein assay (Bio-Rad).

### 2.12.2 Cell lysis using denaturing buffers

The volume of denaturing buffer used to lyse one 15 cm dish of cells of 90% confluence is 1 ml. The denaturing buffers used in this thesis contain the following additives, which were added to the buffers just before use at the concentrations outlined in **Table 2.2**: Ni-NTA Buffer A (NEM), urea lysis buffer for IP K63 (NEM, MG-132), IP lysis buffer for IP K63 (NEM, MG-132), denaturing buffer for Strep-tag pull-down (NEM, DTT, PIC, NaF, β-glycerophosphate, sodium orthovanadate, PR-619, 1,10-Phenanthroline, MG-132).

Dishes were washed twice with cold PBS by gentle addition to the wall of the dishes, and any cells that had detached were pelleted by centrifugation to be combined with the cell lysate. Cold denaturing buffer was added to cells, and cells were immediately scraped on ice using a cell scraper. Cell lysates (2 ml samples if scraped from two 15 cm dishes) were transferred to pre-chilled 2 ml tubes and sonicated on ice using the Q125 Sonicator (QSonica) and the standard 1/8" diameter probe. The optimised sonication settings for the denaturing Strep pull-down protocol (**Section 2.17.2**) are as follows: 40% amplitude, 9 pulses, each 10 s on, 40 s off. The probe was cleaned with ethanol before sonicating the next sample. After sonication, tubes were centrifuged at 13,000 x g at 4°C for 10 min. The supernatants were transferred to fresh tubes and the protein concentration was measured using the Bio-Rad protein assay dye and Bradford protein assay (Bio-Rad).

For the lysis of cells for Ni-NTA purification, dishes were washed in a similar manner and cells were scraped in cold PBS into tubes. The tubes were centrifuged at 13,000 x g for 1 min. The supernatant was removed and cell pellets were lysed by

resuspending in Buffer A, followed by sonication and measurement of the protein concentration.

### 2.12.3 Protein concentration quantification

Protein concentration was quantified using the Bio-Rad protein assay dye and Bradford protein assay (Bio-Rad). Briefly, bovine serum albumin (BSA) (Sigma-Aldrich) protein standards were prepared by serial dilution according to the instructions from Bio-Rad. 1 ml of 1X protein assay dye was added to each semi-micro cuvette (Thermo Fisher Scientific). The BSA protein standards and samples were mixed with the protein assay dye and the absorbance at 595 nm was read in a spectrophotometer. A standard curve was constructed using the absorbance values of the protein standards, and the protein concentration of the samples was calculated by interpolation from the standard curve.

### 2.12.4 Protein sample preparation

Protein samples were prepared based on Bradford assay calculations of protein concentration. 100 µl samples were prepared for SDS-PAGE and Western blotting. Each sample consists of 1X LDS sample buffer (Thermo Fisher Scientific), 10% DTT (Thermo Fisher Scientific), the calculated volume of protein, and lysis buffer to make up the remaining volume. Samples were heated at 70°C for 10 min. Samples were cooled prior to loading or stored in -20°C.

## 2.13 Western blotting

Protein samples were run on NuPAGE 4-12% or 8% Bis-Tris Protein Gels (Thermo Fisher Scientific). The former gel was used when immunoblotting for ubiquitylated proteins. The 4-12% gels were run in 1X NuPAGE MES SDS running buffer (Thermo Fisher Scientific) while 8% gels were run in 1X NuPAGE MOPS SDS running buffer (Thermo Fisher Scientific). The gels were run at 150V until adequate separation of proteins was achieved as indicated by the SeeBlue Plus2 Pre-stained Protein Standard (Thermo Fisher Scientific). When immunoblotting for UBR5, a 6% gel was prepared using SureCast reagents (Thermo Fisher Scientific) according to the recipe specified by the manufacturer, and the gel was run in 1X SDS running buffer at 150V until adequate protein separation was achieved as indicated by the HiMark Pre-stained Protein Standard (Thermo Fisher Scientific).

The Trans-Blot Turbo Transfer System was used for transferring proteins from gels onto PVDF membranes for 30 min (Bio-Rad). Membranes were incubated in blocking buffer (**Table 2.1**) for 1 h. Primary antibodies specific for vinculin, FLAG, total ubiquitin, Twin-Strep-tag and RFP, along with the secondary antibodies, were diluted in blocking buffer (see **Table 2.6** for antibody information). All other primary antibodies were diluted in 5% BSA in TBST, and membranes were washed 3 times in TBST at 5-min intervals after blocking, prior to their incubation with primary antibodies diluted in 5% BSA. Membranes were incubated with primary antibodies overnight at 4°C. Membranes were then washed 3 times in TBST at 10-min intervals, and incubated with the appropriate HRP-conjugated secondary antibody for 1 h at room temperature. Membranes were washed 3 times in TBST at 10-min intervals and treated with Pierce ECL Western blotting substrate (Thermo Fisher Scientific) or, for a more sensitive detection, Clarity Western ECL substrate (Bio-Rad). The antibody signal was visualised using Hyperfilm ECL films (GE Healthcare) and an X-ray film processor (Euroteck Systems).

## 2.14 Coomassie staining

For the staining of proteins in SDS-PAGE gels, the gel was rinsed in MilliQ $H_2O$ then incubated with InstantBlue stain reagent (Expedeon) for at least 1 h at room temperature. The gel was rinsed in MilliQ $H_2O$ several times, then imaged using the GelDoc imager (BioRad).

## 2.15 Immunoprecipitation

### 2.15.1 IP of FLAG

Cells were plated in 10 cm dishes at a density of 1.6 - 2 x $10^6$ cells in each dish, such that cells were 80-90% confluent on the day of harvest. The day after plating, cells were transfected with FLAG-tagged constructs using PEI reagent (**Section 2.3**). 24 h post-transfection, the growth medium was replaced with fresh medium. 24 h later, cells were harvested by lysing in Triton X-100 as described in **Section 2.12.1**. Micro Bio-Spin chromatography columns (Bio-Rad) were prepared by adding Triton X-100 lysis buffer to wet the columns, followed by the addition of 100 µl anti-FLAG M2 affinity gel (Sigma-Aldrich) to each column using a pipette tip with its end cut off. The affinity gel was washed 3 times with cold lysis buffer by gravity flow. The protein concentration of the cell lysates was measured using the Bradford assay. The column ends were closed with a cap, and the calculated protein amount was added to the columns. Lysis buffer was added to make up a total of 900 µl in each column. The columns were closed at both ends and rotated at 4°C for 15 min. Meanwhile, 1% of the IP protein amount was used to prepare the input protein samples as described in **Section 2.12.4**. The columns were washed 5 times with cold lysis buffer, after which the affinity gel was resuspended in 200 µl lysis buffer and transferred to pre-chilled tubes. The tubes were centrifuged at 1000 x g for 2 min at 4°C. The supernatant was removed carefully and 100 µl IP protein samples were prepared. The input and IP protein samples were subsequently used for SDS-PAGE and Western blotting to determine protein binding to the FLAG constructs.

### 2.15.2 IP of RFP

Cells were plated in two 15 cm dishes for each condition at a density of 6 x $10^6$ cells per dish. The next day, cells were transfected with the PCNA chromobody (pCCC-TagRFP, Chromotek) or mCherry empty vector using PEI reagent (**Table 2.3**, **Section 2.3**). 24 h post-transfection, the medium was removed and cells were treated with 1 µM MMC for 24 h. After the treatment, cells were harvested by lysing cells in Triton X-100 buffer as described in **Section 2.12.1**. 60 µl RFP-Trap agarose (Chromotek) was added to a Protein LoBind tube (Eppendorf) using a pipette tip with its end cut off. The resin was washed 3 times in Triton X-100 lysis buffer by inverting the tube several times, followed by centrifugation at 2500 x g at 4°C for 5 min, then aspirating the supernatant. Nearly all the protein lysate was added to the tube containing the resin, and the tube was rotated at 4°C for 1 h. Meanwhile, 1% of the IP protein amount was used to prepare the input protein samples as described in **Section 2.12.4**. After rotating for 1 h, the resin was centrifuged at 2500 x g at 4°C for 5 min. The supernatant was removed and the resin was washed 3 times in lysis buffer, where each wash involved rotating tubes at 4°C for 3 min followed by centrifugation. These washes were performed to remove contaminating DUBs, DUB inhibitors and free ubiquitin. After the final wash, the supernatant was aspirated and 10 µl DUB reaction buffer was added to the resin prior to the DUB assay as detailed in **Section 2.16**.

### 2.15.3 IP of K63-linked ubiquitin

This protocol was performed as previously described (Hewings et al., 2018). Cells were plated in two 15 cm dishes for each condition at a density of 5 x $10^6$ cells per dish. The next day, cells were treated with 2 mM HU or an equivalent volume of $H_2O$ for 2.5 h, in the presence or absence of 20 µM MG-132 or an equivalent volume of DMSO. Cells were harvested by lysing in urea lysis buffer as described in **Section 2.12.2**. Cell lysates were transferred to 2 ml tubes and sonicated on ice using the Q125 Sonicator (QSonica) and the standard 1/8” diameter probe, with the following settings: 50% amplitude, 3 pulses, each 5s on, 30s off. Protein A Dynabeads (Thermo

Fisher Scientific) were washed 3 times in wash buffer using a magnetic rack. For the pre-clearing step, cell lysates were incubated with 20 µl Dynabeads by rotating for 2 h at 4°C. The protein concentration of the pre-cleared lysates was measured using the Bradford assay. The lysates were diluted 2-fold in IP lysis buffer, and the calculated protein amount was added to tubes containing anti-K63 linkage-specific IP antibody, diluting in IP lysis buffer if necessary to give a total of 1.5 ml in each tube. The tubes were rotated overnight at 4°C. 2% of the IP protein amount was used to prepare the input protein samples as described in **Section 2.12.4**. After overnight rotation, 25 µl beads were incubated with each IP sample by rotating for 2 h at 4°C, to allow the attachment of immunocomplexes to the beads. The beads were then washed 4 times in wash buffer and proteins were eluted by resuspending beads in sample buffer to prepare 80 µl protein samples for subsequent SDS-PAGE and Western blotting.

## 2.16 Deubiquitylase assay

As a continuation from **Section 2.15.2**, the RFP-Trap agarose was resuspended in DUB reaction buffer and distributed equally into 6 tubes after the IP. The tubes were centrifuged at 2500 x g for 2 min at 4°C and the supernatant was removed. Recombinant USP2, or ZUP1 in combination with RPA, were diluted in DUB reaction buffer (to which DTT was added to a final molarity of 5 mM just before use) in a 50 µl reaction volume and incubated with the agarose to result in the following final molarities: 0.5 µM USP2, or 1 µM ZUP1 together with 1 µM RPA. The tubes were gently flicked to mix and incubated at 37°C for the indicated timepoints in a Thermomixer (Eppendorf ThermoMixer C) at 600 rpm. After incubation, the tubes were centrifuged at 2500 x g for 5 min. The supernatants were transferred to fresh tubes to prepare protein samples for visualisation by Coomassie staining. The resin was resuspended in sample buffer, DTT and DUB reaction buffer to prepare 50 µl protein samples as described in **Section 2.12.4**. Protein samples were subsequently used for SDS PAGE and immunoblotting.

## 2.17 Affinity purification

### 2.17.1 Ni-NTA purification of His-ubiquitin

This protocol was adapted from Elia et al. (Elia et al., 2015). Cells were plated in two 15 cm dishes for each condition and allowed to adhere overnight. The next day, cells were transfected with His-ubiquitin (pDEST12.2-FLAG-linker-His-linker-ubiquitin) using PEI reagent (**Section 2.3**). 24 h later, the medium was removed and cells were treated with 2 mM HU. Meanwhile, the Ni-NTA buffers were prepared fresh (**Table 2.1**). 2 h later, cells were harvested by lysing in Buffer A as described in **Section 2.12.2**. After sonication on ice using the Q125 Sonicator (QSonica) and the standard 1/8" diameter probe (50% amplitude, 10 pulses, each 1 s on, 20 s off), the protein concentration was measured using the Bradford assay (**Section 2.12.3**) and 50 µl of HisPur Ni-NTA resin (Thermo Fisher Scientific) was washed 3 times in Buffer A. The resin was resuspended in 50 µl of Buffer A then incubated with the calculated protein amount from the cell lysates which was diluted in Buffer A. 2% of this protein amount was used to prepare the input protein samples as described in **Section 2.12.4**. The tubes containing resin were rotated for 3 h at room temperature. After rotation, tubes were centrifuged at 13,000 x g for 2 min. The supernatant was discarded, and the resin was washed once in Buffer A by inverting the tubes followed by centrifugation, twice in 1:3 buffer and once more in TI buffer. The supernatant was removed and a 26G needle fitted onto a syringe was plunged into the resin to remove the residual liquid. The resin was resuspended in sample buffer and DTT to prepare 100 µl protein samples, which were diluted in $H_2O$ and also included 25% 1 M imidazole (Sigma-Aldrich). Protein samples were subsequently used for SDS PAGE and immunoblotting.

### 2.17.2 Strep purification (Strep-tag system)

Cells were plated in two 15 cm dishes for each condition at a density of 1.5 x $10^6$ cells per dish (293T wild-type) or 2 x $10^6$ cells per dish (293T ZUP1 knockouts). Approximately 24 h later, cells were synchronised by double thymidine block as described in **Section 2.8**. During the first 9 h thymidine release, cells were transfected with Strep-ubiquitin (pDEST12.2-TwinStreptag-ubiquitin) or the pDEST12.2 empty vector using PEI reagent as outlined in **Section 2.3**. Upon release from the second thymidine treatment, dishes were washed once with medium before treating cells with 1 μM MMC or an equivalent volume of DMSO for the indicated durations. After the treatment, dishes were washed and either frozen in -80°C overnight or harvested immediately by lysing in Strep-tag denaturing buffer as described in **Section 2.12.2**. Cell lysates (2 ml from two 15 cm dishes as described in **Section 2.12.2**) in 2 ml tubes were sonicated using the Q125 Sonicator (QSonica) and the standard 1/8" diameter probe, with the following settings: 40% amplitude, 9 pulses, each 10 s on, 40 s off. 25 μl of Strep-Tactin Sepharose resin (IBA Lifesciences) was added to Protein LoBind tubes using a pipette tip with its end cut off, and the resin was washed 3 times in denaturing buffer (without additives) by tapping the tube, followed by centrifugation at 2500 x g for 30 s at 4°C. A small volume of the lysate was diluted 5-fold in Triton X-100 buffer prior to the measurement of protein concentration using the Bradford assay (**Section 2.12.3**). The calculated protein amount was added to the tubes containing Strep-Tactin resin to give a final volume of 900 μl in denaturing buffer. The tubes were rotated for 2 h at 4°C. Meanwhile, 1% of the calculated pull-down protein amount was used to prepare the input protein samples as described in **Section 2.12.4**. After the 2 h rotation, tubes were centrifuged at 2500 x g for 30 s and the resin was washed 5 times in denaturing buffer including additives (**Section 2.12.2**). The resin was resuspended in sample buffer to prepare 50 μl protein samples as described in **Section 2.12.4**, which were subsequently used for SDS-PAGE and Western blotting.

## 2.18 Statistical analysis

Statistical analyses were performed in GraphPad Prism 9. For clonogenic assays, the difference in the surviving fraction between the wild-type cells and ZUP1 knockout clones at each drug dose was analysed across 3 independent experiments (each consisting of technical triplicates) using two-way ANOVA with Dunnett's test. For the LMNA HDR assay, the difference in HDR efficiency between the wild-type cells and ZUP1 knockout clones was analysed across 3 independent experiments (each consisting of technical triplicates) using one-way ANOVA with Dunnett's test.

# 3

# Characterising ZUP1-Dependent DNA Repair Phenotypes

## Contents


**3.1 Introduction……..…..82**

**3.2 Results……..……85**

3.2.1 Consideration of ZUP1 splice isoforms……85

3.2.2 CRISPR-Cas9 sgRNA design and strategy……..…..……88

3.2.3 Validation of ZUP1 knockout in single cell-derived clones……..……91

3.2.4 ZUP1 knockouts are sensitive to replication stress induced by genotoxic agents……..……...…….107

3.2.5 ZUP1 hypomorphs also exhibit sensitivity to genotoxic agents……113

**3.3 Discussion……..……..116**

3.3.1 Challenges in the generation of CRISPR-Cas9 knockouts in cell lines with complex karyotypes……..……...…….116

3.3.2 Evaluation of knockout strategy to eliminate ZUP1……..……..…….118

3.3.3 ZUP1 has a role in replication-coupled DNA repair…….……...…….119

3.3.4 The N-terminus of ZUP1 may be important for its DNA repair function.....121

## 3.1 Introduction

Following the discovery of ZUP1 as the founding member of a novel DUB class, four independent groups extended their biochemical investigation to assess the cellular roles of ZUP1 (Kwasna et al., 2018; Haahr et al., 2018; Hermanns et al., 2018; Hewings et al., 2018). Proteomic approaches revealed the interaction between ZUP1 and proteins involved in DNA replication and repair, including the RPA complex (Kwasna et al., 2018; Hermanns et al., 2018; Hewings et al., 2018). This led the groups to use RNAi approaches to analyse ZUP1-dependent effects on DNA damage accumulation and RPA ubiquitylation as summarised below.

Kwasna et al. depleted ZUP1 in U2OS cells using siRNAs and reported the accumulation of chromatin-bound 53BP1 and γH2AX in unchallenged conditions, which indicates spontaneous DNA damage (Kwasna et al., 2018). To address potential off-target effects, a panel of independent siRNAs were used to individually deplete ZUP1, which demonstrated a consistent phenotype. The accumulation of 53BP1 foci resulting from ZUP1 knockdown was prevented by the inducible expression of siRNA-resistant WT ZUP1 but not the catalytically inactive (C360S) ZUP1 allele. This suggests that the DUB activity of ZUP1 may be required to protect cells from spontaneous DNA damage. ZUP1 knockdown was also found to sensitise cells to exogenous DNA damage, namely ionising radiation and camptothecin (CPT) which forms double-strand DNA breaks and inhibits topoisomerase I, respectively (Vignard et al., 2013; Pommier et al., 2006).

Haahr et al. demonstrated that siRNA-mediated ZUP1 knockdown in U2OS cells resulted in elevated levels of RPA32 foci upon CPT treatment, and micronuclei upon treatment with CPT, aphidicolin or hydroxyurea (HU) (Haahr et al., 2018). Aphidicolin inhibits B-family DNA polymerases, whereas hydroxyurea inhibits ribonucleotide reductase which catalyses the formation of deoxyribonucleotides (Baranovskiy et al., 2014; Krakoff et al., 1968). The effect of aphidicolin on micronuclei formation was rescued by complementation with WT ZUP1 but not with catalytically inactive or ubiquitin-binding-deficient ZUP1 mutants. The study further showed that ZUP1 knockdown increased the levels of K63-linked polyubiquitin levels at replication forks

stalled at the Lac repressor (LacR)-bound *LacO* array. From these findings, the authors proposed that ZUP1 has a role in maintaining genome stability, and may regulate K63-linked ubiquitylation of proteins at stressed forks.

Given the findings that ZUP1 interacts with the RPA complex, and that ZUP1 is specific for cleaving K63-linked polyubiquitin chains, Hewings et al. assessed the effects of siRNA-mediated ZUP1 knockdown on the K63 ubiquitylation status of the RPA complex (Hewings et al., 2018). ZUP1-depleted HeLa cells exhibited higher levels of endogenous RPA70 and RPA32 modified by K63-linked polyubiquitin upon hydroxyurea treatment. While this suggests a novel hypothesis that ZUP1 regulates the ubiquitylation of the RPA complex, for which a regulatory DUB is yet to be identified, it assumes that the single siRNA tested did not induce confounding ZUP1-independent effects. The contribution of ZUP1 DUB activity to this effect also remains to be examined.

Overall, the preliminary evidence presented by independent groups report a common theme that ZUP1 has an important role in maintaining genome stability. This merits the use of more robust and comprehensive approaches to investigate the repair pathway(s) that ZUP1 functions within. One major caveat of the RNAi methodology utilised in these studies is the possible induction of off-target effects that may confound the results (Boutros et al., 2008). An example of how siRNA off-target effects can generate false positives for DNA repair defect phenotypes was illustrated by a previous genome-wide siRNA-based screen in human cells that identified the HR factor, RAD51 as a common off-target of siRNAs (Adamson et al., 2012). In addition, while the ZUP1 siRNAs were shown by the authors to have depleted the largest ZUP1 isoform, it is not known if the siRNAs had silenced the other ZUP1 splice isoforms. Therefore, it cannot be excluded that residual or compensatory ZUP1 splice isoforms may have limited the strength or robustness of the observed phenotypes.

More broadly, the role of ZUP1 as a DUB in DNA repair has not been fully characterised. This chapter describes the generation of ZUP1 knockout cells using the CRISPR-Cas9 system which addresses the limitations of published RNAi

experiments. Guide RNAs were designed using algorithm-based tools to target different exons and eliminate ZUP1 isoforms or truncated variants that may retain functionality. To investigate ZUP1-dependent DNA repair phenotypes, ZUP1 knockout cells were assessed for survival defects in the presence of genotoxic agents that induce a range of lesions. This chapter also describes the challenges arising from deriving complete knockouts in cell lines with underlying chromosomal and karyotype instability, and highlight the importance of using effective screening methods to detect complex editing outcomes.

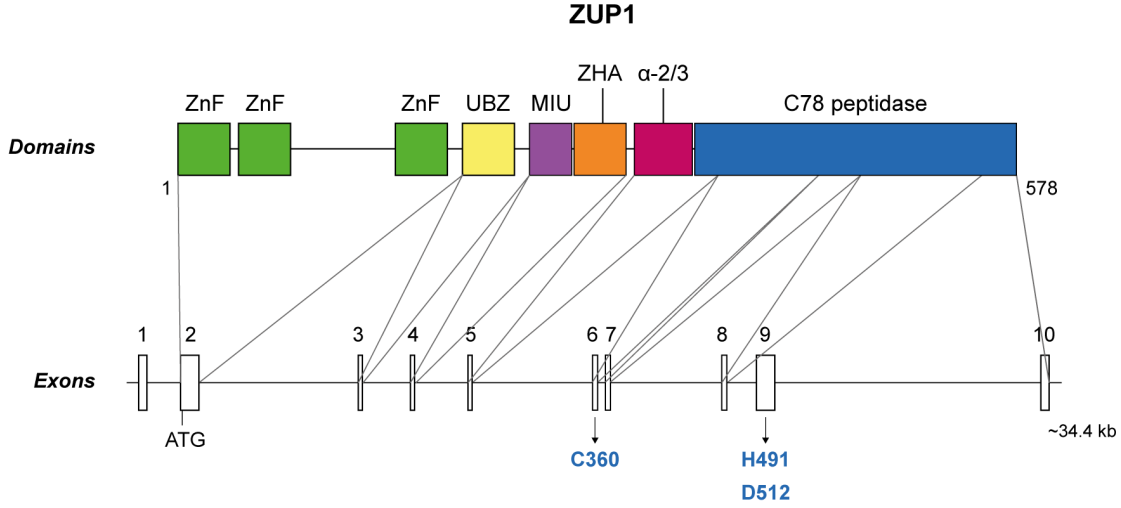
## 3.2 Results

### 3.2.1 Consideration of ZUP1 splice isoforms

To date, four distinct ZUP1 protein-coding transcripts are described on the UCSC Genome Browser and Ensembl databases (**Fig. 3.1B**). The ATG start codon is present in what is determined as exon 2. Exon 6, also common to all isoforms, encodes the catalytic cysteine residue, Cys360 that forms the catalytic triad together with His491 and Asp512 in full-length ZUP1 (Hermanns et al., 2018; **Fig. 3.1A**).

Although alternative splicing mechanisms are highly complex and require comprehensive transcriptome analysis, it is conceivable that exon skipping may have produced the 280 aa (1225 bp) isoform, while intron retention may have occurred in the 578 aa (2588 bp) isoform (Wang et al., 2015). The 280 aa splice isoform lacks two out of three catalytic triad residues since it does not contain exon 9. The 3' truncation in the 280 aa isoform therefore suggests extensive differences in its structure and function compared to the other isoforms. In the absence of catalytic activity, cellular functions of this isoform may be executed via non-catalytic domains encoded by the remaining exons. Chapter 4 describes novel roles for some of the ZUP1 non-catalytic domains which were found to provide protein-protein interaction sites.

A




B

| Transcript ID | Exon map | Protein (aa) | Calculated molecular weight (Da) | Length (bp) |
|---|---|---|---|---|
| NM_001361189.2 | 1 Intron 2 3 4 5 6 7 8 9 10 | 578 | 65828 | 2588 |
| NM_145062.3 ENST00000368576.8 | 1 2 3 4 5 6 7 8 9 10 | 578 | 65828 | 2167 |
| NM_001361190.2 | 1 2 3 4 5 6 7 8 9 10 | 410 | 46842 | 1872 |
| ENST00000368573.5 | 1 2 3 4 6 | 280 | 32286 | 1225 |

**Figure 3.1: ZUP1 domains, exons and reported splice isoforms.** A) Schematic representation of ZUP1 exons mapped to protein domains. The ZUP1 catalytic triad residues are indicated in blue below the exons that encode them. B) ZUP1 splice transcripts and their indicated features as currently reported (UCSC Genome Browser, Ensembl). The pink arrow denotes the ATG initiation codon. The relative size of each exon is represented by boxes which are not drawn exactly to scale.

The function of individual ZUP1 splice isoforms remain unknown and their relative expression has not been investigated. In addition, it has yet to be determined whether these isoforms are co-expressed in the same cell, either by assessing a clonal cell population or by analysing single cells by RNA sequencing. Following the discovery of ZUP1, the Gibbs-Seymour lab generated mouse monoclonal and polyclonal antibodies against ZUP1, and validated their superior performance compared to commercially available antibodies. The minimal region recognised by the in-house ZUP1 antibody is the helix-turn-helix hairpin protrusion, annotated as α-2/3, that spans 35 residues upstream of the catalytic domain (**Fig. 1.10, Appendix A: Fig. 1**). It was previously suggested that the α-2/3 region is required for ZUP1 DUB activity, as an internal deletion of the α-2/3 significantly reduced the ability of ZUP1 to cleave free K63-linked polyubiquitin chains (Hermanns et al., 2018).

Using the ZUP1 antibody, four bands were detected in 293T cell lysates. These were verified as ZUP1 gene products by the siRNA-mediated knockdown of ZUP1 in **Fig. 3.3A**, and are hereafter referred to as isoforms A, B, C and D, where isoform A is the full-length and most abundant isoform. The relative expression of each isoform is consistent at basal conditions, with isoform A being the most highly expressed followed by isoforms C, B and D (**Fig. 3.2B**). Based on the antibody recognition site, these isoforms should contain the α-2/3 region that extends from the catalytic core (**Fig. 1.10**). One caveat of using this ZUP1 antibody is that it may not detect the 280 aa isoform represented on the databases as shown in **Fig. 3.1B**, due to the absence of exon 5 which encodes the α-2/3 region. This was later addressed by utilising multiple genotyping approaches during the generation of ZUP1 knockouts to ensure the complete loss or mutation of the targeted exon, as described in the following sections.

To assess ZUP1-dependent phenotypes and understand the cellular roles of ZUP1, the first aim was to achieve the complete elimination of all known ZUP1 isoforms in the knockout cells. This is feasible given that ZUP1 is not an essential gene (Tsherniak et al., 2017; Dempster et al., 2019). Whether the ZUP1 isoforms are functionally distinct or redundant, residual isoform expression could obscure or limit the strength

of cellular phenotypes. In addition, the generation of complete ZUP1 knockouts also involved the removal of potentially functional in-frame variants or truncations resulting from CRISPR-Cas9 editing. This chapter describes the approaches tested to derive complete ZUP1 knockouts, and the obstacles encountered in generating the desired edits.

### 3.2.2 CRISPR-Cas9 sgRNA design and strategy

The CRISPR-Cas9 vector used to knock out ZUP1 contains a U6 promoter-driven single guide RNA (sgRNA) cassette, and encodes wild-type *S. pyogenes* Cas9 (SpCas9) (Ran et al., 2013a). ZUP1 knockouts were generated in the 293T cell line which was considered a suitable cell line for the phenotypic assays presented in Chapter 5, due to its rapid growth rate and high transfection efficiency.

Exon 2 is the first coding exon and is present in all reported ZUP1 splice variants (**Fig. 3.1A, B**). The first strategy to knock out ZUP1 involved targeting exon 2 using a single or paired sgRNA approach (**Fig. 3.2A**). The paired sgRNA approach involved the co-transfection of two sgRNA/Cas9 vectors in which the sgRNAs target two sites within exon 2 where Cas9-mediated DSBs will result in the deletion of the region, rather than the 'double-nicking' strategy that utilises the Cas9 nickase (D10A mutant) (Ran et al., 2013b). The sgRNAs were designed using CRISPOR and CHOPCHOP, which are computational tools that identify potential target sites based on protospacer adjacent motif (PAM) sequences on the exon, and predicts off-target activity by analysing sequences across the genome that display homology to the target sequence (Concordet et al., 2018; Labun et al., 2019). The sgRNA efficiency is scored based on guanine enrichment, adenine depletion, DNA accessibility and self-complementarity, amongst other metrics collated from published screens and meta-analyses (Labun et al., 2019).

The sgRNA sequences with the highest specificity scores were selected and cloned into the sgRNA/Cas9 vector, which was transiently expressed in 293T wild-type cells

(**Appendix A: Fig. 2, 3**). For the paired sgRNA approach, cells were co-transfected with two vectors, each bearing one sgRNA targeting a specific sequence within exon 2. A limiting dilution method was used to obtain single cell-derived clones from a pooled population of transfected cells that had been selected for plasmid expression. Following clonal expansion, the knockout was validated by western blotting, PCR, Sanger sequencing and indel analysis, as described in this chapter.

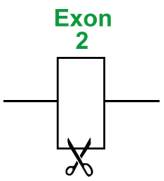
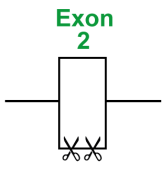
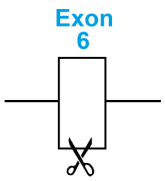
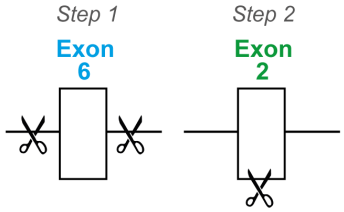
The combined activity of the exon 2-targeting sgRNA and DSB-generating Cas9 nuclease were expected to cause frameshift insertions or deletions (indels) as a result of NHEJ or MMEJ, and introduce a premature termination codon that would trigger nonsense-mediated mRNA decay (Popp et al., 2016). However, as detailed in the next section, this strategy yielded incomplete ZUP1 knockouts (**Fig. 3.3B**, **3.4B**). Although the efficiency of knocking out the primary ZUP1 isoform A was approximately 50% using the exon 2-targeting sgRNA #33, residual ZUP1 gene products were detected in most clones which could be truncated variants or splice isoforms. This was concerning as the residual ZUP1 protein may possess catalytic activity or cellular functions that could complicate phenotypic analysis.

The next ZUP1 knockout strategy utilised exon 6-targeting sgRNAs, with the rationale that the loss or mutation of exon 6 would disrupt the catalytic cysteine residue and therefore the DUB activity of ZUP1 isoforms (**Fig. 3.2A**). Using the same workflow as above, single sgRNAs were designed to target exon 6, however these were found to result in a low knockout efficiency where most clones were found to retain isoform A (**Fig. 3.5B**, **Appendix A: Fig. 4**).

To generate complete ZUP1 knockouts, a two-step approach was tested where a pair of intronic sgRNAs flanking exon 6 was first used to delete the entire exon (**Fig. 3.2A**). Single cell-derived clones were validated for exon 6 deletion and subjected to a second round of editing where exon 2 was targeted using a single sgRNA, which successfully eliminated the residual ZUP1 proteins (**Fig. 3.2A, 3.2B, 3.7A, 3.7B**).

The ZUP1 knockout strategies and outcomes are summarised in **Fig. 3.2**, and are described in more detail in the following section. The expression of multiple splice isoforms, truncated variants and the complex karyotype of the 293T cell line warranted multiple editing rounds and knockout validation methods to ensure the complete loss of ZUP1 in the ZUP1 knockout clones used for subsequent phenotypic assays in this thesis.

**A**

| Strategy | ΔZUP1_Ex2 | ΔZUP1_Ex2 | ΔZUP1_Ex6 | ΔZUP1_Ex6/2 |
|---|---|---|---|---|
| sgRNA(s) | • sgRNA #33 exon 2 | • sgRNA #11 exon 2<br>• sgRNA #23 exon 2 | • sgRNA #8 exon 6<br>• sgRNA #71 exon 6 | • sgRNA #2 exon 6<br>• sgRNA #3 exon 6<br>• sgRNA #33 exon 2 |
| Target site(s) |  |  |  |  |
| Outcome | Incomplete knockout | Incomplete knockout | Low knockout efficiency | High knockout efficiency (complete knockout) |

**B**

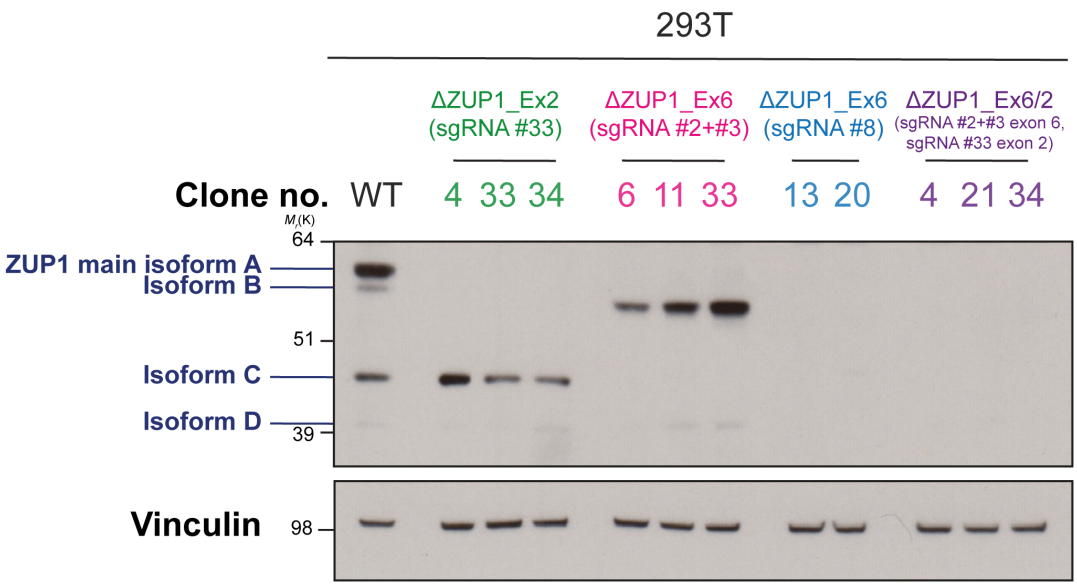



**Figure 3.2: CRISPR-Cas9 ZUP1 knockout strategies and outcomes.** A) Summary of ZUP1 knockout strategies, sgRNAs, targeted exons or sites (represented in a schematic showing the approximate locations of the targeted sequence within ZUP1)

and editing outcomes. The strategies are referred to as 'Ex2', 'Ex6' or 'Ex6/2' corresponding to the targeted ZUP1 exons, and these are preceded with 'ΔZUP1' when naming the single cell-derived clones edited with the indicated strategy. Ex6/2 refers to the targeting of exon 6 followed by exon 2 in two separate editing rounds. The purple bracket denotes the use of the sgRNAs as a pair. B) Representative single cell-derived clones generated from the indicated strategies. Shown are representative clones out of the following total number of clones screened: 34 (ΔZUP1_Ex2); 46 [ΔZUP1_Ex6 (sgRNA #2+#3)]; 35 [ΔZUP1_Ex6 (sgRNA #8)]; 28 (ΔZUP1_Ex6/2). Note that ΔZUP1_Ex6 (sgRNA #8) Clones 13 and 20 were the only two clones identified as complete ZUP1 knockouts using this strategy, and therefore do not reflect the actual low efficiency of the strategy as described in the later sections. This and subsequent Western blots in this chapter were assessed using the in-house ZUP1 antibody as described in the main text.

### 3.2.3 Validation of ZUP1 knockout in single cell-derived clones

To assess the efficiency of the paired sgRNAs designed to target exon 2, ZUP1 expression was first analysed in the edited 293T cell pool by Western blotting. After editing, cell lysates contained an abundant level of ZUP1 protein around the molecular weight of isoform D (**Fig. 3.3A**). The band directly above it may be the monoubiquitylated form, given that the band observed above isoform A in the wild-type cells was confirmed by other members of the lab to be monoubiquitylated ZUP1 using denaturing ubiquitin pull-down methods (data not shown). A faster-migrating band was also present at low levels in the edited pool.

The bands identified in the edited pool were confirmed to be ZUP1 gene products, as they were effectively silenced by a siRNA pool targeting ZUP1 (**Fig. 3.3A**). ZUP1 siRNAs also depleted a ~45 kDa protein expressed at low levels in single cell-derived U2OS clones that had previously been generated in the lab using a sgRNA targeting ZUP1 exon 2 (**Fig. 3.3A**). It is not known if the residual ~45 kDa ZUP1 protein in the

U2OS edited clones is functional or exerts any cellular roles, and these clones were considered ZUP1 hypomorphs given the incomplete knockout. The edited 293T pool was not taken forward for single cell cloning given the expression of residual ZUP1 variants, therefore alternative ZUP1 knockout approaches were explored instead.

The ~39 kDa residual ZUP1 protein in the edited 293T pool resembles isoform D at first glance, which may have upregulated its expression to compensate for the loss of the other isoforms (**Fig. 3.3A**). However, this would assume that isoform D is not one of the four isoforms reported on the databases since it appears to have escaped editing by sgRNAs targeting exon 2, which is present in all four reported isoforms (**Fig. 3.1B, 3.3A**). Alternatively, the sgRNAs may have generated a novel truncation of ZUP1, for example through in-frame exon skipping which has been demonstrated to arise from CRISPR-Cas9 editing (Lalonde et al., 2017; Mou et al., 2017; Tuladhar et al., 2019).

The next strategy utilised a single sgRNA to target exon 2, which resulted in the loss of ZUP1 isoform A at an efficiency of approximately 50% based on a Western blot screen of single cell-derived clones (**Fig. 3.3B**). However, faster-migrating ZUP1 proteins were detected in most clones. As speculated in the previous strategy, these proteins may be novel truncated variants or unedited isoforms. The latter may be applicable to isoforms C and/or D despite the slight mismatch in their molecular weights compared to the wild-type, possibly caused by the use of a wild-type protein sample that was prepared on a different day.

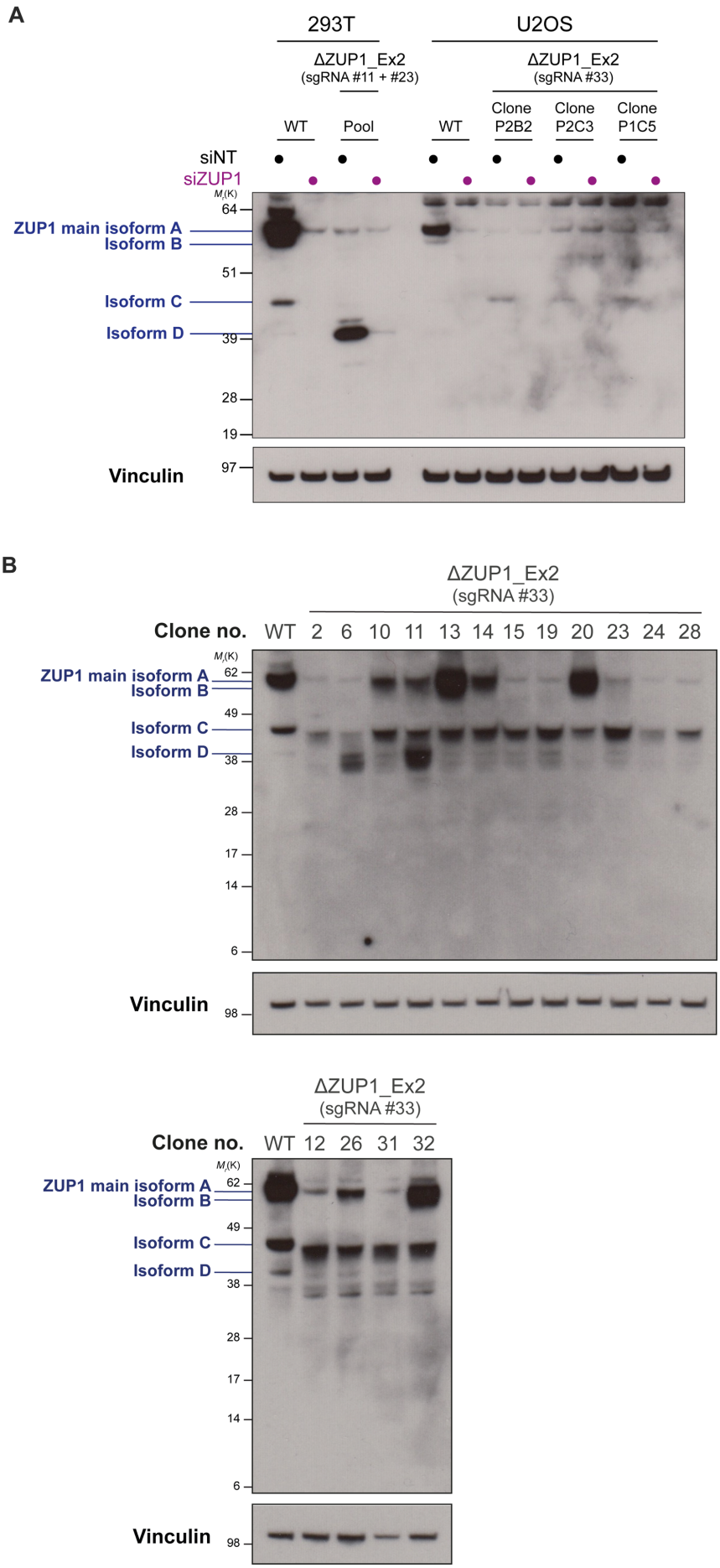
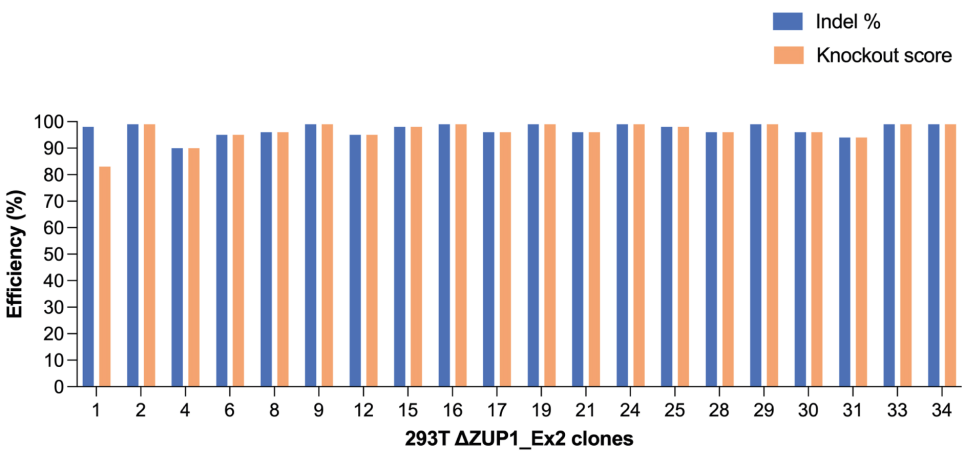

A
293T
U2OS
ΔZUP1_Ex2
(sgRNA #11 + #23)
ΔZUP1_Ex2
(sgRNA #33)
WT
Pool
WT
Clone P2B2
Clone P2C3
Clone P1C5
siNT
siZUP1
M,(K)
64
51
39
28
19
ZUP1 main isoform A
Isoform B
Isoform C
Isoform D
Vinculin
97
B
ΔZUP1_Ex2
(sgRNA #33)
Clone no.
WT 2 6 10 11 13 14 15 19 20 23 24 28
M,(K)
62
49
38
28
17
14
6
ZUP1 main isoform A
Isoform B
Isoform C
Isoform D
Vinculin
98
ΔZUP1_Ex2
(sgRNA #33)
Clone no.
WT 12 26 31 32
M,(K)
62
49
38
28
17
14
6
ZUP1 main isoform A
Isoform B
Isoform C
Isoform D
Vinculin
98

**Figure 3.3: Residual ZUP1 proteins were detected in cells edited using paired or single sgRNAs targeting exon 2.** A) 293T wild-type cells were edited using paired ZUP1 exon 2-targeting sgRNAs, then selected with puromycin and recovered for a week. The edited cell pool was transfected with a non-targeting (siNT) or ZUP1-targeting (siZUP1) siRNA pool. The siRNA transfection was also performed in WT cells as the control. ZUP1 siRNA knockdown was also performed in the indicated independent U2OS single cell-derived clones previously edited using a single sgRNA targeting ZUP1 exon 2 (Appendix A: Fig. 5). B) Western blot analysis of single cell-derived clones edited using a single sgRNA targeting ZUP1 exon 2. Note that the WT sample was prepared on a different day from the clones in these blots, which may have affected migration patterns. Shown are representative clones out of 34 clones screened in total.

From the Western blotting analysis in **Fig. 3.3B**, the clones that seemed to have lost ZUP1 isoform A were brought forward for further assessment. The method for validating exon 2 loss involved PCR amplification of the edited exon followed by Sanger sequencing and analysis using the Interference of CRISPR Edits (ICE) software. ICE compares the Sanger sequencing traces of the wild-type and edited sample, generates a profile of the type and relative proportion of frameshift-causing indels, and finally calculates the overall editing efficiency (Hsiau et al., 2019). Briefly, the algorithm predicts editing outcomes based on the sgRNA target sequence, and the predictions are fitted to the sequence data using linear regression. The indel percentage represents the percentage of traces containing any indels within the targeted sequence, whether or not they induce frameshifts. The knockout score denotes the proportion of traces containing frameshift-inducing indels or ≥ 21 base pair (bp) indels. Here, it is important to consider that the scoring of editing efficiency favours mutations that strictly match the predicted indels, which can limit interpretations, as discussed later for **Fig. 3.5D**.

The exon 2 region was PCR amplified in the clones shortlisted from the representative blots in **Fig. 3.3B** and other blots not included in the figure. ICE analysis revealed a high indel percentage and knockout score for most clones, and none were found to contain the wild-type sequence, suggesting complete exon 2 loss (**Fig 3.4A**). The indel profiles differed substantially between clones and displayed homozygosity, heterozygosity, diploidy, or polyploidy. The heterozygous editing outcomes are in line with the well-established concept that CRISPR-mediated DSB induction can lead to diverse editing outcomes and generate a mixed population with unequal allele sequences, as summarised in the Discussion (Kosicki et al., 2018; Adikusuma et al., 2018; Xia et al., 2020). As demonstrated later in this section, this could be further complicated by the complex karyotype of the 293T cell line. Clones that were assigned high knockout scores were nevertheless considered incomplete ZUP1 knockouts due to the expression of faster-migrating ZUP1 proteins (**Fig. 3.4B**).

A




| ΔZUP1_Ex2 clone no. | Indel contribution | Model fit ($R^2$) | Presence of WT sequence |
|---|---|---|---|
| **1** | +1 (83%), -3 (11%), -3 (4%) | 0.98 | None |
| **2** | +1 (99%) | 0.99 | None |
| **4** | +1 (30%), -10 (30%), -2 (17%), -2 (13%) | 0.90 | None |
| **6** | -23 (47%), -28 (42%), -28 (6%) | 0.95 | None |
| **8** | +1 (71%), -22 (14%), -22 (11%) | 0.96 | None |
| **9** | +1 (99%) | 0.99 | None |
| **12** | -4 (33%), -2 (33%), +1 (29%) | 0.95 | None |
| **15** | +1 (86%), -5 (12%) | 0.98 | None |
| **16** | +1 (99%) | 0.99 | None |
| **17** | -22 (39%), -22 (29%), +1 (25%), -22 (3%) | 0.96 | None |
| **19** | +1 (99%) | 0.99 | None |
| **21** | +1 (70%), -2 (26%) | 0.96 | None |
| **24** | +1 (99%) | 0.99 | None |
| **25** | +1 (82%), -20 (16%) | 0.98 | None |
| **28** | +1 (96%) | 0.96 | None |
| **29** | +1 (99%) | 0.99 | None |
| **30** | +1 (75%), -8 (21%) | 0.96 | None |
| **31** | +1 (56%), -10 (18%), -4 (15%), -4 (5%) | 0.94 | None |
| **33** | +1 (99%) | 0.99 | None |
| **34** | +1 (99%) | 0.99 | None |

B

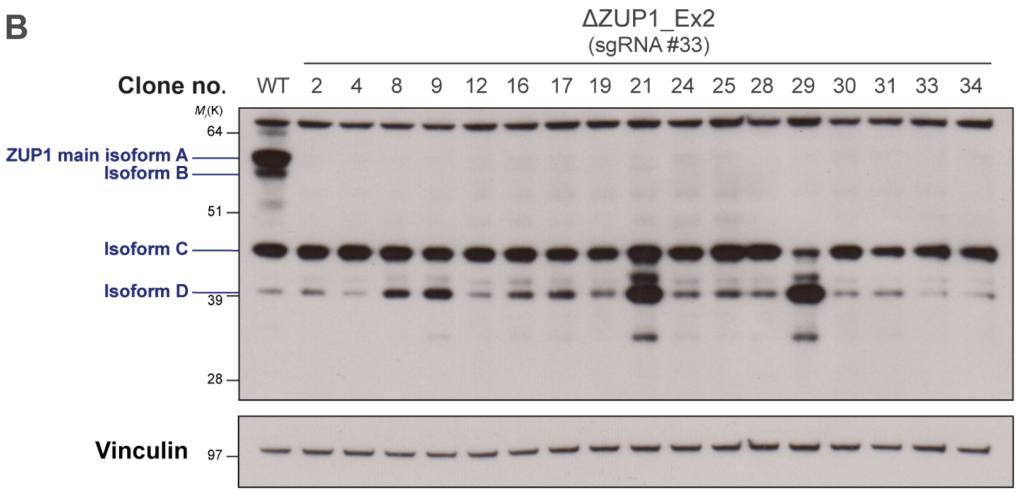


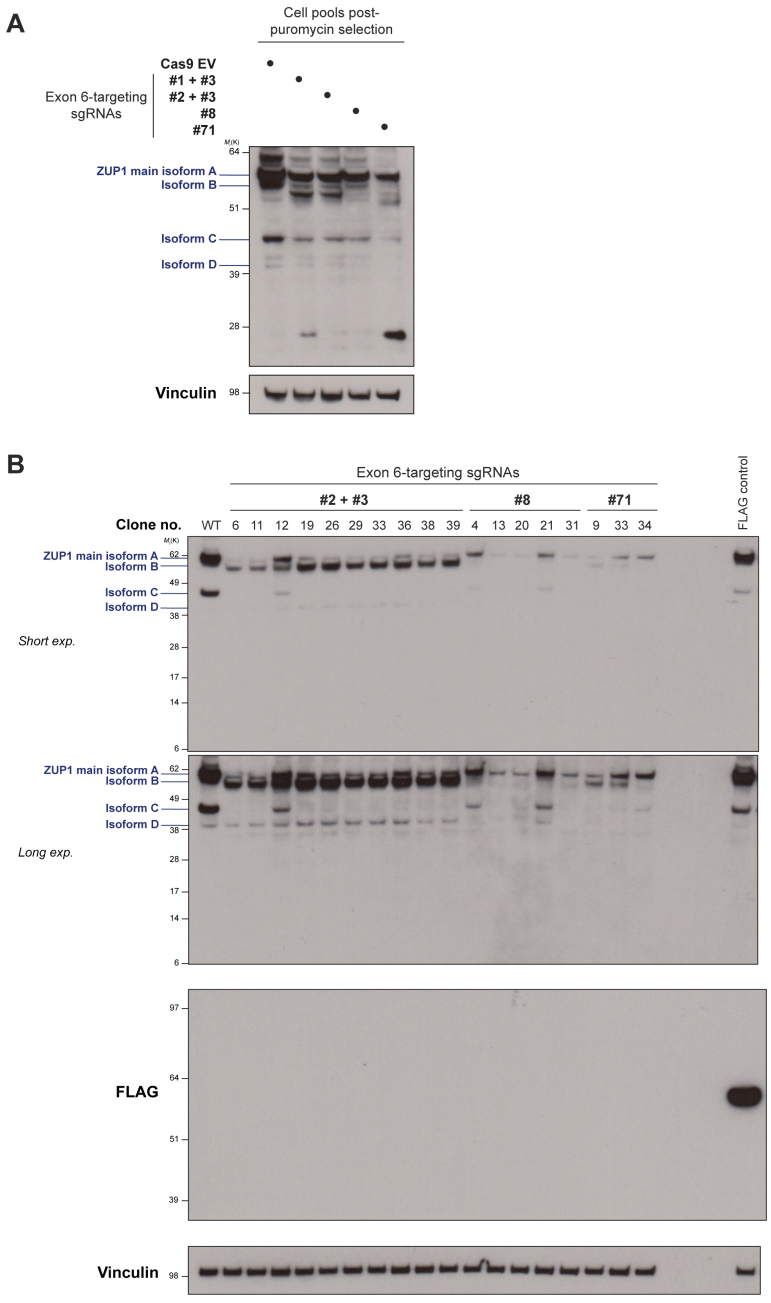
**Figure 3.4: Analysis of frameshift-inducing indel formation and ZUP1 protein loss in 293T clones edited using a single sgRNA targeting exon 2.** A) ICE analysis of clones shortlisted from Fig. 3.3B. Definitions for indel % and knockout score are described in the main text above (Hsiau et al., 2019). Model fit ($R^2$) is a goodness-of-fit measure for how closely the ICE prediction of indels fit the Sanger sequencing data of the edited sample. B) Western blot analysis of the clones analysed in A.

Another strategy involved sgRNAs that were designed to target ZUP1 exon 6, with the aim of disrupting the catalytic cysteine residue encoded by this exon and therefore DUB activity (**Appendix A: Fig. 2, 3**). After editing cells with a single exon 6-targeting sgRNA, isoform A was still abundant in the cell pools indicating a low efficiency of nonsense-mediated mRNA decay (**Fig. 3.5A**). Indeed, single cell-derived clones edited using this strategy displayed a low overall knockout efficiency (**Appendix A: Fig. 4**). However, a handful of clones were genotyped further as they seemed to have lost ZUP1 expression based on the undetectable ZUP1 protein levels (**Fig. 3.5B**).

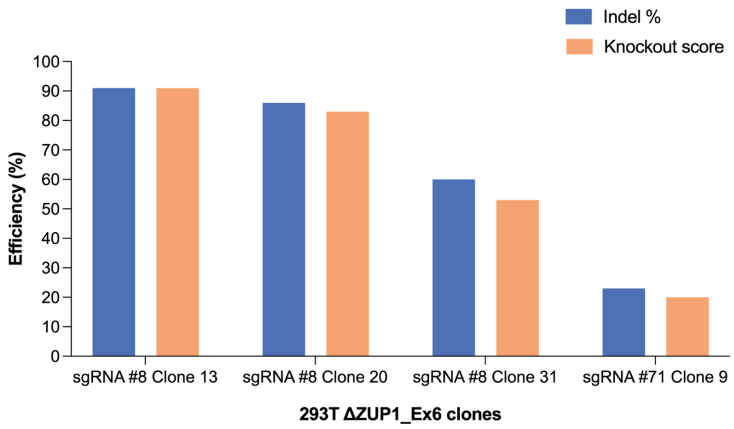
To validate the mutation of exon 6, a fragment containing exon 6 was amplified, Sanger sequenced and analysed by ICE. The indel profile of Clone 13 indicates a tetraploid population in which each allele contains a different indel (**Fig. 3.5C**). The high scores assigned by ICE, together with the absence of ZUP1 protein in Clone 13, support the claim that Clone 13 may be a complete ZUP1 knockout (**Fig. 3.5B, 3.5C**). The low overall knockout efficiency resulting from the single sgRNA targeting exon 6 suggests that although exon 6 is common to all reported isoforms as shown in **Fig. 3.1B**, the target site within the exon may not favour effective nonsense-mediated mRNA decay (**Appendix A: Fig. 4**).

Clone 9 did not score highly despite the absence of the wild-type sequence (**Fig. 3.5C**). Amplification of the exon 6 region for this clone resulted in multiple bands of varying lengths (**Fig. 3.5D**). This demonstrates allele diversity, in which some contain

large insertions or deletions as indicated by two notably large and small amplicon sizes. One limitation of the ICE software is that the indel limits are set at 30 bp for deletions, and 14 bp for insertions (Hsiau et al., 2019). Given that the algorithm predicts a limited number of edits based on the input sgRNA sequence, the large indels generated within exon 6 of Clone 9 may not match the ICE predictions, despite potentially causing frameshifts and exon 6 loss. The deviation of these large indels from the ICE predictions may have reduced the goodness of fit ($R^2$). If Clone 9 was truly a knockout, this provides a note of caution that ICE scores may not accurately reflect knockout efficiency when complex edits are involved.



C




| ΔZUP1_Ex6 clone no. | Indel contribution | Model fit ($R^2$) | Presence of WT sequence |
|---|---|---|---|
| **sgRNA #8 Clone 13** | +1 (25%), -10 (24%), +10 (21%), -8 (21%) | 0.91 | None |
| **sgRNA #8 Clone 20** | -28 (29%), +1 (25%), -7 (16%), -7 (11%), -9 (3%), -19 (2%) | 0.86 | None |
| **sgRNA #8 Clone 31** | -1 (34%), -1 (13%), 0 (8%), -12 (3%), other (<3%) | 0.68 | Yes |
| **sgRNA #71 Clone 9** | -4 (7%), -16 (3%), -4 (3%), -22 (2%), other (<3%) | 0.23 | None |

D

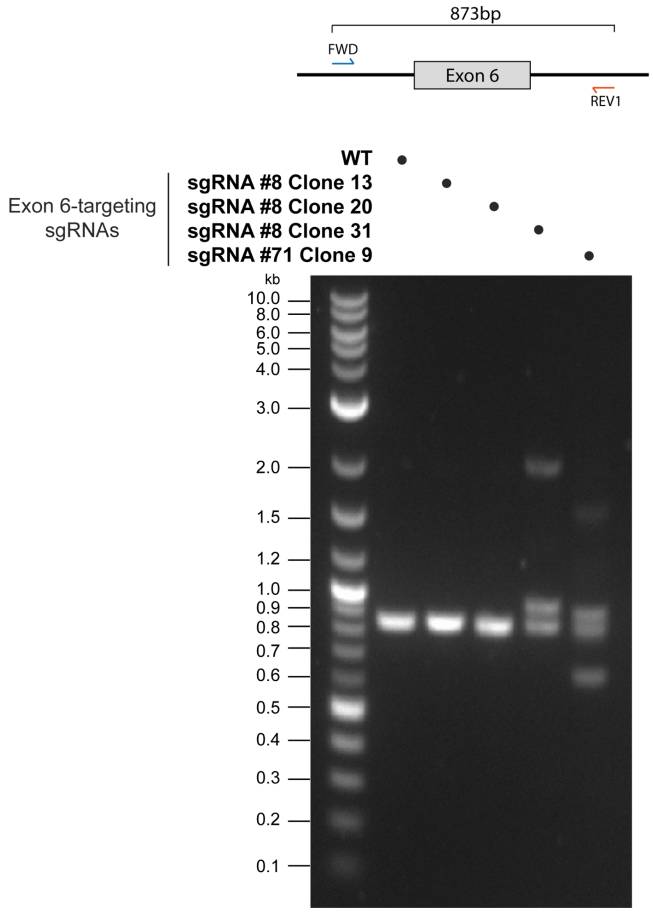


**Figure 3.5: Editing outcomes in clones edited with sgRNA(s) targeting ZUP1 exon 6.** A) Analysis of ZUP1 protein levels in cell pools after cells were edited using the indicated single or paired exon 6-targeting sgRNAs, and selected in puromycin. B) Western blot analysis of single cell-derived clones edited using the indicated sgRNAs targeting exon 6. Shown are representative clones out of the following total number of clones screened: 46 [ΔZUP1_Ex6 (sgRNA #2+#3)]; 35 [ΔZUP1_Ex6 (sgRNA #8)]; 28 (ΔZUP1_Ex6/2). C) ICE analysis of potential ZUP1 knockout clones identified in B that had been edited using the indicated single exon 6-targeting sgRNAs. D) PCR products resulting from the amplification of a 873 bp region containing exon 6 from the genomic DNA of the indicated clones.

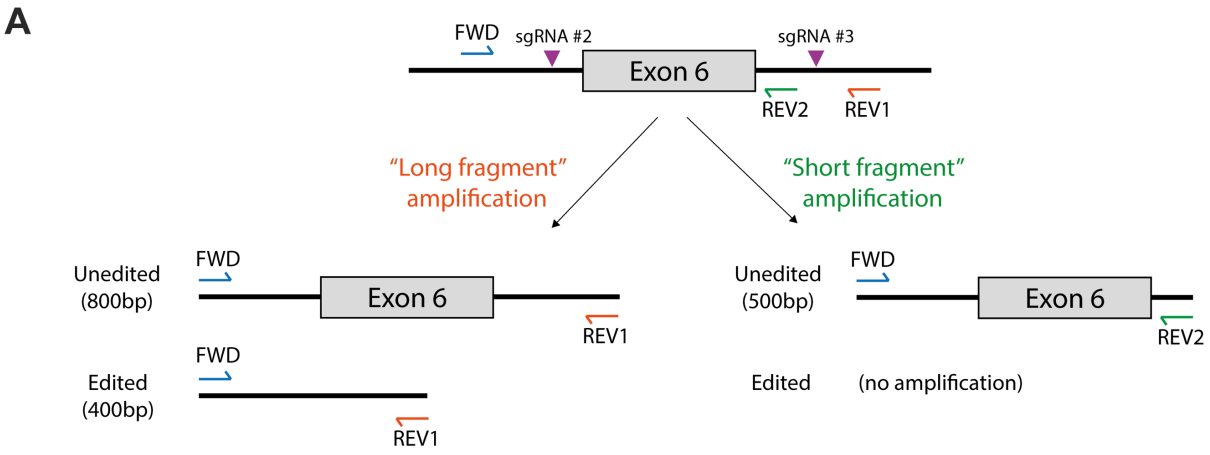
Paired intronic sgRNAs flanking exon 6 were also designed to delete a ~600 bp (sgRNAs #1 + #3) or ~450 bp (sgRNAs #2 + #3) region spanning exon 6 and the immediate surrounding introns (**Fig. 3.5A, Appendix A: Fig. 2**). To genotype single cell-derived clones edited using the latter sgRNA pair, two sets of primers were designed to amplify the targeted exon 6 region, yielding two different fragment sizes of ~800 bp ('long fragment') and ~500 bp ('short fragment') in unedited or wild-type cells (**Fig. 3.6A**). The size of the PCR products discriminate the edited from unedited samples due to the binding site of the reverse primers relative to the Cas9 cleavage site. The deletion of exon 6 by the paired sgRNAs is identified by a ~400 bp long fragment and an unamplified short fragment (**Fig. 3.6A, 3.6B**). For example, the band patterns of Clone 11 in **Fig. 3.6B** indicate that exon 6 is deleted in all alleles.

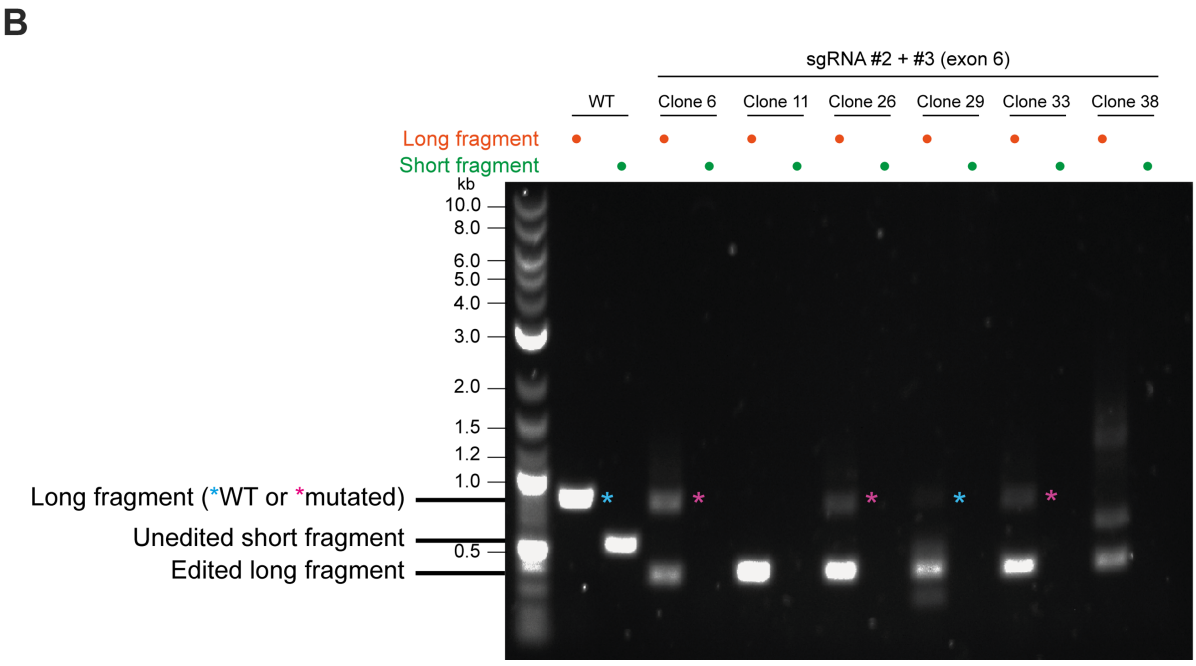
The PCR products would migrate as multiple bands if heterozygous edits have occurred and resulted in mixed alleles (**Fig. 3.6B**). Two distinct bands were observed in some clones when the long fragment was amplified, the larger of which had the same size as the unedited long fragment. While this reflected a mixture of unedited and edited alleles, it was puzzling that the short fragment, which should be intact in unedited alleles, was not amplified in three of these clones. This lack of amplification indicates the inactivation of the REV2 reverse primer binding site, which would be

expected of clones that had lost exon 6 such as Clone 11 (**Fig. 3.6A, B**). It was thus unclear why the long fragment amplicon was present in some clones indicating unedited alleles, while the short fragment primers failed to amplify across exon 6 in these same clones.

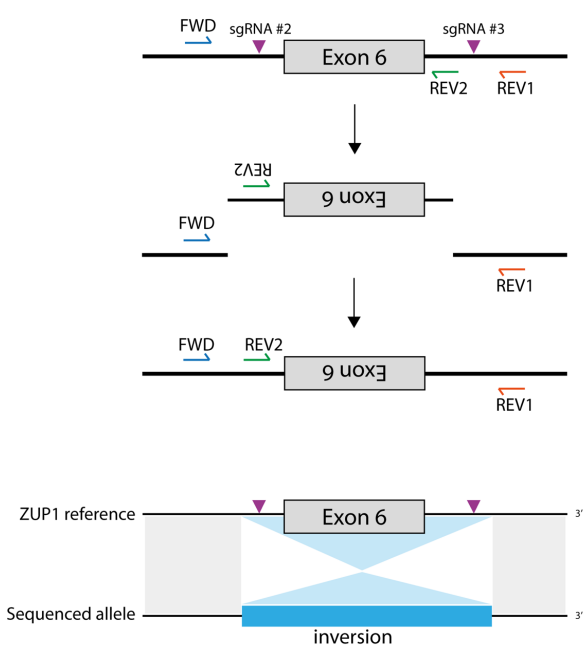
To clarify the ambiguous nature of these edits, the CRISPR-Cas9 machinery was re-visited and other complex repair outcomes were considered. Given that the aforementioned clones retained the length of the exon 6 fragment whilst lacking the exon itself, it was considered whether an inversion mutation of exon 6 may have occurred during the repair of the Cas9-induced DSBs. A possible scenario is the re-insertion of the excised exon 6 region into targeted site, in an inverted orientation (**Fig. 3.6C**). This would maintain the size of the 'long fragment' amplicon, but cause a mutation of exon 6 that would prevent binding of the reverse primer REV2 to the reverse strand (**Fig. 3.6A**).

If the excised fragment had re-integrated into the targeted genome in this manner, the new binding position of the reverse primer REV2 would assume the orientation of a forward primer (**Fig. 3.6C**). PCRs were therefore performed using REV2 as the forward primer, along with REV1 as the reverse primer. This revealed that the inverted fragment was indeed amplified in some ambiguous clones, in contrast to the wild-type and homozygous Clone 11 which served as negative controls (**Fig. 3.6D**). The inversion of the excised exon 6 fragment was confirmed in the 800 bp 'long fragment' amplicons of three clones by Sanger sequencing. Although this inversion mutation may have resulted in the desired loss of the catalytic cysteine, it cannot be excluded it may have produced neomorphic mutations of ZUP1, leading to novel functions. The homozygous Clone 11 was therefore selected instead for a second round of ZUP1 editing (by targeting exon 2) in the next strategy since exon 6 was confirmed to be deleted across all alleles in Clone 11.

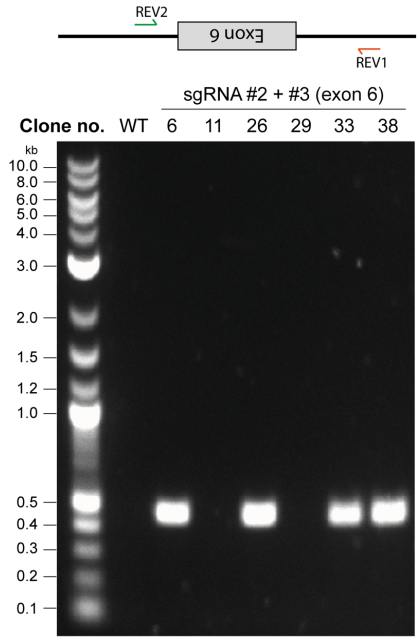

A
FWD
sgRNA #2
sgRNA #3
Exon 6
REV2
REV1
"Long fragment" amplification
"Short fragment" amplification
Unedited (800bp)
FWD
Exon 6
REV1
Edited (400bp)
FWD
REV1
Unedited (500bp)
FWD
Exon 6
REV2
Edited
(no amplification)


B
sgRNA #2 + #3 (exon 6)
WT
Clone 6
Clone 11
Clone 26
Clone 29
Clone 33
Clone 38
Long fragment
Short fragment
kb
10.0
8.0
6.0
5.0
4.0
3.0
2.0
1.5
1.2
1.0
0.5
Long fragment (*WT or *mutated)
Unedited short fragment
Edited long fragment

C




D




| Clone no. (sgRNA #2 + #3, exon 6) | 'Long fragment' (FWD + REV1) | 'Short fragment' (FWD + REV2) | Inverted exon 6 (REV2 + REV1) | Conclusion |
|---|---|---|---|---|
| WT | 800bp<br>Sequence: WT | 500bp | Not amplified | Unedited |
| 6 | 800bp, 400bp<br>800bp sequence: Inversion | Not amplified | Amplified | Heterozygous edit: Exon 6 deletion; inversion |
| 11 | 400bp | Not amplified | Not amplified | Homozygous edit: Exon 6 deletion |
| 26 | 800bp, 400bp<br>800bp sequence: Inversion | Not amplified | Amplified | Heterozygous edit: Exon 6 deletion; inversion |
| 29 | 800bp, 400bp<br>800bp sequence: WT. | Not amplified/ undetected | Not amplified | Heterozygous edit: WT; exon 6 deletion |
| 33 | 800bp, 400bp<br>800bp sequence: Inversion | Not amplified | Amplified | Heterozygous edit: Exon 6 deletion; inversion |
| 38 | 400bp, multiple higher MW bands | Not amplified | Amplified | Heterozygous edit: Exon 6 deletion; inversion with possible additional insertions/deletions |

**Figure 3.6: PCR genotyping of clones edited using paired intronic sgRNAs flanking exon 6.** A) Schematic of PCR setup to amplify the 'long' or 'short' fragments that discriminate the unedited samples from those in which exon 6 has been deleted. The grey box denotes exon 6 while the horizontal line represents the immediate flanking introns. The purple arrows denote Cas9 cleavage sites as guided by the indicated sgRNAs. FWD = forward primer; REV = reverse primer. B) Amplification of the 'long' or 'short' fragments in single cell-derived clones edited using the indicated paired sgRNAs. C) Schematic depicting the possible phenomenon in which the excised exon 6 fragment re-integrates into the targeted genome, causing an inversion mutation. D) Top: Identification of inverted exon 6 sequence in the clones by PCR amplification using the indicated primers, where REV2 was used as the forward primer and REV1 was used as the reverse primer. Bottom: Summary of genotyping results including the Sanger sequencing data of the amplified 'long fragment'. The column headers refer to the fragments amplified by PCR using the primer pair indicated in brackets.

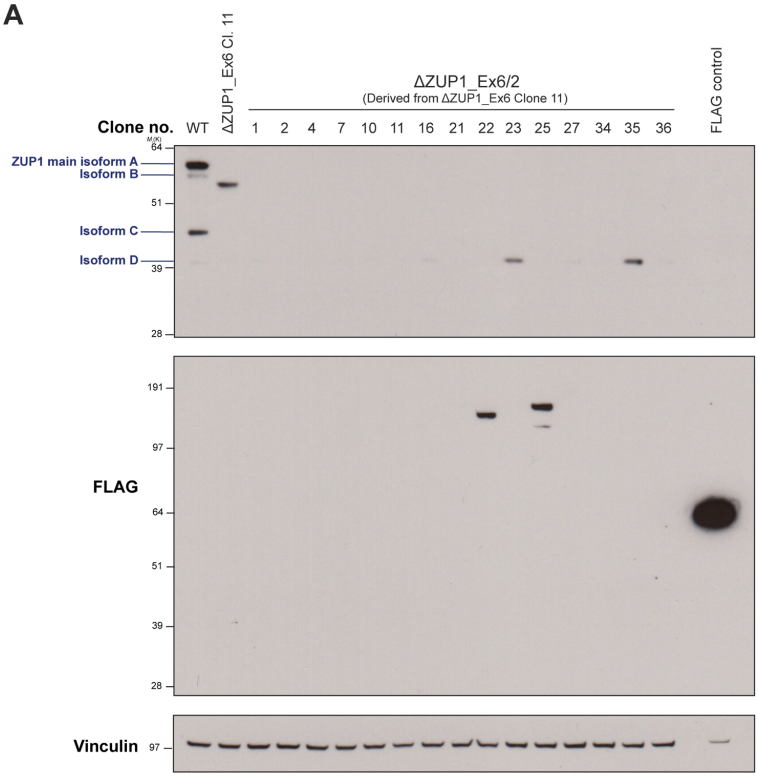
The most effective strategy identified for knocking out ZUP1 involved two separate rounds of editing and clonal expansion. 293T ΔZUP1_Ex6 Clone 11, generated from the previous exon 6 deletion approach in **Fig. 3.6**, was assumed not to express any enzymatically active ZUP1 protein due to the homozygous deletion of exon 6 (**Fig. 3.6B, 3.6D**). This clone was therefore selected for the subsequent editing round in which a single sgRNA targeting exon 2 was used to remove the residual ZUP1 protein and generate complete ZUP1 knockouts.

Following the derivation of single cell-derived clones using this strategy, the loss of ZUP1 protein in the clones was examined by Western blotting (**Fig. 3.7A**). The exon 2 region was sequenced and analysed by ICE to assess frameshift-inducing indels (**Fig. 3.7B**). In the panel of clones screened, some were heterozygously-edited where their indel proportions reflect diploidy or polyploidy. This testifies to the reported karyotype complexity of the 293T cell line, as described further in the Discussion

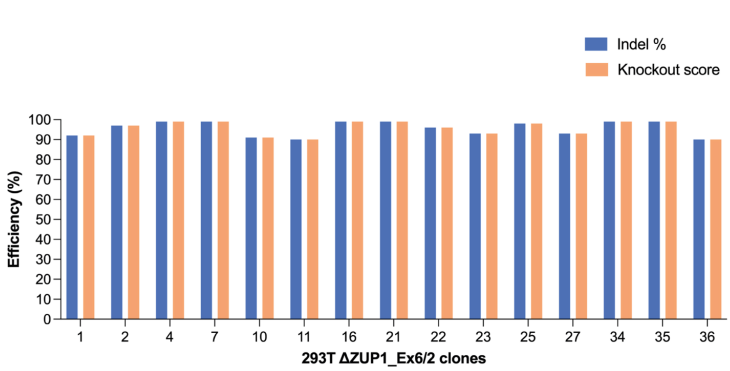
(Cullot et al., 2019). The clones selected for subsequent phenotypic analysis in Chapter 5 include 293T ΔZUP1_Ex6/2 Clones 4 and 21 which had high knockout scores and $R^2$ values, and contain the same indel across all alleles.

Despite the transient transfection setup, two clones were found to express FLAG which was tagged in the sgRNA/Cas9 vector, indicating random and stable integration of the vector (**Fig. 3.7A**). These clones were discarded due to potential constitutive Cas9 expression, gene disruption at the integration sites and/or off-target effects. Random integration of the vector may have also allowed promoter-driven expression of the antibiotic selection marker, a likely reason for the selection of some 'false positive' antibiotic-resistant ZUP1 knockout clones.

A




B




| ΔZUP1_Ex6/2 clone no. | Indel contribution | Model fit ($R^2$) | Presence of WT sequence |
|---|---|---|---|
| **1** | +1 (86%), +5 (5%), -13 (1%) | 0.92 | None |
| **2** | +1 (70%), -10 (27%) | 0.97 | None |
| **4** | +1 (99%) | 0.99 | None |
| **7** | +1 (99%) | 0.99 | None |
| **10** | +1 (30%), -4 (27%), -10 (27%), -4 (4%), -10 (3%) | 0.91 | None |
| **11** | +2 (31%), +1 (31%), -5 (28%) | 0.90 | None |
| **16** | +1 (99%) | 0.99 | None |
| **21** | +1 (99%) | 0.99 | None |
| **22** | +1 (46%), -2 (44%), -2 (6%) | 0.96 | None |
| **23** | -4 (43%), -23 (40%), -23 (5%), other (<5%) | 0.93 | None |
| **25** | -2 (98%) | 0.98 | None |
| **27** | +1 (66%), -25 (27%) | 0.93 | None |
| **34** | +1 (99%) | 0.99 | None |
| **35** | +1 (99%) | 0.99 | None |
| **36** | +1 (31%), -5 (27%), -1 (25%), -1 (7%) | 0.90 | None |

**Figure 3.7: Assessment of ZUP1 loss in single cell-derived clones generated by targeting exon 2 within ΔZUP1_Ex6 Clone 11.** A) Western blot analysis of single cell-derived clones generated by the ΔZUP1_Ex6/2 strategy. A FLAG-expressing control, which is 293T wild-type cells over-expressing FLAG-ZUP1, served a positive control for FLAG expression. Shown are representative clones out of 28 clones screened in total. B) ICE analysis of the clones assessed in A.

### 3.2.4 ZUP1 knockouts are sensitive to replication stress induced by genotoxic agents

The above sections describe the generation of ZUP1 knockouts in the 293T cell line which were used for the assays presented in Chapter 5. The clonogenic survival assays shown in the remaining sections of this chapter were performed in U2OS ZUP1 knockout cells instead, given that it is a widely used cancer cell line for assessing DNA damage and repair. U2OS is an osteosarcoma cell line that has high transfection efficiency and is extensively used in the DNA repair field for immunofluorescence and imaging studies, clonogenic survival and other DNA repair or replication assays. U2OS ZUP1 knockout cells were generated by others in the Gibbs-Seymour lab by first targeting the ZUP1 gene at exon 2. A validated clone was taken forward for a second round of editing where exon 6 was deleted using paired sgRNAs as described for the 293T cell line (**Appendix A: Fig. 5**). To identify the DNA repair pathway(s) that ZUP1 is involved in, the clonogenic survival of U2OS wild-type and ZUP1 knockout cells was assessed by exposing cells to genotoxic agents that activate various repair pathways (Franken et al., 2006; **Fig. 3.8**). Given that the phenotypes in Chapter 5 were observed in 293T ZUP1 knockouts, it would be important for future work to also assess the clonogenic survival of 293T ZUP1 knockouts to this panel of genotoxic agents.

Among the genotoxic agents assessed in the clonogenic survival assays is mitomycin C (MMC), which is reductively activated upon entering the cell and utilises its alkylating function to react with the exocyclic amino group of deoxyguanosine to form monoadducts with DNA (Tomasz et al. 1987; Bizanek et al., 1992). MMC generates intrastrand crosslinks between adjacent bases in the same strand, and interstrand crosslinks between complementary DNA strands (Iyer et al., 1963). Interstrand crosslinks (ICLs) induce replication stress and engage the Fanconi Anemia pathway to prevent accumulation of the lesion (Chapter 1, Section 1.6.3).

Olaparib is a PARP inhibitor used in the treatment of HR-deficient tumours such as BRCA1/BRCA2-mutant ovarian and breast cancers based on the synthetic lethal interaction between PARP inhibition and BRCA deficiency (Chapter 1, Section 1.2.5). In addition to the catalytic inhibition of PARP, PARP inhibitors cause PARP trapping onto DNA, and the stabilisation of PARP-DNA complexes was suggested to be an important determinant of PARP inhibitor toxicity (Murai et al., 2012). It was later demonstrated that PARP inhibitors markedly increase replication fork elongation speed which results in replication stress (Maya-Mendoza et al., 2018). Recently, it was shown that BRCA1-deficient cells treated with PARP inhibitors have higher levels of exposed lagging strand ssDNA gaps resulting from defective Okazaki fragment processing. This phenomenon was proposed to exhaust RPA pools and contribute to PARP inhibitor synthetic lethality (Cong et al., 2021). Talazoparib is another PARP inhibitor that inhibits PARP catalytic activity at a potency comparable to olaparib but is ~100-fold more efficient in trapping PARP onto the DNA (Murai et al., 2014). Olaparib and talazoparib were tested in the clonogenic assays to assess if the potent PARP trapping effect reported for talazoparib may create a greater dependence of cells on ZUP1 for survival.

Topotecan is a topoisomerase I (TOP1) inhibitor that generates toxic DNA-protein crosslinks (DPCs) (Pommier et al., 2009). TOP1 forms a transient covalent intermediate with DNA when the catalytic tyrosine attacks the DNA phosphate group. TOP1 relieves DNA torsional stress and introduces a single-strand break to allow controlled rotation of the free DNA strand (Stewart et al., 1998; Pommier et al., 2016).

TOP1 cleavage complexes are removed by tyrosyl-DNA phosphodiesterases, structure-specific endonucleases and DPC proteases such as SPRTN (Kühbacher et al., 2020; Sun et al., 2020). Topotecan prevents the removal of TOP1 and traps it onto the DNA, forming persistent DPCs and replication stress (Pommier et al., 2009).

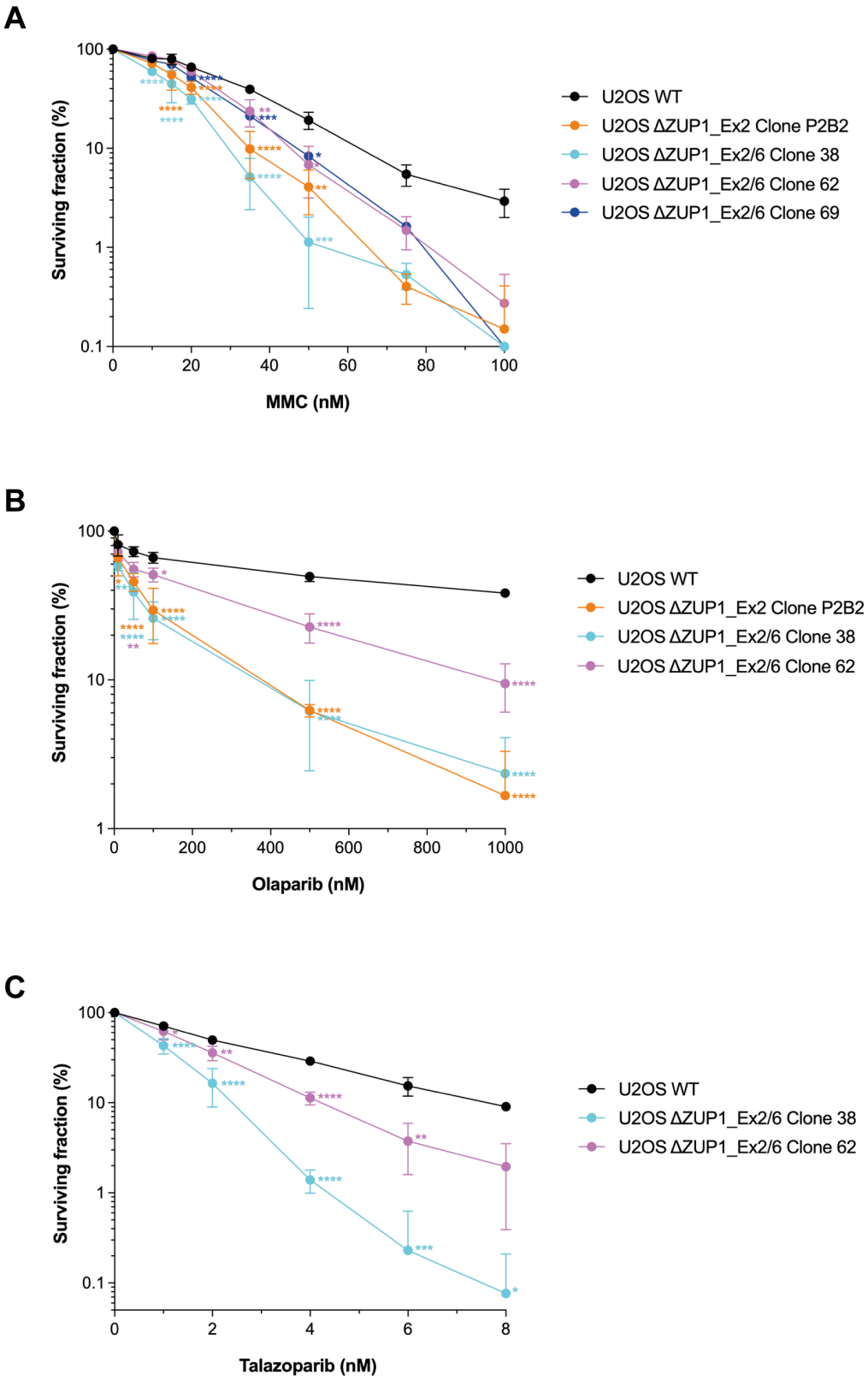
AZD6738 was also included in the panel of genotoxic compounds assessed in clonogenic assays, as it is an inhibitor of ATR, which has a key role in modulating the replication stress response and DNA damage checkpoints (Yazinski et al., 2016; Foote et al., 2018). As described in Chapter 1, one important function of ATR during replication stress is to limit origin firing through the CHK1 kinase. Toledo et al. showed that ATR deficiency leads to unscheduled origin firing, excessive levels of ssDNA which exhausts the nuclear RPA pool, and irreversible nucleus-wide fork breakage (Toledo et al., 2013).

Compared to the wild-type, ZUP1 knockouts were found to be significantly more sensitive to MMC, olaparib, talazoparib, topotecan and AZD6738 (**Fig. 3.8A-E**). This suggests that ZUP1 may have an important role in a common pathway that repairs DNA lesions generated by these genotoxic compounds. When the replication machinery encounters such lesions, or repair intermediates, forks can stall and collapse into DSBs if they do not undergo timely repair or restart (Chapter 1, Section 1.2.4; Berti et al., 2016). To further investigate the DNA repair function of ZUP1, the potential substrates of ZUP1 and its role in HR repair were explored in Chapter 5. Other members of the lab have shown that the MMC sensitivity phenotype in ZUP1 knockout cells can be rescued by the stable re-expression of ZUP1 (data not shown). To confirm the dependence of the other drug hypersensitivity phenotypes on ZUP1, it would be essential for future work to examine the rescue ability of ZUP1 for the complete panel of genotoxic agents tested in **Fig. 3.8**.

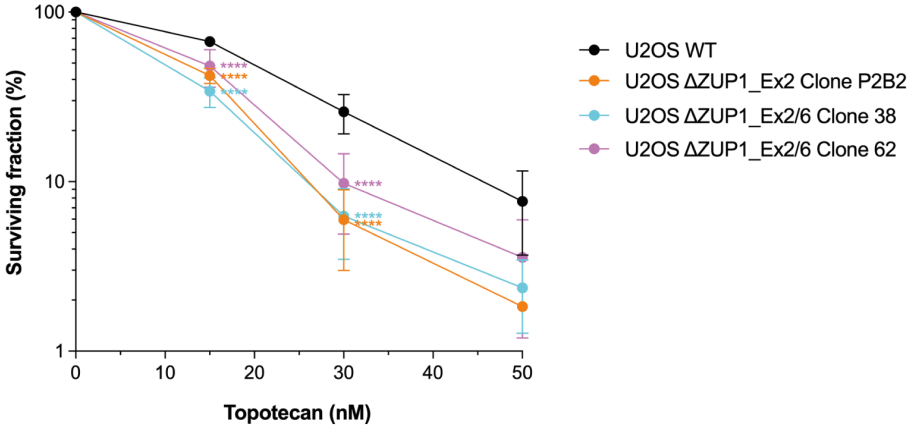
It was previously reported that talazoparib is approximately 100-fold more efficient at trapping PARP-DNA complexes compared to olaparib (Murai et al., 2014). ZUP1 knockouts demonstrate hypersensitivity to both olaparib and talazoparib treatments (**Fig. 3.8B, C**). Relative to the wild-type, the survival defects of ZUP1 knockouts

treated with talazoparib were not more dramatic than that of ZUP1 knockouts treated with olaparib. Based on this observation, it is reasonable to speculate that the PARP trapping effect of PARP inhibitors may not play a major role in PARP inhibitor hypersensitivity in ZUP1 knockouts. As described above, other reported effects of PARP inhibition are potentially more important for the phenotype (Maya-Mendoza et al., 2018; Cong et al., 2021).

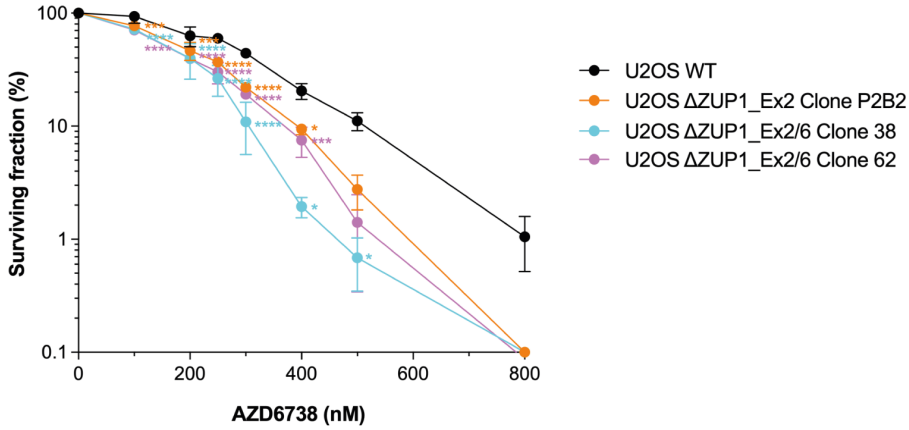
The only compound in the panel to which ZUP1 loss did not confer additional sensitivity is hydroxyurea (**Fig. 3.8F**). Hydroxyurea inhibits ribonucleotide reductase, the enzyme responsible for catalysing the conversion of ribonucleotides to deoxyribonucleotides (Krakoff et al., 1968). In human cells, a 30-minute hydroxyurea treatment induces fork slowdown (at 50 μM) and stalling (at 1 mM), and also alters cellular metabolism by increasing reactive oxygen species (ROS) levels (at 50 μM) (Somyajit et al., 2017). The generation of hydroxyl radicals in *E. coli* upon hydroxyurea treatment was shown to be a major contributor to hydroxyurea-induced cytotoxicity (Davies et al., 2009). Given that cells were treated with up to 30 mM hydroxyurea for 24 hours in the clonogenic assays shown in **Fig. 3.8F**, it is likely that ROS may have accumulated to levels that cause DNA damage by inducing base oxidation, as previously reported. Cells rely on base excision repair and mismatch repair pathways to prevent the incorporation of oxidised bases into DNA (Nakabeppu et al., 2014). As ZUP1 knockout cells did not exhibit additional sensitivity to hydroxyurea compared to the wild-type, it is possible that ZUP1 may not play a major role in the repair of ROS-induced DNA damage upon hydroxyurea treatment. This is in contrast to DNA lesions generated by the other five genotoxic compounds tested that potentially require ZUP1 for efficient repair, as described above.


A
Surviving fraction (%)
MMC (nM)
U2OS WT
U2OS ΔZUP1_Ex2 Clone P2B2
U2OS ΔZUP1_Ex2/6 Clone 38
U2OS ΔZUP1_Ex2/6 Clone 62
U2OS ΔZUP1_Ex2/6 Clone 69
B
Surviving fraction (%)
Olaparib (nM)
U2OS WT
U2OS ΔZUP1_Ex2 Clone P2B2
U2OS ΔZUP1_Ex2/6 Clone 38
U2OS ΔZUP1_Ex2/6 Clone 62
C
Surviving fraction (%)
Talazoparib (nM)
U2OS WT
U2OS ΔZUP1_Ex2/6 Clone 38
U2OS ΔZUP1_Ex2/6 Clone 62

**D**


100
10
1
Surviving fraction (%)
0
10
20
30
40
50
Topotecan (nM)
U2OS WT
U2OS ΔZUP1_Ex2 Clone P2B2
U2OS ΔZUP1_Ex2/6 Clone 38
U2OS ΔZUP1_Ex2/6 Clone 62

**E**


100
10
1
0.1
Surviving fraction (%)
0
200
400
600
800
AZD6738 (nM)
U2OS WT
U2OS ΔZUP1_Ex2 Clone P2B2
U2OS ΔZUP1_Ex2/6 Clone 38
U2OS ΔZUP1_Ex2/6 Clone 62

**F**

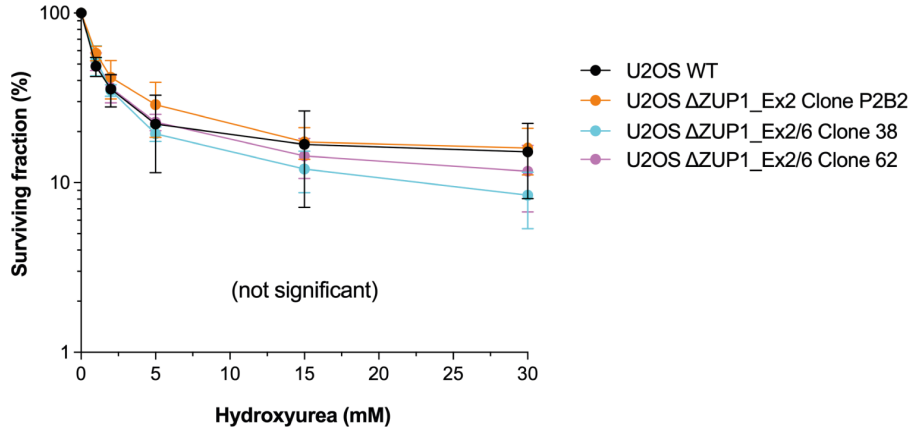

100
10
1
Surviving fraction (%)
(not significant)
0
5
10
15
20
25
30
Hydroxyurea (mM)
U2OS WT
U2OS ΔZUP1_Ex2 Clone P2B2
U2OS ΔZUP1_Ex2/6 Clone 38
U2OS ΔZUP1_Ex2/6 Clone 62

**Figure 3.8: Clonogenic survival assays in U2OS ZUP1 knockout clones.** The indicated independent U2OS ZUP1 knockout clones were assessed for their clonogenic survival in the presence of genotoxic agents: A) MMC, B) olaparib, C) talazoparib, D) topotecan, E) AZD6738 and F) hydroxyurea. The drug treatment and growth conditions are described in the Methods. U2OS ΔZUP1_Ex2 refers to clones edited using a single sgRNA targeting exon 2 (considered ZUP1 hypomorphs) whereas ΔZUP1_Ex2/6 (complete ZUP1 knockouts) refers to clones generated using paired sgRNAs targeting exon 6 within a ΔZUP1_Ex2 clone as described in the main text. Values (mean ± S.D.) represent three independent experiments (n = 3), each consisting of technical triplicates. A two-way ANOVA was performed with Dunnett's test. *P < 0.05, **P < 0.01, ***P < 0.001, ****P < 0.0001.

### 3.2.5 ZUP1 hypomorphs also exhibit sensitivity to genotoxic agents

To understand the extent to which ZUP1 contributes to DNA repair, partial or hypomorphic ZUP1 knockouts (named U2OS ΔZUP1_Ex2) were also assessed for their survival in the presence of genotoxic agents. Three independent ZUP1 hypomorphic clones that retain a ~45 kDa ZUP1 gene product as shown in **Fig. 3.3A**, were found to be sensitive to MMC and olaparib (**Fig. 3.9A-C**). To rule out experimental artifacts, one hypomorphic clone (U2OS ΔZUP1_Ex2 Clone P2B2) was tested alongside the complete knockout clones in the same experimental setup in **Fig. 3.8**. The ZUP1 hypomorph showed hypersensitivity to MMC, olaparib, topotecan and AZD6738, and also mirrored the lack of hydroxyurea sensitivity in the complete knockouts (**Fig. 3.8A, 3.8B, 3.8D, 3.8E, 3.8F**).

Two possible explanations are outlined here for how the partial loss of ZUP1 in the hypomorphic clones may have effectively sensitised cells to the replication stress agents mentioned. Firstly, the efficient repair of genotoxic lesions may require sufficient levels of ZUP1 which could not be achieved with the low level of the ~45 kDa ZUP1 protein present in the hypomorphic clones. Alternatively, since the clones

were generated by inducing frameshift mutations within exon 2, it is possible that the three N-terminal zinc fingers encoded by exon 2 are important for ZUP1-mediated DNA repair (**Fig. 3.1A**). This provides a basis for investigating the roles of these zinc finger domains within ZUP1, which are unclear to date and are characterised in more detail in Chapter 4.

Either scenario suggests that ZUP1 has an important role in DNA repair, which supports previous reports and motivates further mechanistic investigation. Stable ZUP1 re-expression was shown to rescue the MMC sensitivity phenotype in ZUP1 knockout cells by other members of the lab (data not shown). To confirm that the other sensitivity phenotypes are dependent on ZUP1, future work should examine the rescue effect of ZUP1 for the other genotoxic agents tested. This would be necessary to exclude the caveats of the CRISPR methodology including potential off-target effects and the selection of compensatory mutations in ZUP1 knockout cells that may have arisen during the single cell cloning or clonal expansion steps (Fu et al., 2013). It would also be important for future work to assess the contribution of ZUP1 catalytic activity to the phenotypes by expressing a ZUP1 catalytically inactive mutant.

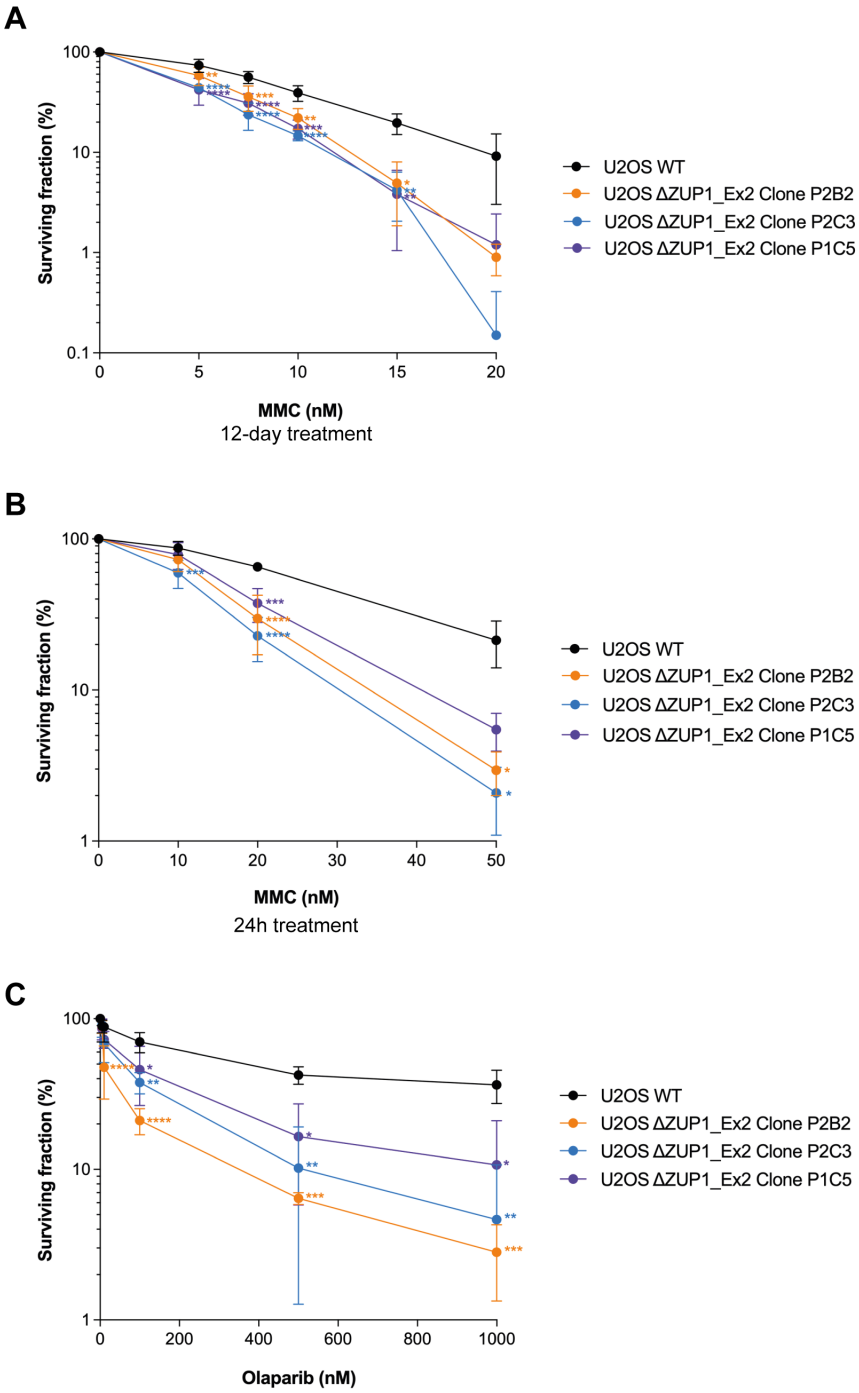



**Figure 3.9: Clonogenic survival assays in U2OS ZUP1 hypomorphic clones.** The indicated independent ZUP1 hypomorphic clones were assessed for their clonogenic survival when treated with: A) MMC (12-day treatment), B) MMC (24h treatment) or C) olaparib. The drug treatment and growth conditions are described in the Methods. Values (mean ± S.D.) represent three independent experiments (n = 3), each consisting of technical triplicates. A two-way ANOVA was performed with Dunnett's test. *P < 0.05, **P < 0.01, ***P < 0.001, ****P < 0.0001.

## 3.3 Discussion

### 3.3.1 Challenges in the generation of CRISPR-Cas9 knockouts in cell lines with complex karyotypes

The 293T cell line, also known as HEK293T, was selected as the cell line model for generating ZUP1 knockouts due to its rapid growth and high transfection efficiency which make them suitable for the assays described in Chapter 5. However, like many cancer cell lines, the 293T line has a complex karyotype and numerous chromosome aberrations (Lin et al., 2014; Stepanenko et al., 2015; Perpiñá et al., 2020). 293T cells are known to exhibit hypertriploidy which can change due to instability, as reflected in the modal chromosome number described by ATCC for its parental 293 line, which is 64 in 30% of cells (Perpiñá et al., 2020; American Type Culture Collection, ATCC). Indeed, analysis of the edited loci in ZUP1 knockouts revealed that indels can be distributed between two to potentially five alleles, which varies from one single cell-derived clone to another (**Fig. 3.4A, 3.7B**).

Cell lines with inherent chromosomal instability, polyploidy or high-copy-number genes have been shown to undergo inefficient CRISPR-Cas9 editing (Rayner et al., 2019; Cullot et al., 2019). The efficiency of generating homozygous edits in 293T cells was low during the attempt to delete ZUP1 exon 6 using paired sgRNAs (**Fig. 3.6B, 3.6D**). Although a reasonable number of clones had not retained the ZUP1 wild-type sequence after CRISPR-Cas9 editing using the strategies described, it is important to consider the risk that a single wild-type allele could have escaped detection, given the polyploidy of 293T cells. This warranted the use of multiple validation steps in this chapter to prevent the misclassification of ZUP1 knockout clones. As discussed below, other validation approaches beyond those presented in this chapter should also be employed in genome editing studies to ensure the accurate genotyping of edited cells.

Complex and undesired DSB repair outcomes are widely reported consequences of CRISPR-Cas9 editing and include inversions, duplications, large deletions and

insertions (Boroviak et al., 2017; Kosicki et al., 2018; Adikusuma et al., 2018; Cullot et al., 2019). The diversity of repair events can stem from the use of multiple DSB repair pathways including NHEJ and MMEJ (Yeh et al., 2019). DNA repair mechanisms in 293T cells are likely defective given the chromosomal abnormalities, which could render them more prone to genomic rearrangements when Cas9-mediated DNA breaks are induced. This could lead to undesired mutations or DNA rearrangements that can confound phenotypic analysis or confer a selective growth advantage to clones derived from single cells.

Some alleles in the edited 293T clones were found to contain an unanticipated inversion of exon 6 after introducing flanking intronic sgRNAs to delete the exon (**Fig. 3.6C, 3.6D**). While this may have produced the desired outcome of disrupting the catalytic cysteine within exon 6, it is not unlikely that the inversion mutation resulted in gain-of-function mutations, resulting in a ZUP1 mutant with novel functions. As with other editing strategies, allelic heterozygosity was observed for this unexpected mutation (**Fig. 3.6B, 3,6D**). If the inversion had occurred by re-insertion of the excised exon 6 fragment into the targeted site, a possible extrapolation is that other untargeted loci in the genome are also susceptible to random integration of the fragment. This risk may be especially high in cell lines such as 293T containing chromosomal instability, if spontaneous DSBs occur frequently as suggested in Chapter 5.

The inversion mutation identified in 293T ZUP1 clones in **Fig. 3.6** provides an example where an effective PCR design can detect chromosomal rearrangements that would have otherwise been missed by Western blotting or the ICE software. However, larger rearrangements will require longer-range PCR for detection. Considering the risk of heterogeneous and complex repair outcomes resulting from CRISPR-Cas9 editing, best practice might be to use higher resolution and more comprehensive genomic analyses that extend beyond the immediate vicinity of the targeted site. These include long-read sequencing, array comparative genomic hybridisation (array-CGH) and fluorescent in-situ hybridization (FISH) (Kosicki et al., 2018; Cullot et al., 2019). Xia et al. developed a homology-directed insertion method to generate CRISPR-Cas9

knockouts in polyploid cell lines (Xia et al., 2020). Briefly, a cassette is designed to contain homology arms and multiple sgRNAs, and is inserted into the target site by homology-directed repair following Cas9 cleavage. The sgRNAs expressed from the inserted cassette can lead to further mutation of the remaining alleles (Xia et al., 2020). The base editing method has also been described that utilises deaminases to directly convert targeted base pairs to the desired base pair, and eliminates the need for DSB generation (Huang et al., 2021).

### 3.3.2 Evaluation of knockout strategy to eliminate ZUP1

This chapter presents the different CRISPR-Cas9 strategies tested to achieve the complete knockout of ZUP1. It has become increasingly evident that simply targeting 5' exons may not abolish gene function due to the potential induction of functional in-frame variants through alternative splicing or other poorly understood mechanisms (Mou et al., 2017; Tuladhar et al., 2019). Indeed, despite the loss of the main ZUP1 isoform, most clones were found to retain faster-migrating ZUP1 proteins after targeting exon 2 in 293T cells (**Fig. 3.4B**).

The only ZUP1 function that has been assessed to date is its deubiquitylating role, as summarised in Chapter 1. When designing the ZUP1 knockout strategies, it was considered that the disruption of its catalytic activity by targeting exon 6 may not be sufficient to eliminate potential non-deubiquitylating functions of ZUP1. The deletion of exon 6 using the flanking sgRNA pair resulted in truncated ZUP1 proteins that may not be active as a deubiquitylase, but could retain functionality through the other non-catalytic domains (**Fig. 3.5B**). This speculation also took into account the putative 280 aa isoform that possibly lacks catalytic activity due to the 3' truncation that removes the His491 and Asp512 catalytic triad residues (**Fig. 3.1B**). This suggests that ZUP1 function may not be limited to its deubiquitylating activity. As described in the next chapter, some of the ZUP1 non-catalytic domains were indeed found to be important for protein-protein interactions with other components of the ZUP1 enzyme complex.

Therefore, a ZUP1 knockout strategy was designed to eliminate all truncated variants resulting from CRISPR-Cas9 editing and residual ZUP1 isoforms. Two editing and clonal expansion rounds were performed where exon 6 was first deleted using paired sgRNAs, followed by the removal of the remaining ZUP1 proteins using a single sgRNA targeting exon 2 (**Fig. 3.7**). The complete loss of ZUP1 enabled subsequent analyses of cellular phenotypes in Chapter 5 that were found to be robust and consistent between the independent clones.

The database information on ZUP1 splice isoforms aided the design of sgRNAs, however the lack of characterisation and functional data on the individual isoforms can limit our understanding of ZUP1 function within cellular processes. A future area of investigation could involve transcriptome analysis to accurately profile ZUP1 splice isoforms, followed by re-expressing individual isoforms in ZUP1 knockout cells for phenotypic analysis. Additional tools will also be essential for detecting the different isoforms or truncated variants resulting from CRISPR-Cas9 editing, including ZUP1 antibodies specific for different domains or regions.

### 3.3.3 ZUP1 has a role in replication-coupled DNA repair

ZUP1 knockouts are hypersensitive to a broad range of genotoxic agents, namely MMC, olaparib, talazoparib, topotecan and AZD6738 (**Fig. 3.8A-E**). Although the panel of compounds generate unique DNA lesions and engage different repair factors, the activated repair processes may converge at a similar pathway in which ZUP1 may have a role. As described earlier, replication stress can be caused by blockage of the replisome and fork uncoupling due to ICLs created by MMC; lesions created by the trapping of proteins onto DNA which can result from PARP inhibitors and topotecan; or uncontrolled origin firing and excessive ssDNA resulting from ATR inhibition; which can lead to DSBs and fork collapse. DNA repair pathways can be engaged during replication to process the damage, which is known as replication-coupled repair (Cortez et al., 2019). Replisomes can bypass lesions, switch templates to utilise the undamaged chromatid for repair, reverse forks or pause their progression to allow time for repair (Chapter 1, Ashour et al., 2021).

Stressed replicating forks are prone to collapse if lesions are not removed in a timely and accurate manner (Chapter 1, Section 1.2.4). For example, single-strand breaks can be converted to DSBs (Hashimoto et al., 2012). DSBs may also form when trapped topoisomerases collide with progressing forks (Cortez et al., 2019). The inevitable DSB formation and fork collapse requires HR for error-free DSB repair (Scully et al., 2019). It is possible that ZUP1 may be involved in the repair of detrimental DSBs induced by the panel of genotoxic compounds. This may align with subsequent findings in Chapter 5 suggesting that ZUP1 has a role in HR.

ZUP1 is specific for cleaving K63-linked polyubiquitin chains, and this linkage type is present on crucial DNA repair factors such as PCNA (Chapter 1, Section 1.6.1). Given the role of ZUP1 in preventing cell lethality in response to genotoxic lesions, this motivated the work presented in Chapter 5 to investigate the function of ZUP1 as a DUB in DNA repair. The broad long-term goal is to assess how ZUP1 contributes to the tight spatiotemporal regulation of ubiquitylation during DNA repair, and how this may enable the accurate repair of DNA lesions and maintain genome stability.

Further dissection of the role of ZUP1 in DNA repair could involve expanding the panel of genotoxic agents used to treat ZUP1 knockout cells. The role of ZUP1 in the repair of DNA replication-independent damage can also be examined. For example, wild-type and ZUP1 knockout cells can be arrested in G0 and exposed to UV, then released and assessed for their clonogenic survival. In addition, genetic interactions between ZUP1 and DNA repair proteins should also be investigated, for example by performing a genome-wide CRISPR dropout screen to identify genetic vulnerabilities in ZUP1 knockout cells, which is an ongoing effort in the Gibbs-Seymour lab (Tzelepis et al., 2016).

An essential next step would be to confirm the dependence of the observed drug sensitivity phenotypes on ZUP1, by assessing whether ZUP1 re-expression (wild-type or catalytically inactive ZUP1) in the knockouts is able to rescue the survival defects of the cells in the presence of genotoxic agents tested in **Fig. 3.8**. This is crucial considering the limitations of the CRISPR methodology such as potential off-

target effects and the possible selection of compensatory mutations that may have emerged while generating the knockouts (Fu et al., 2013). It would also be important to perform the clonogenic survival assays in other cell lines to determine if ZUP1 function in DNA repair is specific to cell type.

### 3.3.4 The N-terminus of ZUP1 may be important for its DNA repair function

The partial loss of ZUP1 was also sufficient to induce hypersensitivity to genotoxic agents, as demonstrated in multiple independent ZUP1 hypomorphic clones (U2OS ΔZUP1_Ex2, **Fig. 3.8, 3.9**). These clones do not express isoforms A and B, but retain a ~45 kDa ZUP1 protein that is expressed at low levels (**Fig. 3.3A**). This suggests that any function retained by the residual ~45 kDa protein expressed at low levels was not sufficient to protect cells against genotoxicity.

ZUP1 is known for its deubiquitylating function against K63-linked polyubiquitin chains (Chapter 1). The hypersensitivity phenotypes in hypomorphic ZUP1 clones may reveal novel functions of ZUP1 that may or may not be related to its deubiquitylating activity. This takes into consideration the exon 2 frameshifts induced by the exon 2-targeting sgRNAs used for the generation of these hypomorphic clones. Exon 2 encodes the first three N-terminal zinc fingers of ZUP1, the functions of which are not known to date (**Fig. 3.1A**). Given the hypersensitivity phenotype in ZUP1 hypomorphic cells that presumably lack the first three N-terminal zinc fingers as a result of this editing strategy, it is possible that ZUP1 performs its DNA repair and genome maintenance role through this N-terminal region.

The first three N-terminal zinc fingers are not essential for ZUP1 deubiquitylase activity or ubiquitin binding (Kwasna et al., 2018). Further investigation of the roles of these zinc fingers may reveal new facets of ZUP1 function in the context of DNA repair, and provide insight into whether the tandem arrangement of these zinc fingers is due to distinct specificity and roles of the individual zinc finger. Additionally, it will

be important to assess whether the role of this N-terminal region of ZUP1 is independent of, or complementary to ZUP1 deubiquitylase activity in DNA repair.

Although exon 2 was disrupted in the hypomorphic clones, it cannot be excluded that other exons may have also been affected by the frameshift mutations. The hypersensitivity observed in the ZUP1 hypomorphic clones in this chapter provided a motivation for the mutagenesis and protein-protein interaction studies in the next chapter, to elucidate the role of non-catalytic ZUP1 domains such as the N-terminal zinc fingers encoded by exon 2.

# 4

# Defining the ZUP1 Complex in Cells

## Contents


**4.1 Introduction……..…..124**

**4.2 Results……..…..128**

4.2.1 Defining the ZUP1 complex in cells……..128

4.2.2 ZUP1 interacts with another DUB, USP11……137

4.2.3 Dissecting USP11-ZUP1 and USP11-TCEAL1 interactions……144

**4.3 Discussion……..154**

4.3.1 A novel interaction between two DUB classes……..…154

4.3.2 Specificity of the second zinc finger of ZUP1 for binding USP11…..……156

4.3.3 USP11-TCEAL1 interaction mapping will aid future functional characterisation of TCEAL1……158

4.3.4 The ZUP1 interactome suggests a role for ZUP1 in ubiquitin signaling and DNA repair……..……160

## 4.1 Introduction

The findings in the previous chapter suggest that ZUP1 plays an important role in DNA repair. One striking observation was the sensitisation of cells to genotoxic stress upon the disruption of exon 2 which encodes the first three N-terminal zinc fingers of ZUP1 (**Fig. 3.9**). The roles of these ZUP1 zinc fingers remain elusive and their structures have yet to be solved. The well-established function of such zinc finger domains as interaction modules prompted me to focus on protein-protein interactions which are a crucial yet largely unexplored aspect of ZUP1 function. This chapter aimed to define the interacting sites between ZUP1 and its binding partners, to provide a basis for understanding how the non-catalytic domains of ZUP1 may mediate its cellular roles.

The ZUP1 interactome was previously characterised using proteomic approaches (Hermanns et al., 2018; Hewings et al., 2018; Kwasna et al., 2018). Briefly, Hermanns et al. induced the stable expression of FLAG-tagged ZUP1 in 293T Flp-In T-Rex cells, immunopurified the construct and performed LC-MS/MS analysis. Proteins that co-purified with the catalytically inactive (C360A) ZUP1 mutant that was transiently transfected, were analysed for comparison. Hewings et al. transiently over-expressed FLAG-ZUP1 in 293T cells which was then immunopurified, and the interacting proteins were analysed by LC-MS/MS. Kwasna et al. immunoprecipitated endogenous nuclear ZUP1 from 293 nuclear extracts for MS analysis using antibodies raised against ZUP1, however details of the antibody characterisation were not provided.

Due to the differences in these approaches, and to generate sufficient biological replicates, the ZUP1 interactome was re-visited by others in the Gibbs-Seymour lab who performed MS analysis of FLAG-ZUP1 expressed in 293T Flp-In T-Rex cells (**Fig. 4.1**). The identified ZUP1 interacting proteins can be categorised into two major groups based on their recognised roles in ubiquitin signalling or DNA replication and repair. In this chapter, I sought to dissect some of these protein-protein interactions in a cellular setting by identifying potential binding sites. The RPA complex was

consistently identified as a top interacting partner of ZUP1 across the independent studies. Alongside RPA, PCNA is another extensively studied DNA repair protein found to interact with ZUP1, and both proteins were examined in this chapter given their critical roles in DNA replication and repair as described in Chapter 1. To understand ZUP1 function in genome stability, it will be important to investigate the nature and functional significance of its interaction with RPA and PCNA.

In the ubiquitin signalling category of ZUP1 interactors, particular focus was placed on USP11, a USP family DUB. Unlike ZUP1 which displays linkage specificity for K63-linked chains, USP11 cleaves multiple ubiquitin chain linkage types including K6-, K11-, K33- and K63-linkages, and has also been suggested to remove K48-linked chains on p21 in cells (Harper et al., 2014; Deng et al., 2018). In addition to providing novel insight into how distinct DUB classes may cooperate, the interaction between ZUP1 and USP11 may also be a key component underlying the DNA repair role of ZUP1. USP11 has been extensively reported to function in DNA repair. USP11 silencing was shown to result in hypersensitivity to PARP inhibitor treatment, ionising radiation, cisplatin and mitomycin C, and led to decreased RAD51 foci at DSB sites following ionising radiation which indicates HR defects (Wiltshire et al., 2010). One important process mediated by USP11 is the formation of a stable BRCA1–PALB2–BRCA2 complex which it achieves by deubiquitylating PALB2 (Orthwein et al., 2015). USP11 has also been proposed to counteract γH2AX ubiquitylation mediated by RNF8/RNF168 (Yu et al., 2016). More recently, USP11 was shown to cleave monoubiquitylated SPRTN to facilitate the role of SPRTN in DNA-protein crosslink repair (Perry et al., 2021).

A poorly characterised protein, transcription elongation factor A like 1 (TCEAL1) was also identified in the ZUP1 interactome. TCEAL1 is frequently observed to co-purify with USP11 (Sowa et al., 2009; Hein et al., 2015; Basic et al., 2021). Its interaction with USP11 may exert an influence on ZUP1 function, therefore this chapter also attempted to identify the sites involved in USP11-TCEAL1 binding. Another ZUP1 interactor, UBR5 was one of two highly enriched E3 ligases assessed for its interaction with ZUP1 domains. UBR5 has been shown to assemble branched

K48/K63 chains, while ZUP1 specifically cleaves K63-linked chains and is able to bind K48-linked chains (Ohtake et al., 2018; Kwasna et al., 2018). The interaction between ZUP1 and UBR5 may suggest the fine-tuning of common substrates by the two opposing and potentially coordinating regulators.

Given that the ZUP1 interactome includes important factors in ubiquitin signalling and DNA repair as outlined above, I aimed to characterise these protein-protein interactions in cells that may define the deubiquitylating and DNA repair function of ZUP1. In this chapter, I describe the mutagenesis screens performed by rational design to identify interacting sites or residues. This approach was complemented with *in vitro* pull-down assays performed by others in the Gibbs-Seymour lab using purified recombinant proteins, the findings of which are presented in the Appendix and referred to where relevant. As a whole, this chapter seeks to examine the protein binding role(s) of non-catalytic ZUP1 domains and investigate other novel interactions that exist in the ZUP1 protein complex, which in turn will help us understand the function of the cellular ZUP1 complex.

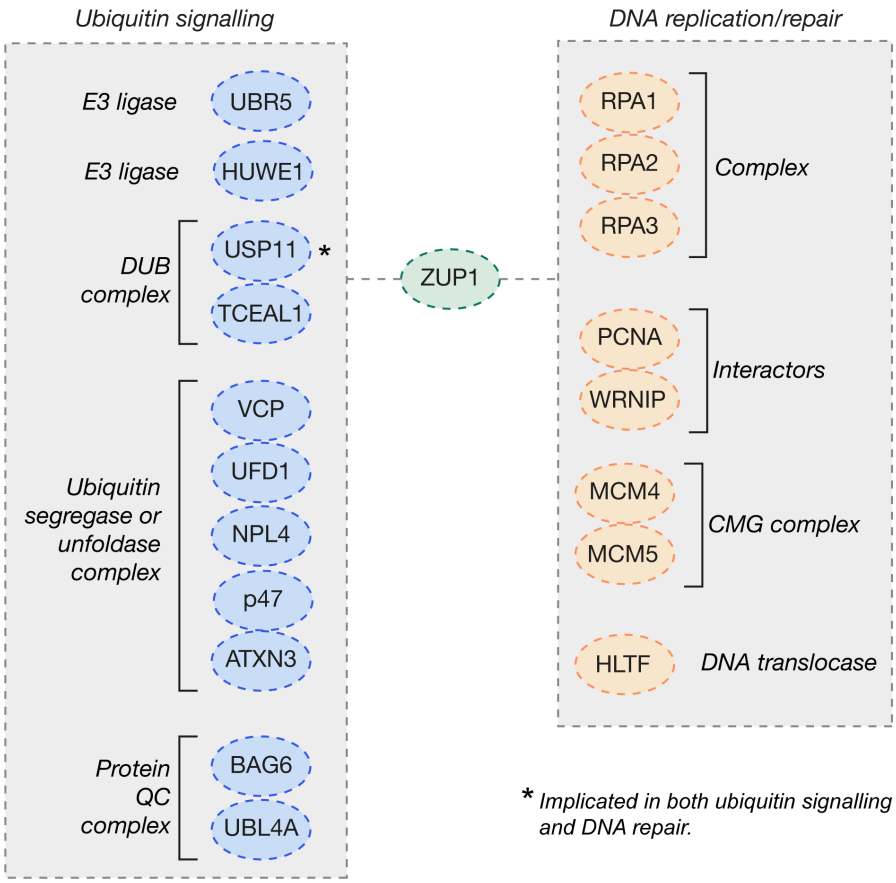



**Figure 4.1: Summary of the ZUP1 interactome previously identified by proteomics.** ZUP1 interacting proteins were identified by MS analysis of FLAG-ZUP1 expressed in and immunoprecipitated from 293T Flp-In T-Rex cells (Martin Attwood, unpublished). Interacting proteins were classified into two groups based on their well-established roles in ubiquitin signaling or DNA replication/repair.

## 4.2 Results

### 4.2.1 Defining the ZUP1 complex in cells

To determine the ZUP1 domains involved in protein-protein interactions, a series of FLAG-tagged ZUP1 truncation mutants were transiently expressed in 293T wild-type cells (**Fig. 4.2A**). The mutants contain deletions of previously annotated domains or structurally characterised regions (Kwasna et al., 2018; Hermanns et al., 2018). The mutants were immunoprecipitated from cells, and their associations with endogenous ZUP1 partner proteins were assessed by Western blotting and compared with the protein levels co-precipitated by full-length ZUP1 and the empty vector control.

Compared to full-length ZUP1, the mutant lacking the α-2/3 helix-turn-helix protrusion directly N-terminal to the catalytic domain (FLAG-ZUP1 Δα-2/3 [Δ275-310]), displayed slightly less binding to the RPA complex (**Fig. 4.2B**). To minimise potential structural artifacts, a flexible GSG linker was added to replace the α-2/3 region which produced a similar effect on RPA binding (FLAG-ZUP1 Δα-2/3 [Δ275-310] + GSG, **Fig. 4.2B**). Deletion of the N-terminal zinc fingers of ZUP1 led to a marked increase in RPA binding, raising the possibility that these N-terminal domains may physically obstruct the binding site of RPA. This interpretation is currently limited by the lack of structural information on the region N-terminal to the MIU domain. Interestingly, the AlphaFold prediction places the first two zinc fingers at close proximity to the α-2/3 protrusion (**Appendix B: Fig. 1**).

In untreated conditions, ectopically expressed ZUP1 tagged with fluorescent proteins was reported to be uniformly localised throughout the cytoplasm and nucleus of U2OS cells (Hermanns et al., 2018). Another study reported that ZUP1 is mainly present in the nucleus (Haahr et al., 2018). The subcellular localisation of ZUP1 therefore requires further clarification, as well as the cell cycle dependence of its localisation, and the region of ZUP1 that may be important for its nuclear localisation. The slight reduction of RPA binding to the ZUP1 construct lacking the α-2/3 region

may not necessarily reflect a decrease in ZUP1 nuclear localisation, given that such a defect should be reversed in the whole cell lysate following cell lysis, where this protein-protein interaction would not be prevented by the nuclear membrane.

In contrast to RPA, the binding of USP11 to ZUP1 decreased significantly in the absence of the first two zinc fingers of ZUP1 and some linker residues preceding the third zinc finger, as shown by the FLAG-ZUP1 146-578 mutant (**Fig. 4.2B**). This suggests that the predominant USP11 binding site may reside in this N-terminal region. The third ZUP1 zinc finger does not appear to be essential for the interaction as its removal did not further reduce the binding of USP11 (FLAG-ZUP1 186-578 compared to FLAG-ZUP1 146-578).

The fourth zinc finger of ZUP1 which was previously defined as the UBZ domain, and the α-2/3 region, may contribute to USP11 interaction since their deletions within the N-terminal truncated mutants led to a further decrease in USP11 binding, albeit to a lesser degree than when only the first two zinc fingers were deleted (**Fig. 4.2B**). Alternatively, USP11 may have an enhanced propensity to recognise these ZUP1 regions in the absence of its main interaction site within the N-terminal zinc fingers. This could explain the reduction in USP11 binding to the catalytic domain (C78)-only mutant (FLAG-ZUP1 311-578) compared to the α-2/3-C78 mutant (FLAG-ZUP1 272-578), whilst the deletion of the α-2/3 only (FLAG-ZUP1 Δα-2/3) did not decrease USP11 binding to ZUP1. This indicates that the α-2/3 region may be dispensable for USP11 interaction.

The binding of TCEAL1 to ZUP1 was found to follow a similar trend to that of USP11, in line with previous proteomic data sets suggesting that TCEAL1 may form a complex with USP11 given their frequent associations (**Fig. 4.2B**, Sowa et al., 2009; Hein et al., 2015; Basic et al., 2021). In addition, the signal detected for TCEAL1 protein in the ZUP1 co-immunoprecipitate was substantially less than that for USP11, and this was later shown in USP11 co-immunoprecipitates to likely reflect the protein amount rather than technical-related issues. This motivated RNAi experiments demonstrated later in this chapter to assess if TCEAL1 binding to ZUP1 may be

USP11-dependent. The effect of ZUP1 truncations on UBR5 binding follows a similar trend to the RPA complex. PCNA was observed to bind all the ZUP1 truncation mutants to a similar extent, suggesting its interaction with the C78 peptidase or an indirect interaction (**Fig. 4.2C**). Experiments shown in **Fig. 4.2B** and **Fig. 4.2C** were performed in the presence of benzonase nuclease to minimise the possibility that DNA is bridging the protein-protein associations examined.

It cannot be excluded that the trends observed from this first mutagenesis screen may reflect structural artifacts due to the large deletions generated within ZUP1. As described in the following figures, further mutagenesis was performed to narrow down some notable binding regions to potential interacting residues.

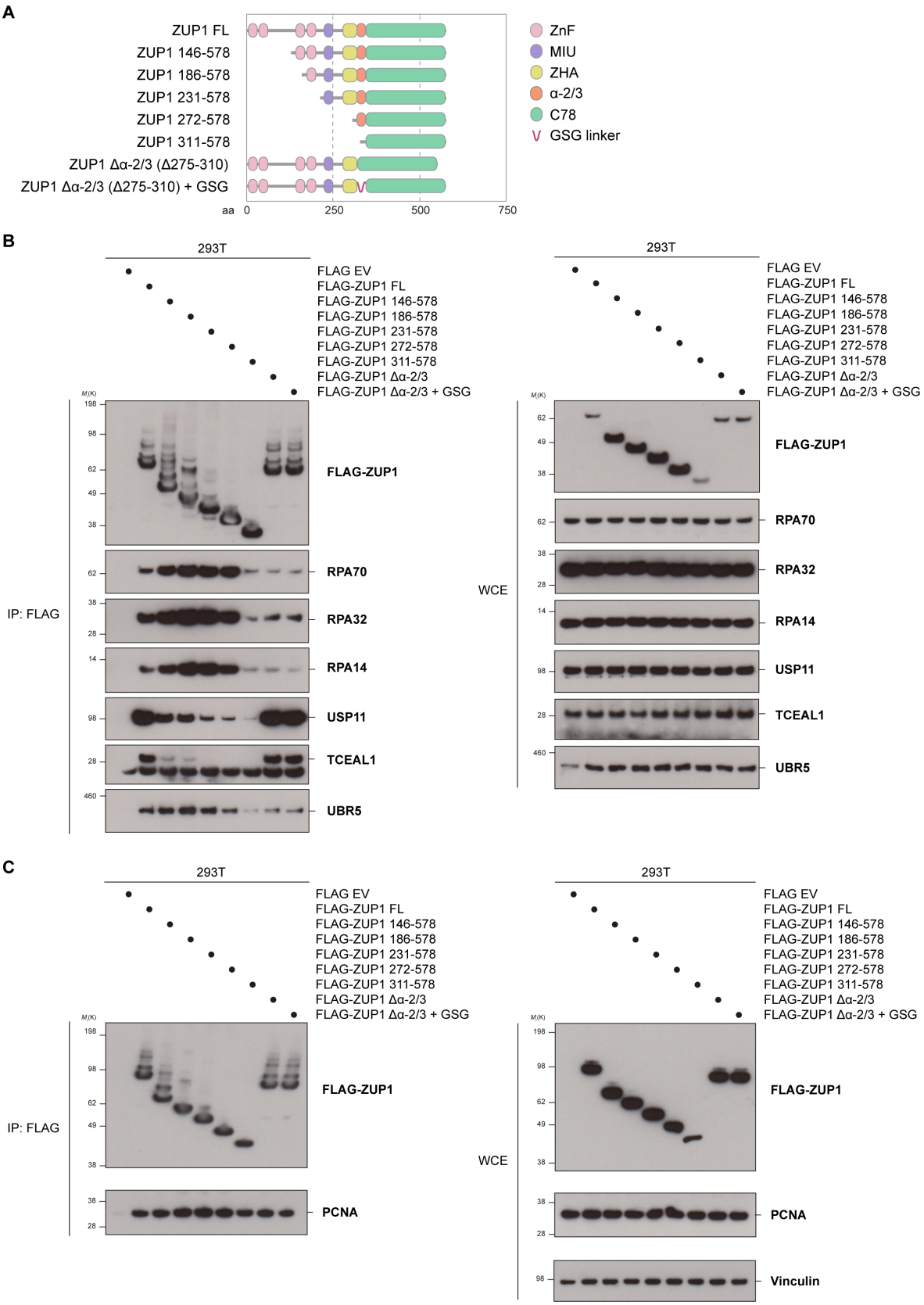

A
ZUP1 FL
ZUP1 146-578
ZUP1 186-578
ZUP1 231-578
ZUP1 272-578
ZUP1 311-578
ZUP1 Δα-2/3 (Δ275-310)
ZUP1 Δα-2/3 (Δ275-310) + GSG
aa 0 250 500 750
ZnF
MIU
ZHA
α-2/3
C78
GSG linker
B
293T
FLAG EV
FLAG-ZUP1 FL
FLAG-ZUP1 146-578
FLAG-ZUP1 186-578
FLAG-ZUP1 231-578
FLAG-ZUP1 272-578
FLAG-ZUP1 311-578
FLAG-ZUP1 Δα-2/3
FLAG-ZUP1 Δα-2/3 + GSG
IP: FLAG
FLAG-ZUP1
RPA70
RPA32
RPA14
USP11
TCEAL1
UBR5
WCE
C
PCNA
Vinculin

**Figure 4.2: Identification of ZUP1 domains involved in protein-protein interactions.** A) Schematic representation of FLAG-tagged ZUP1 truncation mutants containing deletions of previously annotated domains or structurally characterised regions. FL: full length. B) Protein binding to ZUP1 mutants was assessed by immunoprecipitating FLAG-tagged mutants transiently expressed in 293T wild-type cells, and immunoblotting with the indicated antibodies. Blots shown are representative of two independent experiments (n = 2). EV: empty vector; IP: immunoprecipitate; WCE: whole cell extract. C) PCNA binding to ZUP1 mutants was assessed by co-immunoprecipitation as in B. Blots shown are representative of two independent experiments (n = 2).

Another noteworthy observation is the presence of multiple higher molecular weight bands above the main ZUP1 species, as seen in the full-length ZUP1 construct (**Fig. 4.2B**). Other members in the lab have performed denaturing ubiquitin pull-down assays and identified these bands as ubiquitylated ZUP1 proteins (data not shown). Compared to full-length ZUP1, more bands were observed above the FLAG-ZUP1 146-578 construct that lacks the first two zinc fingers and some linker residues preceding the third zinc finger (**Fig. 4.2B**). This may suggest a role for the first two zinc fingers of ZUP1 in regulating ZUP1 ubiquitylation. The binding of the E3 ligase, UBR5 to ZUP1 does not correlate with the number of higher molecular weight bands above the ZUP1 constructs (**Fig. 4.2B**). However, this does not exclude UBR5 as a potential E3 ligase for ZUP1, given that the ubiquitylation sites of ZUP1 are not yet known. The ubiquitylation sites of ZUP1 may be removed by some truncations which could explain the absence of multiple higher molecular weight bands for certain constructs, rather than any differences in UBR5 binding. As shown in **Fig. 4.1**, HUWE1 is another E3 ligase found to interact with ZUP1, and can be assessed together with UBR5 in future work as potential E3 ligases that mediate ZUP1 ubiquitylation, for example by examining the impact of HUWE1 or UBR5 knockdown on ZUP1 ubiquitylation.

To further examine the interaction between ZUP1 and the RPA complex in cells, the contribution of the α-2/3 region to RPA binding observed in **Fig. 4.2B** was first confirmed in a separate co-immunoprecipitation experiment that assessed only the mutants lacking the α-2/3 (**Fig. 4.3A**). *In vitro* pull-down assays performed by others in the lab demonstrated the direct interaction between purified recombinant ZUP1 and RPA, and a significant disruption of RPA binding when the ZUP1 α-2/3 region was deleted (**Appendix B: Fig. 2**). Gel filtration experiments with the ZUP1-RPA complex have reported approximately 1:1 stoichiometry, and ZUP1 forms a monomer in solution (data not shown). The co-immunoprecipitation assays in cells showed residual RPA binding to ZUP1 mutants lacking the α-2/3, and the effect of deleting the α-2/3 was not as substantial as shown *in vitro* (**Fig. 4.2B, 4.3A**). It is important to consider that ZUP1-RPA interaction in cells, as opposed to *in vitro* settings, may be influenced by other binding components. Possible influencing cellular components include ubiquitin, which has been speculated to bind to the α-2/3 region that potentially provides the S1' ubiquitin binding site based on the crystal structure (Hermanns et al., 2018). The same group demonstrated that RPA binding to ZUP1 may be DNA-dependent, which also adds to the complexity of this interaction.

Considering the reported DNA dependence of ZUP1-RPA interaction, and the ssDNA-binding ability of RPA proteins, it was speculated whether the ZUP1-RPA interaction may be bridged by DNA. Previous electrophoretic mobility shift assays (EMSA) demonstrated the slight binding of ZUP1 to ssDNA (Hermanns et al., 2018). ZUP1 was still able to co-precipitate RPA to a similar extent in the presence of benzonase nuclease, which correspondingly did not prevent residual RPA binding to ZUP1 mutants lacking the α-2/3 (**Fig. 4.3B**). Although the results in **Fig. 4.3B** were obtained from a single experiment and more repeats are needed, a similar experimental setup by others in the lab showed that the interaction between ZUP1 and RPA is independent of DNA, and the digestion of nucleic acid by benzonase was also verified in the setup (**Appendix B: Fig. 3**). Subsequent co-immunoprecipitation experiments shown in this chapter were performed in the presence of benzonase to minimise the contribution of DNA binding to the protein associations examined.

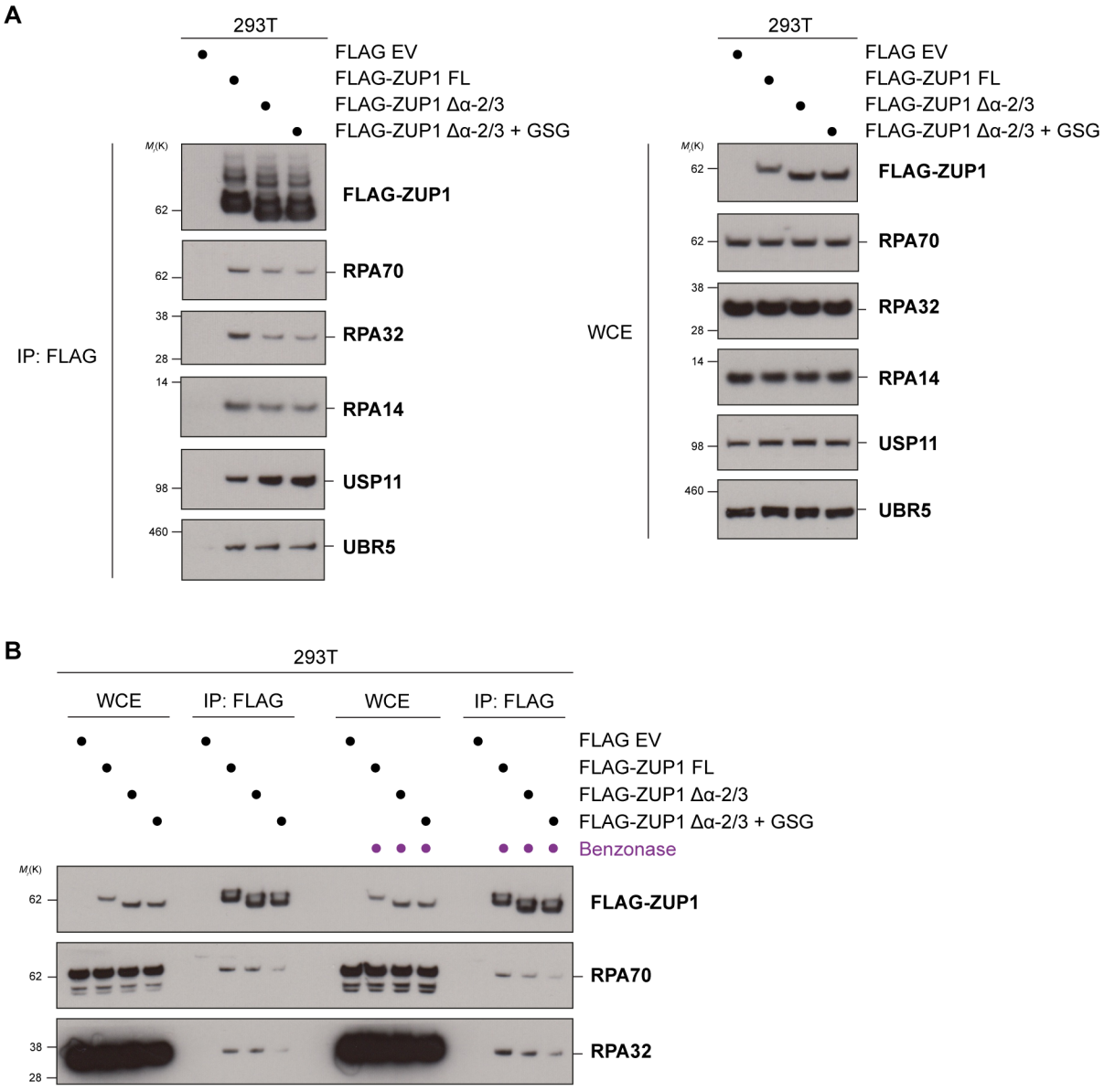



**Figure 4.3: Residual RPA binding to ZUP1 was observed when the α-2/3 region was deleted.** A) The contribution of the α-2/3 region of ZUP1 to RPA binding was assessed using mutants in which the region was deleted or replaced by a flexible linker. The binding of other indicated ZUP1 interacting proteins were also examined by immunoblotting. Blots shown are representative of two independent experiments (n = 2). B) The effect of benzonase on RPA70 and RPA32 binding was investigated by dividing each cell lysate into two samples, where 1:500 benzonase and 2 mM $MgCl_2$ was added to one of the samples. The remaining steps were performed as previously described. Blots shown were obtained from a single experiment (n = 1).

Next, it was considered whether the contribution of the ZUP1 α-2/3 region to RPA binding may not be depicted accurately in the assays shown above due to possible structural changes induced by the α-2/3 deletion which may not have been mitigated by the addition of the flexible GSG linker. Therefore, single-residue mutations were generated within the α-2/3 region to identify potential interacting residues. The α-2/3 residues selected for mutagenesis were surface residues deduced from the published crystal structure that potentially mediate protein interactions based on their side chain orientation (PDB: 6FGE, **Fig. 4.4B**). These residues were substituted with alanine or other residues whose side chains, in comparison to the wild-type residue, have a reduced size or are uncharged.

Some α-2/3 surface residue mutations were found to result in a slight decrease in RPA binding (**Fig. 4.4A**). Subsequent cross-linking mass spectrometry analyses in our lab demonstrated the proximity of the RPA complex to multiple regions throughout ZUP1 including the α-2/3, C78 domain and N-terminal zinc fingers (data not shown). The RPA binding data across the different assays and systems therefore suggest that multiple interacting sites within ZUP1 are involved in binding RPA.

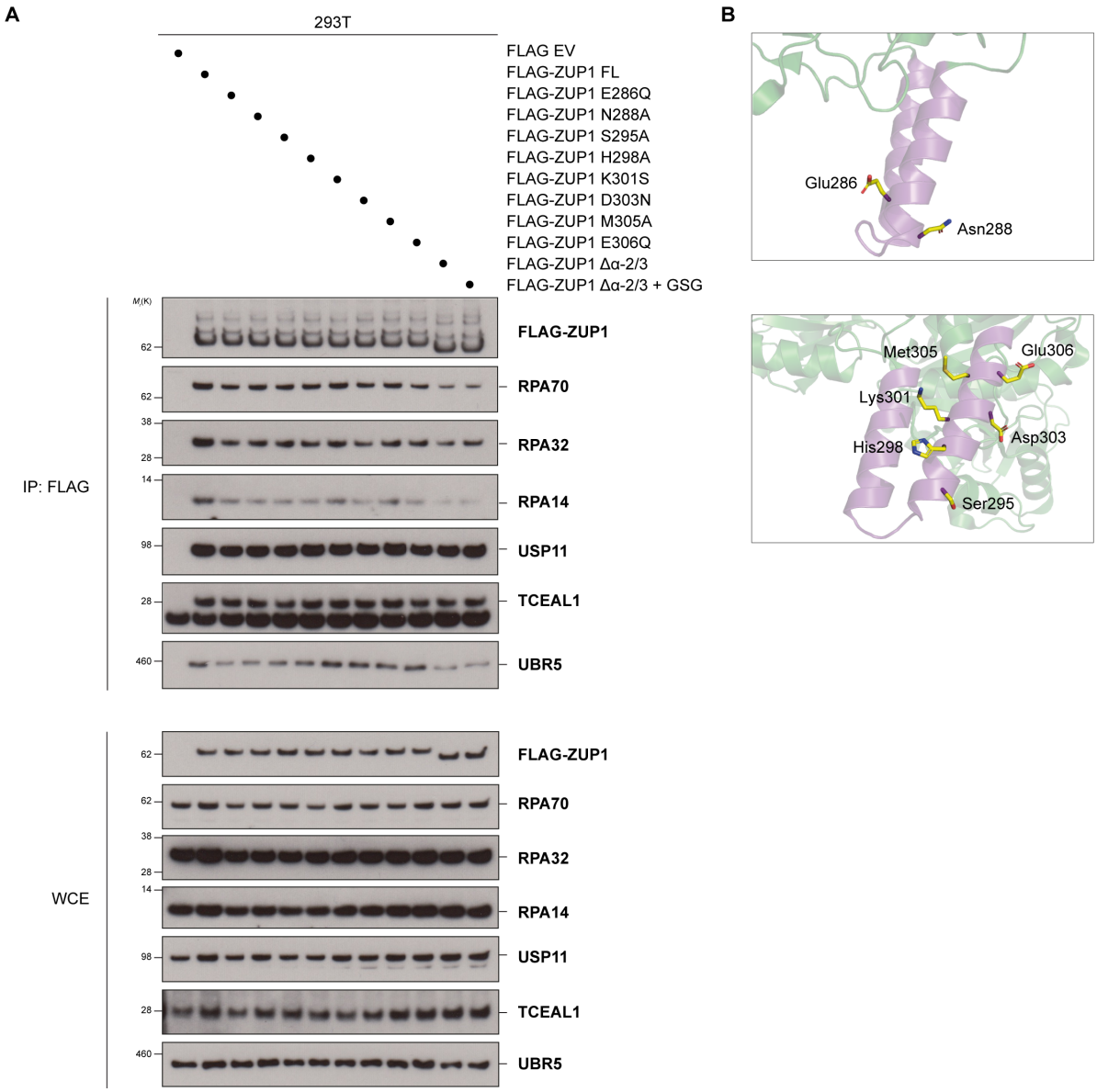



**Figure 4.4: Assessing surface residues in the α-2/3 region of ZUP1 for their contribution to RPA interaction.** A) ZUP1 mutants were generated by Ben Foster and potential α-2/3 surface residues were mutated as inferred from the crystal structure shown in B. The ZUP1 mutants were co-immunoprecipitated from 293T cells as described previously to assess their binding to RPA. Blots shown are representative of three independent experiments (n = 3). B) Crystal structure of ZUP1 α-2/3 showing surface residues selected for mutagenesis (PDB: 6FGE). Figures were prepared in Pymol.

### 4.2.2 ZUP1 interacts with another DUB, USP11

ZUP1 exhibited less binding to USP11 in the absence of its first two zinc fingers and some linker residues preceding the third zinc finger (FLAG-ZUP1 146-578, **Fig. 4.2A, 4.2B**). To define the USP11 binding site in this N-terminal region, the first two zinc fingers of ZUP1 (ZnF1 and ZnF2) were deleted individually or in combination (**Fig. 4.5A**). The combined deletion of ZnF1 and ZnF2 did not include the linker region preceding ZnF3 unlike the previous truncation in **Fig. 4.2A**.

The deletion of ZnF2 within ZUP1 (FLAG-ZUP1 ΔZnF2 [Δ31-52]) revealed that ZnF2 may harbour the main binding site of USP11 (**Fig. 4.5B**). The disruption of USP11 binding caused by ZnF2 deletion was comparable to that resulting from larger truncations which removed the other zinc fingers (FLAG-ZUP1 146-578, FLAG-ZUP1 186-578). Neither ZnF1 nor ZnF3 were considered as major or essential sites for USP11 interaction since their deletions did not affect the level of USP11 bound to ZUP1. TCEAL1 also displayed specificity for ZnF2 and was observed to followed the binding trend of USP11, consistent with all the co-immunoprecipitation assays demonstrated in this chapter.

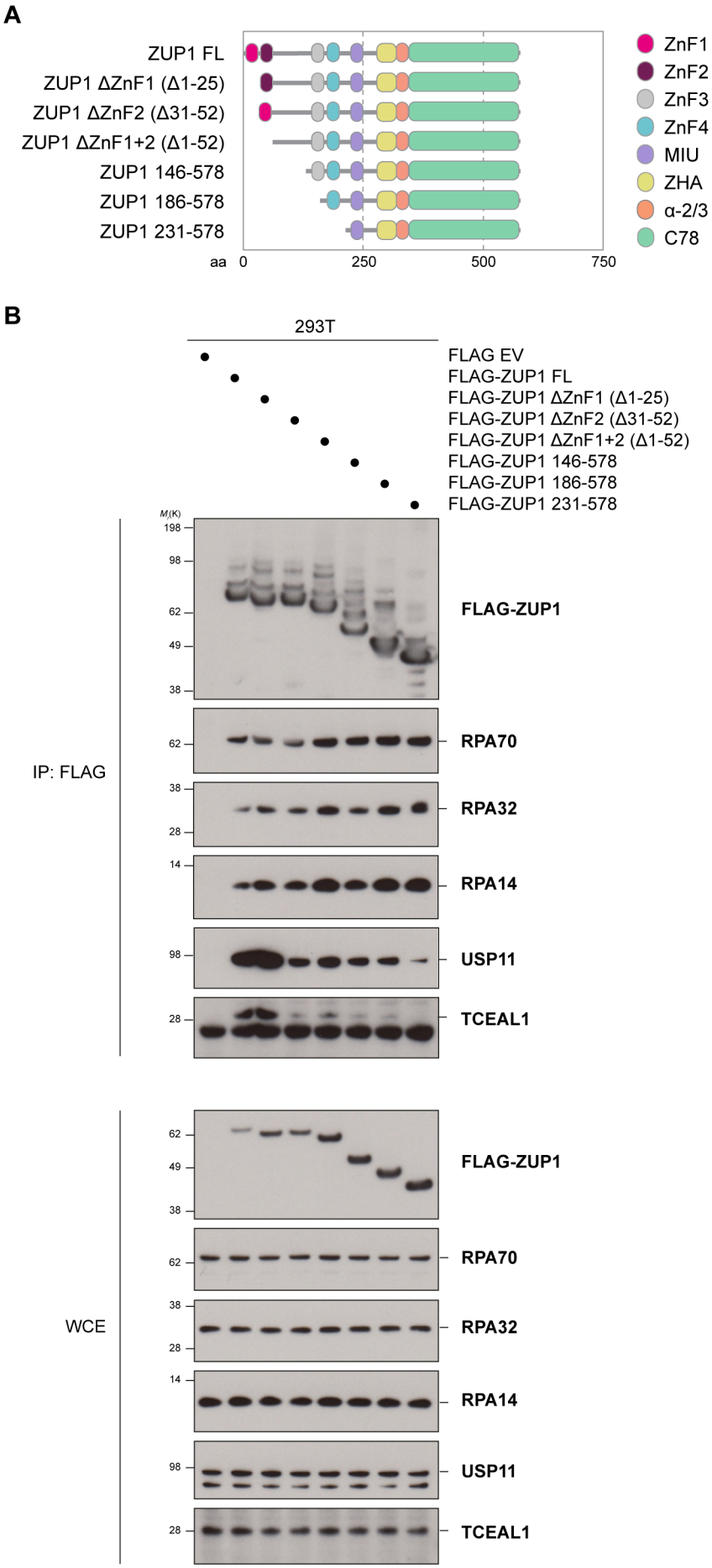

A
ZUP1 FL
ZUP1 ΔZnF1 (Δ1-25)
ZUP1 ΔZnF2 (Δ31-52)
ZUP1 ΔZnF1+2 (Δ1-52)
ZUP1 146-578
ZUP1 186-578
ZUP1 231-578
aa 0 250 500 750
ZnF1
ZnF2
ZnF3
ZnF4
MIU
ZHA
α-2/3
C78
B
293T
FLAG EV
FLAG-ZUP1 FL
FLAG-ZUP1 ΔZnF1 (Δ1-25)
FLAG-ZUP1 ΔZnF2 (Δ31-52)
FLAG-ZUP1 ΔZnF1+2 (Δ1-52)
FLAG-ZUP1 146-578
FLAG-ZUP1 186-578
FLAG-ZUP1 231-578
M(K)
198
98
62
49
38
IP: FLAG
FLAG-ZUP1
62
RPA70
38
28
RPA32
14
RPA14
98
USP11
28
TCEAL1
WCE
62
49
38
FLAG-ZUP1
62
RPA70
38
28
RPA32
14
RPA14
98
USP11
28
TCEAL1

**Figure 4.5: Identification of the ZUP1 zinc finger that mediates USP11 binding.** A) Schematic representation of ZUP1 mutants containing zinc finger deletions. Truncations starting at positions 146, 186 and 231 were previously assessed in Fig. 4.2 and were included in this experiment for comparison. B) ZUP1 was examined for its ability to co-precipitate USP11 when the indicated zinc fingers were deleted. The interactions of other indicated ZUP1 binding partners were also assessed for comparison. Blots shown are representative of two independent experiments (n = 2).

Having identified ZUP1 ZnF2 as the predominant binding site for USP11, this interaction was investigated further to identify potential interacting residues. The role of the ZUP1 C2H2-type zinc fingers remain unclear apart from ZnF4 which was shown to be a ubiquitin-binding UBZ (Hermanns et al., 2018; Kwasna et al., 2018; Haahr et al., 2018). Two common binding partners of the C2H2 zinc finger type are ubiquitin and DNA, which were previously assessed for their binding to ZUP1 zinc fingers. NMR work by Hewings et al. demonstrated that, in isolation, ZnFs 2, 3 and 4 interact with monoubiquitin and with M1-, K48- and K63-linked di-ubiquitin (Hewings et al., 2018). However, ZnFs 1, 2 and 3 did not show significant interaction with polyubiquitin based on *in vitro* pull-down assays performed by Kwasna et al., and EMSAs shown by Hermanns et al. suggested that the binding of ZUP1 to the common DNA templates tested does not depend on ZUP1 ZnFs (Kwasna et al., 2018; Hermanns et al., 2018).

USP11 contains two ubiquitin-like (UBL) domains, one adjacent to the 'domain present in USPs' (DUSP) at the N-terminus and the other embedded in its catalytic domain. As the name suggests, UBL domains share relatively close structural similarity with ubiquitin as they form the characteristic β-grasp fold architecture composed of a central α-helix cradled by a β-sheet (Vijay-Kumar et al., 1987; Hochstrasser et al., 2009; Faesen et al., 2012; **Fig. 4.6A**). UBL domains are best known for their role in mediating protein associations with the proteasome, where

they bind to ubiquitin-binding motifs within ubiquitin receptors (Kang et al., 2007; Husnjak et al., 2008; Shi et al., 2016).

ZUP1 zinc fingers share some sequence similarity with the extensively studied ubiquitin-binding UBZ of DNA polymerase eta (Pol η) (Bomar et al., 2007; Hermanns et al., 2018; **Fig. 4.6B**). Considering the possibility that ZnF2 binds ubiquitin based on previous NMR studies mentioned above, it was speculated whether ZnF2 may be able to recognise the UBL domain(s) of USP11 based on their structural similarity with ubiquitin.

Based on the sequence alignment between ZUP1 zinc fingers and the UBZ domain of Pol η, a conservatively replaced and an invariant residue were noted at positions 43 and 44 for ZnF2 (Hermanns et al., 2018; **Fig. 4.6B**). These residue positions align with two ubiquitin-binding residues previously suggested for ZnF4, Ile207 and Leu208 (Kwasna et al., 2018; **Fig. 4.6B**). Both residues in ZnF2 were substituted with alanine to assess their contribution to USP11 interaction, and residues in other zinc fingers that aligned with these ZnF2 residues were also mutated to serve as negative controls, given the observation in **Fig. 4.5** that they are unlikely to play any major role in the interaction.

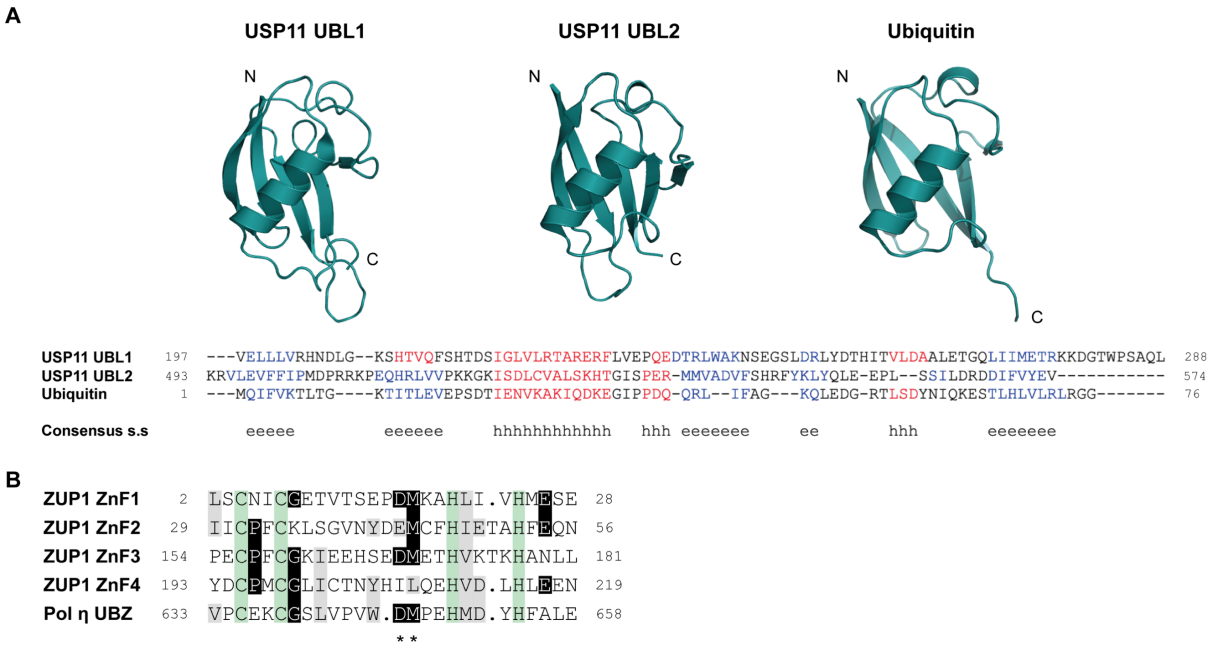



**Figure 4.6: Comparison between USP11 UBL domains and ubiquitin, or ZUP1 zinc fingers and DNA polymerase eta (Pol η) UBZ domain.** A) Structures of human USP11 UBL1 (PDB: 4MEL) and UBL2 (AlphaFold prediction, Jumper et al., 2021) domains were compared to that of ubiquitin (PDB: 1UBQ). Structural similarity is evident between USP11 UBL1, UBL2 and ubiquitin despite poor sequence conservation as shown in the sequence alignment. Predicted secondary structures from the sequence (red: α-helix; blue: β-strand), consensus predicted secondary structure (s.s) symbols (h: α-helix; e: β-strand) (PROMALS3D, Pei et al., 2008). Figures were prepared in Pymol. B) Sequence alignment between ZUP1 zinc fingers and Pol η UBZ domain (modified from Hermanns et al., 2018). Black background: invariant residues; grey background: conservatively replaced; green background: conserved cysteine and histidine residues in C2H2-type zinc fingers. The asterisks denote the residues mutated within ZUP1 ZnFs for the assay in Fig. 4.7.

Mutation of the two ZnF2 residues, Glu43 and Met44 revealed that these residues are important for the ZUP1-USP11 interaction. Alanine substitution of these ZnF2 residues disrupted USP11 binding with an effect comparable to deleting ZnF2 (**Fig. 4.7**). This reinforces the hypothesis that ZUP1 ZnF2 has a binding site specific for USP11. Based on *in vitro* pull-down assays performed by others in the lab using purified recombinant proteins, ZUP1 was shown to directly bind USP11 composed of the N-terminal DUSP-UBL1 domains. Consistent with the observation shown here, alanine substitution of both Glu43 and Met44 in recombinant ZUP1 was also found to prevent USP11 binding *in vitro* (**Appendix B: Fig. 4**).

To gain a deeper understanding of the ZUP1-USP11 interaction, experiments presented in the next section focused on determining the USP11 domains or regions that mediate its interaction with ZUP1. Given also that TCEAL1 binds to ZUP1 mutants in a similar fashion to USP11, binding sites were mapped between USP11 and TCEAL1, and the dependence of TCEAL1 on USP11 for its binding to ZUP1 was explored.

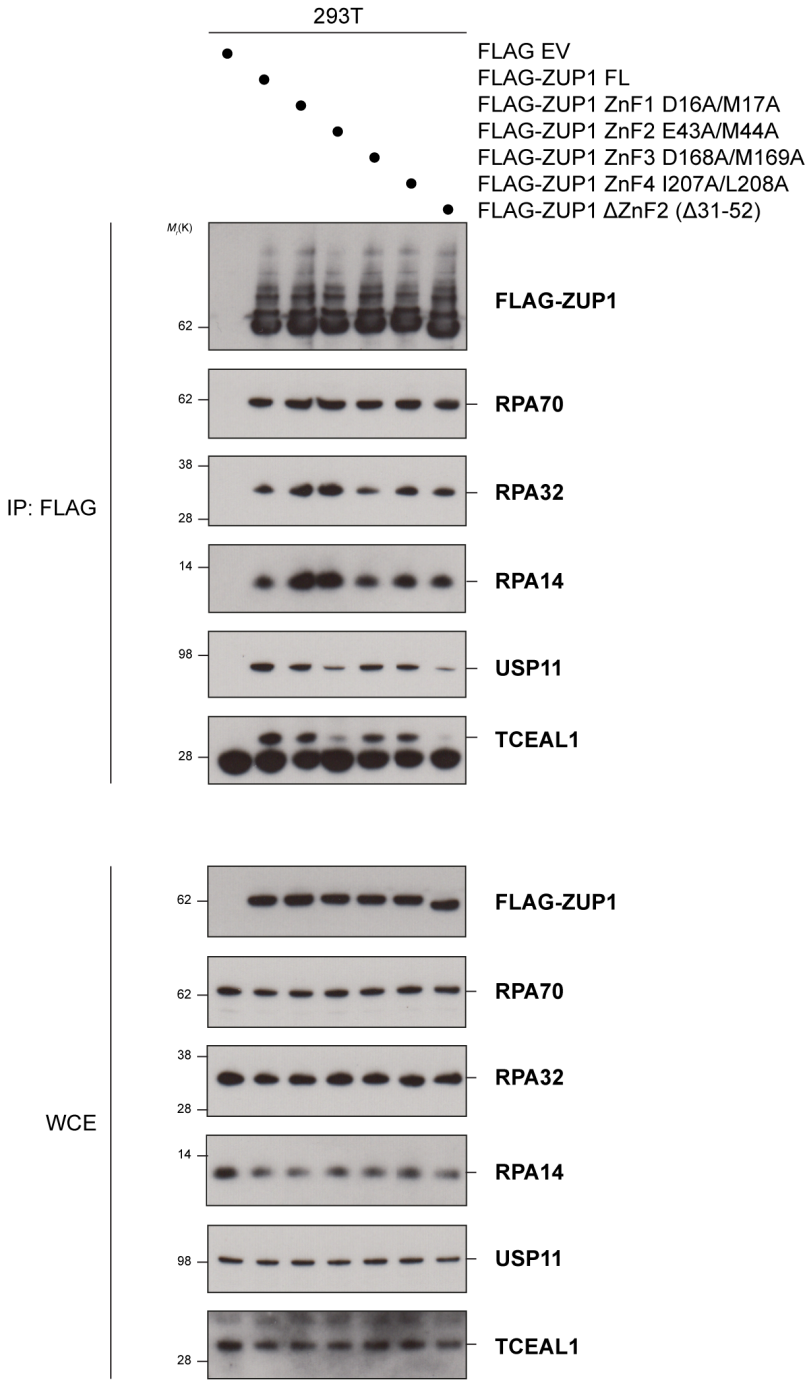



**Figure 4.7: Glu43 and Met44 in ZUP1 ZnF2 are potential interacting residues that mediate USP11 binding.** ZUP1 ZnF alanine mutants were generated based on the sequence alignment shown in Fig. 4.6B. The binding of ZUP1 ZnF mutants to USP11 and other indicated ZUP1 interactors was assessed by co-immunoprecipitation as previously described. The ΔZnF2 mutant that was previously examined in Fig. 4.5 was also included for comparison. Blots shown are representative of two independent experiments (n = 2).

### 4.2.3 Dissecting USP11-ZUP1 and USP11-TCEAL1 interactions

With the knowledge that ZUP1 binds to USP11 specifically via ZnF2, I sought to identify the domain of USP11 that participates in this interaction. USP11 domains were deleted based on published domain annotations and boundaries (**Fig. 4.8A**, Georges et al., 2018). The N-terminal region preceding the DUSP domain is a relatively large disordered region that was deleted in one construct (FLAG-USP11 67-963) to assess whether it contributes to protein binding. The catalytic domain of USP11 is separated into two parts by a large insert containing the second UBL domain (UBL2) and an additional region referred to as the 'insert' (Harper et al., 2014). To examine the role of the UBL2 in protein interaction, both the UBL2 and remaining insert region were deleted together in the first instance, which was later revised in **Fig. 4.9**.

Although recombinant full-length ZUP1 was shown to bind a USP11 fragment consisting of the DUSP and UBL1 region *in vitro*, these N-terminal domains may not play a major or essential role in the interaction in cells as their deletion did not significantly alter the level of ZUP1 binding (FLAG-USP11 288-963, **Fig. 4.8B**). In contrast, deletion of the UBL2 and insert region of USP11 (FLAG-USP11 Δ489-778) significantly disrupted the binding of TCEAL1 while reducing that of ZUP1. In an attempt to validate this result, a different approach was tested where the FLAG-tagged USP11 deletion mutants were co-expressed with YFP-tagged full-length ZUP1 in cells. However, all the USP11 mutants co-precipitated the same level of YFP-ZUP1, suggesting that ectopic expression of both proteins may introduce differences to the interactions and may not accurately mimic the endogenous protein complex (**Fig. 4.8C**). As the results in **Fig. 4.8C** were obtained from a single experiment, more experimental repeats will be needed before interpreting the results.

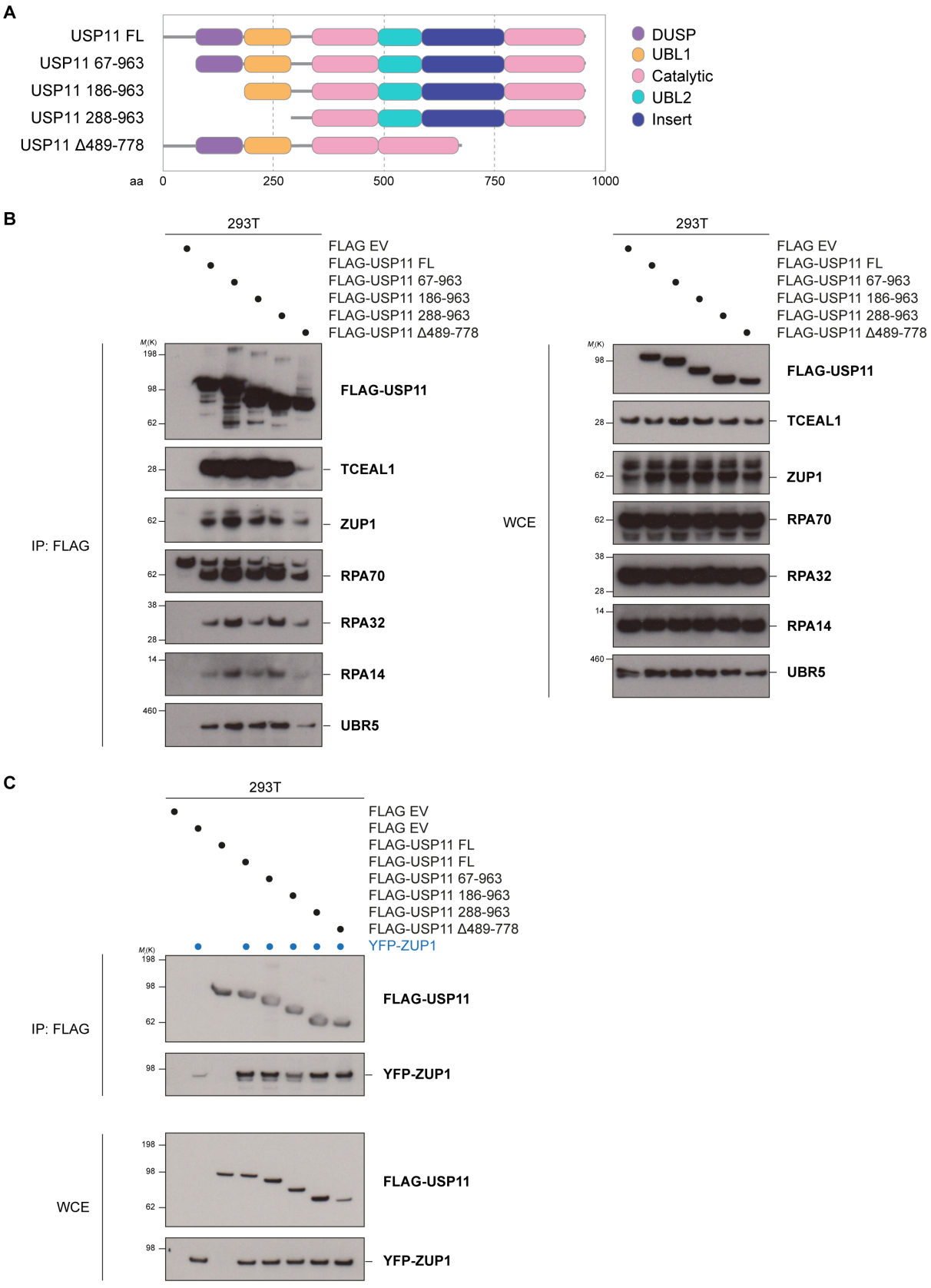

A
USP11 FL
USP11 67-963
USP11 186-963
USP11 288-963
USP11 Δ489-778
aa
0
250
500
750
1000
DUSP
UBL1
Catalytic
UBL2
Insert
B
293T
FLAG EV
FLAG-USP11 FL
FLAG-USP11 67-963
FLAG-USP11 186-963
FLAG-USP11 288-963
FLAG-USP11 Δ489-778
IP: FLAG
WCE
FLAG-USP11
TCEAL1
ZUP1
RPA70
RPA32
RPA14
UBR5
C
293T
FLAG EV
FLAG EV
FLAG-USP11 FL
FLAG-USP11 FL
FLAG-USP11 67-963
FLAG-USP11 186-963
FLAG-USP11 288-963
FLAG-USP11 Δ489-778
YFP-ZUP1
IP: FLAG
WCE
FLAG-USP11
YFP-ZUP1

**Figure 4.8: Deletion of previously annotated USP11 domains or regions to identify potential sites involved in ZUP1 and TCEAL1 binding.** A) Schematic illustration of FLAG-tagged USP11 mutants generated by deleting previously annotated domains or regions (Georges et al., 2018). B) USP11 mutants were assessed for their binding to ZUP1 and TCEAL1 as previously described. Other indicated ZUP1 interactors were also included in the immunoblot. Blots shown are representative of two independent experiments (n = 2). C) Full-length YFP-tagged ZUP1 was co-expressed with FLAG-tagged USP11 mutants in cells and their binding was assessed. Blots shown were obtained from a single experiment (n = 1).

The deletion mutagenesis suggests that the UBL2 and insert region may be important for binding ZUP1 and TCEAL1 (**Fig. 4.8A, 4.8B**). However, this deletion spanned a large region and may have caused global structural rearrangements. Another source of artifacts may the domain boundaries used to generate the deletions within USP11, as these were defined differently from one study to another (Harper et al., 2014; Georges et al., 2018; Spiliotopoulos et al., 2019). Importantly, the structure of USP11 has not been solved beyond the N-terminal DUSP-UBL1 region, therefore it should be considered that the UBL2 and insert region may not have been annotated accurately.

The domain boundaries of USP11 were therefore revised to generate new deletion mutants. Domain boundaries are typically deduced by sequence homology or predictions of secondary structure, solvent accessibility and contact maps (Zheng et al., 2020; Wang et al., 2021). However, the delineation of domain boundaries directly from experimental structures is considered more reliable.

In re-analysing the domain boundaries for the UBL2 and insert (UBL2-insert) region, USP11 domain annotations were retrieved from the InterPro database (Blum et al., 2021). These annotations did not separate the UBL2 domain from the remaining insert, and were found to differ from other boundary predictions (Zhu et al., 2007;

Harper et al., 2014; Georges et al., 2018; Spiliotopoulos et al., 2019). The AlphaFold prediction of USP11 structure was used to visualise the secondary structures within the UBL2-insert region (Jumper et al., 2021). Using the published annotations to guide the approximate domain positions, the UBL2 domain was defined as a structurally compact region from position 493 to 574, while the remaining insert region was defined as a largely disordered region from 575 to 775 (**Fig. 4.9A**).

The UBL2 domain and disordered insert were deleted separately to assess their individual contribution to ZUP1 and TCEAL1 binding (**Fig. 4.9B**). The deleted regions were replaced with a 7 aa flexible linker to allow adequate separation between domains which may minimise the structural impact of the deletion. The deletion of either the UBL2 domain (FLAG-USP11 ΔUBL2 only [Δ493-574] + GSGSGSG) or insert region (FLAG-USP11 ΔInsert only [Δ575-775] + GSGSGSG) in USP11 led to a decrease in ZUP1 binding, and severely disrupted TCEAL1 binding (**Fig. 4.9C**). If this effect was not due to global structural artifacts of the deletion, the results suggest that ZUP1 and TCEAL1 binding may require the presence of both the UBL2 domain and disordered insert, indicating that these regions may act as one binding unit rather than having distinct specificity. The role of the UBL2-insert region is not known, but has been speculated to mediate protein interactions or trafficking since the UBL2 domain does not demonstrate direct autoregulatory functions nor contribute to catalysis (Harper et al., 2014).

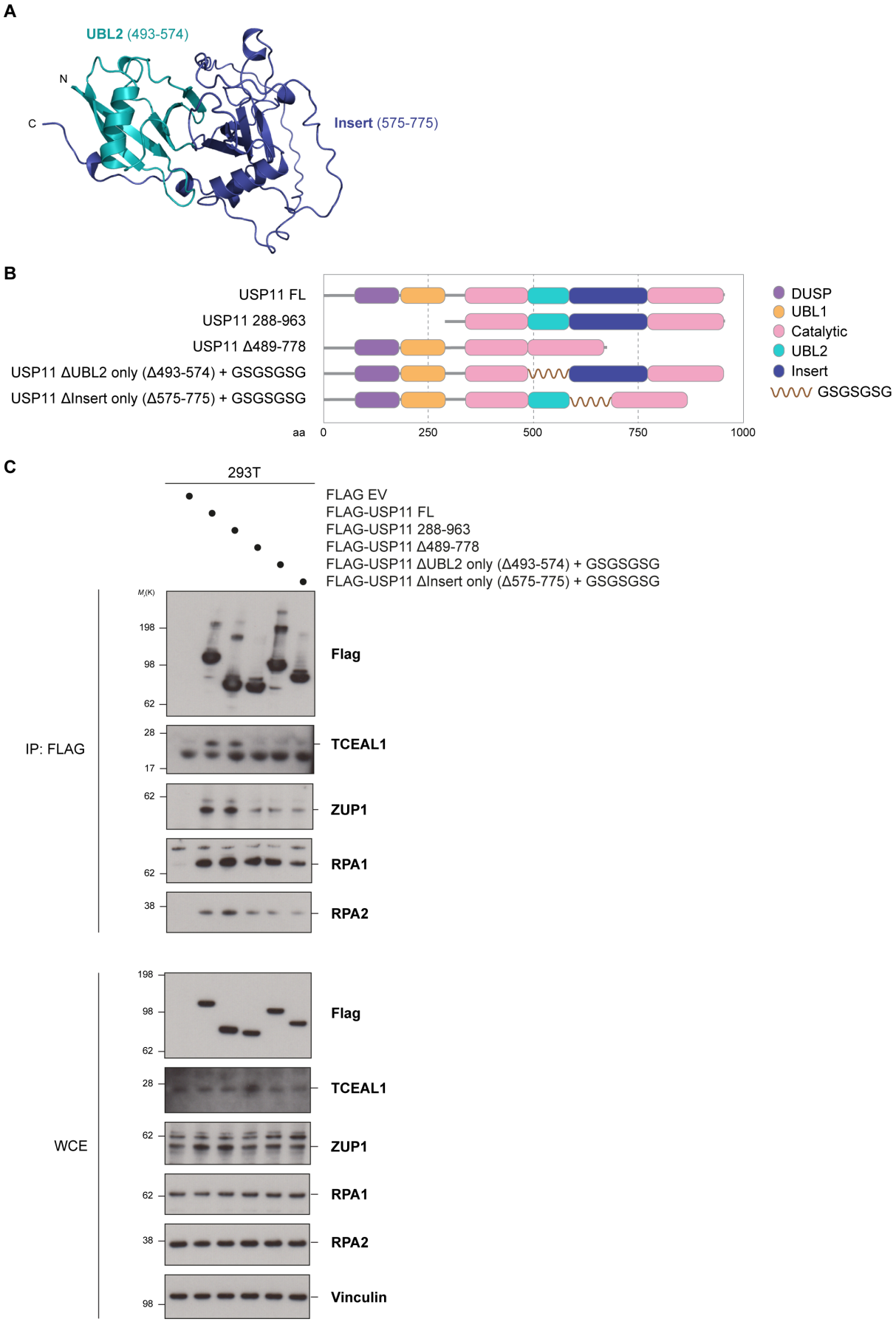

A
UBL2 (493-574)
N
C
Insert (575-775)
B
USP11 FL
USP11 288-963
USP11 Δ489-778
USP11 ΔUBL2 only (Δ493-574) + GSGSGSG
USP11 ΔInsert only (Δ575-775) + GSGSGSG
aa
0
250
500
750
1000
DUSP
UBL1
Catalytic
UBL2
Insert
GSGSGSG
C
293T
FLAG EV
FLAG-USP11 FL
FLAG-USP11 288-963
FLAG-USP11 Δ489-778
FLAG-USP11 ΔUBL2 only (Δ493-574) + GSGSGSG
FLAG-USP11 ΔInsert only (Δ575-775) + GSGSGSG
M(K)
198
98
62
28
17
62
62
38
IP: FLAG
Flag
TCEAL1
ZUP1
RPA1
RPA2
198
98
62
28
62
62
38
98
WCE
Flag
TCEAL1
ZUP1
RPA1
RPA2
Vinculin

**Figure 4.9: USP11 UBL2 domain and the disordered insert region may bind to TCEAL1 and ZUP1.** A) AlphaFold structure prediction of human USP11 UBL2 domain and the insert region (Jumper et al., 2021). Figure was prepared in Pymol. B) Schematic illustration of FLAG-tagged USP11 mutants generated by deleting the UBL2 or insert region in A individually. FLAG-USP11 288-963 and FLAG-USP11 Δ489-778 were previously assessed in Fig. 4.8, and were included in this experiment for comparison. C) USP11 mutants were assessed for their binding to ZUP1 and TCEAL1. Other indicated ZUP1 interactors were also included in the immunoblot. Blots shown are representative of two independent experiments (n = 2).

A BLAST search of USP11 UBL2 domain and the disordered insert region indicated homology to its USP homologues, USP4 (56.79% similarity) and USP15 (50% similarity). Unlike USP11, neither USP4 nor USP15 have been shown to significantly enrich with ZUP1 or TCEAL1 (Sowa et al., 2009; Hermanns et al., 2018). To examine residues in the USP11 UBL2-insert region that may be involved in its interaction with ZUP1 and TCEAL1, a potential starting point may be to compare the UBL2 domain of USP11 with that of USP4 and USP15. Sequence alignment of the predicted α-helix of the UBL2 domain reveals surface residues that potentially distinguish the binding partners of USP11 from that of its homologues (**Appendix B: Fig. 5**). One notable difference is found between Val527 of USP11 and Glu520 of USP4 that are hydrophobic and charged respectively, and may therefore generate vastly different binding specificities. Similarly, the charged Lys531 of USP11 contrasts with the hydrophobic Ala511 of USP15. The contribution of these USP11 UBL2 domain residues can therefore be assessed in the future by mutagenesis and similar co-immunoprecipitation approaches. However, the disordered insert region of USP11 may add to the complexity of the interaction, given that it may also contribute to the binding as shown in **Fig. 4.9C**.

TCEAL1 is a poorly characterised 159 aa protein with no annotated functional domains, established roles or solved structures to date. It is encoded by the *TCEAL* gene family that originated from transposable element domestication events and exists in a cluster with *BEX* genes (Navas-Pérez et al., 2020). The TCEAL and BEX families share a conserved C-terminal α-helical region which, for BEX proteins, are known to mediate interactions with their binding partners (Fernandez et al., 2015).

To determine the potential binding sites involved in TCEAL1 interaction with USP11 and ZUP1, the AlphaFold structure prediction of TCEAL1 was visualised to identify ordered regions. Two α-helices were predicted at the C-terminus and are named α1 and α2 referring to the short and long helices respectively (**Fig. 4.10A**, Jumper et al., 2021). Deletion of α1 within TCEAL1 led to a slight decrease in USP11 and ZUP1 binding, while the deletion of α2 significantly disrupted the binding of USP11 and ZUP1 (**Fig. 4.10B**). It is important to note that the deletion of α2 removes a large ordered region of TCEAL1 which would likely disrupt the protein structure. Therefore, the decrease in USP11 and ZUP1 binding could be a result of structural artifacts rather than the loss of binding sites. To investigate if α2 has a binding site for USP11 and/or ZUP1, individual residues within α2 can be mutated in future studies to identify potential interacting residues.

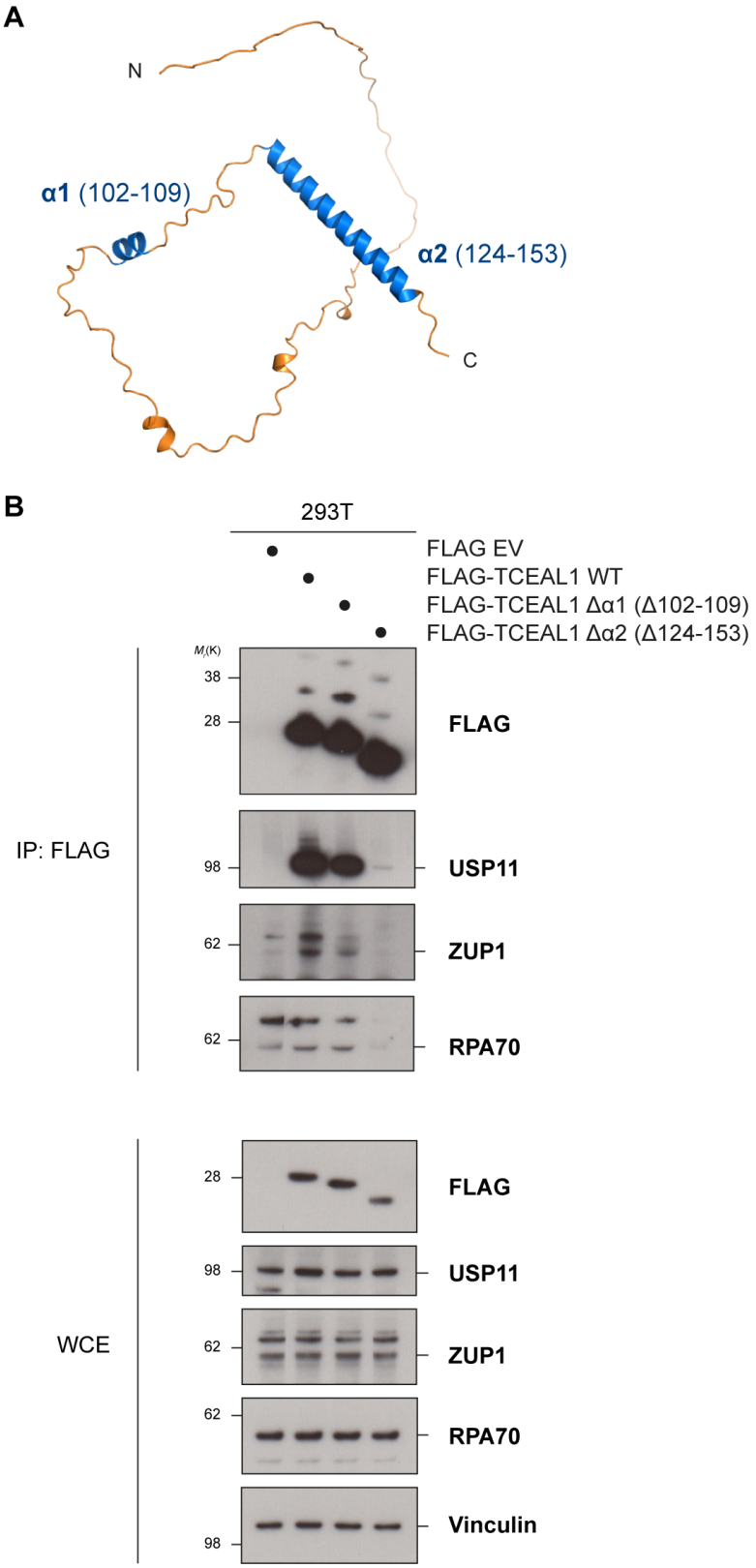

A
N
α1 (102-109)
α2 (124-153)
C
B
293T
FLAG EV
FLAG-TCEAL1 WT
FLAG-TCEAL1 Δα1 (Δ102-109)
FLAG-TCEAL1 Δα2 (Δ124-153)
M(K)
38
28
FLAG
IP: FLAG
98
USP11
62
ZUP1
62
RPA70
28
FLAG
98
USP11
WCE
62
ZUP1
62
RPA70
98
Vinculin

**Figure 4.10: Assessing the effects of deleting TCEAL1 α1 and α2 on USP11 and ZUP1 binding.** A) AlphaFold structure prediction of human TCEAL1 protein (159 aa) (Jumper et al., 2021). Two predicted α-helices are named α1 (short helix) and α2 (long helix) and the residue positions are indicated. Figure was prepared in Pymol. B) The effects of TCEAL1 α1 or α2 deletion on USP11 and ZUP1 binding were assessed by immunoprecipitating FLAG-tagged TCEAL1 and checking protein binding as previously described. RPA70 was included in the immunoblot as a ZUP1 interacting protein. Blots shown are representative of two independent experiments (n = 2).

The binding of TCEAL1 to ZUP1 mutants was consistently observed to follow a similar trend to that of USP11 (**Fig. 4.2B, 4.5B, 4.7**). As TCEAL1 is frequently found to co-purify with USP11, it was considered whether TCEAL1 may depend on USP11 for its interaction with ZUP1 (Sowa et al., 2009; Hein et al., 2015; Basic et al., 2021). To investigate this in cells, USP11 was silenced by a siRNA pool and the binding of TCEAL1 to ZUP1 was assessed. USP11 knockdown severely disrupted TCEAL1 binding to ZUP1 whilst having a negligible effect on total cellular TCEAL1 protein for which a decrease, if any, is extremely slight in comparison (**Fig. 4.11A**). This suggests that USP11 may bridge the interaction between TCEAL1 and ZUP1. TCEAL1 and ZUP1 may not directly interact, however this remains to be clarified using purified recombinant proteins *in vitro*. Intriguingly, the level of ectopically-expressed ZUP1 in the whole cell extracts correlated with that of endogenous USP11, a trend also observed in **Fig. 4.11B**. This suggests potential regulatory mechanisms between ZUP1 and USP11 in relation to protein stability, as described in the Discussion.

To understand how USP11 may reciprocally depend on TCEAL1 for its interaction with ZUP1, the effect of TCEAL1 knockdown was assessed. USP11 binding to ZUP1 was impaired after TCEAL1 knockdown but was not entirely prevented (**Fig. 4.11B**). Of note, the loss of TCEAL1 markedly enhanced the total cellular level of USP11 protein. This suggests a role of TCEAL1 in simultaneously promoting USP11 turnover and its binding to ZUP1, which can be explored in future work as outlined in the

Discussion. TCEAL1 knockdown was also accompanied by an increase in FLAG-ZUP1 in the whole cell extracts. The increase in FLAG-ZUP1 could have occurred through the enhanced levels of total USP11 protein, based on the correlation observed between USP11 and FLAG-ZUP1 protein levels in **Fig. 4.11A**.

The results in **Fig. 4.11A and 4.11B** should be interpreted with caution as they were obtained from a single experiment (n = 1). Therefore, more biological repeats will be required confirm the observations. Considering the potential pleiotropic effects of protein knockdown, future work can also utilise knockout cells or other protein depletion systems such as the degron system to investigate the dependence of USP11 and TCEAL1 on one another for binding to ZUP1.

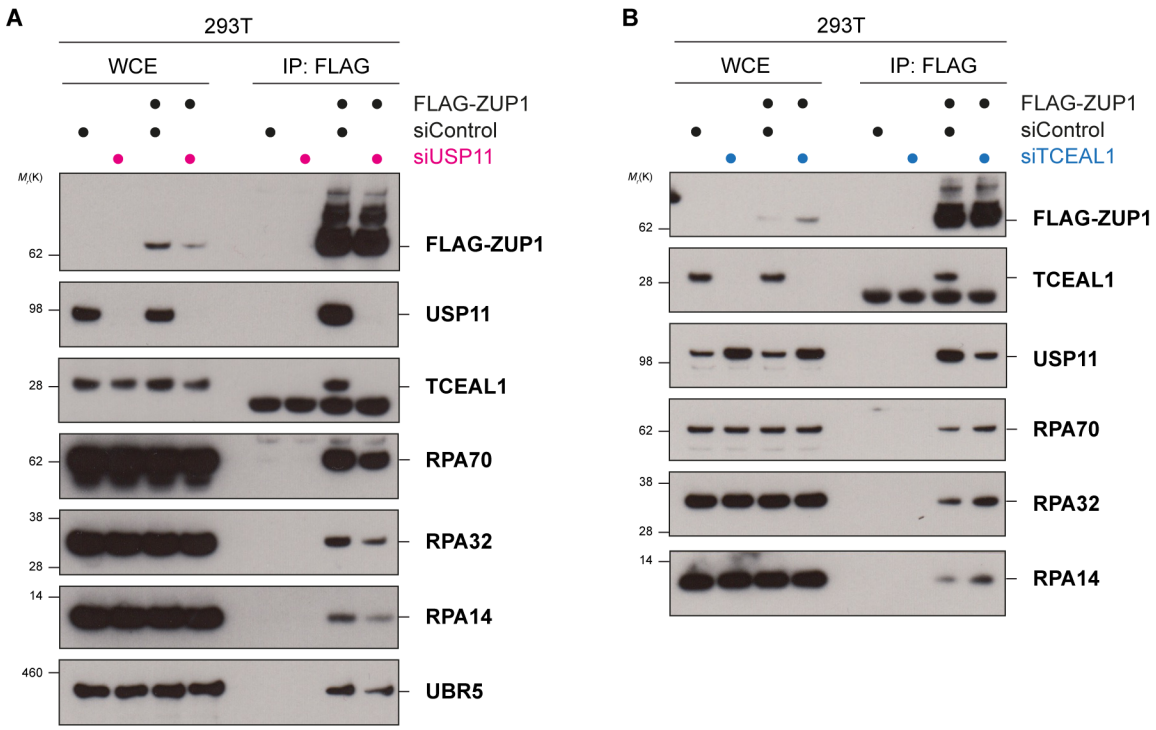



**Figure 4.11: TCEAL1 binding to ZUP1 may be USP11-dependent, and TCEAL1 may have a regulatory role that influences USP11 protein abundance and binding to ZUP1.** A) USP11 was depleted using a siRNA pool and the effects on TCEAL1 binding was assessed as previously described. RPA and UBR5 were included in the immunoblot as ZUP1 interactors. Blots shown were obtained from a

single experiment (n = 1). B) As in A, the effects of TCEAL1 knockdown on protein binding was examined. Blots shown were obtained from a single experiment (n = 1).

## 4.3 Discussion

### 4.3.1 A novel interaction between two DUB classes

DUBs of the same family such as USPs have been shown to interact, and this is thought to be related to their regulation of common targets or binding partners. For example, USP7 interacts with USP11, and both were shown to co-purify with and regulate the ubiquitylation status of Polycomb repressive complex 1 (PRC1) components (Sowa et al., 2009; Maertens et al., 2010; Georges et al., 2018).

This chapter demonstrates a novel interaction between ZUP1 and USP11 which belong to distinct DUB families and share little overlap in their interactome. It will be important to determine if their functions intersect in DNA repair, which are extensively reported for USP11 (Section 4.1), and beginning to emerge for ZUP1. In Chapter 3, it was shown that ZUP1 knockout significantly sensitised cells to various genotoxic agents. USP11 loss has also been shown to cause hypersensitivity to genotoxic stress including PARP inhibitor treatment, ionising radiation, cisplatin and mitomycin C (Wiltshire et al., 2010; Nishi et al., 2014). This hints at essential and unique roles of ZUP1 and USP11 in DNA repair that may not be redundant with other proteins, thereby suggesting the importance of this interaction in genome maintenance.

ZUP1 acts as an endo-DUB and specifically cleaves long K63-linked polyubiquitin chains (Hewings et al., 2018; Hermanns et al., 2018; Haahr et al., 2018; Kwasna et al., 2018). USP11 cleaves various linkage types including K6-, K11-, K33- and K63-linked chains *in vitro*, and experiments in cells have suggested that USP11 removes K48-linked chains on p21 (Harper et al., 2014; Deng et al., 2018). USP11 is also known to cleave monoubiquitin on SPRTN (Perry et al., 2021). In a cellular setting

where ZUP1 cleaves long polyubiquitin chains, it is possible that USP11 may remove the remaining di- or monoubiquitin moiety on the same chain targeted by ZUP1. As discussed in Chapter 5, ZUP1 was shown to remove K63-linked polyubiquitin chains on PCNA but not the monoubiquitin on PCNA, which reflects its preference for cleaving longer chains (**Appendix C: Fig. 4**; Kwasna et al., 2018). An important next step would be to assess if USP11 can complement ZUP1 DUB activity by removing the monoubiquitin moiety on PCNA. This will reveal whether ZUP1 and USP11 can cooperate to deubiquitylate substrates in the same vicinity, which may explain the biological role for their physical interaction.

The interaction between ZUP1 and USP11 may also enable them to regulate the ubiquitylation status of one another. An example of DUB-mediated regulation is the removal of degradation signals dictated by K48-linked ubiquitin chains that will lead to protein stabilisation. DUBs can also remove other non-degradative signals such as K63-linked chains (Yau et al., 2016). From the ZUP1-USP11 interaction, it is conceivable that one DUB may dynamically regulate various aspects of the other's function. **Fig. 4.11** presents an interesting observation that the level of ZUP1 that was ectopically expressed correlated with that of USP11 in the whole cell extracts, suggesting potential regulatory mechanisms between the two that have an influence on protein stability. **Fig. 4.7** suggests that ubiquitin recognition by ZUP1 via UBZ may not be a prerequisite for its binding to USP11, since the interaction was not significantly affected by a previously characterised UBZ mutation.

To understand potential regulatory mechanisms between ZUP1 and USP11, future work can examine how the loss of one DUB or its catalytic activity affects the ubiquitylation status or protein stability of the other. For example, ubiquitin chain formation on ZUP1 and USP11 can firstly be assessed in USP11 and ZUP1 knockout cells respectively, by performing affinity purification of ubiquitylated proteins from cells using the techniques described in Chapter 5. Cycloheximide chase assays can also be performed to analyse the protein stability of each DUB over time, after modulating the expression levels or functional status of the other DUB (Kao et al., 2015).

The role of the ZUP1-USP11 interaction may also relate to the binding sites involved. Deletion mutagenesis suggests that ZUP1 binds to the UBL2-insert region of USP11 that separates the two lobes of the catalytic domain (**Fig. 4.9**). Although Harper et al. has shown that the UBL2 domain may not influence the catalytic activity of USP11, it is possible that the binding of an interacting protein such as ZUP1 to this region may induce allosteric changes that affect catalysis. USP11 binds to ZUP1 ZnF2, the roles of which are also not completely understood. Hermanns et al. observed that the deletion of ZnF1 and ZnF2 of ZUP1 slightly increased its catalytic activity which suggests a possible autoregulatory role (Hermanns et al., 2018). To examine these potential roles, *in vitro* DUB assays can be performed to assess the effect of USP11 binding on ZUP1 catalytic activity, and vice versa.

The mapping of ZUP1 ZnF2 to the UBL2 domain of USP11 in this chapter reveals novel roles for these domains and provides tools for future investigation into the biological role of this interaction. This discovery will not only lead to a more complete picture of how the domains of the individual DUBs function as one unit, but will also advance our understanding of the ubiquitin machinery in relation to how two unrelated DUBs may depend on each other for regulating cellular processes.

### 4.3.2 Specificity of the second zinc finger of ZUP1 for binding USP11

Zinc finger domains are protein structures stabilised by the coordination between $Zn^{2+}$ and well-conserved metal-binding residues, typically Cys and His (Cassandri et al., 2017; Kluska et al., 2018). They are classified based on their structure and the Cys/His combination. Discovered in transcription factors, zinc fingers are best known for their DNA-binding role but have also been reported to interact with RNA and protein in diverse cellular processes (Hall et al., 2005; Brayer et al., 2008).

ZUP1 has four C2H2-type zinc fingers at its N-terminus where the first two, ZnF1 and ZnF2 are separated from ZnF3 by a linker of approximately 100 residues (**Fig. 4.5A**). ZnF4 was shown to be the dominant ubiquitin-binding UBZ domain and precedes

two other ubiquitin-binding domains, the MIU and ZHA (Hermanns et al., 2018; Kwasna et al., 2018; Haahr et al., 2018). These tandem ubiquitin-binding domains are thought to form a polyubiquitin-binding module for long chains hydrolysed by ZUP1.

The linker length between zinc fingers arranged in tandem has been shown to dictate the spacing between DNA sequences recognised by the individual zinc fingers (Fukushima et al., 2012). In ZUP1, the separation of ZnF1 and ZnF2 from the other zinc fingers by a long disordered linker raises the question of whether the binding targets of ZnF1 and ZnF2 may be distinct from that of the ubiquitin-binding ZnF4. This also takes into consideration the lack of consistent evidence for the ability of ZUP1 zinc fingers apart from ZnF4, to bind ubiquitin as mentioned earlier (Section 4.2.2; Hermanns et al., 2018; Kwasna et al., 2018). Indeed, this chapter and complementary *in vitro* work in the lab suggest that the major role of ZnF2 may be to provide a specific binding site for USP11.

Mutagenesis screens in cells revealed that the ZUP1 ZnF2 is critical for USP11 interaction which was partially mapped to interacting ZnF2 residues, Glu43 and Met44 (**Fig. 4.7**). Protein-protein interactions mediated by zinc fingers have been shown to involve multiple zinc fingers as demonstrated by FOG1 in its interaction with GATA1, or require a single zinc finger within a tandem array such as the LIM domain that was shown to be individually sufficient in binding Ldb1-LID (Fox et al., 1999; Deane et al., 2004). Although **Fig. 4.5** suggests that ZUP1 ZnF1 may be dispensable for USP11 binding, it may be placed in close proximity to ZnF2 to stabilise the binding of USP11 on ZnF2, albeit in a redundant manner. Alternatively, a specific USP11 binding site may only exist within ZnF2, while ZnF1 may recognise distinct targets.

The disruption of ZUP1 exon 2 encoding ZnF1, 2 and 3 was shown in Chapter 3 (**Fig. 3.9**) to cause significant survival defects upon the induction of genotoxic stress. To determine if ZUP1-USP11 interaction via ZnF2 may be important for DNA repair and cell survival upon exposure to the genotoxic agents, the ZUP1 ZnF2 E43A/M44A mutant can be expressed in the ZUP1 hypomorphs or knockouts to test its ability to rescue the survival defects. It would also be interesting for future investigations to

explore the binding targets of the other zinc fingers, ZnF1 and ZnF3 that have unknown roles to date. EMSAs performed by Hermanns et al. suggested that ZUP1 ZnFs may not be required for the binding of ZUP1 to common DNA templates (Hermanns et al., 2018). This can be examined further by exploring diverse DNA sequences to identify potential DNA sequence specificity of the ZnFs (Najafabadi et al., 2015).

### 4.3.3 USP11-TCEAL1 interaction mapping will aid future functional characterisation of TCEAL1

*TCEAL* (transcription elongation factor A (SII)-like) genes originated from transposable element domestication events and at least nine of these genes have been identified in humans (Navas-Pérez et al., 2020). TCEAL1 was discovered decades ago as a nuclear phosphoprotein with notable sequence similarities to the human transcription elongation factor A (TCEA), however evidence for its biological function remains scarce (Yeh et al., 1994a; Pillutla et al., 1999). TCEAL1 displays homology with the RNA polymerase binding site of TCEA (Yeh et al., 1994a). To date, only one study has suggested a role of TCEAL1 in transcription, where it was proposed to mediate the transcriptional repression of Rous sarcoma virus long terminal repeat (Yeh et al., 1994b). Physiologically, TCEAL1 has been implicated in tumorigenesis and chemotherapy response based on small-scale gene expression profiling and screens (Makino et al., 2005; Rushworth et al., 2020). Another TCEAL family protein, TCEAL3 was suggested to have a role in axon regeneration, and TCEAL7 is thought to regulate the transcriptional activity of NF-κB (Lukomska et al., 2021; Rattan et al., 2009).

The presence of TCEAL1 in a complex comprising USP11 and ZUP1 that may have intersecting roles as discussed previously, could provide an avenue to expand our limited understanding of TCEAL1 function. This chapter identifies the UBL2-insert of USP11 as an important region that mediates USP11-TCEAL1 interaction, however

further mutagenesis screens and structural information will be essential to identify the interacting residues and exclude potential structural artifacts of the deletion.

This chapter also presents an intriguing observation that TCEAL1 knockdown significantly increased USP11 protein levels whilst decreasing USP11 binding to ZUP1 (**Fig. 4.11B**). Given the crucial roles of USP11 as a DUB in HR repair of DSBs (described in Section 4.1), it will be important to dissect how TCEAL1 may regulate its turnover, protein stability, expression and/or binding affinity to ZUP1 (Orthwein et al., 2015). For example, if TCEAL1 promotes USP11 turnover as suggested in **Fig. 4.11B**, TCEAL1 over-expression in cells should lead to a more rapid degradation of USP11 in cycloheximide chase assays compared to wild-type cells with physiological TCEAL1 expression (Kao et al., 2015). The proteasome dependence can then be assessed using proteasome inhibitors. Alternative systems to ectopic TCEAL1 expression or RNAi such as TCEAL1 knockout cells may also be used to investigate the effects of TCEAL1 on USP11 protein stability or binding to ZUP1.

To understand these potential processes and the broader cellular role of TCEAL1, it may also be necessary to investigate if TCEAL1 is directly involved in transcription as previously suggested. Interestingly, transcription is closely intertwined with DNA replication, and transcription-associated damage is a source of genome instability (Lans et al., 2019; Chapter 1). Overall, the small size and simple domain architecture of TCEAL1 should not spare it from thorough functional characterisation as it may play important roles that support the genome stability functions of USP11 and/or ZUP1.

### 4.3.4 The ZUP1 interactome suggests a role for ZUP1 in ubiquitin signalling and DNA repair

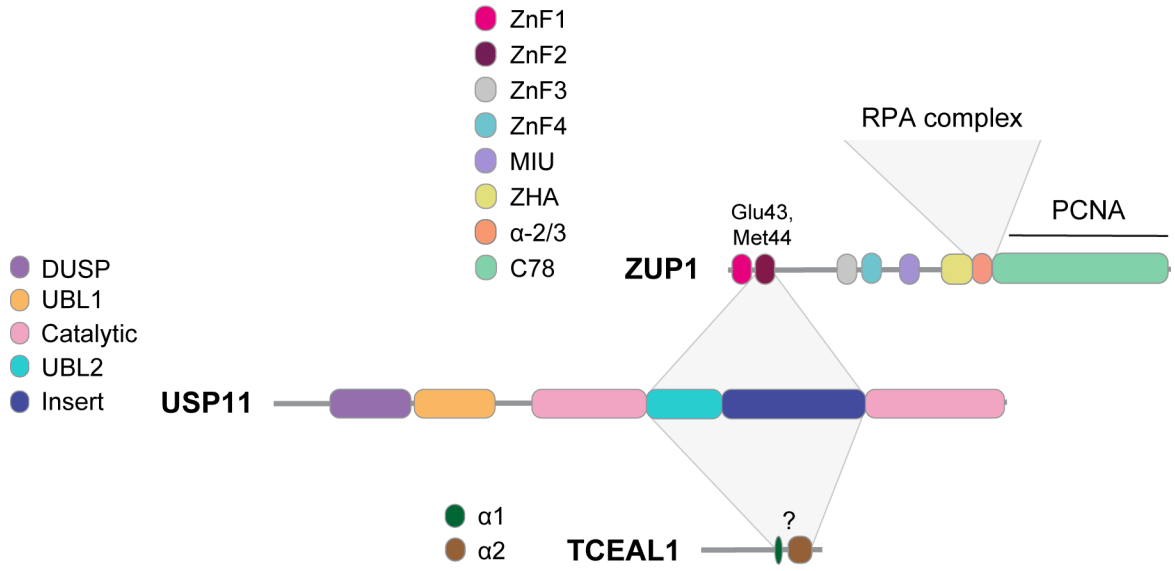



**Figure 4.12: Summary of potential interacting domains of ZUP1, USP11 and TCEAL1 identified from mutagenesis studies in this chapter.**

In this chapter, I verified the association of ZUP1 with interacting partners ascertained from previous proteomic approaches to define the ZUP1 interactome in cells. I investigated potential binding sites with a focus on proteins with established roles in ubiquitin signalling and/or DNA repair. USP11 and its binding partner TCEAL1 were mapped to ZUP1 ZnF2, and the α-2/3 region of ZUP1 participates in ZUP1-RPA interaction. The UBL2-insert region of USP11 may be important for binding TCEAL1 and ZUP1. PCNA was not mapped to a specific site within ZUP1 and possibly binds the catalytic domain. *In vitro* pull-down assays in the lab have demonstrated that ZUP1 cleaves K63-linked polyubiquitin chains on PCNA as discussed further in Chapter 5 (**Appendix C: Fig. 4**). Interestingly, other members in the lab have shown that RPA significantly enhances ZUP1 activity in hydrolysing both free K63-linked polyubiquitin chains and those formed on PCNA (**Appendix C: Fig. 4, 5**).

The presence of multiple proteins involved in ubiquitin signalling and DNA repair or replication in the ZUP1 interactome lends support to the hypothesis that ZUP1 operates as a DUB in DNA repair. It will be important to determine which of these interacting proteins are ZUP1 substrates, and the specific context in which they are regulated by ZUP1. RPA and PCNA are particularly compelling candidates that were assessed in Chapter 5, given the importance of ubiquitylation for their DNA repair roles (described in Chapter 1), alongside the lack of known DUBs to date that regulate their polyubiquitylation.

The hypersensitivity of ZUP1 hypomorphs to the genotoxic agents in Chapter 3 (**Fig. 3.9**) could be related to the loss of USP11 binding to ZUP1 ZnF2. This can be assessed by expressing the ZUP1 ZnF2 E43A/M44A mutant in the ZUP1 hypomorphs or knockouts, and evaluating whether the mutant is able to rescue the survival defects. Considering the observation in **Fig. 4.2B** that USP11 and RPA display opposite ZUP1-binding patterns, it is also possible that the significant increase of RPA binding to ZUP1 in the absence of the N-terminal zinc fingers of ZUP1 may contribute to the drug sensitivity phenotypes. RPA was observed by other members in the lab to stimulate ZUP1 catalytic activity *in vitro*, which raises the possibility that enhanced RPA binding to ZUP1 lacking the N-terminal zinc fingers may result in aberrant ZUP1 activity in cells (**Appendix C: Fig. 4, 5**). It was previously shown that ZUP1 lacking the first two zinc fingers had slightly higher activity than full-length ZUP1 in cleaving K63-linked polyubiquitin chains *in vitro* (Hermanns et al., 2018). This may indicate an autoregulatory role for the first two zinc fingers, which could potentially also contribute to the phenotypes shown in Chapter 3.

The known role of USP11 in HR repair and its interaction with ZUP1 raises the question of whether ZUP1 may also be involved in HR (Orthwein et al., 2015; Yu et al., 2016). In addition to the possibility that ZUP1-USP11 interaction may be important for the cell survival phenotypes observed in Chapter 3, the genotoxic agents to which ZUP1 knockouts are hypersensitive generate lesions that can cause replication-associated DSBs, which require accurate repair by HR. Altogether, the findings presented so far in this thesis provided a focus and motivation for the next chapter

which explores how ZUP1 regulates RPA and PCNA ubiquitylation during replication stress, and investigates the role of ZUP1 in HR repair.

# 5

# Investigating the Roles of ZUP1 in DNA Repair

## Contents


**5.1 Introduction……164**

**5.2 Results……168**

5.2.1 Optimising affinity purification and immunoprecipitation methods, and treatment conditions to detect ubiquitylated PCNA and RPA in cells……..168

5.2.2 ZUP1 loss is associated with elevated levels of PCNA polyubiquitylation during replication stress……184

5.2.3 Attempts to rescue PCNA polyubiquitylation in ZUP1 knockout cells……..198

5.2.4 ZUP1 has a role in homologous recombination repair……...212

**5.3 Discussion……..219**

5.3.1 ZUP1 is a DUB that potentially reverses PCNA ubiquitylation……..219

5.3.2 ZUP1 may have an anti-HR role……222

## 5.1 Introduction

The work presented in this thesis so far illustrates that ZUP1 has an important role in preserving cancer cell survival following DNA damage (Chapter 3) and interacts with proteins involved in ubiquitin signalling, DNA replication and repair (Chapter 4). These findings led to the hypothesis that ZUP1 utilises its DUB activity to regulate one or more of its interacting proteins that function in DNA repair. In this chapter, I examined whether ZUP1 regulates the ubiquitylation of two key DNA repair proteins in its interactome during replication stress using ZUP1 knockout cells generated in Chapter 3. This also addresses the critical question of whether any of these identified interacting partners may be cellular substrates of ZUP1.

To investigate how ZUP1 functions as a DUB to maintain genome stability, I focused on two ZUP1 interacting partners, PCNA and the RPA complex, both of which play critical roles in DNA replication and repair as described in Chapter 1. The first protein examined, PCNA is a homotrimer that encircles and slides along the DNA helix whilst tethering DNA polymerases to enhance their processivity during DNA replication (Chapter 1, Section 1.1.2; Slade et al., 2018). In the presence of DNA lesions, PCNA serves as a recruitment platform that interacts with numerous effector proteins to engage the appropriate repair process (Mailand et al., 2013; Slade et al., 2018). The highly dynamic interactions between PCNA and its binding proteins during replication stress are mediated by post-translational modifications including ubiquitylation (Chapter 1, Section 1.6.1; Mailand et al., 2013).

At stalled replication forks, exposed ssDNA stretches are coated by RPA, and this triggers the recruitment of the E2-E3 RAD6-RAD18 ubiquitin ligase complex (Davies et al., 2008). RAD18 is the principal E3 ligase that monoubiquitylates PCNA at K164, while other identified ubiquitin ligases such as RNF8 and $CRL4^{Cdt2}$ are considered to play minor roles in PCNA monoubiquitylation or, in the case of RFWD3, are not currently well-defined (Hoege et al., 2002; Watanabe et al., 2004; Zhang et al., 2008; Terai et al., 2010; Gallina et al., 2021). In addition to the interactions mediated by PCNA-binding motifs or domains, TLS polymerases contain ubiquitin-binding UBZ (Pol η and Pol κ) or UBM domains (REV1) that allow them to bind with high affinity to

monoubiquitylated PCNA at stalled forks (Bienko et al., 2005; Guo et al., 2006). TLS polymerases enable DNA replication to proceed across the lesion, albeit in an error-prone manner (Chapter 1, Section 1.2.2).

Monoubiquitylated PCNA at K164 can be further extended into K63-linked polyubiquitin chains during DNA damage through poorly understood mechanisms (Slade et al., 2018). Based on studies in yeast, polyubiquitylated PCNA was proposed to promote an error-free damage bypass pathway referred to as template switching that utilises recombination mechanisms (Chapter 1, Section 1.2.2). However, the exact roles of polyubiquitylated PCNA in template switching and the factors involved are not well defined. Another mechanism thought to be mediated by polyubiquitylated PCNA is fork reversal through its interaction with the DNA translocase ZRANB3, which modulates fork reversal and restart (Chapter 1, Section 1.2.3; Ciccia et al., 2012; Vujanovic et al., 2017).

The E3 ligases shown to promote PCNA polyubiquitylation in human cells include HLTF and SHPRH, the former of which was proposed to function together with RAD6-RAD18 and was also identified in the ZUP1 interactome (Unk et al., 2006; Motegi et al., 2006; Unk et al., 2008; Masuda et al., 2018; **Fig. 4.1**). However, UV-induced PCNA polyubiquitylation was not completely prevented in HLTF/SHPRH double-knockout mouse embryonic fibroblasts (Krijger et al., 2011). Consistent with this finding, Gallina et al. found that siRNA-mediated depletion of both HLTF and SHPRH in U2OS cells did not affect PCNA ubiquitylation upon UV exposure (Gallina et al., 2021). The group observed the effects of RFWD3 depletion in UV-treated *Xenopus* egg extracts and human cells and reported that RFWD3 has a role in promoting PCNA mono- and polyubiquitylation via RAD18.

USP1 was shown to negatively regulate PCNA monoubiquitylation in UV-irradiated cells (Huang et al., 2006). Following UV exposure, USP1 undergoes autocleavage and becomes inactivated, allowing monoubiquitylated PCNA to accumulate and promote TLS. Other DUBs such as USP7 and USP10 have also been suggested to deubiquitylate monoubiquitylated PCNA (Park et al., 2014; Kashiwaba et al., 2015).

To date, no DUB has been shown to target polyubiquitylated PCNA. The interaction between ZUP1 and PCNA proteins, and the specificity of ZUP1 for cleaving K63-linked polyubiquitin chains raises the question of whether ZUP1 deubiquitylates PCNA. This chapter evaluates this possibility, which is an important area of investigation in relation to PCNA regulation and function given that ubiquitin signalling represents a crucial component in DNA repair processes coordinated by PCNA.

The RPA complex is another ZUP1 interacting partner that was assessed in this chapter as a potential cellular substrate of ZUP1. The ubiquitylation of the RPA complex was shown to be induced by UV, HU, CPT or APH (Elia et al., 2015). PRP19 and RFWD3 are two E3 ligases previously proposed to mediate RPA ubiquitylation (Chapter 1, Section 1.6.2; Maréchal et al., 2014; Elia et al., 2015; Inano et al., 2017; Dubois et al., 2017; de Moura et al., 2018). Using the ubiquitin K63R mutant, it was suggested that RPA32 is ubiquitylated with K63-linked chains upon DNA damage, although it is not certain whether this is the predominant linkage type (Maréchal et al., 2014; Elia et al., 2015).

The role of RPA ubiquitylation in maintaining genome stability remains poorly understood and has been suggested to trigger ATR activation and homologous recombination (Chapter 1, Section 1.6.2). RFWD3-hypomorphic cells were observed to display elevated sensitivity to MMC, a phenotype that was also apparent in ZUP1 knockout cells (Feeney et al., 2017; Chapter 3). Another unclear aspect surrounding this modification is the involvement of DUBs, and the role of ZUP1 as a potential DUB for RPA was explored in one study in the context of ZUP1-silenced cells. Hewings et al. showed that siRNA-mediated ZUP1 knockdown enhanced the levels of K63-linked polyubiquitylation of RPA70 and RPA32 in HeLa cells after HU treatment (Hewings et al., 2018). In this chapter, ZUP1 knockout cells were subjected to similar DNA damage conditions to determine whether the published observations reflect a role of ZUP1 in counteracting RPA ubiquitylation.

ZUP1 knockouts were observed in Chapter 3 to exhibit hypersensitivity to MMC, olaparib, talazoparib, topotecan and AZD6738 (ATRi). The lesions created by these

genotoxic compounds, in addition to repair intermediates, can obstruct the replication machinery and result in stalled forks. If stalled forks do not undergo timely repair or restart, they can collapse into DSBs which require repair by HR (Chapter 1, Section 1.2.4; Berti et al., 2016). In Chapter 4, it was demonstrated that ZUP1 ZnF2 interacts with USP11, an important DUB in HR that facilitates the formation of the BRCA1-PALB2-BRCA2 complex by deubiquitylating PALB2 (Chapter 4, Section 4.1; Orthwein et al., 2015; Yu et al., 2016). Considering these observations that potentially link ZUP1 to HR, the final aim of this chapter was to investigate if ZUP1 has a role in HR repair of site-specific DSBs. This may help to further elucidate the DNA repair function of ZUP1, which will be crucial for defining the cellular context in which ZUP1 maintains genome stability.

## 5.2 Results

### 5.2.1 Optimising affinity purification and immunoprecipitation methods, and treatment conditions to detect ubiquitylated PCNA and RPA in cells

To examine the role of ZUP1 in regulating ubiquitylated PCNA and RPA, I first attempted to replicate published affinity purification and immunoprecipitation methods that have successfully detected ubiquitylated RPA at endogenous levels. These protocols were performed under denaturing conditions to disrupt non-covalent protein-protein interactions (Elia et al., 2015; Hewings et al., 2018). Denaturing conditions are also expected to inhibit DUB activity, which is important in such assays to maintain the ubiquitylation state of proteins as they were in intact cells (Emmerich et al., 2015). However, to further minimise the impact of any remaining DUB activity, preserve the ubiquitylation state, and improve the detection of the ubiquitylated proteins of interest, other DUB inhibitors were included in the assay buffers throughout this chapter, and are mentioned where relevant. This section only describes additives that are unique to ubiquitin detection methods, while other conventional lysis buffer additives are listed accordingly in the Methods.

Elia et al. transfected HeLa cells with 6xHis-tagged ubiquitin for 24 h before treating cells with DNA damaging agents such as 4NQO, UV, CPT or HU (Elia et al., 2015). His-ubiquitin was purified by incubating cell lysates with the widely used nickel-charged nitrilotriacetic acid (Ni-NTA) resin which contains four chelation sites for nickel ions that coordinate with histidine side chains with high specificity and affinity. As ZUP1 knockout cells had been generated in the U2OS cell line, I attempted to detect ubiquitylated RPA in U2OS wild-type and ZUP1 knockout cells using a similar approach to that shown by Elia and colleagues (Elia et al., 2015). This was performed by transiently transfecting cells with ubiquitin tagged with 1xFlag and 6xHis tags, followed by HU treatment to induce RPA ubiquitylation. The Ni-NTA purification was performed as in the published protocols, where the lysis and wash buffers were supplemented with N-ethylmaleimide (NEM) that alkylates the active site cysteine residues of cysteine proteases thereby inhibiting the function of cysteine protease

DUBs (Elia et al., 2015; Emmerich et al., 2015). Nickel-purified proteins were then immunoblotted for endogenous RPA70 and RPA32. Despite several attempts of Ni-NTA affinity purification of His-Ub from U2OS cells, which includes testing higher cell densities and different RPA70- and RPA32-specific antibodies, ubiquitylated RPA could not be detected clearly (**Fig. 5.1A**). Proteins modified by His-ubiquitin were successfully purified by Ni-NTA and not the empty vector control as indicated by the Flag blot. However, HU-induced ubiquitylated RPA was difficult to detect when cells were subjected to the same treatment conditions described by Elia et al. (2 mM HU, 2 h) even upon overexposure of the immunoblots, some of which were excluded from the representative blots shown in **Fig. 5.1A**.

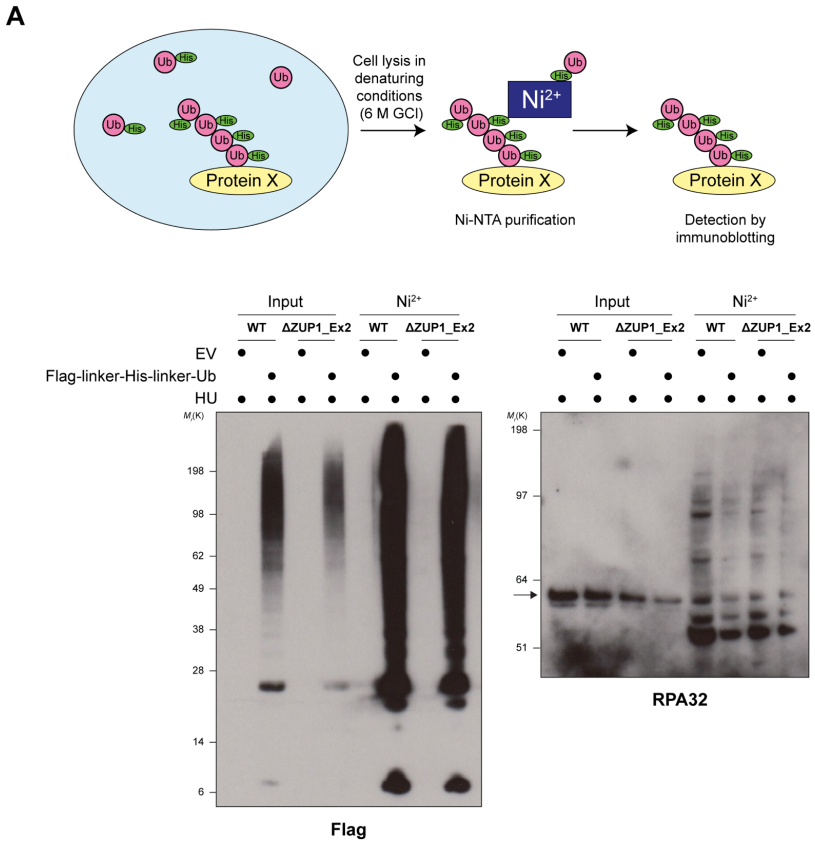
This challenge was also recognised by Elia et al. who reasoned that ubiquitylated RPA may constitute a small fraction of the total cellular pool of RPA, and that the modification may be limited to the vicinity of DNA damage sites or to chromatin-bound RPA (Elia et al., 2015). In agreement with this idea, the authors observed detectable levels of ubiquitylated RPA70 and RPA32 in chromatin extracts upon 4NQO treatment, but not in soluble extracts. In addition to the fundamental biology, it is also important to consider other technical factors that can be manipulated to improve the detection of ubiquitylated proteins in cells, including the use of a higher cell density, alternative cell lines or DNA damage treatment conditions, synchronous cell populations, or including additional DUB inhibitors beyond the cysteine protease inhibitor NEM and/or a proteasome inhibitor to inhibit protein degradation (Emmerich et al., 2015; **Table 5.1**). Some of these modifications were implemented in my work as described later in this section.

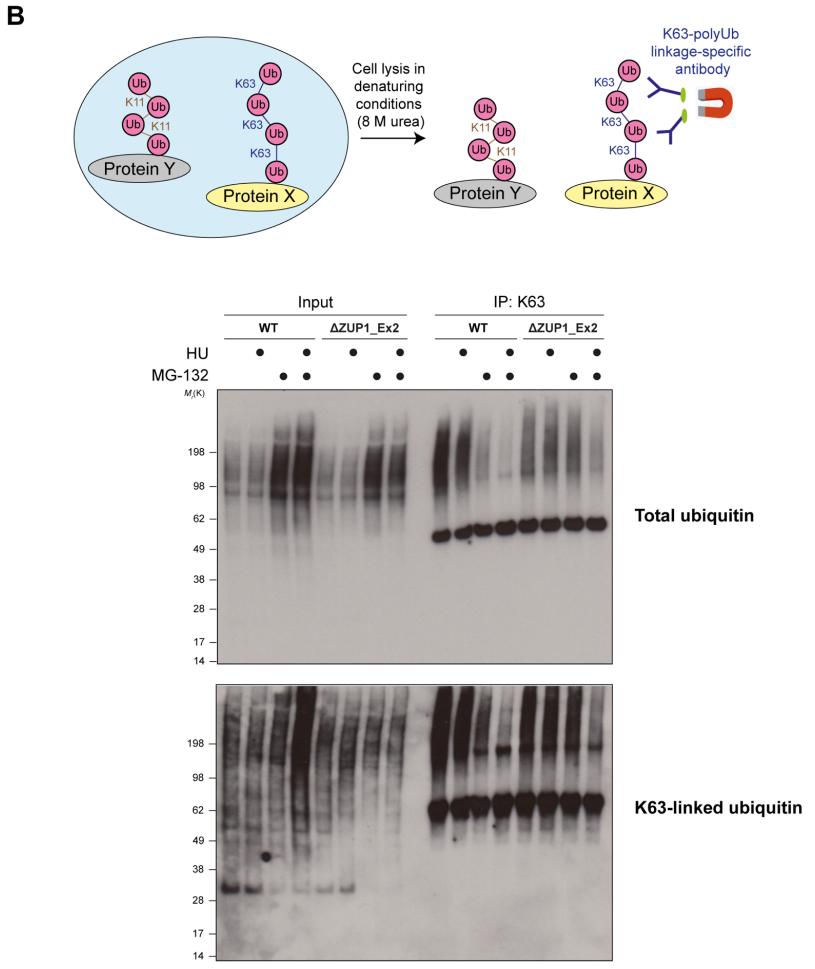
RPA modified by K63-linked polyubiquitin chains was detected in a previous study using a linkage-specific antibody to immunoprecipitate total K63-linked polyubiquitin from cells. This approach was utilised by Hewings et al. to assess if ZUP1 has a role in counteracting K63-linked polyubiquitylation on RPA, given the specificity of ZUP1 for cleaving K63-linked polyubiquitin chains and preliminary evidence that RPA may be ubiquitylated by this chain linkage type (Hewings et al., 2018; Maréchal et al., 2014; Elia et al., 2015). The authors demonstrated that siRNA-mediated ZUP1

knockdown in 293T cells enhanced the levels of endogenous RPA70 ubiquitylated by the K63 linkage upon HU treatment, and K63-modified RPA32 in untreated conditions (Hewings et al., 2018). Using the same immunoprecipitation protocol, I evaluated the reproducibility of this phenotype in U2OS wild-type and ZUP1 knockout cells.

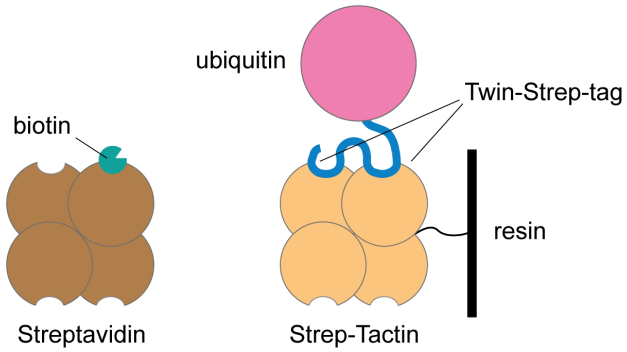
The denaturing immunoprecipitation of K63-linked polyubiquitin chains was performed after HU treatment as previously described (Hewings et al., 2018; Newton et al., 2012). Some samples were exposed to a short treatment with the proteasome inhibitor, MG-132 prior to cell lysis to prevent the proteasomal degradation of proteins modified by degradative ubiquitin signals (Emmerich et al., 2015). Although the K63 linkage type is considered a non-degradative signal, it can form heterotypic chains such as branched chains with other linkage types that are targeted to the proteasome (Ohtake et al., 2018; French et al., 2021). Therefore, the short MG-132 treatment was potentially useful to minimise the loss of RPA ubiquitylated by a combination of K63-linked chains and other proteasome-targeting linkage types. In addition to NEM, the buffers used for lysing all the samples were also supplemented with MG-132 (Emmerich et al., 2015; **Table 5.1**).

Total cellular protein modified by K63-linked ubiquitin chains was detected clearly in the immunoprecipitated fraction using an antibody specific for the K63 linkage (**Fig. 5.1B**). Samples treated with MG-132 prior to cell lysis showed an increase in total ubiquitin as expected, while the effect of MG-132 on total K63-linked ubiquitin was unclear (**Fig. 5.1B**). After multiple attempts, RPA modified by K63-linked polyubiquitin could not be detected (data not shown). If a small fraction of RPA is ubiquitylated during DNA damage as speculated by Elia et al., it is possible that K63-ubiquitylated RPA may represent a fraction that is smaller still. In future investigations, K63-polyubiquitylated proteins can be purified from cell extracts using K63 tandem ubiquitin-binding entities (TUBEs), followed by diGly IP to enrich trypsin-digested ubiquitylated peptides and MS analysis to detect K63-ubiquitylated RPA (Hjerpe et al., 2009; Sims et al., 2012).


A
Cell lysis in denaturing conditions (6 M GCl)
Protein X
Ni-NTA purification
Detection by immunoblotting
Input
Ni2+
WT
ΔZUP1_Ex2
EV
Flag-linker-His-linker-Ub
HU
Flag
RPA32


B
Cell lysis in denaturing conditions (8 M urea)
K63-polyUb linkage-specific antibody
Protein Y
Protein X
Input
IP: K63
WT
ΔZUP1_Ex2
HU
MG-132
Total ubiquitin
K63-linked ubiquitin

C


ubiquitin
Twin-Strep-tag
biotin
resin
Streptavidin
Strep-Tactin

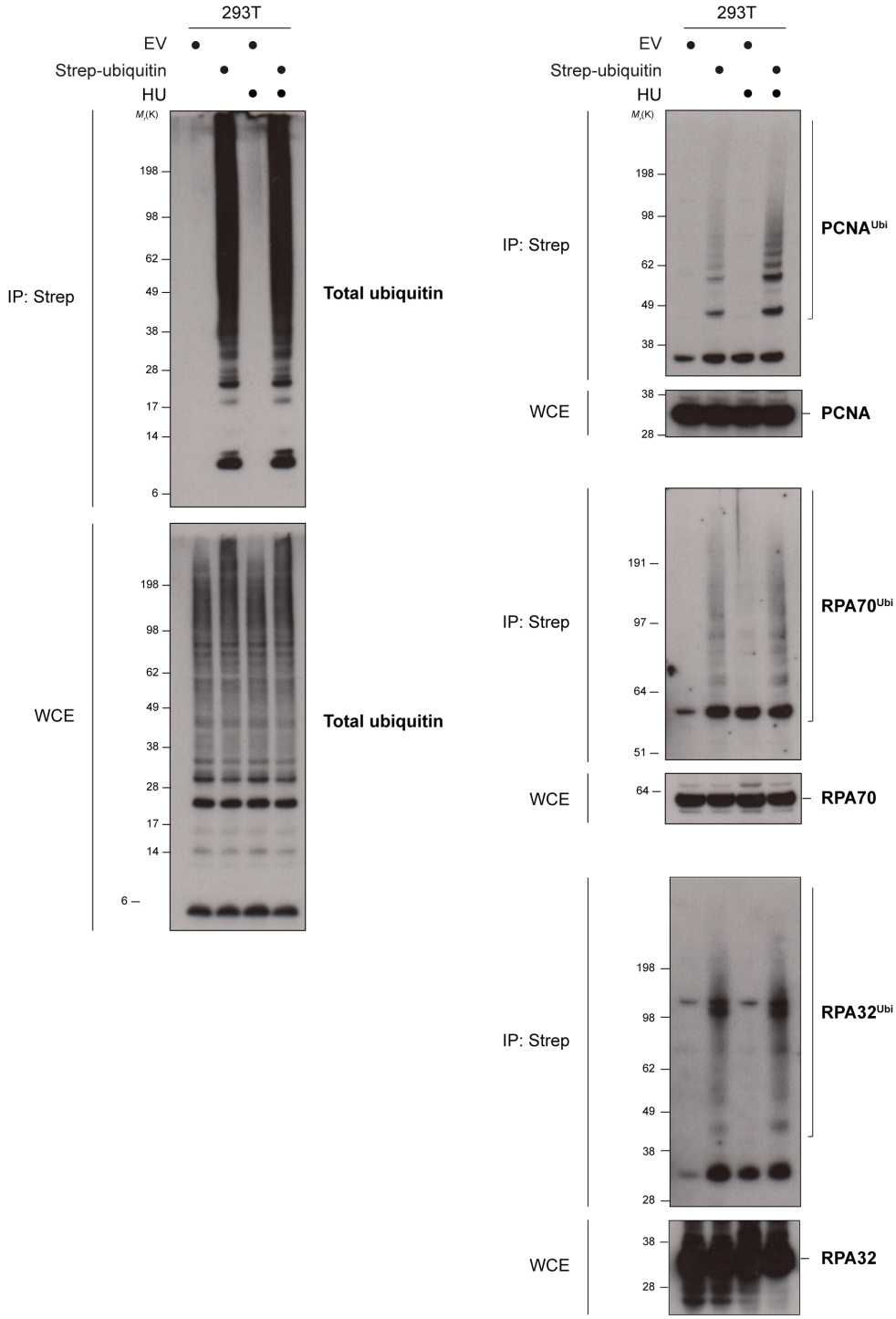

293T
EV
Strep-ubiquitin
HU
M,(K)
198
98
62
49
38
28
17
14
6
IP: Strep
Total ubiquitin
WCE
Total ubiquitin
293T
EV
Strep-ubiquitin
HU
M,(K)
198
98
62
49
38
IP: Strep
PCNAUbi
WCE
38
28
PCNA
191
97
64
51
IP: Strep
RPA70Ubi
WCE
64
RPA70
198
98
62
49
38
28
IP: Strep
RPA32Ubi
WCE
38
28
RPA32

**Figure 5.1: Denaturing affinity purification and immunoprecipitation methods for detecting ubiquitylated RPA and PCNA in cells.** A) Top: Schematic illustration summarising the Ni-NTA purification of His-ubiquitin covalently conjugated to endogenous proteins in cells. Bottom: U2OS wild-type cells or ΔZUP1_Ex2 Clone P2B2 were transfected with the indicated His-ubiquitin vector and treated with 2 mM HU for 2 h. The representative blots show the input and $Ni^{2+}$-purified fractions of total protein (Flag) and RPA32 ubiquitylated by His-ubiquitin. B) Top: Schematic illustration summarising the immunoprecipitation of endogenous proteins covalently modified with K63-linked ubiquitin chains, performed using an antibody specific to the K63 linkage type. Bottom: U2OS wild-type cells or ΔZUP1_Ex2 Clone P2B2 were treated with 2 mM HU or an equivalent volume of $H_2O$ for 2.5 h, in the presence or absence of 20 μM MG-132 or an equivalent volume of DMSO for 2.5 h. The representative blots show the input and IP fractions of total ubiquitin or K63-linked ubiquitin. C) Top: Schematic illustration of the streptavidin derivative, Strep-Tactin which contains binding pockets to which the synthetic Twin-Strep-tag peptide binds with high affinity (IBA Life Sciences). Ubiquitin fused to Twin-Strep-tag was transiently expressed in cells, followed by denaturing purification using the Strep-Tactin resin. Bottom: 293T wild-type cells were transfected with ubiquitin tagged with Twin-Strep-tag (Strep-ubiquitin) or the empty vector. Cells were treated with 2 mM HU or an equivalent volume of $H_2O$ for 2 h. The representative blots show input/whole cell extracts (WCE) and Strep-purified (IP: Strep) fractions of total ubiquitin, ubiquitylated PCNA, RPA70 and RPA32.

Next, an alternative denaturing affinity purification approach was tested, which utilised the Strep-tag system that was developed based on the natural streptavidin-biotin interaction (IBA Life Sciences, **Fig. 5.1C**). Ubiquitin was tagged at the N-terminus with Twin-Strep-tag and transiently expressed in 293T cells. The Twin-Strep-tag binds with high affinity to two engineered biotin-binding pockets within the streptavidin derivative, Strep-Tactin. The advantages of this system are manifold, including the high specificity and binding affinity of Twin-Strep-tag to Strep-Tactin; its compatibility with various buffer conditions, additives and a larger pH range; its ability to purify diverse protein classes; and the inert amino acid composition of the peptide tag (IBA Life Sciences). In contrast, the His-tag system tested in **Fig. 5.1A** has been shown to result in lower protein purity and is unable to tolerate certain reducing agents such as DTT, chelating agents such as EDTA, and other buffer components (IBA Life Sciences). DTT and EDTA were both included in the buffer for the Strep-tag system, the latter of which sequesters heavy metal ions and inhibits metalloprotease DUBs, and may preserve the ubiquitylated form of proteins along with the cysteine protease inhibitor, NEM (Emmerich et al., 2015; Nakayasu et al., 2015).

Using the Strep-tag system, a strong signal of Strep-purified total ubiquitin was detected upon short exposures of the immunoblot. Ubiquitylated PCNA, RPA70 and RPA32 were detected clearly at basal levels, and PCNA ubiquitylation was significantly induced by HU treatment (**Fig. 5.1C**). The Strep-tag system was therefore selected as the main technique for subsequent experiments in this chapter to investigate the role of ZUP1 in regulating PCNA and RPA ubiquitylation during replication stress. The clear detection of ubiquitylated proteins in 293T cell lysates could be attributed to the rapid growth rate and abundant total protein obtained from this cell line. Therefore, 293T (wild-type and ZUP1 knockouts) was selected as the cell line to investigate ZUP1-dependent effects.

Using the Strep-tag system, the affinity purification protocol and treatment conditions were further optimised to achieve robust detection of ubiquitylated PCNA and RPA in cells, and experimental reproducibility. Sonication is an essential step for shearing

genomic DNA that is released by the denaturing lysis buffer containing sodium dodecyl sulfate (SDS) and sodium deoxycholate detergents (DeCaprio et al., 2020). The ultrasound treatment produces heat which can result in protein degradation, and this is typically minimised by applying short pulses and keeping samples on ice throughout the sonication procedure (Fuentes-Iglesias et al., 2020). Two separate Strep-ubiquitin purification experiments were performed, each using different sonication conditions (sonicator details are described in Section 2.12.2 and 2.17.2), which resulted in vastly different signal strengths for ubiquitylated PCNA detected by immunoblotting (**Fig. 5.2A, 5.2B**). Despite involving more frequent (i.e 9) pulses, the sonication setting of 40% amplitude led to a more robust detection of ubiquitylated PCNA compared to when 60% amplitude was used in 3 pulses. However, this was inferred from two independent experiments that were not designed to optimise sonication settings in a systematic manner, which would be necessary for understanding the effect of each parameter on the purification efficiency or detection signal. Subsequent experiments that utilised the sonication settings, cell density and suspension volumes as in **Fig. 5.2A** were found to yield detectable levels of ubiquitylated PCNA, and these settings were therefore used throughout this chapter (**Table 5.1**).

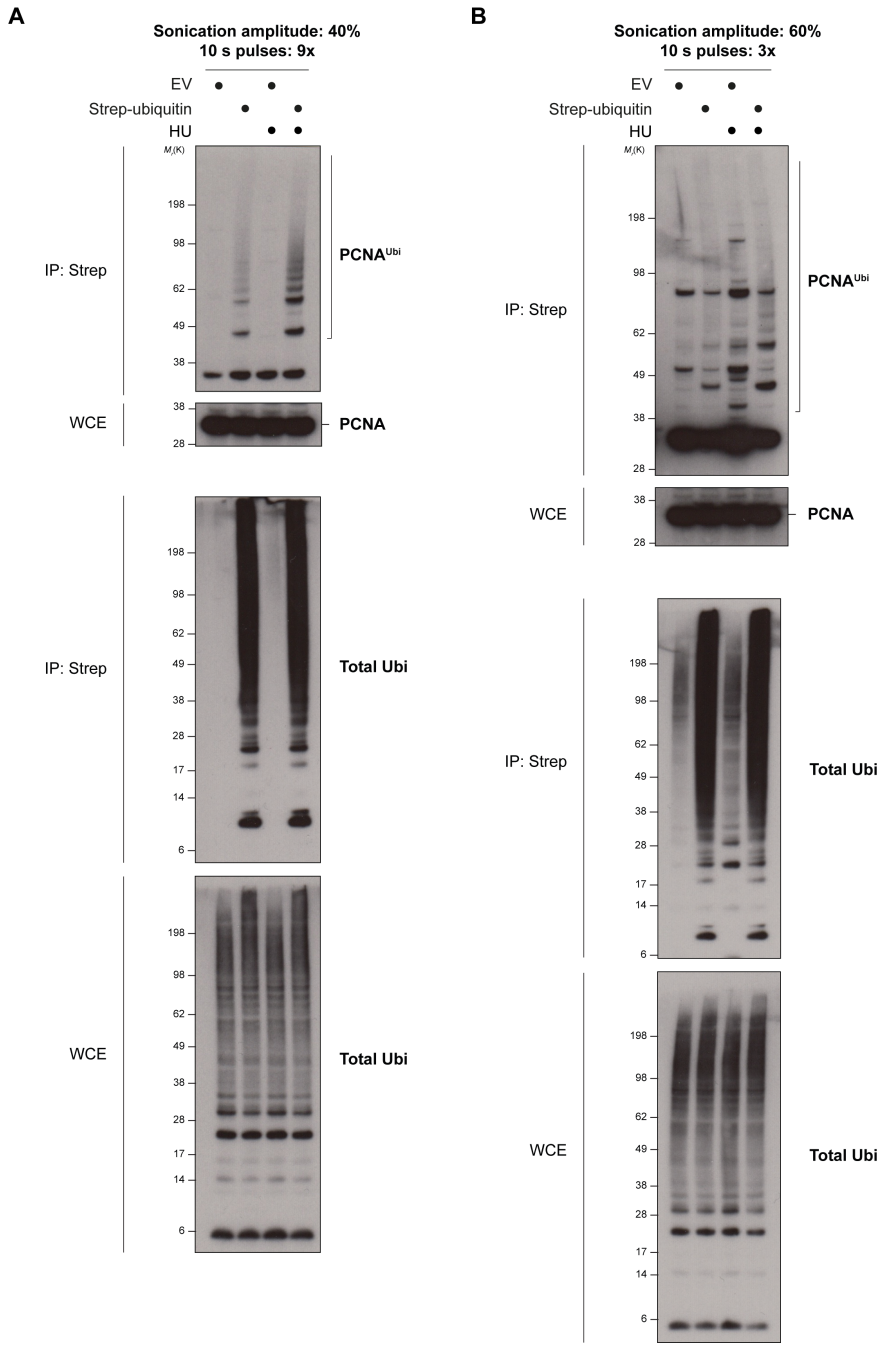



**Figure 5.2: Sonication settings may have an impact on the detection of ubiquitylated PCNA by denaturing Strep pull-down.** A) 293T wild-type cells were transiently transfected with Strep-ubiquitin or the empty vector, then treated with 2 mM HU or an equivalent volume of $H_2O$ for 2 h. The sonication settings used were: 40% amplitude, 9 pulses, each 10 s on, 40 s off. Blots shown are representative of two independent experiments (n = 2). B) Cells were transfected as in A and treated with 2 mM HU or an equivalent volume of $H_2O$ for 4 h. The sonication settings used

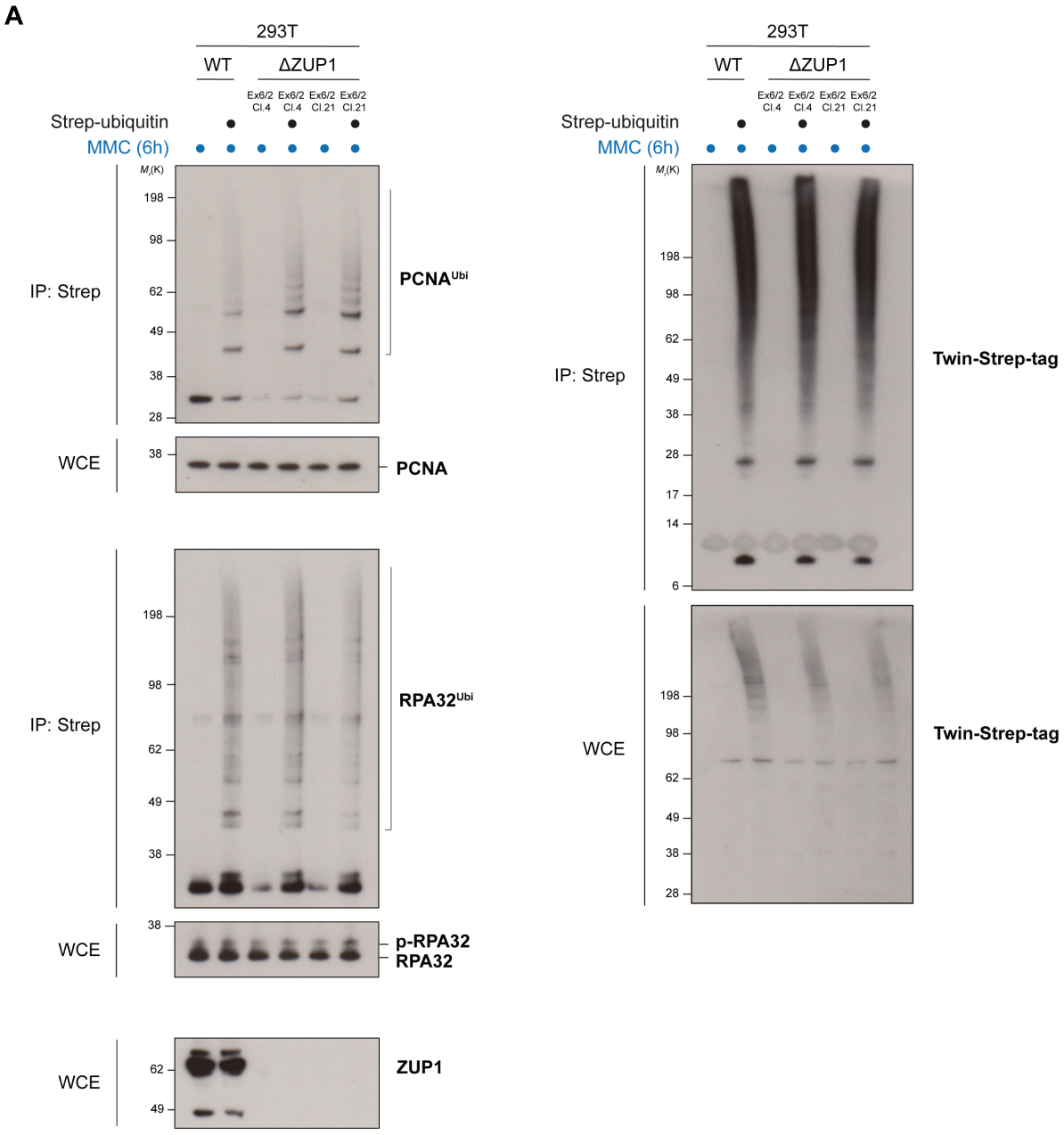
were: 60% amplitude, 3 pulses, each 10 s on, 40 s off. Blots shown were obtained from a single experiment (n = 1).

In Chapter 3, MMC was identified as one of the genotoxic compounds to which U2OS ZUP1 knockouts display significant hypersensitivity. MMC forms interstrand crosslinks (ICLs) which trigger FANCI–FANCD2 ubiquitylation, leading to the recruitment of Fanconi anemia pathway proteins that mediate repair (Chapter 1, Section 1.6.3; Semlow and Walter, 2021). Feeney et al. reported that RFWD3-hypomorphic cells are hypersensitive to ICL-inducing agents including MMC (Feeney et al., 2017). The authors attributed this to the importance of RFWD3 in ICL repair at stalled forks and showed that RFWD3 recruitment may be mediated by RPA. It remains to be clarified whether RPA ubiquitylation is involved in this process, and whether ZUP1 regulates RPA ubiquitylation. Considering the ZUP1-RPA interaction and the MMC hypersensitivity phenotype observed in U2OS ZUP1 knockouts, MMC was used in all the Strep pull-down experiments to create a DNA damage environment in which ZUP1 may have a repair role. However, the 293T cell line (wild-type and ZUP1 knockouts) was used in these experiments for technical reasons as described earlier, and the MMC sensitivity of 293T ZUP1 knockouts has yet to be assessed (further discussed on page 212).

To identify the MMC treatment condition that induces detectable levels of PCNA and RPA ubiquitylation, two different treatment durations were first tested in independent experiments (**Fig. 5.3A, 5.3B**). To minimise technical variation between experiments, the treatment durations were later optimised side by side in the same experiment as shown in **Fig. 5.5**. After a 6 h MMC treatment, two independent 293T ZUP1 knockout clones were found to have slightly higher levels of ubiquitylated PCNA compared to the wild-type (**Fig. 5.3A**). The difference in ubiquitylated RPA32 was less clear. I considered whether a longer MMC treatment, which should lead to the accumulation of replication stress, would result in higher levels of ubiquitylated PCNA and/or RPA that may enable a clearer comparison between the wild-type and ZUP1 knockouts.

The difference in ubiquitylated PCNA levels between the wild-type and ZUP1 knockout was accentuated upon MMC treatment for 16 h, which induced a significantly higher level of ubiquitylated PCNA in the knockout cells (**Fig. 5.3B**). The level of ubiquitylated RPA32 was also markedly higher in the knockout cells compared to the wild-type. However, the observation for ubiquitylated RPA32 could not be reproduced in subsequent biological replicates (data not shown). Conversely, the PCNA phenotype was consistent across experiments as demonstrated in the following figures.

The Strep pull-down experiments performed in **Fig. 5.3** included two other DUB inhibitors, PR-619 and 1,10-phenanthroline in the buffers in addition to NEM and the proteasome inhibitor MG-132. PR-619 is a broad-spectrum DUB inhibitor whereas 1,10-phenanthroline inhibits metalloprotease DUBs by chelating the active site $Zn^{2+}$ (Altun et al., 2011; Cooper et al., 2009; Kumari et al., 2018). It was reasoned that the experimental conditions in **Fig. 5.3** such as the cell density, sonication settings and additional DUB inhibitors, may have collectively contributed to the clear detection of ubiquitylated PCNA and RPA. These technical conditions were therefore implemented in subsequent pull-down experiments as summarised in **Table 5.1**.


A
293T
WT
ΔZUP1
Ex6/2 Cl.4
Ex6/2 Cl.4
Ex6/2 Cl.21
Ex6/2 Cl.21
Strep-ubiquitin
MMC (6h)
IP: Strep
WCE
PCNA^Ubi
PCNA
RPA32^Ubi
p-RPA32
RPA32
ZUP1
Twin-Strep-tag
Twin-Strep-tag

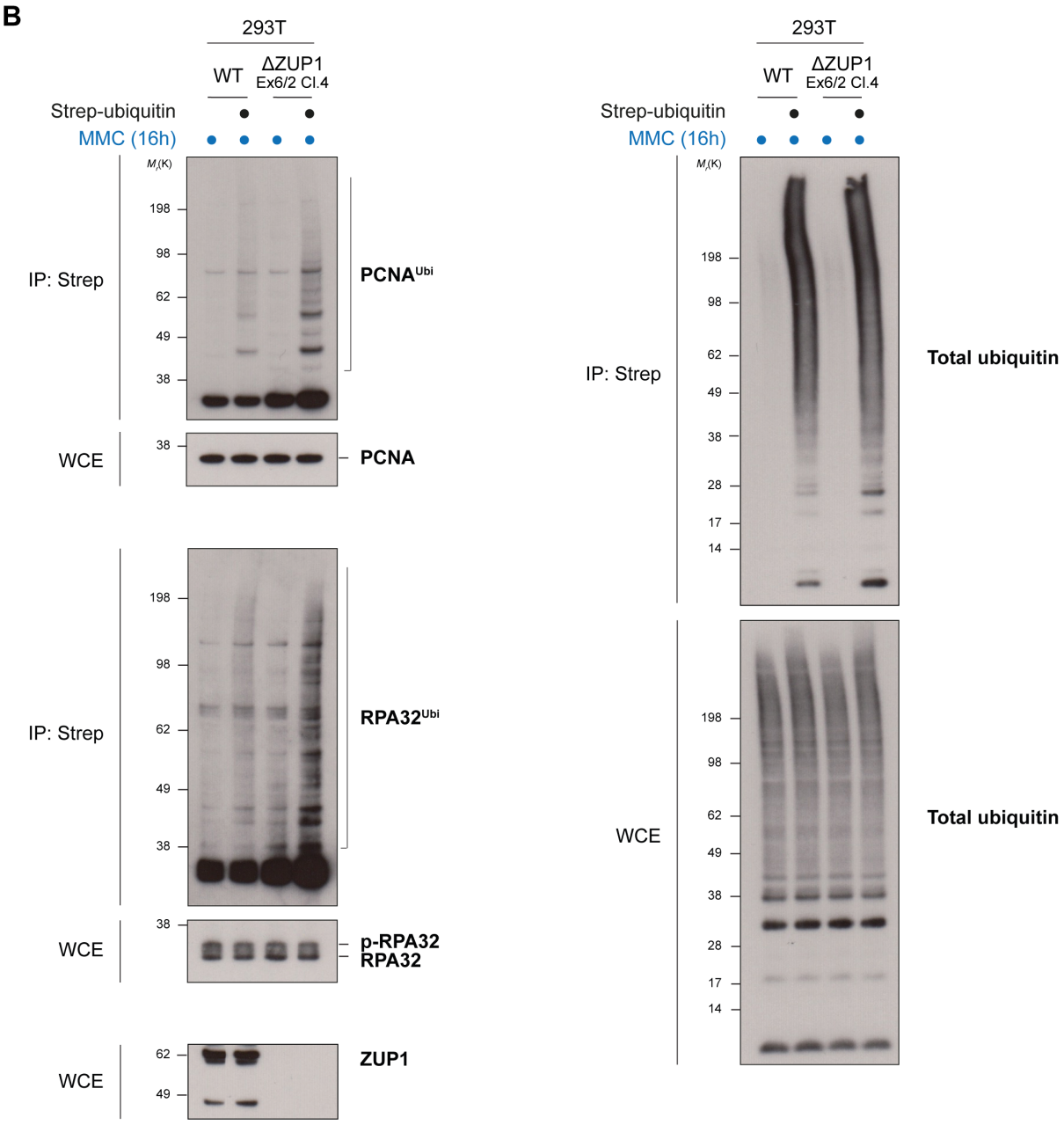



**Figure 5.3: Optimisation of MMC treatment durations to analyse the effect of ZUP1 loss on PCNA and RPA ubiquitylation.** A) 293T wild-type cells and two independent ZUP1 knockout clones, ΔZUP1_Ex6/2 Clone 4 and Clone 21 were transfected with Strep-ubiquitin or the empty vector, then treated with 1 μM MMC for 6 h prior to the denaturing Strep pull-down. The DMSO control was excluded to minimise sample handling in this optimisation experiment. Blots were obtained from a single experiment (n = 1). B) 293T wild-type cells and ΔZUP1_Ex6/2 Clone 4 were transfected as in A and treated with 1 μM MMC for 16 h, followed by the denaturing

Strep pull-down protocol as performed in A. Blots shown are representative of three independent experiments (n = 3).

| | His-ubiquitin pull-down (Ni-NTA) | IP of endogenous K63-linked polyubiquitin | Strep-ubiquitin pull-down (Strep-tag system) |
|---|---|---|---|
| **Cell line** | U2OS | U2OS | 293T |
| **Cell density per sample** | 2x 15 cm dishes (3.3 x $10^6$ cells/dish) | 2x 15 cm dishes (5 x $10^6$ cells/dish) | 2x 15 cm dishes (4.8 x $10^6$ cells/dish)<br>With double thymidine block:<br>2 x $10^6$ cells/dish |
| **Drug treatment** | HU: 2 mM, 2 h | HU: 2 mM, 2.5 h | • HU: 2 mM, 2-4 h<br>• MMC: 1 µM, 6-30 h |
| **Sonication settings** | Amplitude: 50%; 10x pulses,<br>1 s on, 20 s off | Amplitude: 50%; 3x pulses,<br>5 s on, 30 s off | Amplitude: 40%; 9x pulses,<br>10 s on, 40 s off |
| **DUB or proteasome inhibitors in buffers** | NEM | NEM, MG-132 | NEM, PR-619, 1,10-phenanthroline, MG-132 |

**Table 5.1: Comparison of experimental conditions used in denaturing pull-down or IP methods for the detection of ubiquitylated PCNA and RPA.** As summarised in the main text, the Strep-tag system, performed with the indicated experimental conditions, yielded the clearest detection of ubiquitylated PCNA and RPA of the three methods.

Given that MMC induces ICLs that prevent DNA unwinding and block replication progression, it was considered that the cell cycle phase of MMC-treated cells may determine the level of DNA damage accumulated at replication forks, and therefore affect experimental reproducibility. Asynchronous cell populations may accumulate replication-associated damage at different levels between experiments, therefore cells were synchronised to minimise such variability. The Strep pull-down protocol was modified to include a double thymidine block to arrest cells at the beginning of S phase prior to MMC treatment (**Fig. 5.5A**). This was done to ensure that the cell population progresses synchronously through S phase in the presence of MMC.

As monitored by flow cytometry, the double thymidine block protocol resulted in the synchronisation of 293T wild-type and ZUP1 knockout cells in S phase, and removal of the second thymidine enabled cells to resume S phase and proceed through the remainder of the cell cycle (Whitfield et al., 2002; **Fig. 5.4A, 5.4B**). At basal conditions, the wild-type and ZUP1 knockout cells exhibited little difference in their cell cycle profiles (**Fig 5.4B**). The double thymidine block was performed prior to MMC treatment in subsequent Strep pull-down experiments to enable comparison between synchronous cell populations. In this modified protocol, the Strep-ubiquitin transfection was performed during the first thymidine release (**Fig. 5.5A**).

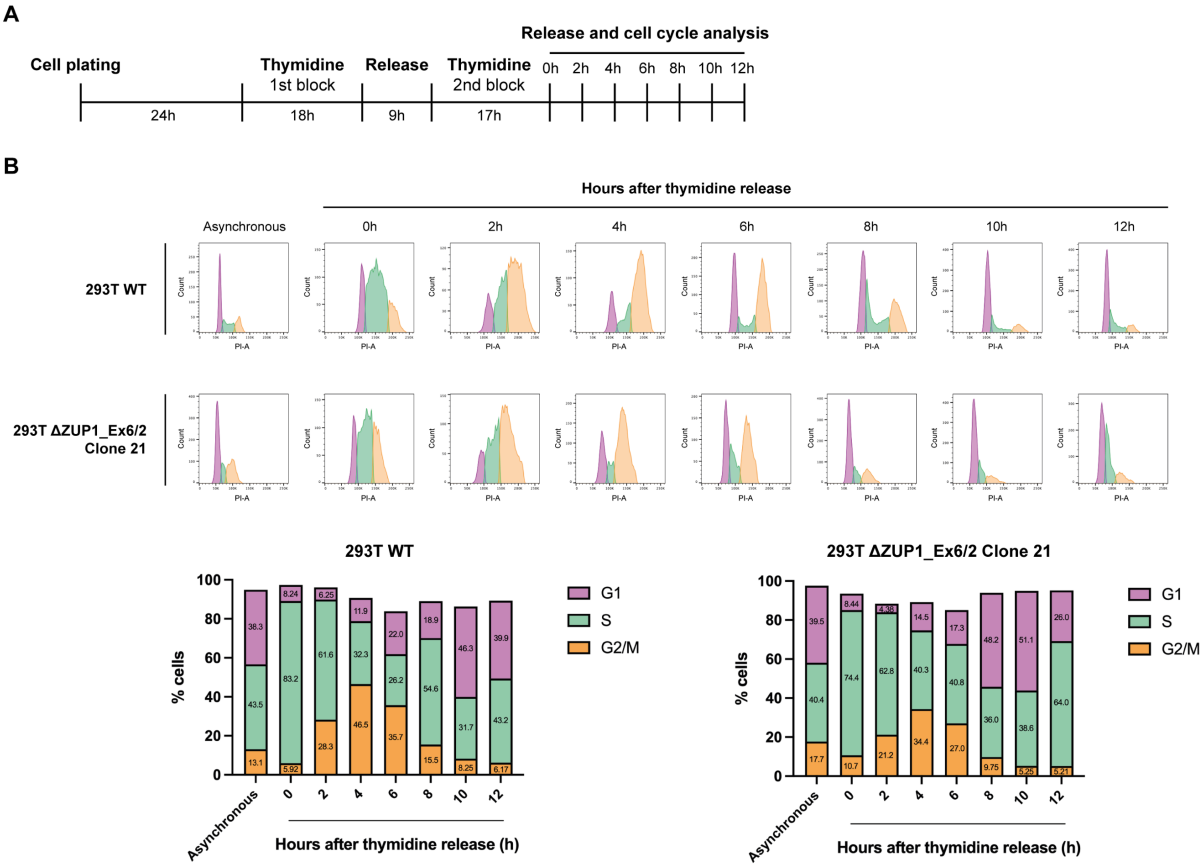



**Figure 5.4: Synchronisation of 293T wild-type and ZUP1 knockout cells in S phase by double thymidine block.** A) Summary of the double thymidine block protocol involving two thymidine treatments. Upon release from the second thymidine treatment, cells were harvested every 2 h from separate dishes for cell cycle analysis. The protocol is detailed in the Methods. B) Cell cycle profiles of 293T wild-type cells and ΔZUP1_Ex6/2 Clone 21 after the second thymidine release as monitored by flow cytometry, where 10000 events were collected per sample. The bar charts represent the proportion of cells in the indicated cell cycle phases based on the flow cytometry analysis. Results are representative of two independent experiments (n = 2).

### 5.2.2 ZUP1 loss is associated with elevated levels of PCNA polyubiquitylation during replication stress

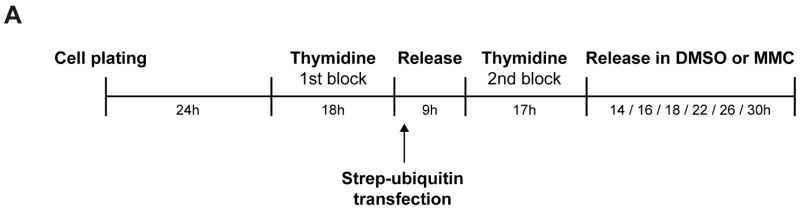
To identify a suitable MMC treatment length for the subsequent phenotyping experiments, the levels of p-RPA32 (at Ser4/Ser8, Thr21, and Ser33) were assessed in synchronised 293T wild-type cells treated with MMC for up to 12 h. Cells treated with MMC for 10 h and 12 h accumulated p-RPA32 to levels higher than in untreated cells, which indicates replication stress, where forks may be obstructed by ICLs as cells progress through S phase (**Appendix C: Fig. 1**; Vassin et al., 2009; Ashley et al., 2014). Based on this, synchronous cell populations were treated with MMC for various durations starting from 14 h, where stressed forks are assumed to be present at levels that induce the replication stress response, even in wild-type cells (**Fig. 5.5A**). PCNA ubiquitylation in 293T wild-type and ZUP1 knockouts was compared under these conditions to examine how this modification may differ in the absence of ZUP1. Cells were treated with MMC for up to 30 h to evaluate any differences in the persistence of PCNA ubiquitylation between the wild-type and ZUP1 knockouts after an extended treatment.

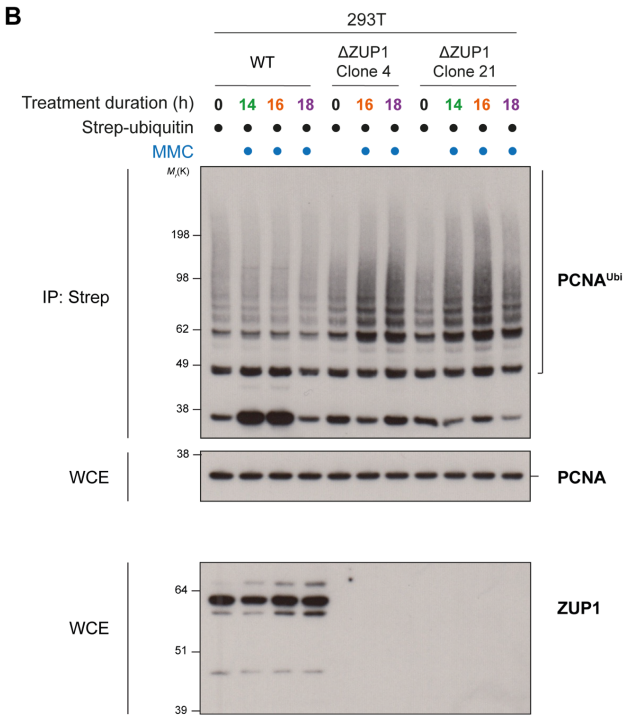
The induction of PCNA polyubiquitylation by MMC was significantly higher in two independent ZUP1 knockout clones compared to the wild-type at all the treatment lengths tested (**Fig. 5.5B, 5.5C**). The induction of ubiquitylated RPA by MMC was less clear in these conditions (data not shown). In both ZUP1 knockout clones, polyubiquitylated PCNA persisted for at least 30 h in the presence of MMC (**Fig. 5.5C**). The phenotype is also presented in **Fig. 5.6** which includes the appropriate transfection and untreated controls.

The elevated levels of polyubiquitylated PCNA in ZUP1 knockout cells may reflect a ZUP1-dependent dysregulation of PCNA polyubiquitylation. A possible underlying mechanism is the direct deubiquitylation of PCNA by ZUP1, which is supported by *in vitro* DUB assays in the Gibbs-Seymour lab demonstrating that recombinant ZUP1 cleaves K63-linked polyubiquitin chains on PCNA, and this was shown to be dependent on ZUP1 catalytic activity (**Appendix C: Fig. 4**). These assays further

revealed that the deubiquitylation of PCNA by ZUP1 is stimulated by RPA, and that ZUP1 does not remove monoubiquitin on PCNA which reflects its preference for cleaving longer chains (**Appendix C: Fig. 4**; Kwasna et al., 2018). The contribution of ZUP1 DUB activity to the PCNA polyubiquitylation phenotype in cells was assessed in the following section.

An alternative explanation for the phenotype is that ZUP1 loss may have caused defective repair through other mechanisms, leading to the accumulation of DNA lesions in the presence of MMC. PCNA polyubiquitylation is associated with fork reversal and recombination-mediated repair, therefore its persistence in ZUP1 knockouts could indicate unresolved or accumulated damage (Chapter 1, Section 1.2.2, Section 1.6.1). Other possible mechanisms of ZUP1 regulation of PCNA and the potential implications of this role are described in the Discussion.


A
Cell plating
Thymidine
1st block
Release
Thymidine
2nd block
Release in DMSO or MMC
24h
18h
9h
17h
14 / 16 / 18 / 22 / 26 / 30h
Strep-ubiquitin
transfection


B
293T
WT
ΔZUP1
Clone 4
ΔZUP1
Clone 21
Treatment duration (h)
0 14 16 18 0 16 18 0 14 16 18
Strep-ubiquitin
MMC
IP: Strep
198
98
62
49
38
PCNAUbi
WCE
38
PCNA
WCE
64
51
39
ZUP1

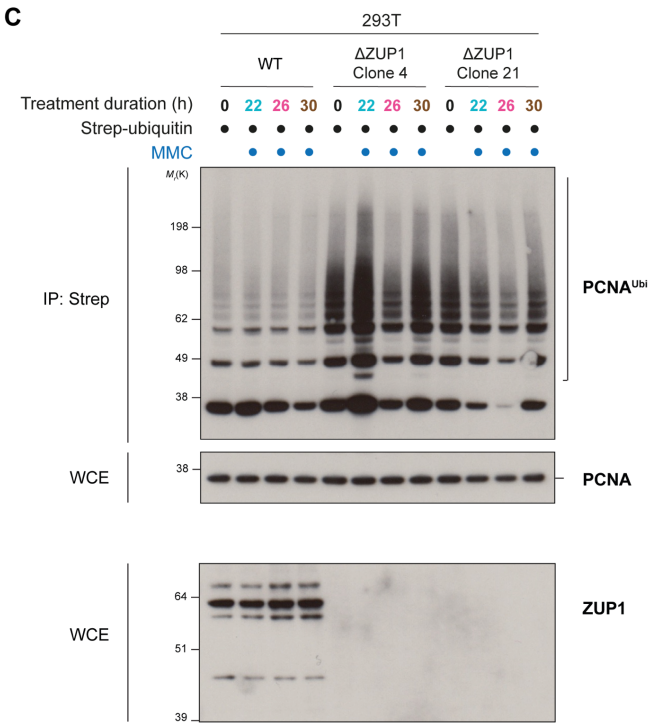

C
293T
WT
ΔZUP1
Clone 4
ΔZUP1
Clone 21
Treatment duration (h)
0 22 26 30 0 22 26 30 0 22 26 30
Strep-ubiquitin
MMC
IP: Strep
198
98
62
49
38
PCNAUbi
WCE
38
PCNA
WCE
64
51
39
ZUP1

**Figure 5.5: Polyubiquitylated PCNA is present at elevated levels and persists for at least 30 h in ZUP1 knockout cells treated with MMC.** A) Summary of the double thymidine block protocol performed prior to MMC/DMSO treatment and the Strep pull-down. Cells were transfected with Strep-ubiquitin during the first release from thymidine. Dishes of cells were treated with MMC for the indicated durations, and washed and frozen overnight before performing the denaturing Strep pull-down protocol as detailed in the Methods. B) 293T wild-type cells, ΔZUP1_Ex6/2 Clone 4 and Clone 21 were transfected with Strep-ubiquitin and treated with 1 μM MMC or an equivalent volume of DMSO for the indicated durations before performing the Strep pull-down as summarised in A. Blots were obtained from a single experiment (n = 1). C) Cells were prepared and treated as in B for 22 h, 26 h or 30 h. Blots were obtained from a single experiment (n = 1).

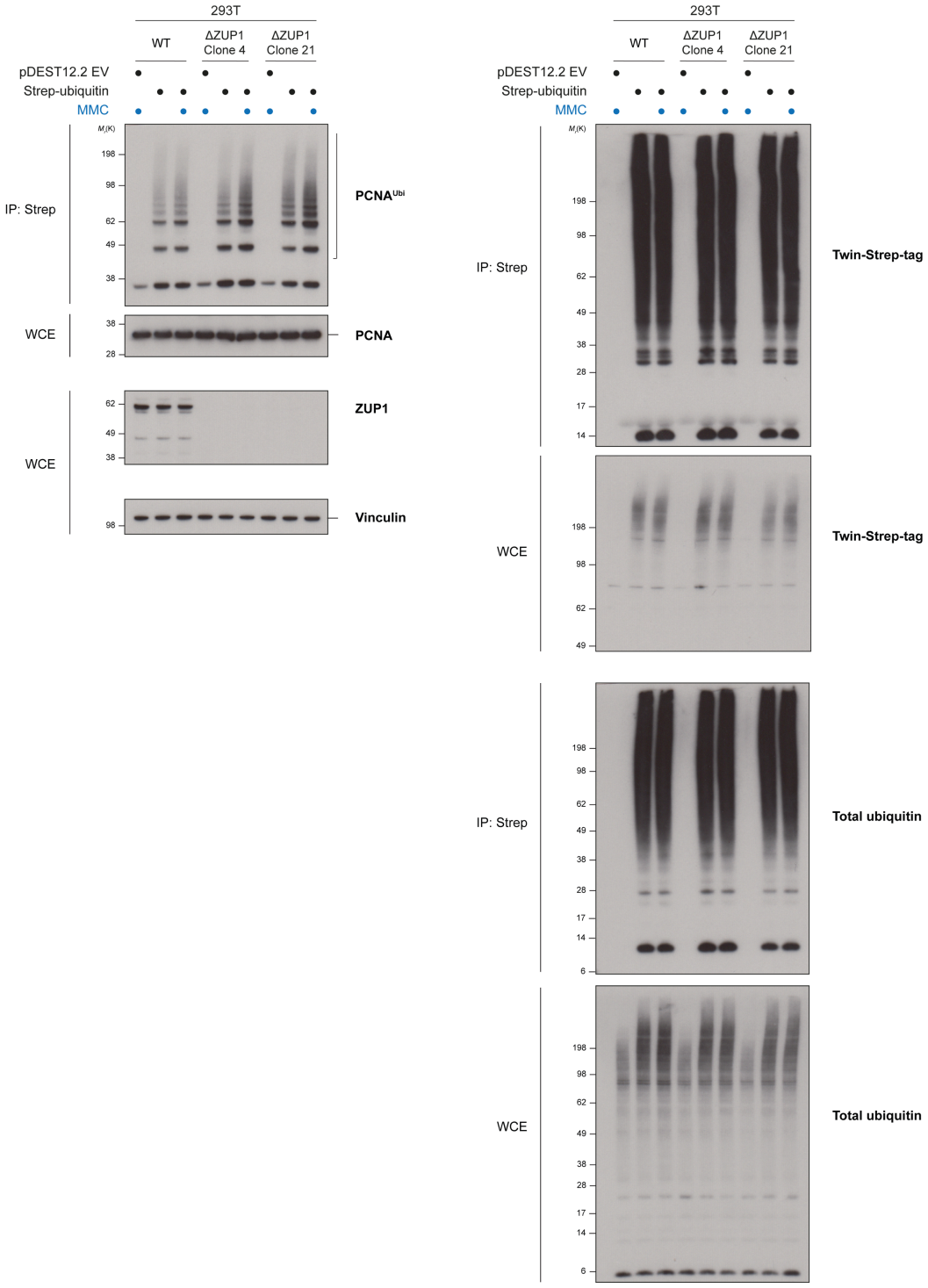



**Figure 5.6: ZUP1 loss is associated with elevated levels of polyubiquitylated PCNA in the presence of MMC.** 293T wild-type cells, ΔZUP1_Ex6/2 Clone 4 and Clone 21 were synchronised by double thymidine block. As in Fig. 5.5, cells were transfected with Strep-ubiquitin or the empty vector during the first thymidine release, and treated with 1 μM MMC or an equivalent volume of DMSO for 24 h upon release

from the second thymidine, followed by the denaturing Strep pull-down. Blots shown are representative of two independent experiments (n = 2).

In response to replication stress, a key step that promotes translesion synthesis is the monoubiquitylation of PCNA at K164 which is predominantly mediated by the E2-E3 complex, RAD6-RAD18 (Chapter 1, Section 1.6.1; Hoege et al., 2002; Watanabe et al., 2004; Mailand et al., 2013; Slade et al., 2018). Monoubiquitin at K164 of PCNA can be further extended into a K63-linked polyubiquitin chain which has been proposed to promote recombination-mediated template switching and fork reversal mechanisms (Chapter 1, Section 1.2.2, Section 1.6.1). In ZUP1 knockout cells, MMC treatment enhanced the levels of PCNA mono- and polyubiquitylation at K164, which were detected using a monoclonal antibody specific for this PCNA modification (**Fig. 5.7**).

To evaluate the RAD18 dependence of PCNA mono- and polyubiquitylation in ZUP1 knockout cells, RAD18 was silenced by siRNA, which impaired the induction of both mono- and polyubiquitylated PCNA upon MMC treatment (**Fig. 5.7**). In untreated conditions, RAD18 knockdown also led to a reduction in monoubiquitylated PCNA whilst strongly decreasing the polyubiquitylated form. This aligns with previous evidence that reported the RAD18 dependence of UV-induced PCNA mono- and polyubiquitylation in 293T and U2OS cells, which was demonstrated by siRNA-mediated RAD18 knockdown (Brun et al., 2008; Gallina et al., 2021). Although it is not known if RAD18 directly extends the monoubiquitin on PCNA into polyubiquitin chains, this finding suggests that PCNA polyubiquitylation may be dependent on RAD18-mediated monoubiquitin conjugation on K164. However, the results shown in **Fig. 5.7** were obtained from a single experiment, therefore more repeats will be needed to confirm the findings.

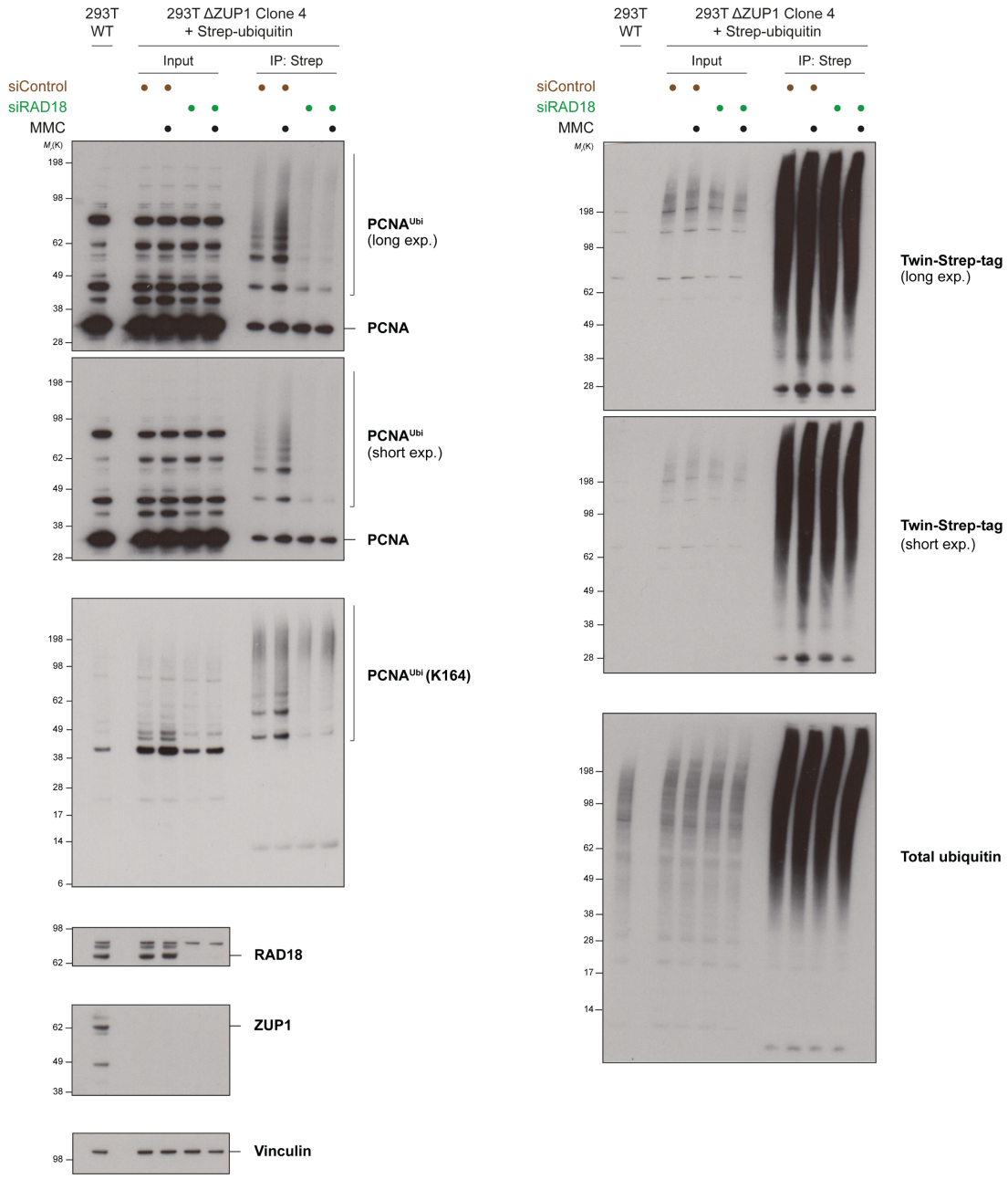



**Figure 5.7: PCNA ubiquitylation in ZUP1 knockout cells may be dependent on RAD18.** 293T ΔZUP1_Ex6/2 Clone 4 cells were reverse transfected with 20 nM of non-targeting (siControl) or RAD18 siRNA (siRAD18) pools during cell plating, 24 h prior to the double thymidine block protocol as previously described. Synchronised cells were treated with 1 μM MMC or an equivalent volume of DMSO for 24 h before performing the denaturing Strep pull-down. Cells were transfected with Strep-ubiquitin or the empty vector during the first thymidine release as previously described. 293T wild-type whole cell extract was loaded onto the gel as a control for ZUP1 expression. Blots shown were obtained from a single experiment (n = 1).

The E3 ligases that mediate PCNA polyubiquitylation are less clearly defined. HLTF and SHPRH have been shown to promote PCNA polyubiquitylation in human cells (Unk et al., 2006; Motegi et al., 2006; Unk et al., 2008; Masuda et al., 2018). However, HLTF/SHPRH double knockout in mouse embryonic fibroblasts did not completely prevent UV-stimulated PCNA polyubiquitylation (Krijger et al., 2011). Gallina et al. also reported that siRNA-mediated depletion of both HLTF and SHPRH in U2OS cells did not affect UV-induced PCNA ubiquitylation (Gallina et al., 2021).

RFWD3 is another E3 ligase proposed to regulate PCNA ubiquitylation in response to DNA damage (Gallina et al., 2021). The study reported that RFWD3 depletion in *Xenopus* egg extracts led to a decrease in mono- and polyubiquitylated PCNA during the replication of UV-damaged chromatin and plasmids containing DNA-protein crosslinks. It was further shown that siRNA knockdown of RFWD3 in U2OS cells resulted in less PCNA ubiquitylation upon UV exposure. This defect was reversed by stable expression of wild-type RFWD3, but not a RING domain mutant lacking E3 ligase activity. The study also presented findings suggesting that RFWD3-mediated PCNA ubiquitylation depends on RAD18.

To assess if RFWD3 may be involved in MMC-induced mono- and polyubiquitylation of PCNA, 293T ZUP1 knockout cells were transfected with a siRNA pool targeting RFWD3 (**Fig. 5.8**). As RFWD3 is essential for cell viability in many cell types, the cell density was optimised to maximise the number of surviving RFWD3-depleted cells that could be harvested for the pull-down (Tsherniak et al., 2017; Dempster et al., 2019; data not shown). A reduction of RFWD3 protein levels was evident after siRNA knockdown, however residual RFWD3 protein could still be detected (**Fig. 5.8**). There was no appreciable effect of RFWD3 knockdown on MMC-induced PCNA ubiquitylation in ZUP1 knockouts. The strength of this effect may be limited by the incomplete RFWD3 knockdown, which is not an uncommon outcome given the essentiality of RFWD3 for viability in many cell types, as seen in previous RFWD3 silencing attempts and the difficulty in generating complete RFWD3 knockouts (Gallina et al., 2021; Feeney et al., 2017). Future work should therefore consider the

use of acute protein depletion systems such as the degron system to understand the role of RFWD3 in mediating PCNA ubiquitylation in ZUP1 knockout cells.

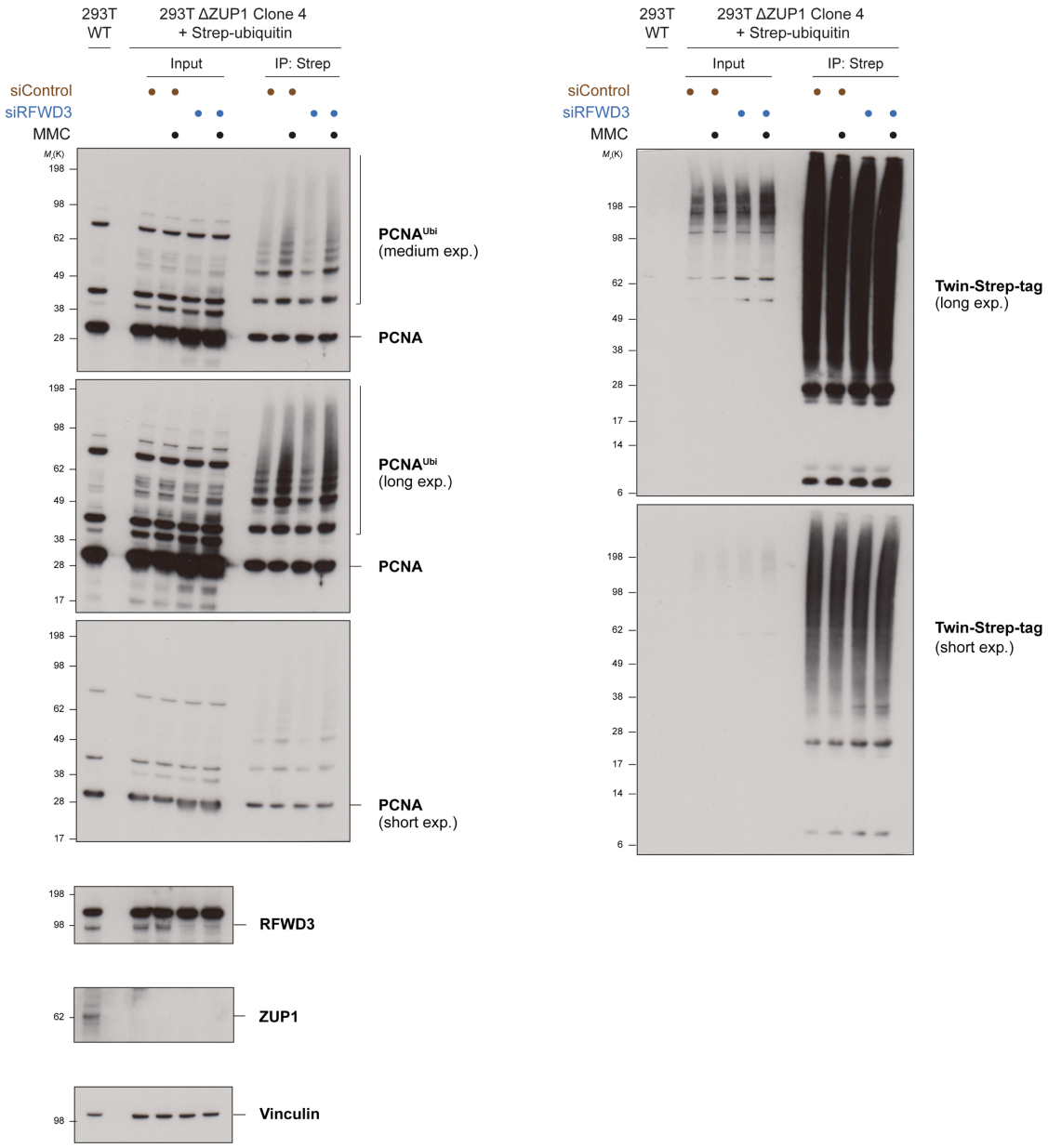



**Figure 5.8: Assessing the effects of RFWD3 knockdown on MMC-induced PCNA ubiquitylation in ZUP1 knockout cells.** 293T ΔZUP1_Ex6/2 Clone 4 cells were reverse transfected with 20 nM of non-targeting (siControl) or RFWD3 siRNA (siRFWD3) pools during cell plating, 24 h prior to the double thymidine block protocol, which was followed by MMC treatment and denaturing pull-down as described in Fig. 5.7. 293T wild-type whole cell extract was loaded onto the gel as a control for ZUP1 expression. Blots shown were obtained from a single experiment (n = 1).

PCNA monoubiquitylation in UV-irradiated cells was shown to be negatively regulated by USP1 (Huang et al., 2006). USP1 exists in a complex with UAF1 which stimulates its catalytic activity (Cohn et al., 2007). Huang et al. reported that USP1 is inactivated by autocleavage following UV exposure, resulting in enhanced levels of PCNA monoubiquitylation which activates TLS (Huang et al., 2006). Based on these findings, the authors proposed a model in which USP1 autocleavage enables TLS to proceed when required, but USP1 may limit monoubiquitylated PCNA and concomitant mutagenic TLS polymerase activity both in unchallenged conditions and in the presence of UV damage.

It is not known whether the autocleavage of USP1 is a common response to DNA lesions apart from UV to enhance the levels of monoubiquitylated PCNA, or whether USP1 also targets polyubiquitylated PCNA for deubiquitylation. Niimi et al. demonstrated that monoubiquitylated PCNA accumulates following UV, MMS or MMC treatment, but only UV-stimulated monoubiquitylated PCNA corresponded to a loss of USP1 (Niimi et al., 2008). Another study reported that HU induction of monoubiquitylated PCNA is associated with a decrease in USP1 (Lim et al., 2018). Given that the role of USP1 as a DUB for monoubiquitylated PCNA may be differentially regulated depending on the type of DNA lesion, it was difficult to predict the effect of USP1 silencing on MMC-induced mono- and polyubiquitylated PCNA in ZUP1 knockout cells.

USP1 knockdown in ZUP1 knockout cells led to the accumulation of monoubiquitylated PCNA in untreated conditions (**Fig. 5.9**). MMC induction of PCNA polyubiquitylation was abolished by USP1 knockdown, while monoubiquitylated PCNA in MMC-treated cells was present at levels higher than basal conditions. Although the effect was clear, this requires further validation given that a complete and efficient knockdown of USP1 could not be achieved, and residual protein was present.

It is plausible that the USP1 partial knockdown led to the accumulation of monoubiquitylated PCNA in MMC-treated cells, which may have resulted in the

excessive recruitment of TLS polymerases. Consistent with this idea, it was previously reported that USP1 depletion resulted in an increase in foci formation of the TLS polymerase, Pol κ which also showed increased interaction with PCNA (Jones et al., 2012). Excessive TLS polymerases may have physically hindered factors such as E3 ligases involved in polyubiquitylating PCNA, and may explain the limited induction of PCNA polyubiquitylation after USP1 knockdown and MMC treatment. However, the observations in **Fig. 5.9** need to be confirmed by performing more biological repeats.

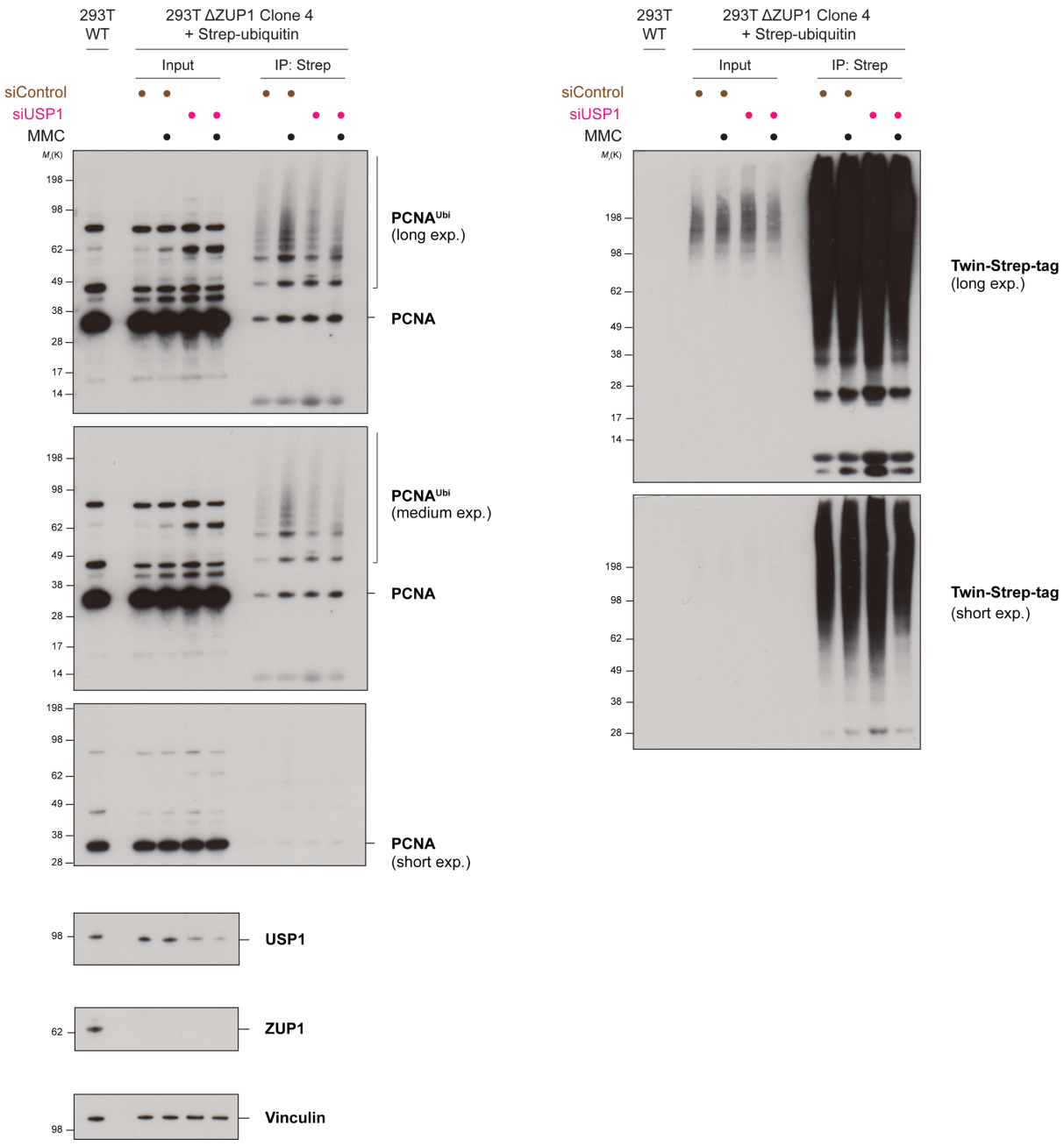



**Figure 5.9: USP1 knockdown abolishes PCNA polyubiquitylation in ZUP1 knockout cells treated with MMC.** 293T ΔZUP1_Ex6/2 Clone 4 was reverse transfected with 20 nM of non-targeting (siControl) or USP1 siRNA (siUSP1) pools. The following steps were performed as in Fig. 5.7. 293T wild-type whole cell extract was loaded onto the gel as a control for ZUP1 expression. Blots shown were obtained from a single experiment (n = 1).

While the phenotype for elevated PCNA polyubiquitylation in MMC-treated ZUP1 knockouts was consistent, the effect on ubiquitylated RPA was less clear. Ubiquitylated RPA remained at low levels in all the conditions tested (data not shown). An alternative Strep pull-down approach was therefore tested where Twin-Strep-tag was fused to RPA32 instead of ubiquitin. Cells were transiently co-transfected with Strep-RPA32, Flag-RPA70 and Flag-RPA14 at a 1:1:1 ratio to enable the exogenous expression of all three RPA subunits in cells (**Fig. 5.10**). The other steps were carried out as previously described, with the cell harvest performed after recovering cells from 24 h MMC treatment in cell culture media for 8 or 24 h.

The wild-type cells exhibited high levels of ubiquitylated RPA32 after 8 h release from MMC, which decreased to basal levels at 24 h. In ZUP1 knockout cells, polyubiquitylated RPA32 was present at elevated levels at 0 h (i.e, immediately after MMC treatment) and after 24 h release from MMC (**Fig. 5.10**). Although a clear trend was not established from these results, ZUP1 knockout cells had more ubiquitylated RPA32 at 24 h release compared to the wild-type, suggesting that it may have persisted for a longer period of time in the ZUP1 knockouts. However, this observation could not be reproduced (data not shown). This may have been due to the asynchronous setup of the experiment, therefore follow-up work should assess if a consistent effect on ubiquitylated RPA32 can be observed in synchronous cell populations. The induction of ubiquitylated RPA32 was less clear or detectable than that of PCNA across multiple approaches, which suggests that ubiquitylated PCNA may constitute a larger fraction of the total PCNA pool during replication stress compared to ubiquitylated RPA.

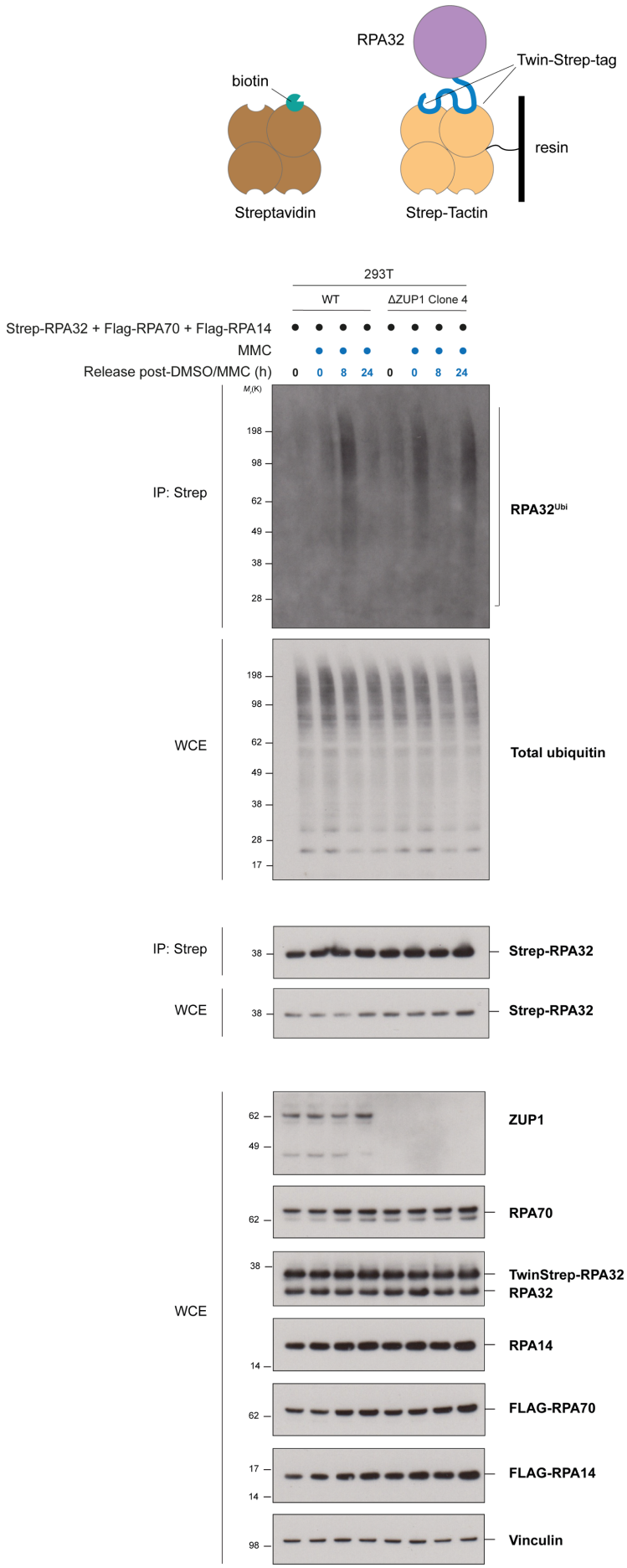

RPA32
Twin-Strep-tag
biotin
resin
Streptavidin
Strep-Tactin
293T
WT
ΔZUP1 Clone 4
Strep-RPA32 + Flag-RPA70 + Flag-RPA14
MMC
Release post-DMSO/MMC (h)
0 0 8 24 0 0 8 24
M,(K)
198
98
62
49
38
28
IP: Strep
RPA32Ubi
WCE
198
98
62
49
38
28
17
Total ubiquitin
IP: Strep
38
Strep-RPA32
WCE
38
Strep-RPA32
WCE
62
49
ZUP1
62
RPA70
38
TwinStrep-RPA32
RPA32
14
RPA14
62
FLAG-RPA70
17
14
FLAG-RPA14
98
Vinculin

**Figure 5.10: Denaturing pull-down of Strep-RPA32 to assess MMC induction of ubiquitylated RPA32.** Top: Schematic illustration of RPA32 tagged with Twin-Strep-tag that binds with high affinity to the streptavidin derivative, Strep-Tactin as described in Fig. 5.1. Bottom: 293T wild-type cells and ΔZUP1_Ex6/2 Clone 4 were co-transfected with Strep-RPA32, Flag-RPA70 and Flag-RPA14 at a 1:1:1 ratio. Cells were prepared using the asynchronous cell setup as described in Fig. 5.3. Cells were treated with 1 μM MMC or an equivalent volume of DMSO for 24 h before releasing in cell culture media for the indicated durations. The denaturing Strep pull-down was performed as previously described. Blots shown represent one out of two independent experiments (n = 2).

### 5.2.3 Attempts to rescue PCNA polyubiquitylation in ZUP1 knockout cells

The elevated levels of polyubiquitylated PCNA in two independent ZUP1 knockout clones upon MMC treatment suggest a ZUP1-dependent dysregulation of PCNA polyubiquitylation. This could involve the direct DUB activity of ZUP1 on PCNA, as suggested by *in vitro* DUB assays performed in parallel in the lab that revealed the ability of recombinant ZUP1 to cleave K63-linked polyubiquitin chains on PCNA, which is dependent on ZUP1 catalytic activity (**Appendix C: Fig. 4**). To assess the contribution of ZUP1 DUB activity to the phenotype in ZUP1 knockout cells, ZUP1 wild-type or the catalytically inactive mutant (C360R) were evaluated for their ability to rescue the phenotype.

ZUP1 knockout cells were transiently co-transfected with Strep-ubiquitin and FLAG-ZUP1 wild-type or C360R during the transfection step in the Strep pull-down protocol. MMC induction of polyubiquitylated PCNA at K164 decreased slightly with the expression of FLAG-ZUP1 wild-type, but not the C360R mutant (**Fig. 5.11**). Although ZUP1 wild-type expression did not completely rescue PCNA polyubiquitylation, the slight effect suggests a regulatory role of ZUP1 for PCNA nonetheless, and the lack of rescue by the C360R mutant could indicate the

involvement of ZUP1 DUB activity. However, the slight rescue effect was difficult to reproduce in subsequent replicates (data not shown).

The effect of FLAG-ZUP1 wild-type on PCNA polyubiquitylation was also assessed in MMC-treated cells released in media for varying durations. The lack of consistency between experiments remained a challenge, and any rescue effect by FLAG-ZUP1 wild-type was modest (**Fig. 5.12A, 5.12B**). It was noted that the co-transfection of the FLAG empty vector plasmid with Strep-ubiquitin corresponded to an inconsistent MMC induction of PCNA polyubiquitylation in the ZUP1 knockouts after 24 h treatment, unlike previous observations in which Strep-ubiquitin was exogenously expressed on its own. I considered whether the transient expression of the FLAG plasmids in addition to Strep-ubiquitin may have introduced technical factors that impacted the phenotype or masked the rescue effect of ZUP1. This was one of the motivations for generating stable ZUP1-expressing rescue cell lines for the next rescue approach (**Appendix C: Fig. 2, Fig. 5.13**). Other possible reasons for the lack of a clear rescue effect upon ZUP1 re-expression are outlined on page 203.

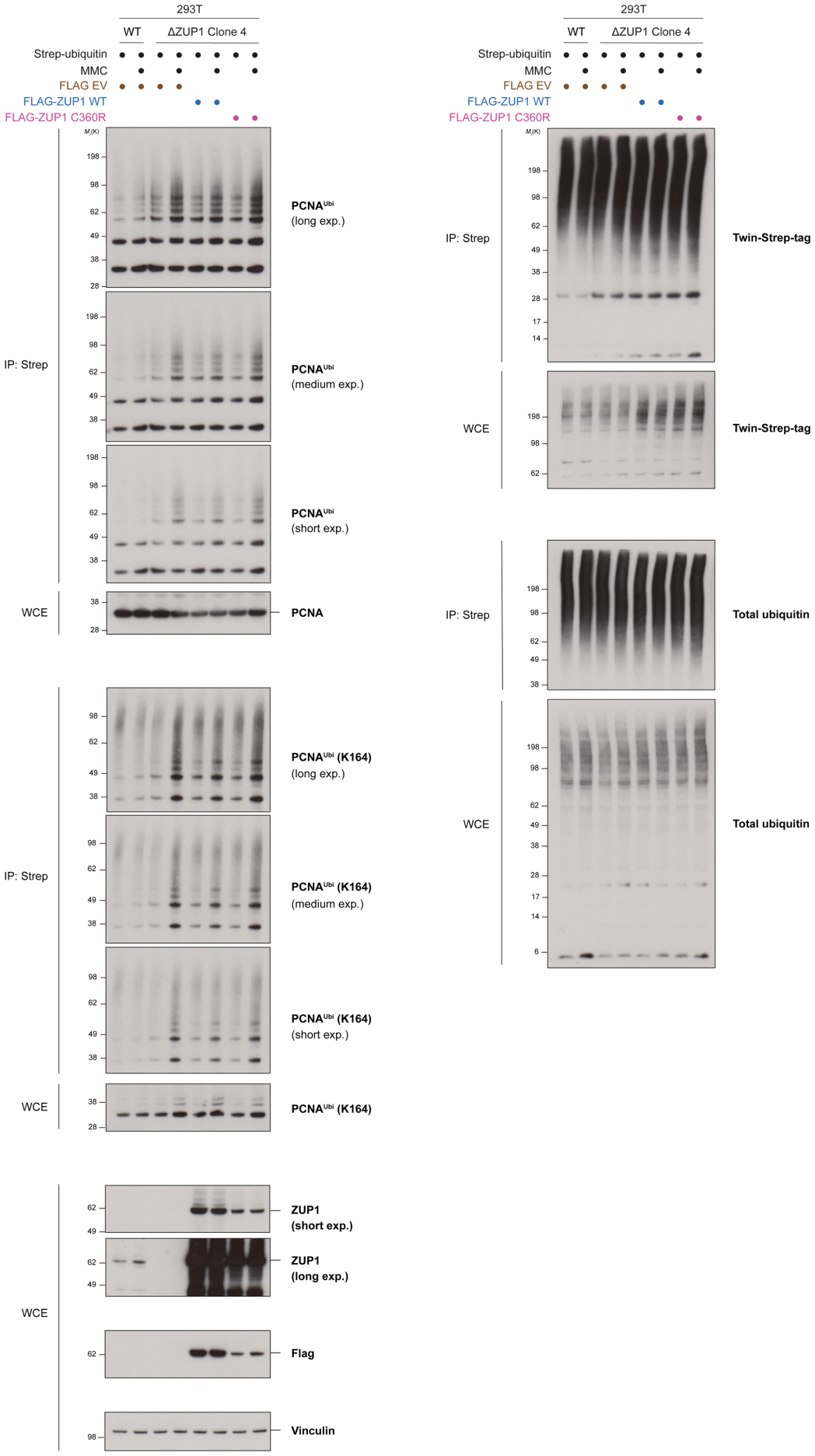

293T
WT
ΔZUP1 Clone 4
Strep-ubiquitin
MMC
FLAG EV
FLAG-ZUP1 WT
FLAG-ZUP1 C360R
$M_r$(K)
198
98
62
49
38
28
17
14
6
IP: Strep
WCE
PCNA$^{Ubi}$ (long exp.)
PCNA$^{Ubi}$ (medium exp.)
PCNA$^{Ubi}$ (short exp.)
PCNA
PCNA$^{Ubi}$ (K164) (long exp.)
PCNA$^{Ubi}$ (K164) (medium exp.)
PCNA$^{Ubi}$ (K164) (short exp.)
PCNA$^{Ubi}$ (K164)
ZUP1 (short exp.)
ZUP1 (long exp.)
Flag
Vinculin
Twin-Strep-tag
Total ubiquitin

**Figure 5.11: Assessing the ability of transiently expressed FLAG-ZUP1 wild-type or C360R to rescue MMC-induced PCNA polyubiquitylation in ZUP1 knockout cells.** 293T wild-type cells and ΔZUP1_Ex6/2 Clone 4 were synchronised by double thymidine block and transiently co-transfected with Strep-ubiquitin and FLAG empty vector, FLAG-ZUP1 WT or C360R. Cells were treated with 1 μM MMC or an equivalent volume of DMSO for 24 h, and the remaining denaturing Strep pull-down steps were performed as previously described. Blots shown represent one out of three independent experiments (n = 3).

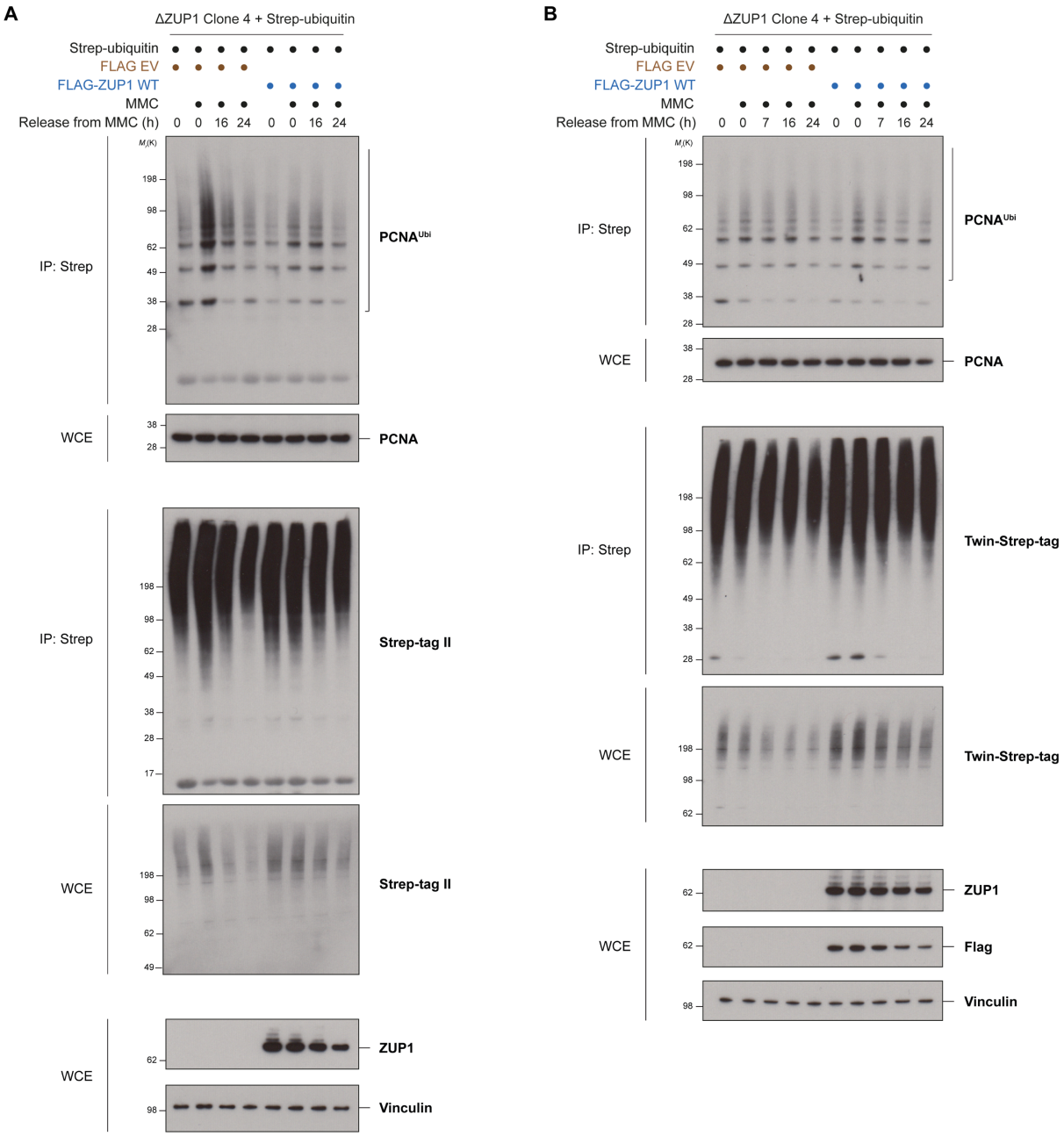



**Figure 5.12: Assessing the effect of FLAG-ZUP1 wild-type on the recovery of MMC-induced PCNA polyubiquitylation in ZUP1 knockout cells.** In A and B, 293T ΔZUP1_Ex6/2 Clone 4 cells were synchronised by double thymidine block and co-transfected with Strep-ubiquitin and FLAG empty vector or FLAG-ZUP1 WT. Cells were treated with 1 μM MMC or an equivalent volume of DMSO for 24 h, then released in cell culture media for the indicated durations. The denaturing Strep pull-down was performed as previously described. Blots shown represent one out of three independent experiments (n = 3).

The transient transfection of FLAG-ZUP1 in **Fig. 5.11** and **5.12** did not show a significant nor reproducible rescue effect. The results shown in **Fig. 5.12** suggests that technical factors may have been introduced by the co-expression of the FLAG and Strep-ubiquitin plasmids, resulting in the inconsistency of an otherwise robust phenotype. Furthermore, the transient transfection of FLAG-ZUP1 in ZUP1 knockouts may not have allowed sufficient time for ZUP1 to restore its cellular function. Another limitation is that exogenous ZUP1 was over-expressed compared to the wild-type, and was therefore not physiological (**Fig. 5.11**).

To address the limitations of the above rescue approach, a ZUP1 knockout clone was complemented with the stable expression of ZUP1 wild-type or C360R, which matched endogenous ZUP1 levels more closely (**Appendix C: Fig. 2**). The stable expression of ZUP1 at near-endogenous levels may allow the assessment of the long-term effect of ZUP1 re-expression on PCNA polyubiquitylation in the knockouts. ZUP1 C360R was also stably expressed to evaluate the contribution of ZUP1 DUB activity to the phenotype.

MMC induction of polyubiquitylated PCNA was examined in the stable rescue cell lines after 24 h treatment. The rescue effect of ZUP1 wild-type was not clear in these conditions (**Fig. 5.13**). It is possible that the 24 h treatment was longer than necessary to detect a rescue effect. In **Fig. 5.5B**, a 14 h or 16 h MMC treatment was sufficient to induce high levels of PCNA polyubiquitylation in the ZUP1 knockouts. The 24 h MMC treatment in **Fig. 5.13** may have resulted in even more substantial levels of stressed forks and polyubiquitylated PCNA that may not be effectively reduced by ZUP1 re-expression. Therefore, it will be worthwhile for future work to analyse a time course of PCNA polyubiquitylation induction starting at shorter treatment lengths, or monitor the recovery of this modification upon the removal of MMC.

It is also important to note that the rescue cell lines in **Fig. 5.13** express only the main ZUP1 isoform and not the other isoforms. It is possible that the smaller ZUP1 isoforms may be important for the regulation of PCNA ubiquitylation, which could explain the lack of a rescue effect upon the re-expression of the main ZUP1 isoform. Conversely,

if the phenotype is not dependent on the smaller isoforms, it is conceivable that ZUP1 knockouts may have irreversibly adapted to ZUP1 loss, in which case the re-expression of ZUP1 may not restore ZUP1 function in regulating PCNA ubiquitylation. As outlined in Chapter 3, the limitations of the CRISPR methodology should also be considered, such as the possible selection of compensatory mutations in the ZUP1 knockouts during the CRISPR protocol, and off-target effects.

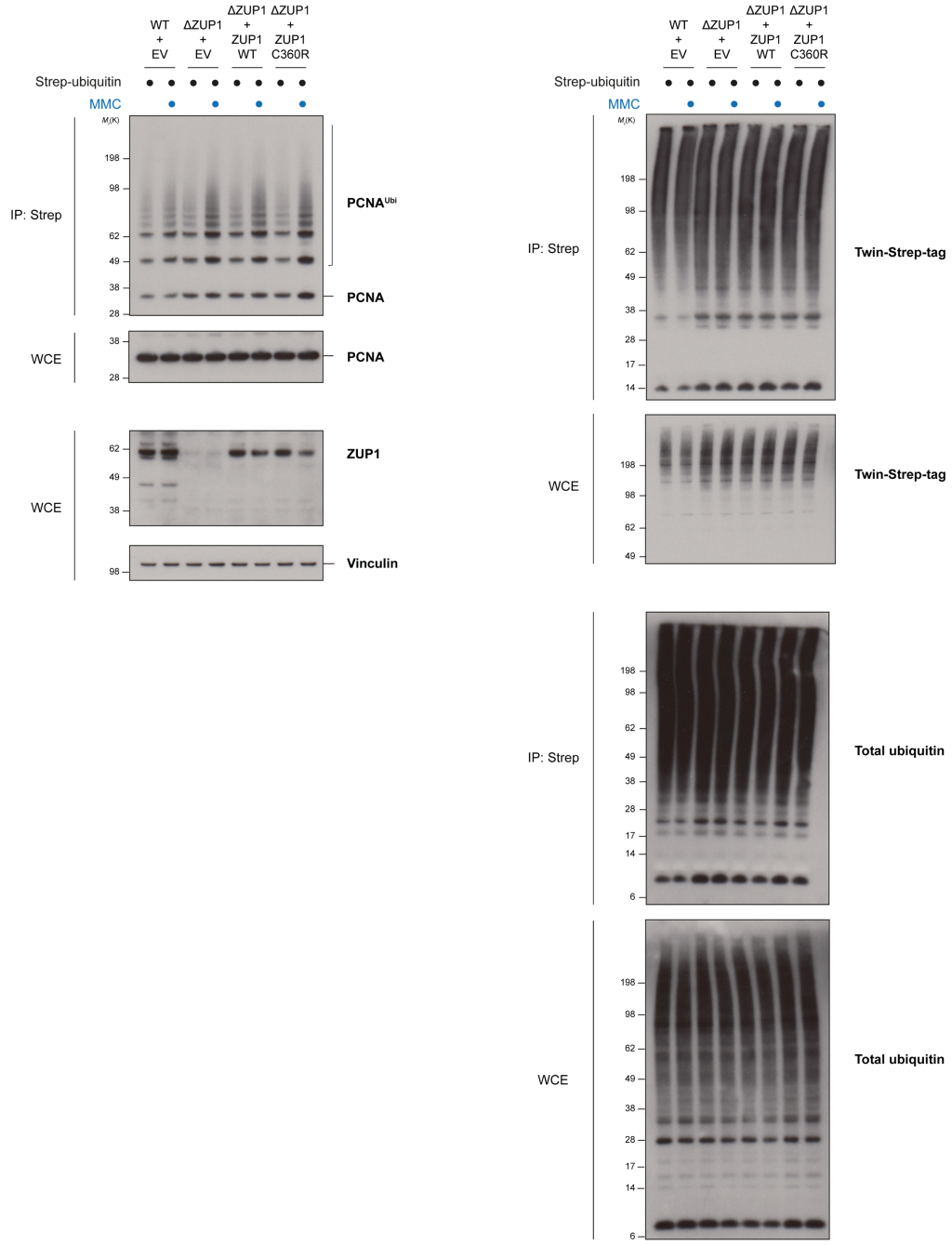



**Figure 5.13: Investigating the ZUP1 rescue effect of MMC-induced PCNA polyubiquitylation using stable ZUP1-complemented cell lines.** Stable cell lines were generated by lentiviral transduction to express ZUP1 wild-type, C360R or the empty vector in 293T ΔZUP1_Ex6/2 Clone 4 (Appendix C: Fig. 2). Wild-type cells that were stably transduced with the empty vector were included in this experiment as the control. Cells were synchronised by double thymidine block, transfected with Strep-ubiquitin and treated with 1 μM MMC or an equivalent volume of DMSO for 24 h prior

to the denaturing Strep pull-down, as previously described. Blots shown are representative of two independent experiments (n = 2).

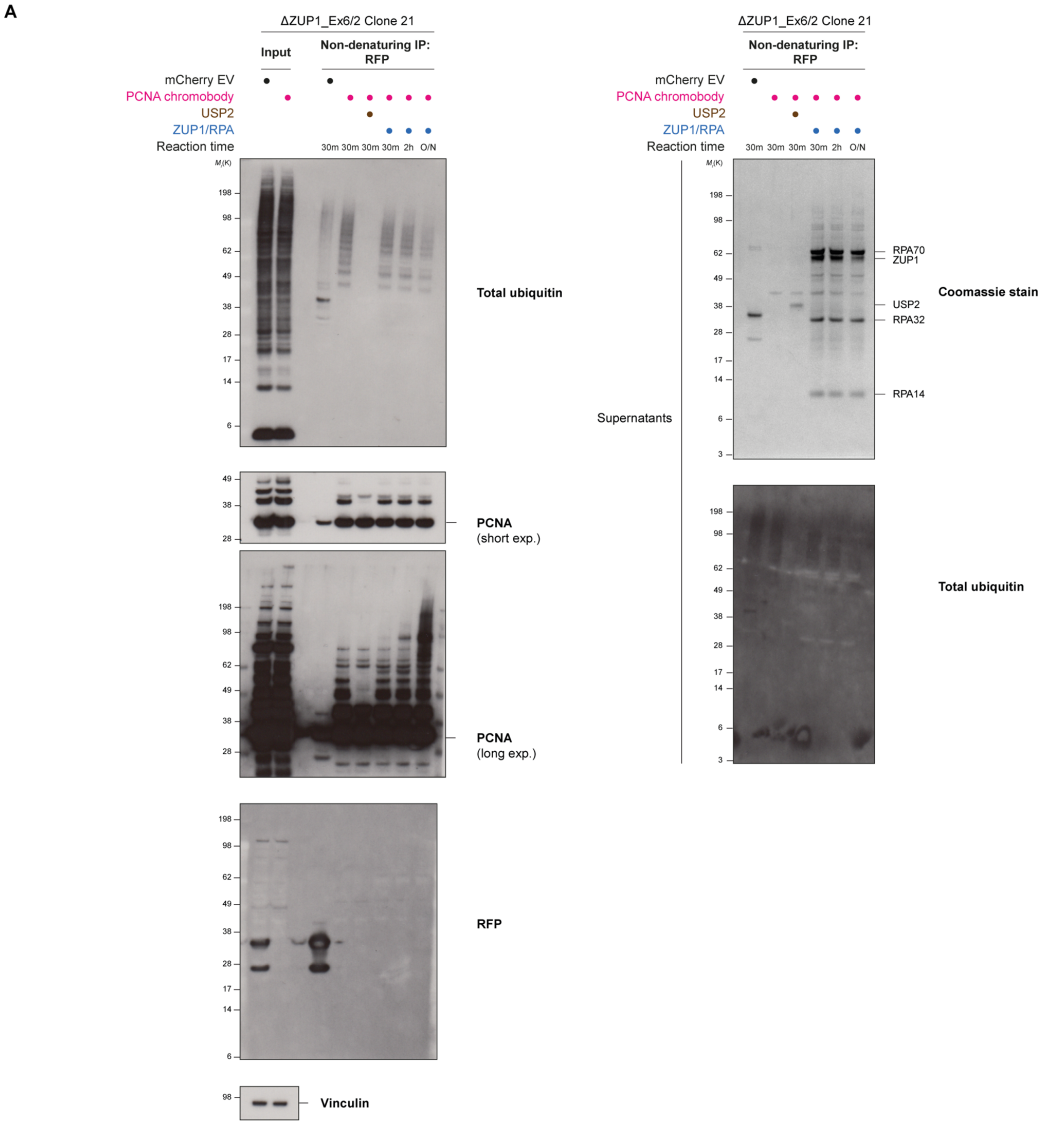
The next method to investigate the dependence of the PCNA polyubiquitylation phenotype on ZUP1 was based on the ubiquitin chain restriction (UbiCRest) assay (Hospenthal et al., 2015). This assay was originally designed to treat ubiquitylated substrates with a panel of DUBs with different linkage specificities and assess the ubiquitin linkage and chain types present on the substrates. Using a similar approach, polyubiquitylated PCNA from MMC-treated ZUP1 knockout cells was used as a substrate for recombinant ZUP1 *in vitro*. This could reveal whether ZUP1 may deubiquitylate polyubiquitylated PCNA, as seen in DUB assays *in vitro* (**Appendix C: Fig. 4**).

GFP-PCNA was expressed in ZUP1 knockout cells which were treated with MMC to induce PCNA polyubiquitylation. However, GFP-PCNA could not be used as a substrate for ZUP1 *in vitro* due to the incompatibility of the GFP magnetic beads with the DUB reaction buffer (data not shown). A DNA plasmid encoding a PCNA chromobody, comprising an anti-PCNA nanobody fused to RFP, was expressed in ZUP1 knockout cells. The expression of the RFP-tagged chromobody was not clear by Western blotting but was seen by fluorescence microscopy to localise in the nuclei, consistent with validation studies for this chromobody (Chromotek, **Fig. 5.14A, 5.14B**). Cells were treated with MMC using previously optimised conditions to induce PCNA polyubiquitylation. RFP immunoprecipitation was then performed to isolate the PCNA-specific chromobody.

The RFP-immunoprecipitated fraction was treated with ZUP1 in the presence of the RPA complex, given the robust observation by other members in the lab that RPA stimulates the DUB activity of ZUP1 against free K63-linked polyubiquitin chains and K63-polyubiquitylated PCNA *in vitro* (**Appendix C: Fig. 4, 5**). USP2 was used as a positive control given its non-selective activity for cleaving various ubiquitin chain linkage types (Clague et al., 2019). PCNA was significantly enriched by RFP

immunoprecipitation compared to the mCherry empty vector control, indicating that a large amount of PCNA remained bound to the chromobody throughout the immunoprecipitation protocol. The total level of ubiquitin chains in the immunoprecipitated fraction decreased slightly in a time-dependent manner in the presence of both ZUP1 and RPA (**Fig. 5.14A**). This suggests that polyubiquitylated PCNA may be deubiquitylated by ZUP1. Notably, the 'smears' that run above PCNA displayed an opposite trend and were enhanced after overnight treatment with ZUP1 and RPA. Such smears do not only reflect the ubiquitylated form but can also indicate SUMO modifications (Parker et al., 2008). The increase in these modifications in the presence of ZUP1 is unlikely to represent ubiquitylation, since the substantial time-dependent increase was not mirrored by the ubiquitin blot, but rather showed an opposite effect to total ubiquitin levels. A potential approach to clarify this is to include SUMO E1 inhibitors in the reaction to prevent any SUMOylation activity in the immunoprecipitated material. Ubiquitin E1 inhibitors can also be used to rule out the identity of these unknown modifications as polyubiquitin.

The time-dependent reduction of ubiquitin chains in the RFP-immunoprecipitated fraction by ZUP1 and RPA was also reproduced in another independent ZUP1 knockout clone (**Fig. 5.15**). Although the effect is slight, the consistent results suggest that ZUP1 may reverse PCNA polyubiquitylation as demonstrated previously *in vitro* (**Appendix C: Fig. 4**). It will be crucial to assess the contribution of ZUP1 DUB activity to this observation using a catalytically inactive ZUP1 mutant. However, it cannot be ruled out that the ubiquitin chains observed are those formed on other proteins that co-precipitated with PCNA. As with all *in vitro* assays, it is also important to consider that this set-up may not provide the complete or optimal physiological setting for ZUP1 to perform its DUB activity. For example, specific protein-protein interactions that influence the DUB function of ZUP1 toward PCNA could be missing *in vitro*.


A
ΔZUP1_Ex6/2 Clone 21
Input
Non-denaturing IP: RFP
mCherry EV
PCNA chromobody
USP2
ZUP1/RPA
Reaction time
30m 30m 30m 30m 2h O/N
M(K)
198
98
62
49
38
28
17
14
6
Total ubiquitin
49
38
28
PCNA
(short exp.)
198
98
62
49
38
28
PCNA
(long exp.)
198
98
62
49
38
28
17
14
6
RFP
98
Vinculin
ΔZUP1_Ex6/2 Clone 21
Non-denaturing IP: RFP
mCherry EV
PCNA chromobody
USP2
ZUP1/RPA
Reaction time
30m 30m 30m 30m 2h O/N
Supernatants
M(K)
198
98
62
49
38
28
17
14
6
3
RPA70
ZUP1
USP2
RPA32
RPA14
Coomassie stain
198
98
62
49
38
28
17
14
6
3
Total ubiquitin

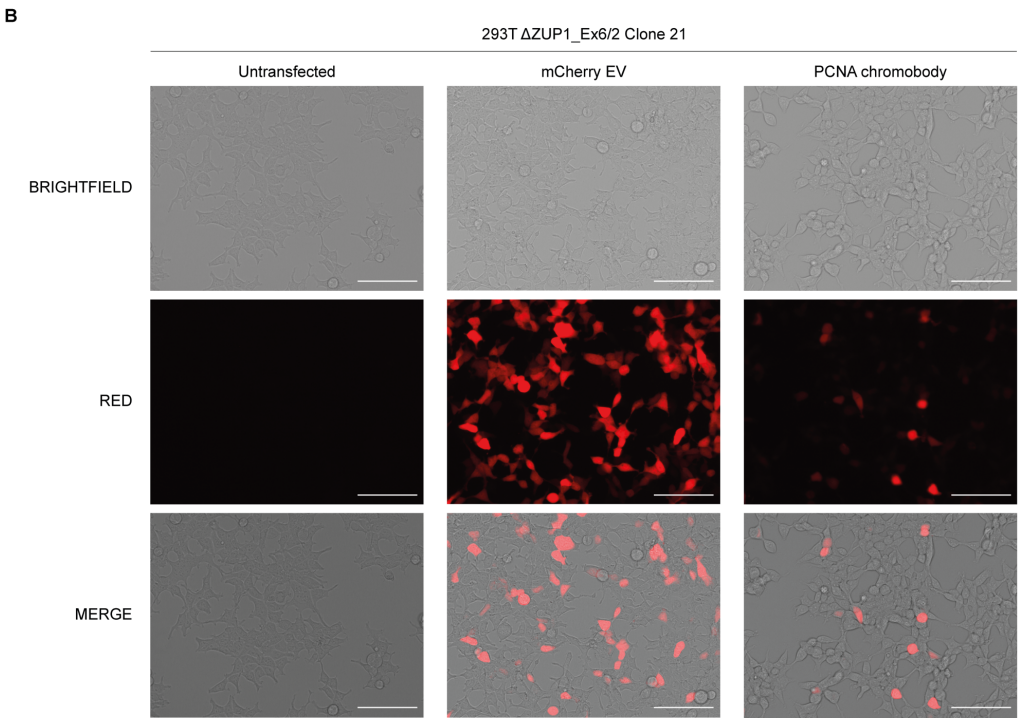
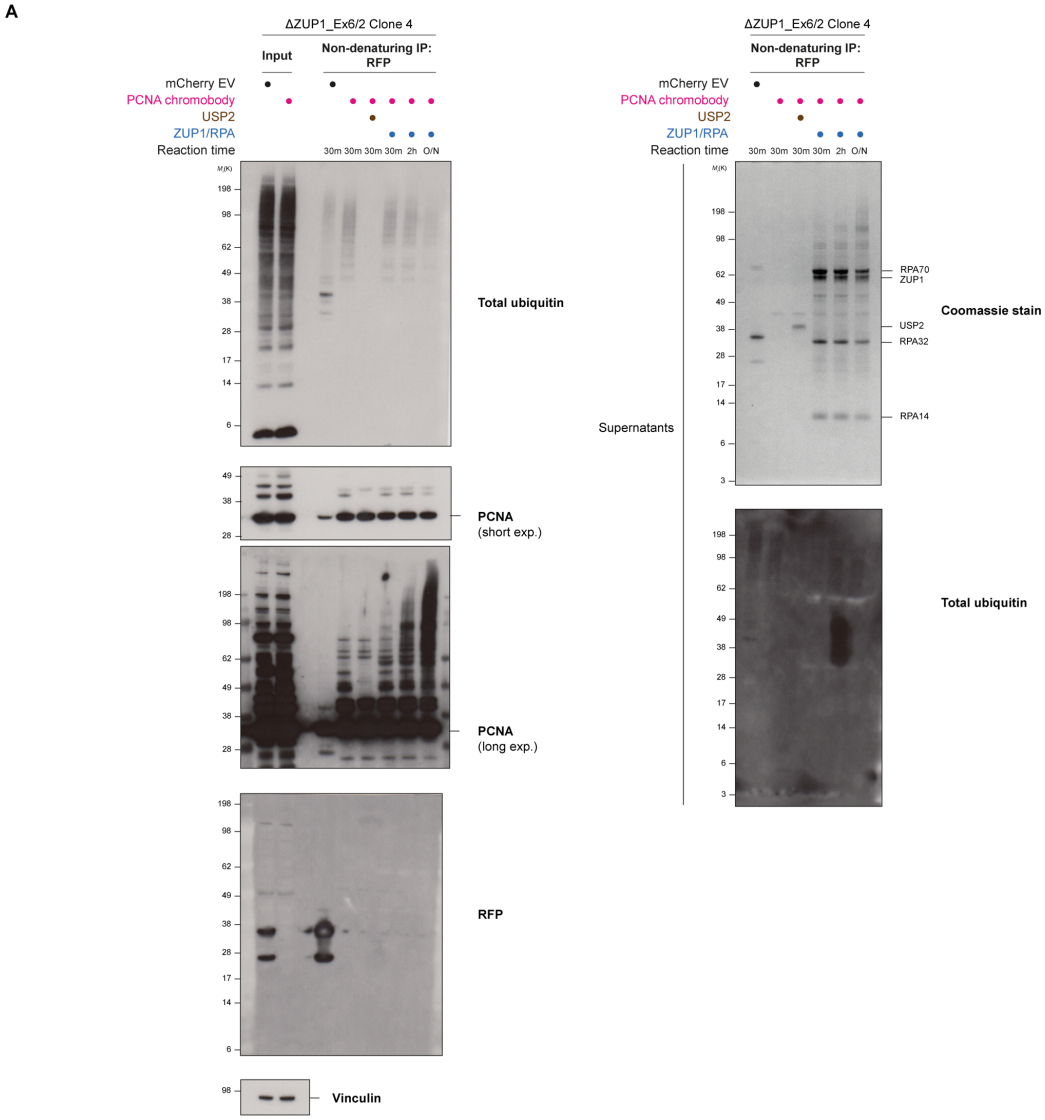

B
293T ΔZUP1_Ex6/2 Clone 21
Untransfected
mCherry EV
PCNA chromobody
BRIGHTFIELD
RED
MERGE

**Figure 5.14: Immunoprecipitation of PCNA from ZUP1 knockout cells to assess the *in vitro* deubiquitylation of polyubiquitylated PCNA by recombinant ZUP1.** A) 293T ΔZUP1_Ex6/2 Clone 21 cells were transfected with a plasmid encoding RFP-tagged PCNA chromobody, or the mCherry empty vector, and all samples were treated with 1 μM MMC for 24 h as detailed in the Methods. The PCNA chromobody was immunoprecipitated under non-denaturing conditions and divided into 6 samples. Each sample was treated with recombinant ZUP1 in the presence of RPA, or with the positive control USP2, or an equivalent volume of DUB reaction buffer for the indicated durations. Blots shown are representative of two independent experiments (n = 2). B) Representative images of the transfected samples in A showing the localisation of the RFP-tagged PCNA chromobody. Samples were transfected with the mCherry empty vector as a control for red fluorescence. Scale bar: 100 μm.


A
ΔZUP1_Ex6/2 Clone 4
Input
Non-denaturing IP: RFP
mCherry EV
PCNA chromobody
USP2
ZUP1/RPA
Reaction time
30m 30m 30m 30m 2h O/N
Total ubiquitin
PCNA (short exp.)
PCNA (long exp.)
RFP
Vinculin
ΔZUP1_Ex6/2 Clone 4
Non-denaturing IP: RFP
Supernatants
RPA70
ZUP1
USP2
RPA32
RPA14
Coomassie stain
Total ubiquitin

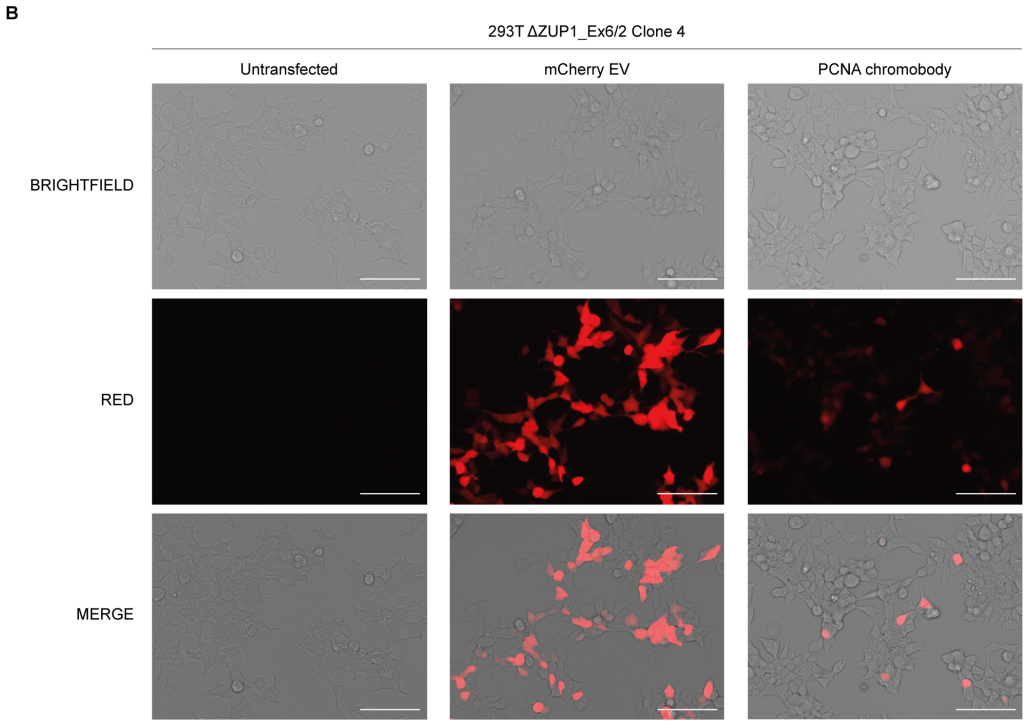

B
293T ΔZUP1_Ex6/2 Clone 4
Untransfected
mCherry EV
PCNA chromobody
BRIGHTFIELD
RED
MERGE

**Figure 5.15: The effect of recombinant ZUP1 on the polyubiquitin chains in the immunoprecipitated PCNA fraction was reproduced in a different ZUP1 knockout clone.** A) The protocol in Fig. 5.14 was repeated in 293T ΔZUP1_Ex6/2 Clone 4. Blots shown were obtained from a single experiment (n = 1). B) Representative images of the transfected samples in A showing the localisation of the RFP-tagged PCNA chromobody. Samples were transfected with the mCherry empty vector as a control for red fluorescence. Scale bar: 100 μm.

As outlined on page 174, the 293T cell line was used for the phenotyping experiments described in this chapter for technical reasons, and MMC was used to induce replication stress based on the hypersensitivity of U2OS ZUP1 knockouts to the drug (observed in Chapter 3). The MMC sensitivity of 293T ZUP1 knockout cells has not been assessed yet, thus the importance of ZUP1 for DNA repair and cell survival of 293T cells in the presence of MMC is not known, but was rather assumed to play an important role based on the survival defects of U2OS ZUP1 knockouts. Given that the two cell lines have different genetic backgrounds and possibly differ in their DNA repair machineries, MMC treatment of both cell lines may not necessarily generate the same dependence on ZUP1 for repair and survival. Although a robust PCNA polyubiquitylation phenotype was observed in this chapter in the 293T ZUP1 knockouts treated with MMC, it would be important for future studies to evaluate the MMC sensitivity of 293T ZUP1 knockouts, in order to support the claim that defective regulation of PCNA polyubiquitylation is related to DNA repair defects in cells.

### 5.2.4 ZUP1 has a role in homologous recombination repair

To assess if ZUP1 plays a role in homologous recombination, a homology-directed repair (HDR) assay was performed to compare the efficiency of CRISPR-mediated HDR in wild-type and ZUP1 knockout cells. In this assay, the GFP variant Clover was knocked in near the start codon of the *LMNA* gene, by transiently co-transfecting cells with a Clover homology repair template (donor) plasmid and a sgRNA/Cas9 plasmid that targets *LMNA* (Pinder et al., 2015; **Fig. 5.16A**). *LMNA* encodes the nuclear lamin A and lamin C isoforms, and the insertion of the Clover sequence in-frame into the gene is indicated by fluorescent nuclei, with enhanced signal at their periphery (Pinder et al., 2015; **Fig. 5.16B**). The readout of HDR efficiency is the percentage of Clover-expressing cells, measured by flow cytometry.

To maximise the capacity of HDR, one of the technical details optimised was the ratio of the two co-transfected plasmids. This was recommended by Pinder et al. who

demonstrated that increasing the ratio of the LMNA sgRNA/Cas9 to the donor plasmid significantly improved HDR efficiency (Pinder et al., 2015). However, the reverse was true for 293T cells, which showed a higher proportion of Clover-positive cells when a 1:5 ratio of the sgRNA/Cas9 to donor plasmid was used, compared to 5:1 or 1:1 (**Fig. 5.17A**). This ratio was therefore utilised in subsequent experiments. On the other hand, U2OS cells exhibited low HDR efficiency for all the ratios tested as seen in other studies (Canny et al., 2018; **Fig. 5.17A**). 293T was the preferred cell line for evaluating the role of ZUP1 in HDR, as any difference in HDR efficiency may be more visible given the higher Clover knock-in rate in 293T (>10% Clover-positive cells) compared to U2OS cells (<3% Clover-positive cells). Although microscopy may also be used to compare Clover-positive cell populations in the wild-type and ZUP1 knockout cells, flow cytometry is an efficient method to quantify these relatively small cell populations and involves fewer sample preparation steps.

CtIP is known for its role in DNA end resection during HR where it activates the MRE11 endonuclease within the MRN complex (Anand et al., 2016; Zhang et al., 2022). CtIP was depleted as a negative control for the assay. As expected, CtIP knockdown corresponded to a decrease in HDR-mediated Clover knock-in (**Fig. 5.17B**).

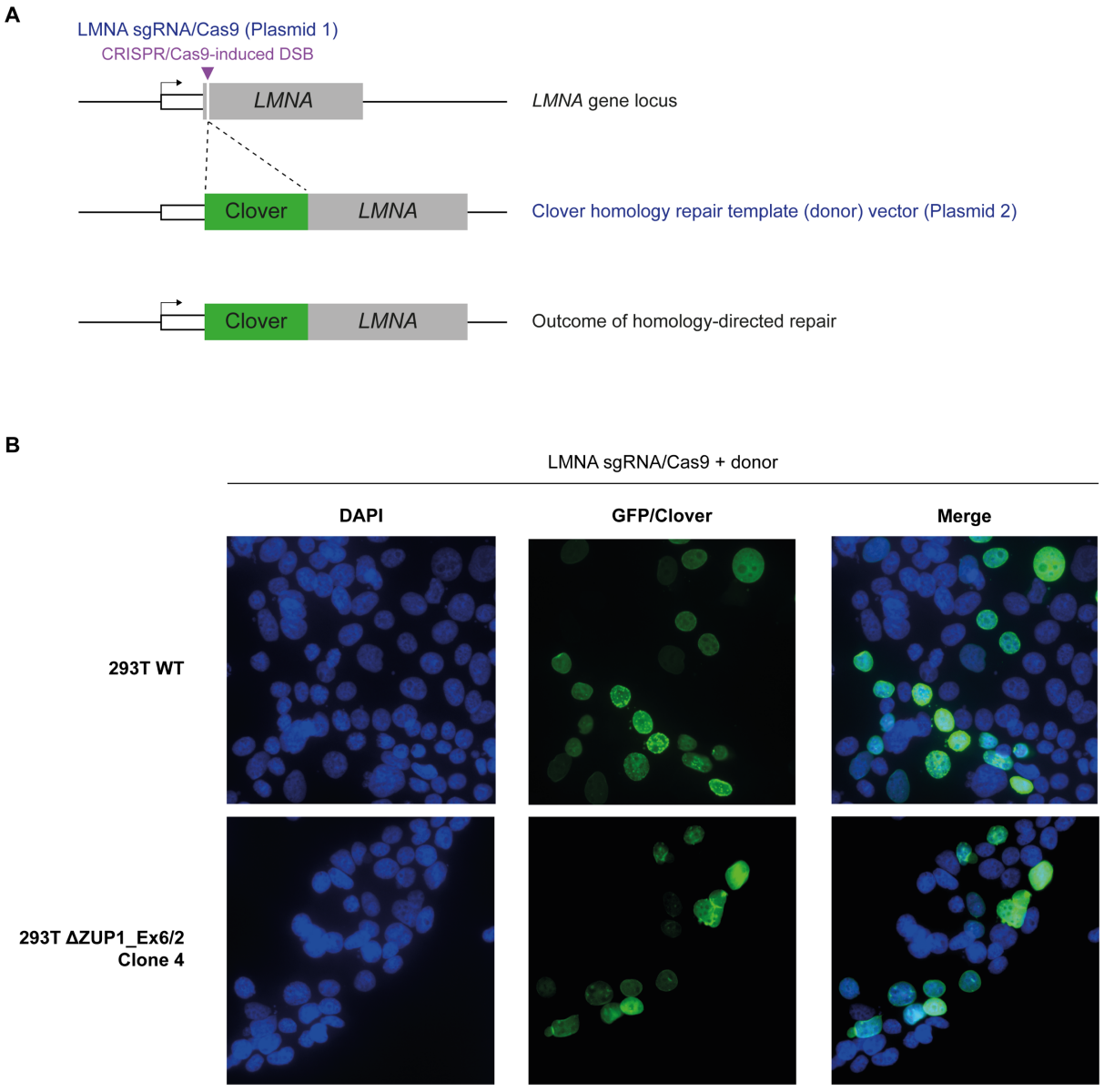



**Figure 5.16: CRISPR-based Clover knock-in assay to assess the efficiency of homology-directed repair in cells.** A) Summary of the HDR assay involving the CRISPR-mediated knock-in of Clover in-frame into the *LMNA* gene to assess HDR efficiency in cells, which was performed by transiently co-transfecting cells with the two indicated plasmids (Pinder et al., 2015). B) Representative images of 293T wild-type and ΔZUP1_Ex6/2 Clone 4 cells co-transfected with the LMNA sgRNA/Cas9 and Clover homology repair template (donor) plasmids indicated in A.

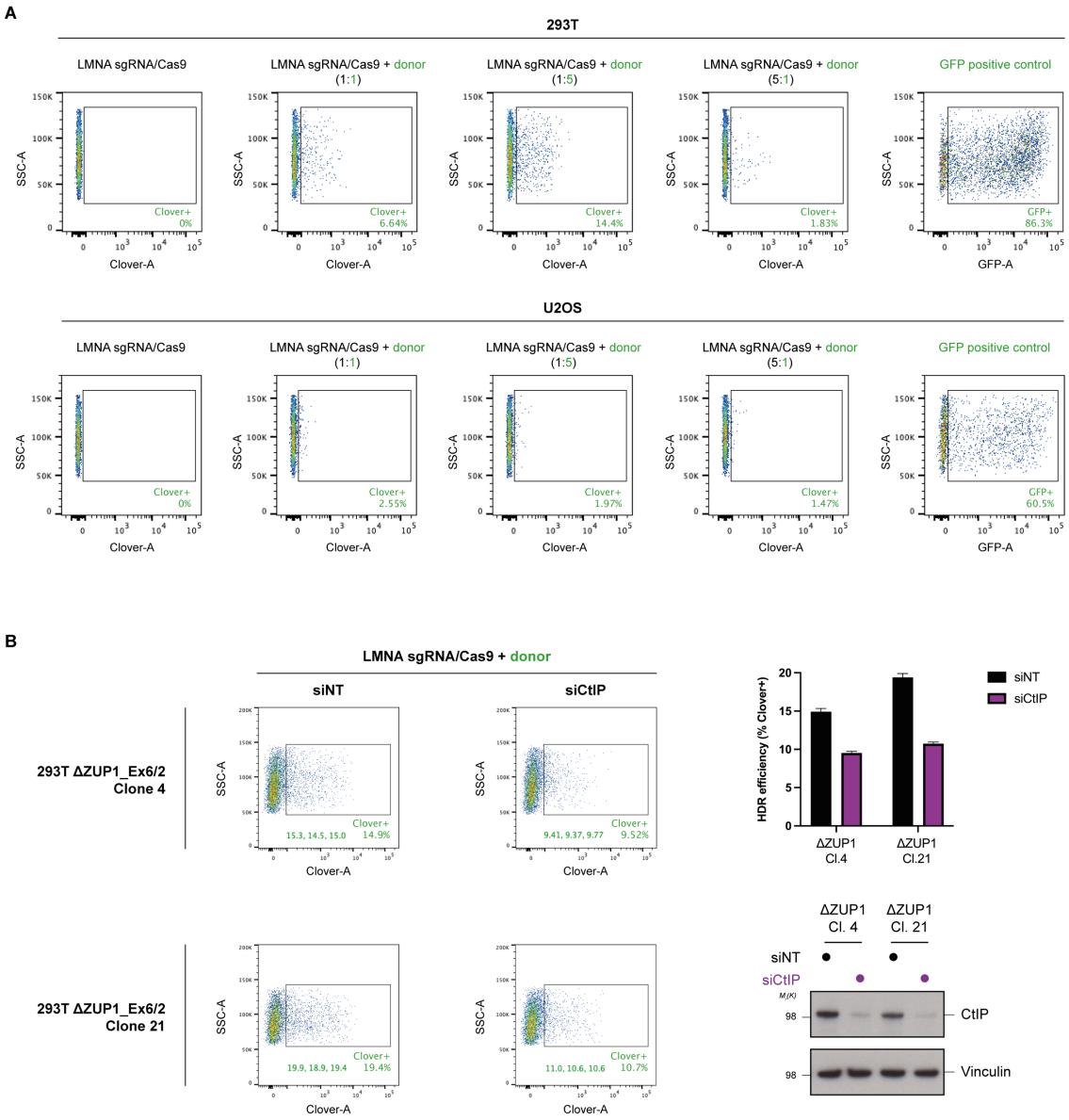



**Figure 5.17: Optimisation of transfected plasmid ratios to maximise Cas9-mediated HDR and Clover knock-in.** A) Flow cytometry analysis of Clover or GFP-positive populations in 293T and U2OS wild-type cells transfected with the indicated ratios of the LMNA sgRNA/Cas9 to Clover homology repair template (donor) plasmid. GFP empty vector was transfected as a control for GFP expression. Results shown were obtained from a single experiment (n = 1). B) ΔZUP1_Ex6/2 Clone 4 and Clone 21 cells were transfected with non-targeting (siNT) or CtIP-targeting (siCtIP) siRNA pools to analyse the suppression of HDR activity by siCtIP. Values (mean ± S.D.) represent 3 technical readings. Results shown were obtained from a single experiment (n = 1).

To analyse the difference in HDR efficiency between 293T wild-type and ZUP1 knockout cells, the Clover knock-in was performed using the optimised plasmid ratios. The control for the assay was cells co-transfected with the donor plasmid and the Cas9 empty vector in place of LMNA Cas9/sgRNA. Two independent ZUP1 knockout clones displayed higher HDR efficiency compared to the wild-type (**Fig. 5.18**). Strikingly, the Cas9 empty vector controls for the ZUP1 knockouts also exhibited a greater proportion of Clover-positive cells compared to the wild-type. This was unexpected given the absence of a gRNA sequence for Cas9-mediated targeting. The Clover fluorescence in these control samples was dispersed throughout the cell (**Appendix C: Fig. 3**). The range of the Clover signal measured by flow cytometry in the control samples was notably larger than that in the LMNA-targeted samples (**Fig. 5.18**). These observations could reflect the random integration of the Clover sequence into spontaneous DSB sites, which may occur at a higher frequency in ZUP1 knockout cells. Alternatively, HR may be dysregulated in the ZUP1 knockouts, as examined further in the Discussion.

To rule out varying transfection efficiencies as a potential confounding factor, the assay was repeated with the inclusion of an mCherry empty vector as the transfection control. Clover-positive cell populations were identified from mCherry-expressing cells (**Fig. 5.19**). The difference between the wild-type and knockouts was accentuated, where the proportion of Clover-expressing cells was significantly higher in all three independent clones compared to the wild-type. The Cas9 empty vector controls for the ZUP1 knockouts were once again observed to have a greater proportion of Clover-positive cells compared to the wild-type.

Rescue experiments will be necessary to assess the contribution of ZUP1 DUB activity to the hyper-recombinogenic characteristics of ZUP1 knockout cells. As described in the Discussion, these results suggest that ZUP1 may have an anti-HR role to limit recombination and prevent the detrimental effects of its dysregulation. This may also be related to the DNA repair defects (Chapter 3) and the aberrant accumulation of PCNA polyubiquitylation in the ZUP1 knockouts during replication stress as presented in this chapter.

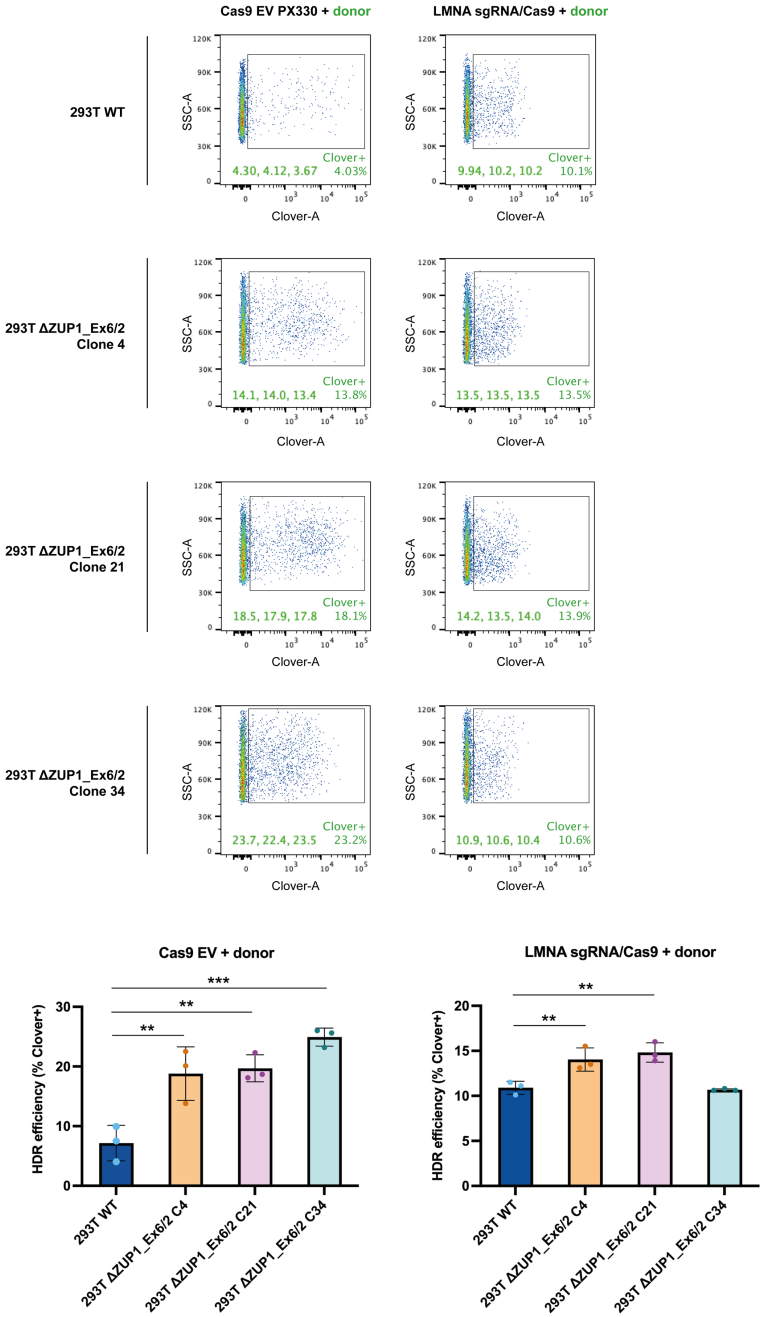



**Figure 5.18: ZUP1 knockouts exhibit enhanced HDR activity as indicated by the efficiency of Clover knock-in.** Flow cytometry analysis of Clover+ populations in 293T wild-type cells, ΔZUP1_Ex6/2 Clone 4 and Clone 21 subjected to the LMNA HDR assay. Cells were co-transfected with either the Cas9 PX330 empty vector or LMNA sgRNA/Cas9 plasmid together with the donor plasmid. Values (mean ± S.D.) represent three independent experiments (n = 3), each consisting of technical triplicates. A one-way ANOVA was performed with Dunnett's test. *P < 0.05, **P < 0.01, ***P < 0.001, ****P < 0.0001.

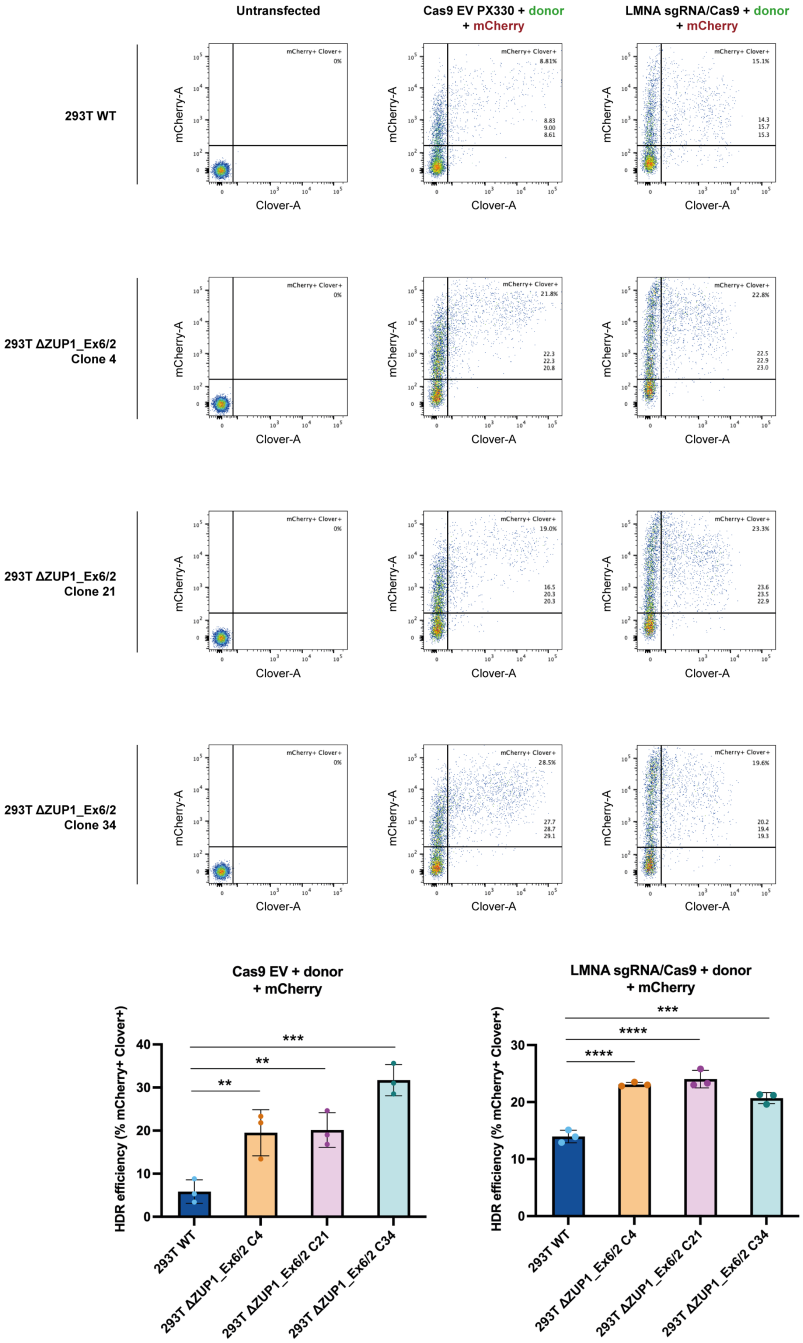



**Figure 5.19: The hyper-recombination phenotype in ZUP1 knockouts was confirmed when a transfection control was included in the LMNA HDR assay.** Flow cytometry analysis of Clover+ populations in 293T wild-type cells, ΔZUP1_Ex6/2 Clone 4 and Clone 21 as in Fig. 5.18. Cells were co-transfected with either the Cas9 PX330 empty vector or LMNA sgRNA/Cas9 plasmid together with the donor plasmid and mCherry empty vector. Values (mean ± S.D.) represent three independent experiments (n = 3), each consisting of technical triplicates. A one-way ANOVA was performed with Dunnett's test. *P < 0.05, **P < 0.01, ***P < 0.001, ****P < 0.0001.

## 5.3 Discussion

### 5.3.1 ZUP1 is a DUB that potentially reverses PCNA ubiquitylation

This chapter demonstrates that ZUP1 knockouts display elevated and persistent levels of ubiquitylated PCNA in response to MMC treatment (**Fig. 5.5, 5.6**). In favour of the hypothesis that ZUP1 may be a DUB for PCNA, DUB assays performed *in vitro* by other members in the lab have shown that recombinant ZUP1 cleaves K63-linked polyubiquitin chains on PCNA, which is dependent on its catalytic activity (**Appendix C: Fig. 4**). These assays revealed that ZUP1 cleavage of polyubiquitin chains on PCNA is further stimulated by RPA, and that ZUP1 does not cleave monoubiquitin on PCNA, consistent with its preference for hydrolysing longer chains (Kwasna et al., 2018).

Although it was challenging to detect a clear ZUP1 rescue effect in cells, there were some modest yet consistent observations suggesting that ZUP1 limits PCNA ubiquitylation, which require further validation. For example, it will be important to clarify if the decrease in polyubiquitin chains after overnight treatment with recombinant ZUP1 and RPA in **Fig. 5.14** and **5.15**, represents chains specifically on PCNA (e.g., using the ubiquitylation-deficient PCNA K164R mutant) and whether this is dependent on ZUP1 catalytic activity (by incubation with catalytically inactive ZUP1).

USP1 is a DUB that negatively regulates UV-induced PCNA monoubiquitylation and was observed to undergo autocleavage following UV exposure, and this enables the accumulation of monoubiquitylated PCNA for TLS activation (Huang et al., 2006). USP7 and USP10 are two other DUBs that have been proposed to deubiquitylate monoubiquitylated PCNA (Park et al., 2014; Kashiwaba et al., 2015). Prior to the work in this thesis, no DUB has been implicated in the deubiquitylation of polyubiquitylated PCNA. Based on the findings in this chapter and supporting *in vitro* DUB assays in the lab, ZUP1 may be the first DUB proposed to regulate polyubiquitylated PCNA.

ZUP1 may act as a DUB to directly target polyubiquitylated PCNA for deubiquitylation as suggested by the *in vitro* DUB assays, or ZUP1 may alternatively regulate PCNA through other mechanisms. Other evidence supporting the possibility that ZUP1 is a direct DUB for PCNA, includes the specificity of ZUP1 for cleaving long K63-linked polyubiquitin chains, which is also the linkage type formed on K164 of PCNA during replication stress (Kwasna et al., 2018; Slade et al., 2018). K63-linked polyubiquitin chains on PCNA have been proposed to mediate template switching and fork reversal mechanisms (Chapter 1, Section 1.2.2, Section 1.6.1).

If polyubiquitylated PCNA is not a direct substrate of ZUP1, ZUP1 may still be an important regulator of PCNA ubiquitylation through alternative mechanisms. For example, ZUP1 may have a role in facilitating the unloading of ubiquitylated PCNA. Ubiquitylated PCNA is known to associate with chromatin (Daigaku et al., 2017; Gallina et al., 2021). ATAD5-RLC performs the unloading of unmodified, mono- and polyubiquitylated PCNA, and was proposed to regulate USP1-mediated deubiquitylation of monoubiquitylated PCNA induced by UV (Kang et al., 2019; Lee et al., 2010). It is possible that the timely unloading of ubiquitylated PCNA is necessary for efficient DNA repair and to enable normal DNA replication to resume. Many chromatin-bound proteins such as the CMG complex are ubiquitylated by K48-linked chains, which are recognised by the ubiquitin-directed AAA-ATPase VCP/p97 that extracts the ubiquitylated protein from the chromatin (Moreno et al., 2014; van den Boom et al., 2018). VCP/p97 was previously identified in the ZUP1 interactome as summarised in **Fig. 4.1**. It is possible that VCP/p97 extracts chromatin-bound ZUP1 interacting proteins that are ubiquitylated such as PCNA. Although VCP/p97 has mostly been shown to recognise and extract target proteins ubiquitylated with K48-linked chains, it is possible that PCNA may have K48/K63 branched chains that are recognised by VCP/p97 (Meyer et al., 2012). Alternatively, VCP/p97 may bind to K63-linked chains on PCNA, based on evidence that the VCP co-factor NPL4 can interact with K63 chains through its NZF domain (Ye et al., 2003). If ZUP1 has a role in facilitating VCP-mediated extraction of PCNA, the loss of ZUP1 could result in dysregulated levels of chromatin-bound ubiquitylated PCNA in the presence of DNA damage.

Most investigations that focus on PCNA mono- and polyubiquitylation have utilised UV and HU to induce this modification (Huang et al., 2006; Niimi et al., 2008; Lim et al., 2018; Gallina et al., 2021). It was previously shown that USP1 loss correlates with accumulated levels of monoubiquitylated PCNA induced by UV and HU, but not those induced by MMC or MMS (Niimi et al., 2008; Lim et al., 2018). This suggests that PCNA ubiquitylation and deubiquitylation may be differentially regulated in response to different DNA lesions, therefore it will be important to define the context in which ZUP1 regulates PCNA polyubiquitylation. In this chapter, synchronised S-phase cell populations were treated with MMC. The panel of DNA damaging agents should be expanded in future investigations to determine if ZUP1 also regulates PCNA polyubiquitylation in the presence of other lesions. It would also be crucial to assess if ZUP1 mediates this role when replication-independent damage is induced, for example by exposing G0-arrested wild-type and ZUP1 knockout cells to UV and comparing the levels of ubiquitylated PCNA.

Considering the hypersensitivity of ZUP1 knockouts to replication stress-inducing compounds as demonstrated in Chapter 3, it is possible that the elevated and persistent levels of PCNA polyubiquitylation in ZUP1 knockouts during replication stress may interfere with the repair process and/or induce more lesions. Aberrant polyubiquitylated PCNA in ZUP1 knockouts may disrupt the binding, recruitment or signalling of appropriate repair factors. PCNA may be polyubiquitylated to promote recombination-mediated template switching mechanisms following replication stress, as previously proposed based on studies in yeast (Chapter 1, Section 1.2.2). Although recombination mechanisms are capable of performing accurate repair, they require tight regulation by anti-recombinogenic factors that prevent excessive or aberrant recombination events (Krejci et al., 2012). Template switching involves the formation of complex DNA structures during strand exchange and fork regression (Giannattasio et al., 2014). Dysregulation of these mechanisms may lead to misalignments, chromosomal rearrangements and/or toxic recombination intermediates. This could be an example of how persistent levels of polyubiquitylated PCNA may account for the hypersensitivity of ZUP1 knockouts to DNA damaging agents. As discussed in the next section, the findings in this chapter may reflect a

role of ZUP1 in limiting recombination-mediated processes to prevent the detrimental effects of excessive recombination.

The observation that ZUP1 regulates PCNA ubiquitylation in cells, combined with *in vitro* DUB assays suggesting that polyubiquitylated PCNA may be a substrate for ZUP1, reveal a crucial role of ZUP1 in DNA repair, given the importance of ubiquitylated PCNA in DNA damage tolerance mechanisms. This provides novel insight into how PCNA, a critical player in DNA replication and repair, is regulated during DNA damage.

### 5.3.2 ZUP1 may have an anti-HR role

This chapter also presents the finding that ZUP1 knockouts have an enhanced HDR activity compared to the wild-type, as measured by CRISPR-mediated Clover knock-in (**Fig. 5.19**). Intriguingly, all three independent ZUP1 knockout clones displayed hyper-recombination not only when DSBs were induced specifically within *LMNA*, but also in the absence of an sgRNA target sequence which was intended as the control. These observations suggest that the loss of ZUP1 results in enhanced HR repair both at targeted DSB sites and also at random or spontaneous DSB sites.

A possible explanation for the enhanced Clover integration into random or untargeted sites is that ZUP1 knockouts intrinsically have a higher level of spontaneous DSBs. This may be due to defective DNA repair in ZUP1 knockouts that fail to prevent the accumulation of spontaneous DNA damage. This is supported by previous work showing that ZUP1 silencing leads to elevated levels of chromatin-bound 53BP1 and γH2AX in unchallenged conditions (Kwasna et al., 2018). Alternatively, the hyper-recombination phenotype may indicate dysregulated HR activity in ZUP1 knockouts, which may reflect a role of ZUP1 in limiting HR repair at any occurring DSB.

HR requires tight regulation by anti-recombinogenic factors to prevent aberrant outcomes and enable accurate repair (Krejci et al., 2012). An example of negative

regulation of HR in human cells is mediated by PARI, a PCNA-interacting protein that restricts recombination events by promoting the disassembly of RAD51-DNA structures (Moldovan et al., 2012; Burkovics et al., 2016). RTEL1 has also been shown to suppress recombination by disrupting the formation of displacement loop (D-loop) intermediates (Barber et al., 2008). Silencing of these factors was found to result in elevated HR activity and DNA damage hypersensitivity. The findings in this chapter suggest that ZUP1 may limit unscheduled or inappropriate recombination to prevent detrimental chromosomal rearrangements. The potential anti-recombinogenic role of ZUP1 may explain both the aberrant HR activity and dysregulated levels of PCNA polyubiquitylation in ZUP1 knockouts, as PCNA polyubiquitylation was previously proposed to promote a recombination-mediated template switching pathway (Chapter 1, Section 1.2.2).

In Chapter 3, ZUP1 knockouts were found to display hypersensitivity to genotoxic compounds that induce replication stress. The resulting DNA lesions may form DSBs upon encounter with the replication machinery. DSBs can be repaired by two major pathways namely HR and NHEJ, the former of which is thought to be highly accurate (Chapter 1, Section 1.2.4; Ackerson et al., 2021). If ZUP1 has an important role in limiting HR in cells, HR may proceed at uncontrolled levels in ZUP1 knockout cells upon exposure to the genotoxic agents. This may result in chromosomal rearrangements or lethal recombination intermediates, and/or inaccurate HR repair of the lesions leading to cell lethality.

As shown in Chapter 4, ZUP1 interacts with USP11 which has critical regulatory roles in HR repair. USP11 was shown to deubiquitylate PALB2 which is a key step in the formation of the BRCA1-PALB2-BRCA2 complex (Orthwein et al., 2015). USP11 was also reported as a deubiquitylase for γH2AX and consequently regulates γH2AX function in DSB repair (Yu et al., 2016). Considering that ZUP1 loss is associated with dysregulated HR, it is possible that the knockout of ZUP1 disrupted the function of USP11 in HR, leading to the observed hyper-recombination phenotype. Future work can evaluate whether USP11 depends on ZUP1 for its reported functions in HR. A

potential tool that can be used for this investigation is the ZUP1 ZnF2 USP11-binding mutant that was identified in Chapter 4.

To confirm the role of ZUP1 in HR, ZUP1 complementation experiments will be essential to evaluate the ability of ZUP1 to rescue the hyper-recombination phenotypes identified in the Clover LMNA HDR assay. It will also be important to determine the contribution of ZUP1 catalytic activity to the observed effects, which may reveal whether the deubiquitylation of PCNA by ZUP1 could be involved in its HR role. Sister chromatid exchange (SCE) assays can be performed as an additional method to examine HR defects in ZUP1 knockout cells in the presence of DSBs induced by UV or compounds such as CPT (Liu et al., 2000; Moldovan et al., 2012; Tumini et al., 2021). SCEs serve as markers of genomic instability or hyperactive HR activity (Painter et al., 1980, Moldovan et al., 2012; Wietmarschen et al., 2016). Excessive levels of SCEs have been observed in cells from Bloom syndrome patients (Chaganti et al., 1974). It will not be surprising if elevated SCE rates are also exhibited by ZUP1 knockouts, or if their metaphase spreads reveal chromosomal aberrations even at basal levels, given the possibility of spontaneous DSBs in ZUP1 knockouts as suggested by the HDR assay. In addition, RAD51 foci formation can be visualised after DSB induction to assess HR activity in ZUP1 knockouts compared to the wild-type (Godin et al., 2016).

Taken together, the findings in this chapter suggest the role of ZUP1 as a DUB for PCNA, which is supported by *in vitro* DUB assays in the lab. In addition, ZUP1 potentially has a role in limiting HR both in unchallenged conditions and in the presence of exogenous DSB-inducing agents. These observations highlight that ZUP1 is an important player in DNA repair, and provide a focus for future investigations to examine how the role of ZUP1 in counteracting PCNA ubiquitylation may extend to its regulation of HR.

# 6

# Final Discussion and Concluding Remarks

ZUP1 was recently discovered as the founding member of a novel DUB class with specificity for cleaving long K63-linked polyubiquitin chains (Kwasna et al., 2018; Hermanns et al., 2018; Hewings et al., 2018; Haahr et al., 2018). Proteomic work from these studies revealed the interaction of ZUP1 with the RPA complex, which is widely known for its roles in DNA replication and repair (Kwasna et al., 2018; Hermanns et al., 2018; Hewings et al., 2018). Preliminary evidence in human cancer cells demonstrated that YFP-ZUP1 is recruited to DNA damage sites, and siRNA-mediated knockdown of ZUP1 resulted in the accumulation of DNA damage markers, hypersensitivity to genotoxic agents, elevated levels of K63-linked polyubiquitin at replication forks stalled at the LacR-bound LacO array, and increased levels of RPA70 and RPA32 modified by K63-linked polyubiquitin chains following hydroxyurea treatment. Although these findings suggest that ZUP1 has a role in maintaining genome stability, the mechanistic basis for its function remains unclear. Some of the outstanding questions in relation to ZUP1 function in DNA repair are as follows:

1. Which DNA repair pathway does ZUP1 function in specifically?
2. Which ZUP1 domains are involved in its binding to components within the cellular ZUP1 complex?
3. What are the cellular substrate(s) of ZUP1?

The questions above shaped the three main aims of this thesis. The major findings and implications of this work are summarised below, while suggestions for future work have been outlined in the respective Discussion sections of the chapters.

To address the first aim, multiple independent ZUP1 knockout clones were generated using the CRISPR-Cas9 methodology, which enabled me to define ZUP1-dependent cellular phenotypes in DNA repair. Unlike previous reports that utilised RNAi to study ZUP1-dependent effects, the generation ZUP1 CRISPR-Cas9 knockout cells took into consideration the expression of ZUP1 splice isoforms in cells which were removed by targeting multiple exons within ZUP1. In addition, the truncated variants resulting from CRISPR targeting were also removed to generate complete ZUP1 knockouts. Clonogenic survival assays revealed that U2OS ZUP1 knockouts are hypersensitive to MMC, PARPi (olaparib and talazoparib), topotecan, and ATRi (AZD6738) in comparison to the wild-type. Intriguingly, ZUP1 hypomorphs or partial knockouts also exhibited significant survival defects following treatment with MMC, olaparib, topotecan and AZD6738 (ATRi). This suggests that ZUP1 plays an important role in maintaining genome stability in the presence of replication stress and that the domains present in the longest isoform play a functional role in genome stability.

Rescue experiments performed by others in the lab have demonstrated that ZUP1 complementation in the knockouts can rescue the MMC sensitivity phenotype (data not shown). Although the findings presented here are consistent in multiple independent ZUP1 knockout clones, it will be important for future studies to confirm that the effects are ZUP1-dependent by evaluating the ability of ZUP1 to rescue the other sensitivity phenotypes, and assess whether ZUP1 catalytic activity contributes to the phenotypes by expressing a ZUP1 catalytically inactive mutant. Some complex, undesired editing events were formed due to the CRISPR-Cas9 editing in 293T cells including inversion mutations and heterozygous edits. While these edits were successfully detected using the screening approaches described, this presents a cautionary note for the utilisation of the CRISPR-Cas9 methodology particularly to generate edits in cell lines with complex karyotypes, such as many cancer cell lines used in DNA repair studies. Such complex edits can lead to undesired gain-of-function mutations or gene disruptions through DNA rearrangements (Anzalone et al., 2020). The CRISPR-Cas9 methodology is therefore constantly being improved to address its limitations whilst maximising on-target editing efficiency, such as the base editing method that edits targeted base pairs without inducing DSBs (Huang et al.,

2021). Perhaps a better future approach will be to generate ZUP1 knockout cells in a more defined cellular background, such as RPE-1 cells that have been edited to remove the p53 protein.

The second aim was addressed in Chapter 4, which presents the novel finding that ZUP1 interacts with another DUB complex, USP11/TCEAL1 via ZnF2 in ZUP1. My data revealed a novel role for the ZUP1 ZnF2 in providing a specific USP11-binding site, with evidence that Glu43 and Met44 are involved in the interaction. This interaction corroborates *in vitro* pull-down assays that utilised recombinant purified proteins and demonstrated the requirement of ZUP1 ZnF2 for its interaction with USP11. Given that the disruption of ZUP1 exon 2 in the ZUP1 hypomorphs, which encodes the first three N-terminal zinc fingers of ZUP1, resulted in survival defects in the presence of genotoxic agents, the binding of ZUP1 ZnF2 to USP11 raises the possibility that this interaction may be important in DNA repair. Interestingly, USP11 has been reported to function within HR and DNA-protein crosslink repair (Wiltshire et al., 2010; Orthwein et al., 2015; Yu et al., 2016; Perry et al., 2021). The ZUP1 ZnF2 mutant that exhibits impaired binding to USP11 can therefore be used as a tool for future work to assess the importance of ZUP1-USP11 interaction for the DNA repair function of ZUP1.

Chapter 4 also revealed that ZUP1 and the uncharacterised protein TCEAL1 potentially binds to the UBL2-insert domain of USP11. Depletion of TCEAL1 using RNAi suggests that TCEAL1 has a role in regulating USP11 turnover, protein abundance and/or binding to ZUP1. A complete understanding of the role of the cellular ZUP1 protein complex will require interrogation of each component, therefore future studies should seek to clarify the mechanisms involved in the regulation of USP11 by TCEAL1, and vice versa. This chapter also showed that the α-2/3 helix-turn-helix region in ZUP1 participates in ZUP1-RPA interaction. Cross-linking mass spectrometry studies in the lab revealed the proximity of the RPA complex to multiple regions throughout ZUP1.

Chapter 5 explored the third aim and presents novel evidence suggesting that ZUP1 regulates PCNA polyubiquitylation during replication stress, based on the aberrant accumulation and persistent levels of polyubiquitylated PCNA observed in ZUP1 knockouts following MMC treatment. This finding was supported by *in vitro* DUB assays performed by other members of the lab showing that ZUP1 cleaves K63-linked polyubiquitin chains on PCNA, which is dependent on its catalytic activity. These observations suggest that ZUP1 may function as a DUB for polyubiquitylated PCNA and highlights that ZUP1 plays an important role in the DNA damage response, given that PCNA is ubiquitylated and acts as a crucial interaction and protein signalling hub during replication stress.

The cellular roles of PCNA polyubiquitylation remain unclear. PCNA was previously suggested to promote a recombination-mediated template switching pathway based on studies in yeast, and PCNA is known to interact with ZRANB3 which promotes fork reversal and restart (Chapter 1, Section 1.2.2, Section 1.6.1). The elevated and persistent levels of polyubiquitylated PCNA in ZUP1 knockouts following MMC treatment, indicate that the repair processes mediated by polyubiquitylated PCNA may be dysregulated in the absence of ZUP1, or that excessive levels of this modification may interfere with the repair of DNA lesions. These factors could contribute to the DNA repair defects observed in the knockouts. Notably, this chapter also demonstrates that ZUP1 knockouts exhibit hyper-recombinogenic characteristics. This suggests a role of ZUP1 in preventing unscheduled recombination events which, if dysregulated, could lead to genome instability. As described in the Discussion, further work to define the function of ZUP1 within HR can include examining HR factors after DSB induction in ZUP1 knockouts, chromosomal aberrations, and evaluating genetic epistasis between ZUP1 and HR genes such as BRCA1 and BRCA2.

Although robust observations were made in Chapter 5, experiments to rescue the PCNA polyubiquitylation phenotype proved to be challenging and require further assessment. The transient or stable expression of ZUP1 in the ZUP1 knockouts were unable to restore polyubiquitylated PCNA to wild-type levels following MMC

treatment, underlining the need for testing alternative conditions such as shorter treatment lengths or monitoring the recovery of the modification after MMC removal. Such rescue experiments are essential to exclude potential off-target effects induced by CRISPR gene editing and/or the selection of compensatory mutations during the single cell cloning or clonal expansion steps. As discussed earlier, one possible reason for the lack of a clear rescue effect could be the absence of the smaller ZUP1 isoforms in the stable rescue cell lines, which express only the main ZUP1 isoform. It is possible that the smaller ZUP1 isoforms play an important role in regulating PCNA ubiquitylation, and therefore need to be re-expressed in the knockouts to rescue the phenotype.

Chapter 5 also attempted to reproduce the published finding that the loss of ZUP1 leads to higher levels of RPA70 and RPA32 modified by K63-linked polyubiquitin following hydroxyurea treatment (Hewings et al., 2018). This effect could not be reproduced in ZUP1 knockout cells, and the challenge encountered was the inability to detect ubiquitylated RPA clearly in the presence of genotoxic agents. This was also noted by Elia et al. who speculated that the level of RPA ubiquitylated during DNA damage may constitute a small fraction of total RPA, which led the authors to purify ubiquitylated RPA from nuclear fractions, rather than whole cell extracts as shown in this thesis.

Collectively, the data presented in this thesis support the hypothesis that ZUP1 has an important role in maintaining genome stability. ZUP1 regulates PCNA polyubiquitylation during replication stress and may function within the HR pathway to suppress or prevent excessive recombination. The finding that ZUP1 interacts with USP11 via ZnF2 also provides a tool for future investigations into how both DUBs may cooperate or regulate one another in DNA repair. **Fig. 6.1** presents a model for the potential role of ZUP1 in DNA repair based on the phenotypes identified in this thesis. It is possible that ZUP1 deubiquitylates PCNA at crosslinked or uncoupled forks. This ZUP1-mediated regulation may in turn regulate the recruitment of ZRANB3 to polyubiquitylated PCNA, resulting in fork reversal. The DUB activity of ZUP1 in cleaving ubiquitin chains on PCNA at stressed forks may be stimulated by the RPA

complex. ZUP1 binding to USP11 may regulate the HR function of USP11 during the repair of ICLs or double-strand breaks, and limit aberrant HR events.

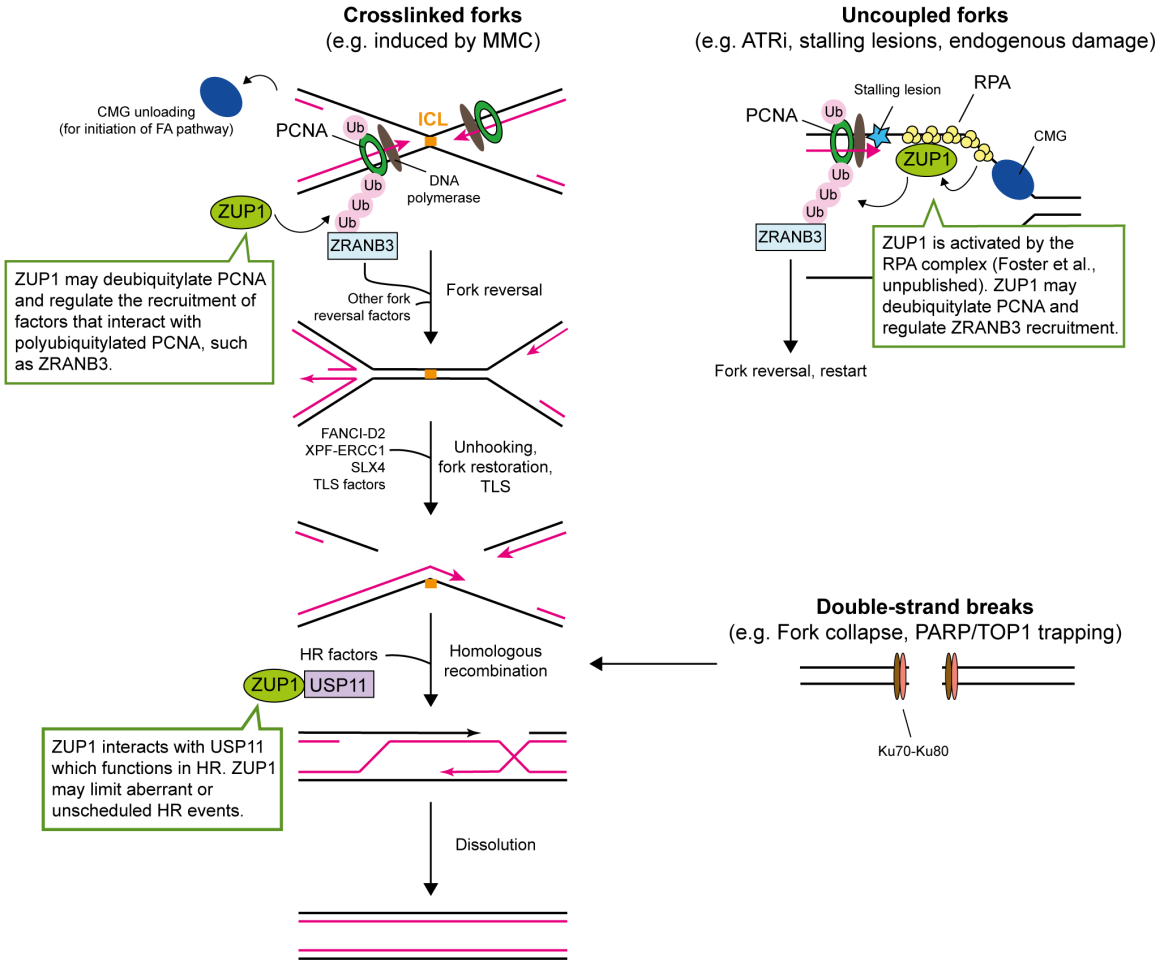



**Figure 6.1: Model for the potential role of ZUP1 in DNA repair.** ZUP1 may be involved in the indicated steps to repair crosslinked or uncoupled forks, or double-strand breaks, as described in the main text. The left panel was modified from Wu and Walter, 2019.

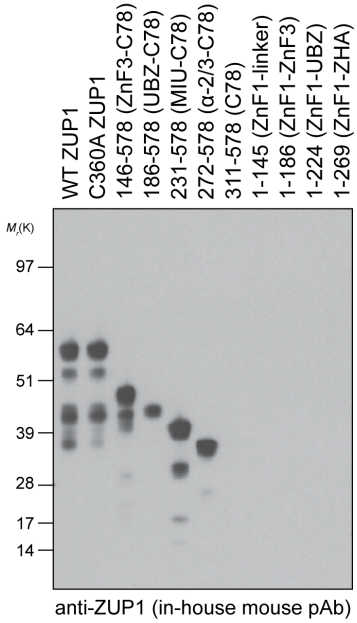
While this work has advanced our understanding of ZUP1 function in DNA repair, it will be important for the future studies to define the context in which ZUP1 deubiquitylates its substrates such as PCNA, and to identify other DNA repair factors or processes influenced by its function. From a broader perspective, the discovery of

key regulators in the DNA damage response such as ZUP1 is crucial to understand dysregulated pathways in cancer, chemoresistance mechanisms and/or potential therapeutic targets. This is particularly important for cancer types with underlying vulnerabilities in the DNA repair machinery. Overall, the work presented here merit further investigation into the function of ZUP1 in DNA repair, which may lead to the discovery of novel druggable targets for cancer therapy.

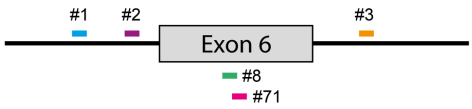
# Appendices

# Appendix A (Supplemental information to Chapter 3)

**1**

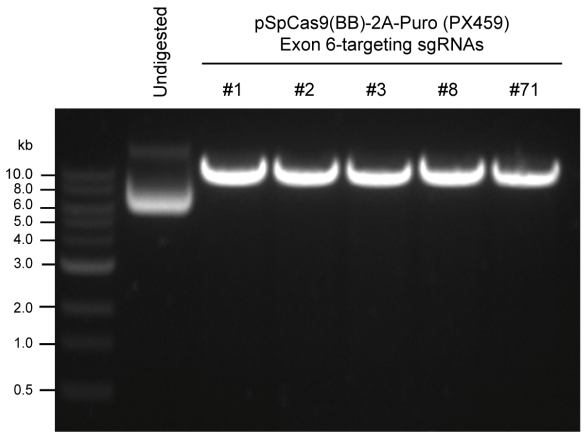


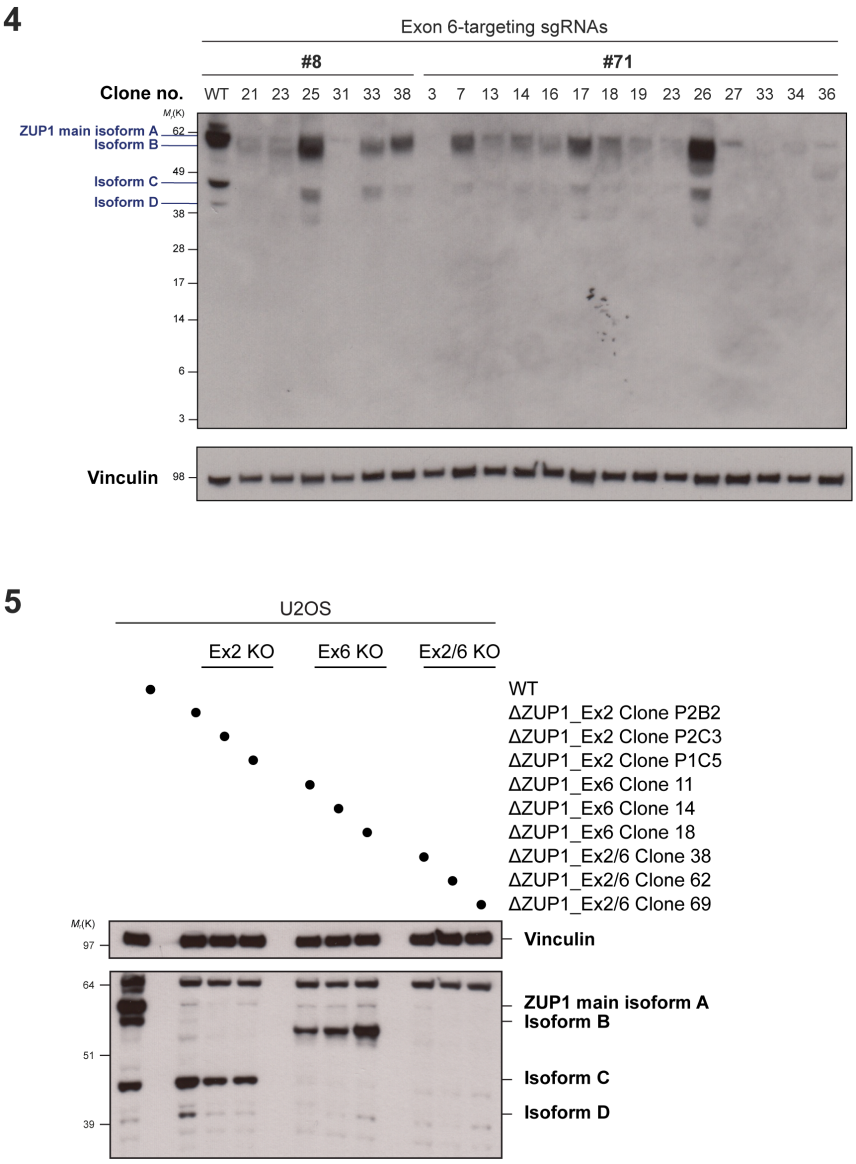

**2**




| sgRNA name (Exon 6-targeting) | Design tool | Scoring |
|---|---|---|
| **#1** | CRISPOR | MIT specificity score = 91<br>CFD. spec. score = 94 |
| **#2** | CRISPOR | MIT specificity score = 73<br>CFD. spec. score = 78 |
| **#3** | CRISPOR | MIT specificity score = 90<br>CFD. spec. score = 93 |
| **#8** | CHOPCHOP | Overall rank = 1<br>Efficiency = 40.98 |
| **#71** | CHOPCHOP | Overall rank = 22<br>Efficiency = 41.56 |

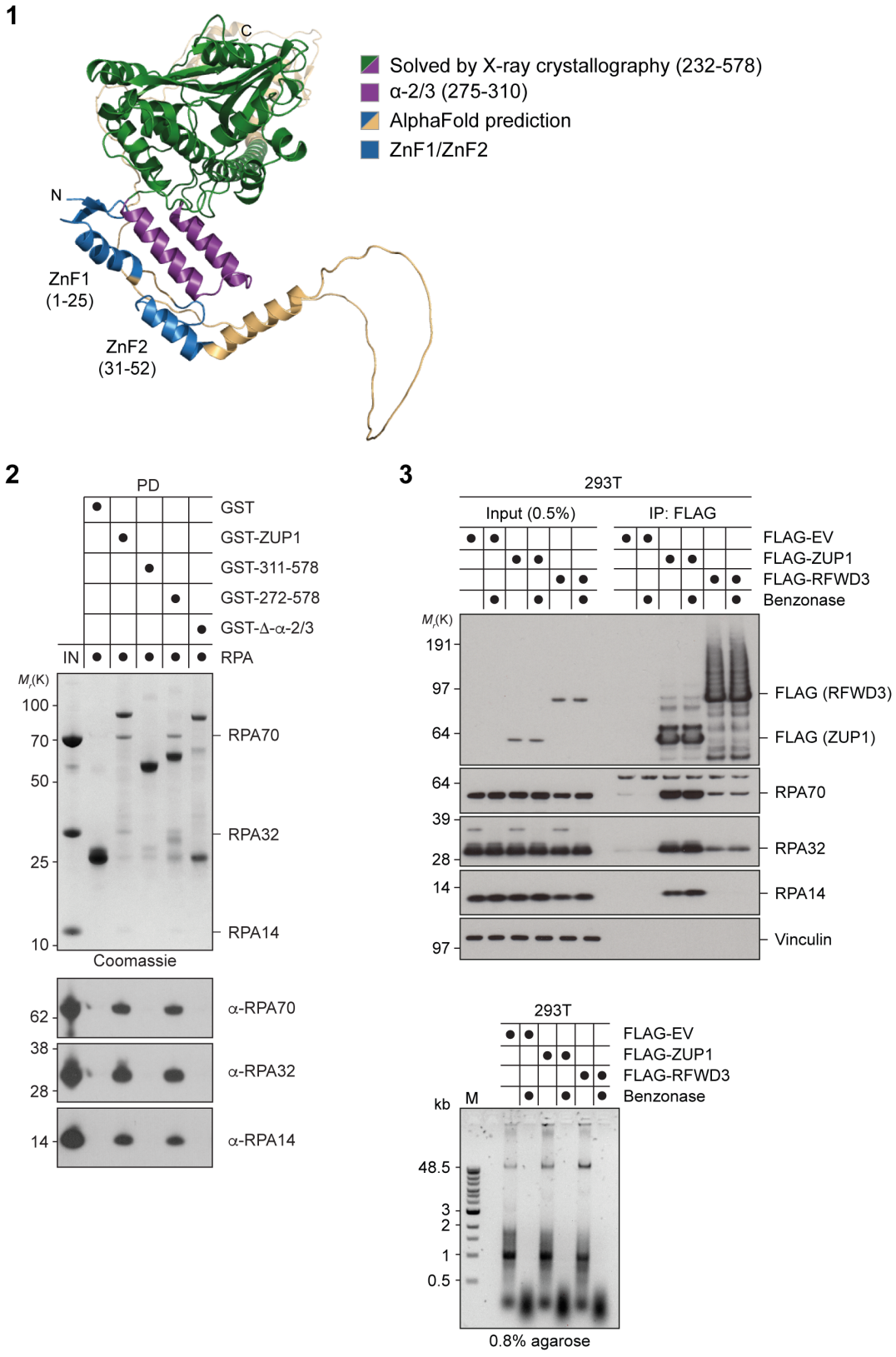
**3**

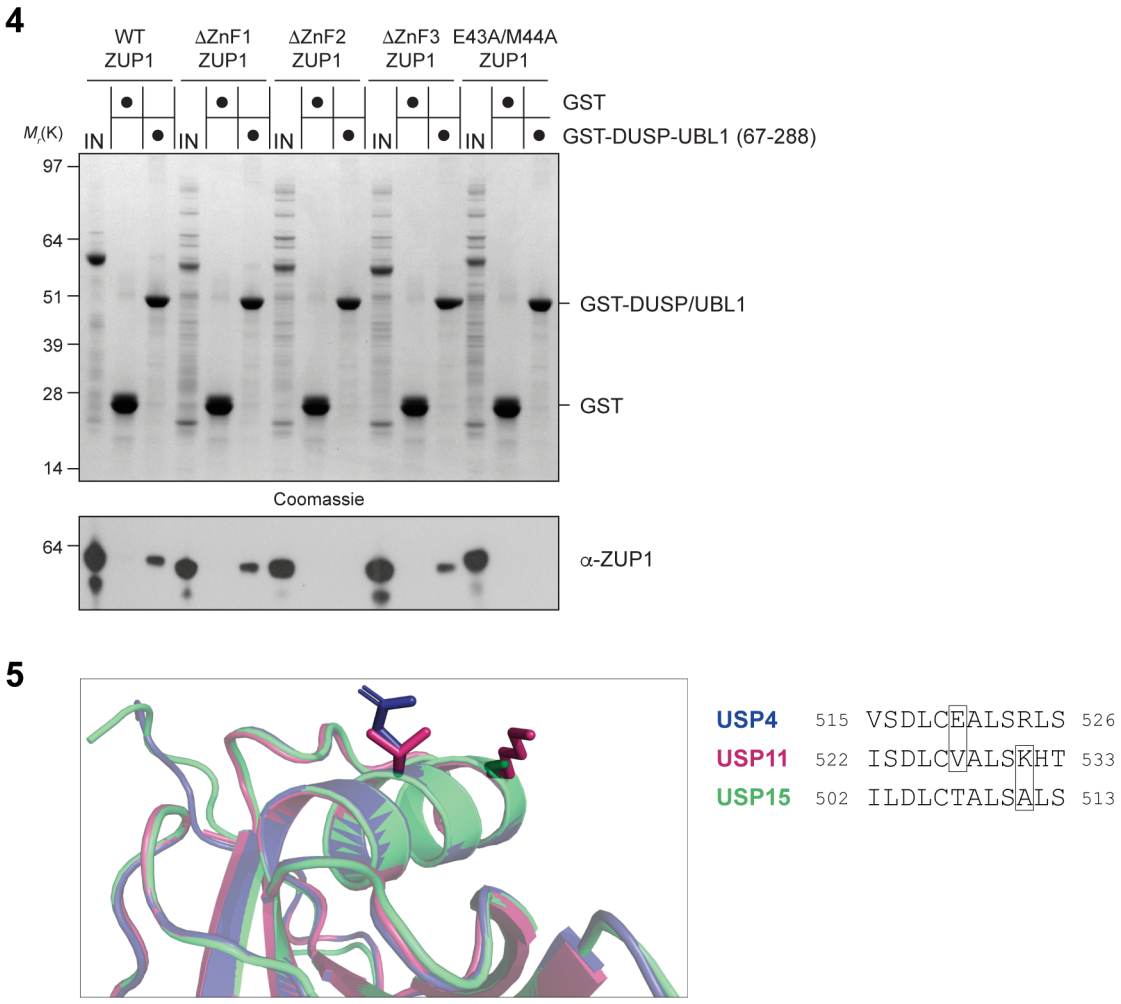





**Appendix A.** 1) Recognition of the indicated purified recombinant ZUP1 fragments by an in-house ZUP1 mouse polyclonal antibody generated against full length ZUP1 (Ben Foster, unpublished). 2) Design of exon 6-targeting sgRNAs using CRISPOR and CHOPCHOP. The approximate target sites of the sgRNAs are illustrated in the diagram. The sgRNA sequences are listed in Chapter 2. 3) Plasmid purification of the indicated cloned Cas9/sgRNA vectors. 4) Western blot analysis of 293T single cell-derived clones edited using the indicated single sgRNAs targeting exon 6. 5) Representative blot showing U2OS ZUP1 knockout clones generated using the indicated strategies (Ex2, Ex6 or Ex2/6) as described in the main text (Matt Drake, unpublished). ΔZUP1_Ex2 and ΔZUP1_Ex2/6 clones were used in the clonogenic assays presented in Fig. 3.8 and 3.9.

## Appendix B (Supplemental information to Chapter 4)



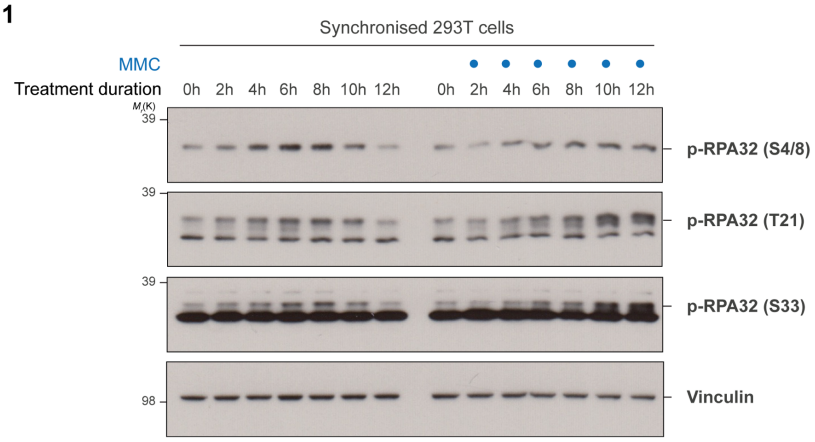



**Appendix B.** 1) AlphaFold prediction of ZUP1 structure showing the positioning of ZnF1 and ZnF2 relative to the regions solved by X-ray crystallography. For the structures predicted by AlphaFold, blue indicates confident predictions (90 > pLDDT > 70) while yellow represents low (70 > pLDDT > 50) or very low (pLDDT < 50) confidence predictions (Jumper et al., 2021). Figure was prepared in Pymol. 2) GST pull-down of GST or the indicated GST-tagged ZUP1 proteins with RPA (Ben Foster, unpublished). GST-ZUP1 indicates full-length ZUP1; GST-311-578 and GST-272-578 denote the remaining ZUP1 residues after truncation; GST-Δ-α-2/3 indicates the deletion of the α-2/3 region only (Δ275-310) within ZUP1. IN: input, PD: pull-down. 3) Top: Co-immunoprecipitation assay to assess RPA binding to FLAG-tagged ZUP1 or RFWD3 transiently expressed in 293T cells (Martin Attwood, unpublished). 1:500 benzonase and 2mM $MgCl_2$ were added to cell lysates in the indicated samples. Bottom: Verification of nucleic acid digestion in the benzonase-treated samples

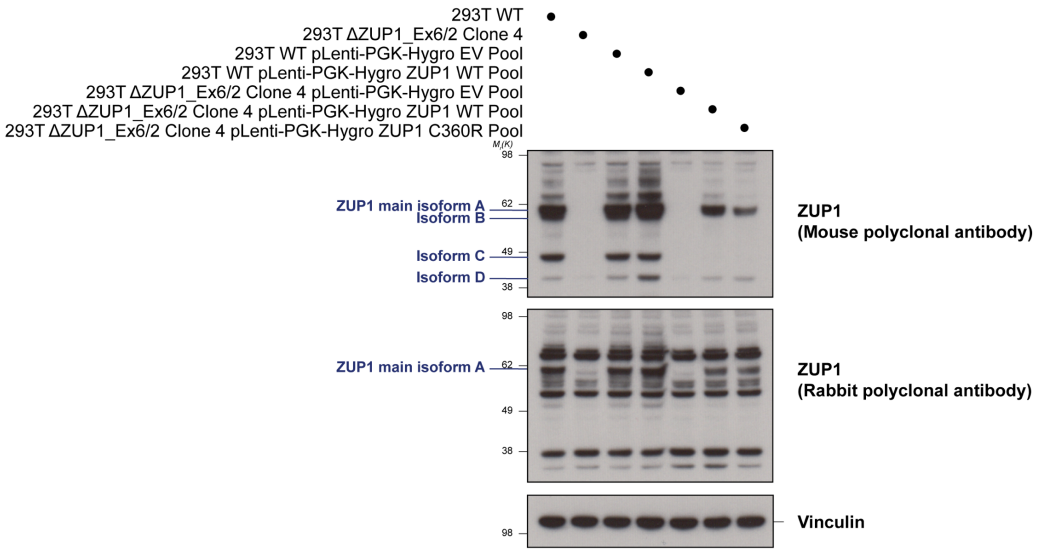
shown above by agarose gel electrophoresis (Martin Attwood, unpublished). 4) GST pull-down of GST or GST-tagged USP11 DUSP-UBL1 (67-288) with the indicated ZUP1 mutants (Ben Foster, unpublished). 5) Superimposition of UBL2 domain structures (AlphaFold predictions) of USP4, USP11 and USP15 showing the residue side chains with notable differences in their properties (Jumper et al., 2021). These superimposed residue side chains are indicated by the box in the sequence. Figure was prepared in Pymol.

# Appendix C (Supplemental information to Chapter 5)

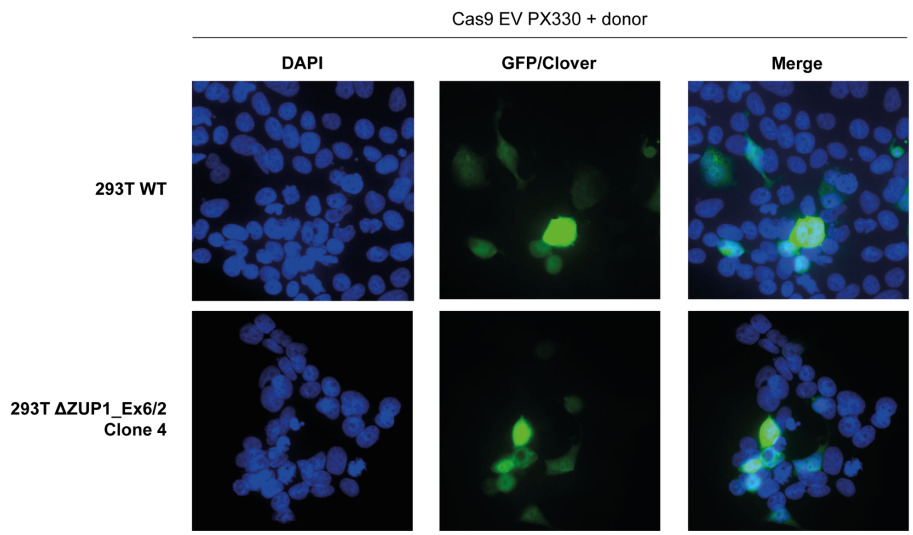
1



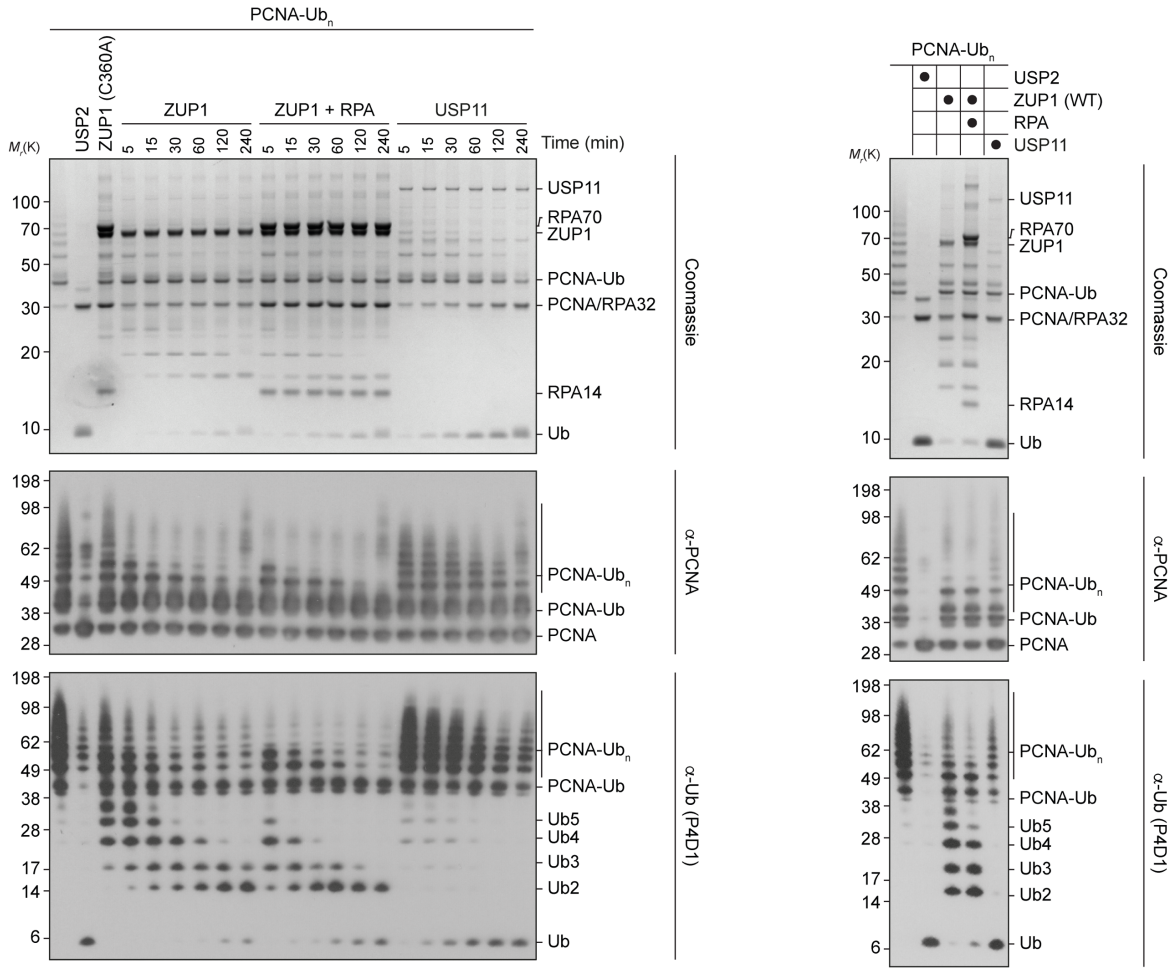

2



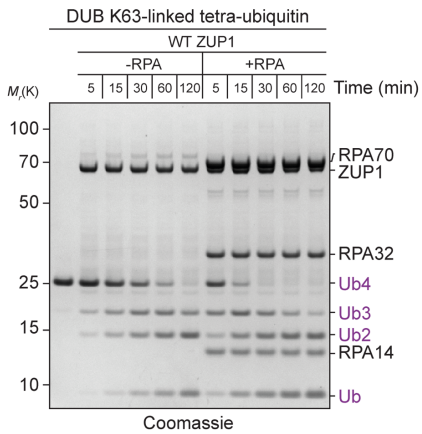

3



**4**


PCNA-Ub$_n$
USP2
ZUP1 (C360A)
ZUP1
ZUP1 + RPA
USP11
5 15 30 60 120 240
Time (min)
$M_r$(K)
100
70
50
30
20
10
USP11
RPA70
ZUP1
PCNA-Ub
PCNA/RPA32
RPA14
Ub
Coomassie
198
98
62
49
38
28
PCNA-Ub$_n$
PCNA-Ub
PCNA
α-PCNA
17
14
6
Ub5
Ub4
Ub3
Ub2
α-Ub (P4D1)
PCNA-Ub$_n$
USP2
ZUP1 (WT)
RPA
USP11

**5**


DUB K63-linked tetra-ubiquitin
WT ZUP1
-RPA
+RPA
5 15 30 60 120 5 15 30 60 120
Time (min)
$M_r$(K)
100
70
50
25
15
10
RPA70
ZUP1
RPA32
Ub4
Ub3
Ub2
RPA14
Ub
Coomassie

**Appendix C.** 1) Analysis of MMC induction of p-RPA32 at S4/8, T21 and S33 in 293T wild-type cells synchronised by double thymidine block. Upon release from the second thymidine treatment (0 h), the 0 h dishes were immediately washed and frozen overnight before Western blot analysis, while the other dishes were treated with 1 μM MMC or an equivalent volume of DMSO for the indicated durations prior to washing and freezing overnight, followed by Western blot analysis. 2) Pools of stable ZUP1-expressing cell lines generated by lentiviral transduction. 293T wild-type cells or ΔZUP1_Ex6/2 Clone 4 were transduced with ZUP1 WT or ZUP1 C360R cloned into the pLenti-PGK-Hygro vector, or the empty vector alone as a control, as described in the Methods. 3) Representative images of 293T wild-type and ΔZUP1_Ex6/2 Clone 4 cells co-transfected with the Cas9 EV PX330 and Clover homology repair template (donor) plasmids as the control for the LMNA HDR assay performed in Fig. 5.18. Some cells were found to express Clover despite the absence of a sgRNA target sequence for Cas9-mediated cleavage. 4) *In vitro* DUB assays performed using purified recombinant PCNA polyubiquitylated with K63-linked chains as the substrate (Ben Foster, unpublished). Left: Recombinant ZUP1 was incubated with polyubiquitylated PCNA (PCNA-$Ub_n$) for the indicated durations in min, in the absence or presence of RPA. USP2 was used as the positive control given that it is not linkage-selective. Right: Overnight incubation of PCNA-$Ub_n$ with the indicated DUBs. ZUP1 was incubated with polyubiquitylated PCNA in the absence or presence of RPA. 5) *In vitro* DUB assay time course where free K63-linked tetra-ubiquitin chains were incubated with recombinant WT ZUP1 in the presence or absence of RPA (Ben Foster, unpublished).

# References


Abdul Rehman, S.A., Kristariyanto, Y.A., Choi, S.Y., Nkosi, P.J., et al. (2016) MINDY-1 Is a Member of an Evolutionarily Conserved and Structurally Distinct New Family of Deubiquitinating Enzymes. Molecular Cell, 63(1), p. 146.

Ackerson, S.M., Romney, C., Schuck, P.L. and Stewart, J.A. (2021) To Join or Not to Join: Decision Points Along the Pathway to Double-Strand Break Repair vs. Chromosome End Protection. Frontiers in Cell and Developmental Biology, 9, p. 1830.

Adamson, B., Smogorzewska, A., Sigoillot, F.D., King, R.W. and Elledge, S.J. (2012) A genome-wide homologous recombination screen identifies the RNA-binding protein RBMX as a component of the DNA damage response. Nature Cell Biology, 14(3), p. 318.

Adikusuma, F., Piltz, S., Corbett, M.A., Turvey, M., et al. (2018) Large deletions induced by Cas9 cleavage. Nature, 2018 560:7717, 560(7717), pp. E8–E9.

Ahuja, A.K., Jodkowska, K., Teloni, F., Bizard, A.H., Zellweger, R., Herrador, R., Ortega, S., Hickson, I.D., Altmeyer, M., Mendez, J., Lopes, M. (2016) A short G1 phase imposes constitutive replication stress and fork remodelling in mouse embryonic stem cells. Nature Communications. 7:10660.

Akutsu, M., Kawasaki, M., Katoh, Y., Shiba, T., et al. (2005) Structural basis for recognition of ubiquitinated cargo by Tom1-GAT domain. FEBS Letters, 579(24), pp. 5385–5391.

Alam, S.L., Langelier, C., Whitby, F.G., Koirala, S., Robinson, H., Hill, C.P. and Sundquist, W.I. (2006) Structural basis for ubiquitin recognition by the human ESCRT-II EAP45 GLUE domain. Nature Structural & Molecular Biology, 2006 13:11, 13(11), pp. 1029–1030.

Alcón, P., Shakeel, S., Chen, Z.A., Rappsilber, J., Patel, K.J. and Passmore, L.A. (2020) FANCD2–FANCI is a clamp stabilized on DNA by monoubiquitination of FANCD2 during DNA repair. Nature Structural & Molecular Biology, 27(3), p. 240.

Alexander, J.L. and Orr-Weaver, T.L. (2016) Replication fork instability and the consequences of fork collisions from rereplication. Genes & Development, 30(20), p. 2241.

Altun, M., Kramer, H.B., Willems, L.I., McDermott, J.L., et al. (2011) Activity-Based Chemical Proteomics Accelerates Inhibitor Development for Deubiquitylating Enzymes. Chemistry & Biology, 18(11), pp. 1401–1412.

Amerik, A.Y. and Hochstrasser, M. (2004) Mechanism and function of deubiquitinating enzymes. Biochimica et Biophysica Acta (BBA) - Molecular Cell Research, 1695(1–3), pp. 189–207.

Amunugama, R., Willcox, S., Wu, R.A., Abdullah, U.B., et al. (2018) Replication Fork Reversal during DNA Interstrand Crosslink Repair Requires CMG Unloading. Cell Reports, 23(12), pp. 3419–3428.

Anand, R., Ranjha, L., Cannavo, E. and Cejka, P. (2016) Phosphorylated CtIP Functions as a Co-factor of the MRE11-RAD50-NBS1 Endonuclease in DNA End Resection. Molecular Cell, 64(5), pp. 940–950.

Aria, V. and Yeeles, J.T.P. (2019) Mechanism of Bidirectional Leading-Strand Synthesis Establishment at Eukaryotic DNA Replication Origins. Molecular Cell, 73(2), pp. 199-211.e10.

Ashley, A.K., Shrivastav, M., Nie, J., Amerin, C., et al. (2014) DNA-PK Phosphorylation of RPA32 Ser4/Ser8 Regulates Replication Stress Checkpoint Activation, Fork Restart, Homologous Recombination and Mitotic Catastrophe. DNA Repair, 21, p. 131.

Ashour, M.E. and Mosammaparast, N. (2021) Mechanisms of damage tolerance and repair during DNA replication. Nucleic Acids Research, 49(6), pp. 3033–3047.

Attali, I., Botchan, M.R. and Berger, J.M. (2021) Structural Mechanisms for Replicating DNA in Eukaryotes. Annual Review of Biochemistry, 2021 Jun 20;90:77-106.

Avvakumov, G. V., Walker, J.R., Xue, S., Allali-Hassani, A., et al. (2012) Two ZnF-UBP domains in isopeptidase T (USP5). Biochemistry, 51(6), p. 1188.

Balakrishnan, L. and Bambara, R.A. (2013) Okazaki Fragment Metabolism. Cold Spring Harbor Perspectives in Biology, 5(2), p. a010173.

Ball, L.G., Zhang, K., Cobb, J.A., Boone, C. and Xiao, W. (2009) The yeast Shu complex couples error-free post-replication repair to homologous recombination. Molecular Microbiology, 73(1), pp. 89–102.

Baranovskiy, A.G., Babayeva, N.D., Suwa, Y., Gu, J., Pavlov, Y.I. and Tahirov, T.H. (2014) Structural basis for inhibition of DNA replication by aphidicolin. Nucleic Acids Research, 42(22), p. 14013.

Barber, L.J., Youds, J.L., Ward, J.D., McIlwraith, M.J., et al. (2008) RTEL1 Maintains Genomic Stability by Suppressing Homologous Recombination. Cell, 135(2), pp. 261–271.

Basar, M.A., Beck, D.B. and Werner, A. (2020) Deubiquitylases in developmental ubiquitin signaling and congenital diseases. Cell Death & Differentiation 2020 28:2, 28(2), pp. 538–556.

Basic, M., Hertel, A., Bajdzienko, J., Bonn, F., et al. (2021) The deubiquitinase USP11 is a versatile and conserved regulator of autophagy. Journal of Biological Chemistry, 297(5), p. 101263.

Bass, T.E., Luzwick, J.W., Kavanaugh, G., Carroll, C., et al. (2016) ETAA1 acts at stalled replication forks to maintain genome integrity. Nature Cell Biology, 18(11), p. 1185.

Békés, M., van der Heden van Noort, G.J., Ekkebus, R., Ovaa, H., Huang, T.T. and Lima, C.D. (2016) Recognition of Lys48-Linked Di-ubiquitin and Deubiquitinating Activities of the SARS Coronavirus Papain-like Protease. Molecular Cell, 62(4), p. 572.

Bellare, P., Kutach, A.K., Rines, A.K., Guthrie, C. and Sontheimer, E.J. (2006) Ubiquitin binding by a variant Jab1/MPN domain in the essential pre-mRNA splicing factor Prp8p. RNA, 12(2), p. 292.

Berti, M., Chaudhuri, A.R., Thangavel, S., Gomathinayagam, S., et al. (2013) Human RECQ1 promotes restart of replication forks reversed by DNA topoisomerase I inhibition. Nature Structural & Molecular Biology, 20(3), p. 347.

Berti, M. and Vindigni, A. (2016) Replication stress: getting back on track. Nature Structural & Molecular Biology, 23(2), p. 103.

Berti, M., Cortez, D. and Lopes, M. (2020) The plasticity of DNA replication forks in response to clinically relevant genotoxic stress. Nature Reviews Molecular Cell Biology 2020 21:10, 21(10), pp. 633–651.

Bétous, R., Mason, A.C., Rambo, R.P., Bansbach, C.E., et al. (2012) SMARCAL1 catalyzes fork regression and Holliday junction migration to maintain genome stability during DNA replication. Genes & Development, 26(2), p. 151.

Bétous, R., Couch, F.B., Mason, A.C., Eichman, B.F., Manosas, M. and Cortez, D. (2013) Substrate-selective repair and restart of replication forks by DNA translocases. Cell Reports, 3(6), p. 1958.

Biau, J., Chautard, E., Verrelle, P. and Dutreix, M. (2019) Altering DNA repair to improve radiation therapy: Specific and multiple pathway targeting. Frontiers in Oncology, 9(SEP), p. 1009.

Bienko, M., Green, C.M., Crosetto, N., Rudolf, F., et al. (2005) Biochemistry: Ubiquitin-binding domains in Y-family polymerases regulate translesion synthesis. Science, 310(5755), pp. 1821–1824.

Bizanek, R., Tomasz, M., McGuinness, B.F. and Nakanishi, K. (1992) Isolation and Structure of an Intrastrand Cross-Link Adduct of Mitomycin C and DNA. Biochemistry, 31(12), pp. 3084–3091.

Blow, J.J. and Dutta, A. (2005) Preventing re-replication of chromosomal DNA. Nature Reviews Molecular Cell Biology, 6(6), p. 476.

Blum, M., Chang, H.Y., Chuguransky, S., Grego, T., et al. (2021) The InterPro protein families and domains database: 20 years on. Nucleic Acids Research, 49(D1), pp. D344–D354.

Boehm, E.M., Gildenberg, M.S. and Washington, M.T. (2016) The many roles of PCNA in eukaryotic DNA replication. The Enzymes, 39, p. 231.

Bomar, M.G., Pai, M.T., Tzeng, S.R., Li, S.S.C. and Zhou, P. (2007) Structure of the ubiquitin-binding zinc finger domain of human DNA Y-polymerase η. EMBO Reports, 8(3), pp. 247–251.

Bomar, M.G., D'Souza, S., Bienko, M., Dikic, I., Walker, G.C. and Zhou, P. (2010) Unconventional Ubiquitin Recognition by the Ubiquitin-Binding Motif within the Y-Family DNA Polymerases ι and Rev1. Molecular Cell, 37(3), p. 408.

Boroviak, K., Fu, B., Yang, F., Doe, B. and Bradley, A. (2017) Revealing hidden complexities of genomic rearrangements generated with Cas9. Scientific Reports 2017 7:1, 7(1), pp. 1–8.

Boutros, M. and Ahringer, J. (2008) The art and design of genetic screens: RNA interference. Nature Reviews Genetics 2008 9:7, 9(7), pp. 554–566.

Bowry, A., Kelly, R.D.W., Petermann, E. (2021) Hypertranscription and replication stress in cancer. Trends in Cancer, 7(9):863-877.

Boyault, C., Gilquin, B., Zhang, Y., Rybin, V., et al. (2006) HDAC6–p97/VCP controlled polyubiquitin chain turnover. The EMBO Journal, 25(14), p. 3357.

Branzei, D., Vanoli, F. and Foiani, M. (2008) SUMOylation regulates Rad18-mediated template switch. Nature 2008 456:7224, 456(7224), pp. 915–920.

Branzei, D. and Psakhye, I. (2016a) DNA damage tolerance. Current Opinion in Cell Biology, 40, pp. 137–144.

Branzei, D. and Szakal, B. (2016b) DNA damage tolerance by recombination: Molecular pathways and DNA structures. DNA Repair, 44, p. 68.

Braten, O., Livneh, I., Ziv, T., Admon, A., et al. (2016) Numerous proteins with unique characteristics are degraded by the 26S proteasome following monoubiquitination. Proceedings of the National Academy of Sciences of the United States of America, 113(32), pp. E4639–E4647.

Brayer, K.J. and Segal, D.J. (2008) Keep your fingers off my DNA: Protein-protein interactions mediated by C2H2 zinc finger domains. Cell Biochemistry and Biophysics, 50(3), pp. 111–131.

Broomfield, S., Chow, B.L. and Xiao, W. (1998) MMS 2, encoding a ubiquitin-conjugating-enzyme-like protein, is a member of the yeast error-free postreplication repair pathway. Proceedings of the National Academy of Sciences of the United States of America, 95(10), pp. 5678–5683.

Brun, J., Chiu, R., Lockhart, K., Xiao, W., Wouters, B.G. and Gray, D.A. (2008) hMMS2 serves a redundant role in human PCNA polyubiquitination. BMC Molecular Biology, 9(1), pp. 1–11.

Brzovic, P.S., Lissounov, A., Christensen, D.E., Hoyt, D.W. and Klevit, R.E. (2006) A UbcH5/Ubiquitin Noncovalent Complex Is Required for Processive BRCA1-Directed Ubiquitination. Molecular Cell, 21(6), pp. 873–880.

Burgers, P.M.J. and Kunkel, T.A. (2017) Eukaryotic DNA Replication Fork. Eukaryotic DNA Replication Fork. Annual Review of Biochemistry, 2017 Jun 20; 86:417-438.

Burkovics, P., Dome, L., Juhasz, S., Altmannova, V., et al. (2016) The PCNA-associated protein PARI negatively regulates homologous recombination via the inhibition of DNA repair synthesis. Nucleic Acids Research, 44(7), p. 3176.

Burnett, B., Li, F. and Pittman, R.N. (2003) The polyglutamine neurodegenerative protein ataxin-3 binds polyubiquitylated proteins and has ubiquitin protease activity. Human Molecular Genetics, 12(23), pp. 3195–3205.

Canny, M.D., Moatti, N., Wan, L.C.K., Fradet-Turcotte, A., et al. (2018) Inhibition of 53BP1 favors homology-dependent DNA repair and increases CRISPR-Cas9 genome-editing efficiency. Nature Biotechnology, 36(1), p. 95.

Cassandri, M., Smirnov, A., Novelli, F., Pitolli, C., et al. (2017) Zinc-finger proteins in health and disease. Cell Death Discovery 2017 3:1, 3(1), pp. 1–12.

Chaganti, R.S.K., Schonberg, S. and German, J. (1974) A Manyfold Increase in Sister Chromatid Exchanges in Bloom's Syndrome Lymphocytes. Proceedings of the National Academy of Sciences, 71(11), pp. 4508–4512.

Chaudhuri, R.A. and Nussenzweig, A. (2017) The multifaceted roles of PARP1 in DNA repair and chromatin remodelling. Nature Reviews Molecular Cell Biology. 18(10), pp. 610–621.

Chen D., Frezza M., Schmitt S., Kanwar J., Dou Q.P. (2011) Bortezomib as the first proteasome inhibitor anticancer drug: current status and future perspectives. Current Cancer Drug Targets. 11(3):239-53.

Chilkova, O., Stenlund, P., Isoz, I., Stith, C.M., et al. (2007) The eukaryotic leading and lagging strand DNA polymerases are loaded onto primer-ends via separate mechanisms but have comparable processivity in the presence of PCNA. Nucleic Acids Research, 35(19), p. 6588.

Ciccia, A., Bredemeyer, A.L., Sowa, M.E., Terret, M.E., Jallepalli, P. V., Harper, J.W. and Elledge, S.J. (2009) The SIOD disorder protein SMARCAL1 is an RPA-interacting protein involved in replication fork restart. Genes & Development, 23(20), p. 2415.

Ciccia, A., Nimonkar, A. V., Hu, Y., Hajdu, I., et al. (2012) Polyubiquitinated PCNA Recruits the ZRANB3 Translocase to Maintain Genomic Integrity after Replication Stress. Molecular Cell, 47(3), pp. 396–409.

Clague, M.J., Urbé, S. and Komander, D. (2019) Breaking the chains: deubiquitylating enzyme specificity begets function. Nature Reviews Molecular Cell Biology 2019 20:6, 20(6), pp. 338–352.

Cohn, M.A., Kowal, P., Yang, K., Haas, W., Huang, T.T., Gygi, S.P. and D'Andrea, A.D. (2007) A UAF1-Containing Multisubunit Protein Complex Regulates the Fanconi Anemia Pathway. Molecular Cell, 28(5), pp. 786–797.

Concordet, J.P. and Haeussler, M. (2018) CRISPOR: intuitive guide selection for CRISPR/Cas9 genome editing experiments and screens. Nucleic Acids Research, 46(W1), pp. W242–W245.

Cong, K., Peng, M., Kousholt, A.N., Lee, W.T.C., et al. (2021) Replication gaps are a key determinant of PARP inhibitor synthetic lethality with BRCA deficiency. Molecular Cell, 81(15), pp. 3128-3144.e7.

Cooper, E.M., Cutcliffe, C., Kristiansen, T.Z., Pandey, A., Pickart, C.M. and Cohen, R.E. (2009) K63-specific deubiquitination by two JAMM/MPN+ complexes: BRISC-associated Brcc36 and proteasomal Poh1. The EMBO Journal, 28(6), p. 621.

Cortez, D. (2019) Replication-coupled DNA Repair. Molecular Cell, 74(5), p. 866.

Costa, A., Ilves, I., Tamberg, N., Petojevic, T., Nogales, E., Botchan, M.R. and Berger, J.M. (2011) The structural basis for MCM2–7 helicase activation by GINS and Cdc45. Nature Structural & Molecular Biology 2011 18:4, 18(4), pp. 471–477.

Craggs, T.D., Hutton, R.D., Brenlla, A., White, M.F. and Penedo, J.C. (2014) Single-molecule characterization of Fen1 and Fen1/PCNA complexes acting on flap substrates. Nucleic Acids Research, 42(3), p. 1857.

Cullot, G., Boutin, J., Toutain, J., Prat, F., et al. (2019) CRISPR-Cas9 genome editing induces megabase-scale chromosomal truncations. Nature Communications 2019 10:1, 10(1), pp. 1–14.

D'Arcy P, Wang X, Linder S. (2015) Deubiquitinase inhibition as a cancer therapeutic strategy. Pharmacology & Therapeutics. 147:32-54.

Daigaku, Y., Etheridge, T.J., Nakazawa, Y., Nakayama, M., et al. (2017) PCNA ubiquitylation ensures timely completion of unperturbed DNA replication in fission yeast. PLOS Genetics, 13(5), p. e1006789.

Damgaard, R.B. (2021) The ubiquitin system: from cell signalling to disease biology and new therapeutic opportunities. Cell Death & Differentiation 2021 28:2, 28(2), pp. 423–426.

Davies, A.A., Huttner, D., Daigaku, Y., Chen, S. and Ulrich, H.D. (2008) Activation of Ubiquitin-Dependent DNA Damage Bypass Is Mediated by Replication Protein A. Molecular Cell, 29(5), pp. 625–636.

Davies B.W., Kohanski M.A., Simmons L.A., Winkler J.A., Collins J.J., Walker G.C. (2009) Hydroxyurea induces hydroxyl radical-mediated cell death in Escherichia coli. Molecular Cell. 36(5):845-60.

De March, M., Merino, N., Barrera-Vilarmau, S., Crehuet, R., Onesti, S., Blanco, F.J. and De Biasio, A. (2017) Structural basis of human PCNA sliding on DNA. Nature Communications 2017 8:1, 8(1), pp. 1–7.

de Moura, T.R., Mozaffari-Jovin, S., Szabó, C.Z.K., Schmitzová, J., et al. (2018) Prp19/Pso4 Is an Autoinhibited Ubiquitin Ligase Activated by Stepwise Assembly of Three Splicing Factors. Molecular Cell, 69(6), pp. 979-992.e6.

Deane, J.E., Ryan, D.P., Sunde, M., Maher, M.J., Guss, J.M., Visvader, J.E. and Matthews, J.M. (2004) Tandem LIM domains provide synergistic binding in the LMO4:Ldb1 complex. The EMBO Journal, 23(18), p. 3589.

Deans, A.J. and West, S.C. (2011) DNA interstrand crosslink repair and cancer. Nature Reviews Cancer 2011 11:7, 11(7), pp. 467–480.

DeCaprio, J. and Kohl, T.O. (2020) Denaturing Lysis of Cells for Immunoprecipitation. Cold Spring Harbor Protocols, 2020(2): pdb.prot098616.

Deegan, T.D. and Diffley, J.F.X. (2016) MCM: one ring to rule them all. Current Opinion in Structural Biology, 37, pp. 145–151.

Dempster, J.M., Rossen, J., Kazachkova, M., Pan, J., Kugener, G., Root, D.E. and Tsherniak, A. (2019) Extracting Biological Insights from the Project Achilles Genome-Scale CRISPR Screens in Cancer Cell Lines. bioRxiv, p. 720243.

Dewar, J.M., Budzowska, M. and Walter, J.C. (2015) The mechanism of DNA replication termination in vertebrates. Nature, 525(7569), p. 345.

Dewar, J.M. and Walter, J.C. (2017) Mechanisms of DNA replication termination. Nature Reviews Molecular Cell Biology, 2017 18:8, 18(8), pp. 507–516.

Dikic, I., Wakatsuki, S. and Walters, K.J. (2009) Ubiquitin-binding domains — from structures to functions. Nature Reviews Molecular Cell Biology 2009 10:10, 10(10), pp. 659–671.

Douglas, M.E., Ali, F.A., Costa, A. and Diffley, J.F.X. (2018) The mechanism of eukaryotic CMG helicase activation. Nature 2018 555:7695, 555(7695), pp. 265–268.

Dubois, J.C., Yates, M., Gaudreau-Lapierre, A., Clément, G., et al. (2017) A phosphorylation-and-ubiquitylation circuitry driving ATR activation and homologous recombination. Nucleic Acids Research, 45(15), p. 8859.

Dueva, R. and Iliakis, G. (2020) Replication protein A: a multifunctional protein with roles in DNA replication, repair and beyond. NAR Cancer, 2(3).

Dupont, S., Mamidi, A., Cordenonsi, M., Montagner, M., et al. (2009) FAM/USP9x, a Deubiquitinating Enzyme Essential for TGFβ Signaling, Controls Smad4 Monoubiquitination. Cell, 136(1), pp. 123–135.

Ekkebus, R., Van Kasteren, S.I., Kulathu, Y., Scholten, A., et al. (2013) On terminal alkynes that can react with active-site cysteine nucleophiles in proteases. Journal of the American Chemical Society, 135(8), pp. 2867–2870.

Elango, R., Sheng, Z., Jackson, J., Decata, J., et al. (2017) Break-induced replication promotes formation of lethal joint molecules dissolved by Srs2. Nature Communications 2017 8:1, 8(1), pp. 1–13.

Elia, A.E.H., Wang, D.C., Willis, N.A., Boardman, A.P., et al. (2015) RFWD3-Dependent Ubiquitination of RPA Regulates Repair at Stalled Replication Forks. Molecular Cell, 60(2), p. 280.

Elu, N., Osinalde, N., Ramirez, J., Presa, N., Rodriguez, J.A., Prieto, G. and Mayor, U. (2022) Identification of substrates for human deubiquitinating enzymes (DUBs): An up-to-date review and a case study for neurodevelopmental disorders. Seminars in Cell and Developmental Biology, 2022 Jan 15:S1084-9521(22)00003-9.

Emmerich, C.H. and Cohen, P. (2015) Optimising methods for the preservation, capture and identification of ubiquitin chains and ubiquitylated proteins by immunoblotting. Biochemical and Biophysical Research Communications, 466(1), pp. 1–14.

Ensminger, M. and Löbrich, M. (2020) one end to rule them all: Non-homologous end-joining and homologous recombination at DNA double-strand breaks. British Journal of Radiology, 93(1115).

Evrin, C., Clarke, P., Zech, J., Lurz, R., et al. (2009) A double-hexameric MCM2-7 complex is loaded onto origin DNA during licensing of eukaryotic DNA replication. Proceedings of the National Academy of Sciences of the United States of America, 106(48), pp. 20240–20245.

Faesen, A.C., Dirac, A.M.G., Shanmugham, A., Ovaa, H., Perrakis, A. and Sixma, T.K. (2011) Mechanism of USP7/HAUSP activation by its C-Terminal ubiquitin-like domain and allosteric regulation by GMP-synthetase. Molecular Cell, 44(1), pp. 147–159.

Faesen, A.C., Luna-Vargas, M.P.A. and Sixma, T.K. (2012) The role of UBL domains in ubiquitin-specific proteases. Biochemical Society Transactions, 40(3), pp. 539–545.

Feeney, L., Muñoz, I.M., Lachaud, C., Toth, R., Appleton, P.L., Schindler, D. and Rouse, J. (2017) RPA-Mediated Recruitment of the E3 Ligase RFWD3 Is Vital for Interstrand Crosslink Repair and Human Health. Molecular Cell, 66(5), pp. 610-621.e4.

Fernandez, E.M., Díaz-Ceso, M.D. and Vilar, M. (2015) Brain Expressed and X-Linked (Bex) Proteins Are Intrinsically Disordered Proteins (IDPs) and Form New Signaling Hubs. Plos One, 10(1), p. e0117206.

Finley, D., Bartel, B. and Varshavsky, A. (1989) The tails of ubiquitin precursors are ribosomal proteins whose fusion to ubiquitin facilitates ribosome biogenesis. Nature 1989 338:6214, 338(6214), pp. 394–401.

Foote, K.M., Nissink, J.W.M., McGuire, T., Turner, P., et al. (2018) Discovery and Characterization of AZD6738, a Potent Inhibitor of Ataxia Telangiectasia Mutated and Rad3 Related (ATR) Kinase with Application as an Anticancer Agent. Journal of Medicinal Chemistry, 61(22), pp. 9889–9907.

Fox, A.H., Liew, C., Holmes, M., Kowalski, K., Mackay, J. and Crossley, M. (1999) Transcriptional cofactors of the FOG family interact with GATA proteins by means of multiple zinc fingers. The EMBO Journal, 18(10), pp. 2812–2822.

Franken, N.A.P., Rodermond, H.M., Stap, J., Haveman, J. and van Bree, C. (2006) Clonogenic assay of cells in vitro. Nature Protocols 2006 1:5, 1(5), pp. 2315–2319.

French, M.E., Koehler, C.F. and Hunter, T. (2021) Emerging functions of branched ubiquitin chains. Cell Discovery 2021 7:1, 7(1), pp. 1–10.

Fu, Q.S., Zhou, C.J., Gao, H.C., Jiang, Y.J., et al. (2009) Structural Basis for Ubiquitin Recognition by a Novel Domain from Human Phospholipase A2-activating Protein. The Journal of Biological Chemistry, 284(28), p. 19043.

Fu, Y., Foden, J.A., Khayter, C., Maeder, M.L., Reyon, D., Joung, J.K. and Sander, J.D. (2013) High-frequency off-target mutagenesis induced by CRISPR-Cas nucleases in human cells. Nature Biotechnology 2013 31:9, 31(9), pp. 822–826.

Fuentes-Iglesias, A., Garcia-Outeiral, V., Pardavila, J.A., Wang, J., Fidalgo, M. and Guallar, D. (2020) An Optimized Immunoprecipitation Protocol for Assessing Protein-RNA Interactions In Vitro. STAR Protocols, 1(2), p. 100093.

Gaillard, H., García-Muse, T. and Aguilera, A. (2015) Replication stress and cancer. Nature Reviews Cancer 2015 15:5, 15(5), pp. 276–289.

Gallina, I., Hendriks, I.A., Hoffmann, S., Larsen, N.B., et al. (2021) The ubiquitin ligase RFWD3 is required for translesion DNA synthesis. Molecular Cell, 81(3), pp. 442-458.e9.

Gambus, A. (2017) Termination of eukaryotic replication forks. Advances in Experimental Medicine and Biology, 1042, pp. 163–187.

Gambus, A., Jones, R.C., Sanchez-Diaz, A., Kanemaki, M., van Deursen, F., Edmondson, R.D. and Labib, K. (2006) GINS maintains association of Cdc45 with MCM in replisome progression complexes at eukaryotic DNA replication forks. Nature Cell Biology 2006 8:4, 8(4), pp. 358–366.

Gan, W., Guan, Z., Liu, J., Gui, T., Shen, K., Manley, J.L. and Li, X. (2011) R-loop-mediated genomic instability is caused by impairment of replication fork progression. Genes & Development, 25(19), p. 2041.

Ganai, R.A. and Johansson, E. (2016) DNA Replication—A Matter of Fidelity. Molecular Cell, 62(5), pp. 745–755.

García-Muse, T. and Aguilera, A. (2016) Transcription–replication conflicts: how they occur and how they are resolved. Nature Reviews Molecular Cell Biology 2016 17:9, 17(9), pp. 553–563.

Garg, P. and Burgers, P.M. (2005) Ubiquitinated proliferating cell nuclear antigen activates translesion DNA polymerases η and REV1. Proceedings of the National Academy of Sciences of the United States of America, 102(51), p. 18361.

Garg, P., Stith, C.M., Sabouri, N., Johansson, E. and Burgers, P.M. (2004) Idling by DNA polymerase δ maintains a ligatable nick during lagging-strand DNA replication. Genes & Development, 18(22), p. 2764.

Ge, X.Q. and Blow, J.J. (2010) Chk1 inhibits replication factory activation but allows dormant origin firing in existing factories. The Journal of Cell Biology, 191(7), p. 1285.

Georges, A., Marcon, E., Greenblatt, J. and Frappier, L. (2018) Identification and Characterization of USP7 Targets in Cancer Cells. Scientific Reports 2018 8:1, 8(1), pp. 1–12.

Giannattasio, M., Zwicky, K., Follonier, C., Foiani, M., Lopes, M. and Branzei, D. (2014) Visualization of recombination-mediated damage bypass by template switching. Nature Structural & Molecular Biology 2014 21:10, 21(10), pp. 884–892.

Gilljam, K.M., Feyzi, E., Aas, P.A., Sousa, M.M.L., et al. (2009) Identification of a novel, widespread, and functionally important PCNA-binding motif. The Journal of Cell Biology, 186(5), p. 645.

Girard, J.R., Tenthorey, J.L. and Morgan, D.O. (2015) An E2 accessory domain increases affinity for the anaphasepromoting complex and ensures E2 competition. Journal of Biological Chemistry, 290(40), pp. 24614–24625.

Godin, S.K., Sullivan, M.R. and Bernstein, K.A. (2016) Novel insights into RAD51 activity and regulation during homologous recombination and DNA replication. Biochemistry and Cell Biology, 94(5), p. 407.

Grice, G.L., Lobb, I.T., Weekes, M.P., Gygi, S.P., Antrobus, R. and Nathan, J.A. (2015) The Proteasome Distinguishes between Heterotypic and Homotypic Lysine-11-Linked Polyubiquitin Chains. Cell Reports, 12(4), pp. 545–553.

Guilliam, T.A., Jozwiakowski, S.K., Ehlinger, A., Barnes, R.P., et al. (2015) Human PrimPol is a highly error-prone polymerase regulated by single-stranded DNA binding proteins. Nucleic Acids Research, 43(2), p. 1056.

Guilliam, T.A., Brissett, N.C., Ehlinger, A., Keen, B.A., et al. (2017) Molecular basis for PrimPol recruitment to replication forks by RPA. Nature Communications 2017 8:1, 8(1), pp. 1–14.

Guilliam, T.A. and Yeeles, J.T.P. (2020) An updated perspective on the polymerase division of labor during eukaryotic DNA replication. Critical Reviews in Biochemistry and Molecular Biology. 2020 Oct;55(5):469-481.

Guilliam, T.A. (2021) Mechanisms for Maintaining Eukaryotic Replisome Progression in the Presence of DNA Damage. Frontiers in Molecular Biosciences, 8:712971, p. 658.

Guo, C., Tang, T.-S., Bienko, M., Parker, J.L., et al. (2006) Ubiquitin-Binding Motifs in REV1 Protein Are Required for Its Role in the Tolerance of DNA Damage. Molecular and Cellular Biology, 26(23), p. 8892.

Haahr, P., Hoffmann, S., Tollenaere, M.A., Ho, T., Toledo, L.I., Mann, M., Bekker-Jensen, S., Räschle, M., Mailand, N. (2016) Activation of the ATR kinase by the RPA-binding protein ETAA1. Nature Cell Biology, 18(11):1196-1207.

Haahr, P., Borgermann, N., Guo, X., Typas, D., et al. (2018) ZUFSP Deubiquitylates K63-Linked Polyubiquitin Chains to Promote Genome Stability. Molecular Cell, 70(1), pp. 165-174.e6.

Hall, T.M.T. (2005) Multiple modes of RNA recognition by zinc finger proteins. Current Opinion in Structural Biology, 15(3), pp. 367–373.

Hanzlikova, H., Kalasova, I., Demin, A.A., Pennicott, L.E., Cihlarova, Z. and Caldecott, K.W. (2018) The Importance of Poly(ADP-Ribose) Polymerase as a Sensor of Unligated Okazaki Fragments during DNA Replication. Molecular Cell, 71(2), pp. 319-331.e3.

Haracska, L., Unk, I., Johnson, R.E., Phillips, B.B., Hurwitz, J., Prakash, L. and Prakash, S. (2002) Stimulation of DNA Synthesis Activity of Human DNA Polymerase κ by PCNA. Molecular and Cellular Biology, 22(3), p. 784.

Harper, S., Gratton, H.E., Cornaciu, I., Oberer, M., Scott, D.J., Emsley, J. and Dreveny, I. (2014) Structure and Catalytic Regulatory Function of Ubiquitin Specific Protease 11 N-Terminal and Ubiquitin-like Domains. Biochemistry, 53(18), p. 2966.

Hashimoto, Y., Puddu, F. and Costanzo, V. (2012) RAD51 and MRE11 dependent reassembly of uncoupled CMG helicase complex at collapsed replication forks. Nature Structural & Molecular Biology, 19(1), p. 17.

Hashimoto, S., Anai, H. and Hanada, K. (2016) Mechanisms of interstrand DNA crosslink repair and human disorders. Genes and Environment, 38(1), pp. 1–8.

He, Y., Hicke, L. and Radhakrishnan, I. (2007) Structural Basis for Ubiquitin Recognition by SH3 Domains. Journal of Molecular Biology, 373(1), p. 190.

He, J., Zhu, Q., Wani, G., Sharma, N., et al. (2014) Ubiquitin-specific Protease 7 Regulates Nucleotide Excision Repair through Deubiquitinating XPC Protein and Preventing XPC Protein from Undergoing Ultraviolet Light-induced and VCP/p97 Protein-regulated Proteolysis. Journal of Biological Chemistry, 289(39), pp. 27278–27289.

He, F., Wollscheid, H.P., Nowicka, U., Biancospino, M., et al. (2016) Myosin VI contains a compact structural motif that binds to ubiquitin chains. Cell Reports, 14(11), p. 2683.

Hein, M.Y., Hubner, N.C., Poser, I., Cox, J., et al. (2015) A Human Interactome in Three Quantitative Dimensions Organized by Stoichiometries and Abundances. Cell, 163(3), pp. 712–723.

Heller, R.C., Kang, S., Lam, W.M., Chen, S., Chan, C.S. and Bell, S.P. (2011) Eukaryotic Origin-Dependent DNA Replication In Vitro Reveals Sequential Action of DDK and S-CDK Kinases. Cell, 146(1), pp. 80–91.

Helmrich, A., Ballarino, M. and Tora, L. (2011) Collisions between Replication and Transcription Complexes Cause Common Fragile Site Instability at the Longest Human Genes. Molecular Cell, 44(6), pp. 966–977.

Hendel, A., Krijger, P.H.L., Diamant, N., Goren, Z., et al. (2011) PCNA Ubiquitination Is Important, But Not Essential for Translesion DNA Synthesis in Mammalian Cells. PLoS Genetics, 7(9).

Herhaus, L. and Dikic, I. (2015) Expanding the ubiquitin code through post-translational modification. EMBO reports, 16(9), pp. 1071–1083.

Herhaus, L., van den Bedem, H., Tang, S., Maslennikov, I., Wakatsuki, S., Dikic, I. and Rahighi, S. (2019) Molecular Recognition of M1-Linked Ubiquitin Chains by Native and Phosphorylated UBAN Domains. Journal of Molecular Biology, 431(17), pp. 3146–3156.

Hermanns, T., Pichlo, C., Woiwode, I., Klopffleisch, K., et al. (2018) A family of unconventional deubiquitinases with modular chain specificity determinants. Nature Communications 2018 9:1, 9(1), pp. 1–13.

Hewings, D.S., Heideker, J., Ma, T.P., Ahyoung, A.P., et al. (2018) Reactive-site-centric chemoproteomics identifies a distinct class of deubiquitinase enzymes. Nature Communications 2018 9:1, 9(1), pp. 1–17.

Hirano, S., Kawasaki, M., Ura, H., Kato, R., Raiborg, C., Stenmark, H. and Wakatsuki, S. (2006) Double-sided ubiquitin binding of Hrs-UIM in endosomal protein sorting. Nature Structural & Molecular Biology 2006 13:3, 13(3), pp. 272–277.

Hjerpe, R., Aillet, F., Lopitz-Otsoa, F., Lang, V., England, P. and Rodriguez, M.S. (2009) Efficient protection and isolation of ubiquitylated proteins using tandem ubiquitin-binding entities. EMBO Reports, 10(11), p. 1250.

Hochstrasser, M. (2009) Origin and function of ubiquitin-like proteins. Nature 2009 458:7237, 458(7237), pp. 422–429.

Hoege, C., Pfander, B., Moldovan, G.L., Pyrowolakis, G. and Jentsch, S. (2002) RAD6-dependent DNA repair is linked to modification of PCNA by ubiquitin and SUMO. Nature 2002 419:6903, 419(6903), pp. 135–141.

Hogg, M., Osterman, P., Bylund, G.O., Ganai, R.A., Lundström, E.B., Sauer-Eriksson, A.E. and Johansson, E. (2013) Structural basis for processive DNA synthesis by yeast DNA polymerase ε. Nature Structural & Molecular Biology 2013 21:1, 21(1), pp. 49–55.

Hong, Y.H., Ahn, H.C., Lim, J., Kim, H.M., et al. (2009) Identification of a novel ubiquitin binding site of STAM1 VHS domain by NMR spectroscopy. FEBS Letters, 583(2), pp. 287–292.

Hospenthal, M.K., Mevissen, T.E.T. and Komander, D. (2015) Deubiquitinase–based analysis of ubiquitin chain architecture using Ubiquitin Chain Restriction (UbiCRest). Nature Protocols, 10(2), p. 349.

Hsiau, T., Conant, D., Rossi, N., Maures, T., et al. (2019) Inference of CRISPR Edits from Sanger Trace Data. bioRxiv, p. 251082.

Hu, M., Li, P., Li, M., Li, W., et al. (2002) Crystal Structure of a UBP-Family Deubiquitinating Enzyme in Isolation and in Complex with Ubiquitin Aldehyde. Cell, 111(7), pp. 1041–1054.

Huang, T.T., Nijman, S.M.B., Mirchandani, K.D., Galardy, P.J., et al. (2006) Regulation of monoubiquitinated PCNA by DUB autocleavage. Nature Cell Biology, 2006 8:4, 8(4), pp. 341–347.

Huang, T.P., Newby, G.A. and Liu, D.R. (2021) Precision genome editing using cytosine and adenine base editors in mammalian cells. Nature Protocols, 2021 16:2, 16(2), pp. 1089–1128.

Hurley, J.H., Lee, S. and Prag, G. (2006) Ubiquitin-binding domains. Biochemical Journal, 399(3), pp. 361–372.

Husnjak, K., Elsasser, S., Zhang, N., Chen, X., et al. (2008) Proteasome subunit Rpn13 is a novel ubiquitin receptor. Nature, 2008 453:7194, 453(7194), pp. 481–488.

Husnjak, K. and Dikic, I. (2012) Ubiquitin-Binding Proteins: Decoders of Ubiquitin-Mediated Cellular Functions. Annual Review of Biochemistry, 2012;81:291-322.

Inano, S., Sato, K., Katsuki, Y., Kobayashi, W., et al. (2017) RFWD3-Mediated Ubiquitination Promotes Timely Removal of Both RPA and RAD51 from DNA Damage Sites to Facilitate Homologous Recombination. Molecular Cell, 66(5), pp. 622-634.e8.

Iyer, V.N and Szybalski, W. (1963) A Molecular Mechanism of Mitomycin Action: Linking of Complementary DNA Strands. Proceedings of the National Academy of Sciences of the United States of America, 50(2), pp. 355–362.

Jones, M.J.K., Colnaghi, L. and Huang, T.T. (2012) Dysregulation of DNA polymerase κ recruitment to replication forks results in genomic instability. The EMBO Journal, 31(4), pp. 908–918.

Jumper, J., Evans, R., Pritzel, A., Green, T., et al. (2021) Highly accurate protein structure prediction with AlphaFold. Nature 2021 596:7873, 596(7873), pp. 583–589.

Kang, R.S., Daniels, C.M., Francis, S.A., Shih, S.C., Salerno, W.J., Hicke, L. and Radhakrishnan, I. (2003) Solution Structure of a CUE-Ubiquitin Complex Reveals a Conserved Mode of Ubiquitin Binding. Cell, 113(5), pp. 621–630.

Kang, Y., Chen, X., Lary, J.W., Cole, J.L. and Walters, K.J. (2007) Defining how Ubiquitin Receptors hHR23a and S5a Bind Polyubiquitin. Journal of Molecular Biology, 369(1), pp. 168–176.

Kang, M.S., Ryu, E., Lee, S.W., Park, J., et al. (2019) Regulation of PCNA cycling on replicating DNA by RFC and RFC-like complexes. Nature Communications, 2019 10:1, 10(1), pp. 1–16.

Kannouche, P.L., Wing, J. and Lehmann, A.R. (2004) Interaction of Human DNA Polymerase η with Monoubiquitinated PCNA: A Possible Mechanism for the Polymerase Switch in Response to DNA Damage. Molecular Cell, 14(4), pp. 491–500.

Kao, S.H., Wang, W.L., Chen, C.Y., Chang, Y.L., Wu, Y.Y., Wang, Y.T., Wang, S.P., Nesvizhskii, A.I., Chen, Y.J., Hong, T.M., Yang, P.C.. Analysis of Protein Stability by the Cycloheximide Chase Assay. Bio Protocol, 2015 Jan 5;5(1):e1374.

Kashiwaba, S. ichiro, Kanao, R., Masuda, Y., Kusumoto-Matsuo, R., Hanaoka, F. and Masutani, C. (2015) USP7 Is a Suppressor of PCNA Ubiquitination and Oxidative-Stress-Induced Mutagenesis in Human Cells. Cell Reports, 13(10), pp. 2072–2080.

Kawasaki, M., Shiba, T., Shiba, Y., Yamaguchi, Y., et al. (2005) Molecular mechanism of ubiquitin recognition by GGA3 GAT domain. Genes to Cells, 10(7), pp. 639–654.

Kelch, B.A., Makino, D.L., O'Donnell, M. and Kuriyan, J. (2011) How a DNA polymerase clamp loader opens a sliding clamp. Science (New York, N.Y.), 334(6063), p. 1675.

Keusekotten, K., Elliott, P.R., Glockner, L., Fiil, B.K., et al. (2013) OTULIN Antagonizes LUBAC Signaling by Specifically Hydrolyzing Met1-Linked Polyubiquitin. Cell, 153(6), p. 1312.

Kile, A.C., Chavez, D.A., Bacal, J., Eldirany, S., et al. (2015) HLTF's Ancient HIRAN Domain Binds 3′-DNA Ends to Drive Replication Fork Reversal. Molecular Cell, 58(6), p. 1090.

Klein Douwel, D., Boonen, R.A.C.M., Long, D.T., Szypowska, A.A., Räschle, M., Walter, J.C. and Knipscheer, P. (2014) XPF-ERCC1 Acts in Unhooking DNA Interstrand Crosslinks in Cooperation with FANCD2 and FANCP/SLX4. Molecular Cell, 54(3), pp. 460–471.

Kliza, K. and Husnjak, K. (2020) Resolving the Complexity of Ubiquitin Networks. Frontiers in Molecular Biosciences, 2020 Feb 27;7:21.

Kluska, K., Adamczyk, J. and Krężel, A. (2018) Metal binding properties, stability and reactivity of zinc fingers. Coordination Chemistry Reviews, 367, pp. 18–64.

Komander, D., Clague, M.J. and Urbé, S. (2009) Breaking the chains: Structure and function of the deubiquitinases. Nature Reviews Molecular Cell Biology. Nature Publishing Group, pp. 550–563.

Komander, D. and Rape, M. (2012) The Ubiquitin Code. Annual Review of Biochemistry, 2012;81:203-29.

Kosicki, M., Tomberg, K. and Bradley, A. (2018) Repair of double-strand breaks induced by CRISPR-Cas9 leads to large deletions and complex rearrangements. Nature Biotechnology, 36(8), p. 765.

Krakoff IH, Brown NC, Reichard P. Inhibition of ribonucleoside diphosphate reductase by hydroxyurea. Cancer Research. 1968 Aug;28(8):1559-65.

Kramara, J., Osia, B. and Malkova, A. (2018) Break-Induced Replication: The Where, The Why, and The How. Trends in Genetics, 34(7), pp. 518–531.

Krijger, P.H.L., Lee, K.Y., Wit, N., van den Berk, P.C.M., et al. (2011) HLTF and SHPRH are not essential for PCNA polyubiquitination, survival and somatic hypermutation: Existence of an alternative E3 ligase. DNA Repair, 10(4), pp. 438–444.

Kristariyanto, Y.A., Abdul Rehman, S.A., Campbell, D.G., Morrice, N.A., Johnson, C., Toth, R. and Kulathu, Y. (2015) K29-Selective Ubiquitin Binding Domain Reveals Structural Basis of Specificity and Heterotypic Nature of K29 Polyubiquitin. Molecular Cell, 58(1), p. 83.

Kristariyanto, Y.A., Rehman, S.A.A., Weidlich, S., Knebel, A. and Kulathu, Y. (2017) A single MIU motif of MINDY-1 recognizes K48-linked polyubiquitin chains. EMBO Reports, 18(3), p. 392.

Kubota, T., Nishimura, K., Kanemaki, M.T. and Donaldson, A.D. (2013) The Elg1 Replication Factor C-like Complex Functions in PCNA Unloading during DNA Replication. Molecular Cell, 50(2), pp. 273–280.

Kühbacher, U. and Duxin, J.P. (2020) How to fix DNA-protein crosslinks. DNA Repair, 94, p. 102924.

Kulathu, Y. and Komander, D. (2012) Atypical ubiquitylation — the unexplored world of polyubiquitin beyond Lys48 and Lys63 linkages. Nature Reviews Molecular Cell Biology 2012 13:8, 13(8), pp. 508–523.

Kumagai, A., Lee, J., Yoo, H.Y. and Dunphy, W.G. (2006) TopBP1 Activates the ATR-ATRIP Complex. Cell, 124(5), pp. 943–955.

Kumari, N., Lee, K.K. and Jha, S. (2018) Targeting the Ubiquitin Proteasome System in Cancer. Neoplasm, IntechOpen, London. 10.5772/intechopen.76705.

Kunkel, T.A. and Burgers, P.M. (2008) Dividing the workload at a eukaryotic replication fork. Trends in Cell Biology, 18(11), pp. 521–527.

Kwasna, D., Abdul Rehman, S.A., Natarajan, J., Matthews, S., et al. (2018) Discovery and Characterization of ZUFSP/ZUP1, a Distinct Deubiquitinase Class Important for Genome Stability. Molecular Cell, 70(1), pp. 150-164.e6.

Labun, K., Montague, T.G., Krause, M., Torres Cleuren, Y.N., Tjeldnes, H. and Valen, E. (2019) CHOPCHOP v3: expanding the CRISPR web toolbox beyond genome editing. Nucleic Acids Research, 47(W1), pp. W171–W174.

Lalonde, S., Stone, O.A., Lessard, S., Lavertu, A., et al. (2017) Frameshift indels introduced by genome editing can lead to in-frame exon skipping. PLoS ONE, 12(6).

Lange, S.M., Armstrong, L.A. and Kulathu, Y. (2022) Deubiquitinases: From mechanisms to their inhibition by small molecules. Molecular Cell, 82(1), pp. 15–29.

Langston, L.D., Zhang, D., Yurieva, O., Georgescu, R.E., et al. (2014) CMG helicase and DNA polymerase ε form a functional 15-subunit holoenzyme for eukaryotic leading-strand DNA replication. Proceedings of the National Academy of Sciences of the United States of America, 111(43), pp. 15390–15395.

Lans, H., Hoeijmakers, J.H.J., Vermeulen, W. and Marteijn, J.A. (2019) The DNA damage response to transcription stress. Nature Reviews Molecular Cell Biology 2019 20:12, 20(12), pp. 766–784.

Lee, J.H. and Paull, T.T. (2005) ATM activation by DNA double-strand breaks through the Mre11-Rad50-Nbs1 complex. Science, 308(5721), pp. 551–554.

Lee, S., Tsai, Y.C., Mattera, R., Smith, W.J., et al. (2006) Structural basis for ubiquitin recognition and autoubiquitination by Rabex-5. Nature Structural & Molecular Biology 2006 13:3, 13(3), pp. 264–271.

Lee, K.Y., Yang, K., Cohn, M.A., Sikdar, N., D'Andrea, A.D. and Myung, K. (2010) Human ELG1 Regulates the Level of Ubiquitinated Proliferating Cell Nuclear Antigen (PCNA) through Its Interactions with PCNA and USP1. The Journal of Biological Chemistry, 285(14), p. 10362.

Lee, K.Y., Fu, H., Aladjem, M.I. and Myung, K. (2013) ATAD5 regulates the lifespan of DNA replication factories by modulating PCNA level on the chromatin. The Journal of Cell Biology, 200(1), p. 31.

Lemonidis, K., Arkinson, C., Rennie, M.L. and Walden, H. (2022) Mechanism, specificity, and function of FANCD2-FANCI ubiquitination and deubiquitination. The FEBS Journal, 289(16), pp. 4811–4829.

León-Ortiz, A.M., Svendsen, J. and Boulton, S.J. (2014) Metabolism of DNA secondary structures at the eukaryotic replication fork. DNA Repair, 19, pp. 152–162.

Leung, W., Baxley, R.M., Moldovan, G.L. and Bielinsky, A.K. (2019) Mechanisms of DNA Damage Tolerance: Post-Translational Regulation of PCNA. Genes, 10(1).

Licchesi, J.D.F., Mieszczanek, J., Mevissen, T.E.T., Rutherford, T.J., et al. (2011) An Ankyrin-repeat ubiquitin binding domain determines TRABID's specificity for atypical ubiquitin chains. Nature Structural & Molecular Biology, 19(1), p. 62.

Lim, K.S., Li, H., Roberts, E.A., Gaudiano, E.F., et al. (2018) USP1 Is Required for Replication Fork Protection in BRCA1-Deficient Tumors. Molecular Cell, 72(6), pp. 925-941.e4.

Lin, Y.C., Boone, M., Meuris, L., Lemmens, I., et al. (2014) Genome dynamics of the human embryonic kidney 293 lineage in response to cell biology manipulations. Nature Communications 2014 5:1, 5(1), pp. 1–12.

Liu, L.F., Desai, S.D., Li, T.K., Mao, Y., Sun, M. and Sim, S.P. (2000) Mechanism of Action of Camptothecin. Annals of the New York Academy of Sciences, 922(1), pp. 1–10.

Liu, Z., Gong, Z., Jiang, W.X., Yang, J., et al. (2015) Lys63-linked ubiquitin chain adopts multiple conformational states for specific target recognition. eLife, 4(June 2015), pp. 1–19.

Lord, C.J. and Ashworth, A. (2017) PARP inhibitors: Synthetic lethality in the clinic. Science, 355(6330), pp. 1152 LP – 1158.

Lovett, S.T. (2017) Template-switching during replication fork repair in bacteria. DNA repair, 56, p. 118.

Lukomska, A., Kim, J., Rheaume, B.A., Xing, J,. Hoyt, A., Lecky, E., Steidl, T., Trakhtenberg, E.F. Developmentally upregulated transcriptional elongation factor a like 3 suppresses axon regeneration after optic nerve injury. Neuroscience Letters. 2021 Nov 20;765:136260.

Maertens, G.N., El Messaoudi-Aubert, S., Elderkin, S., Hiom, K. and Peters, G. (2010) Ubiquitin-specific proteases 7 and 11 modulate Polycomb regulation of the INK4a tumour suppressor. The EMBO Journal, 29(15), pp. 2553–2565.

Mailand, N., Gibbs-Seymour, I. and Bekker-Jensen, S. (2013) Regulation of PCNA–protein interactions for genome stability. Nature Reviews Molecular Cell Biology 2013 14:5, 14(5), pp. 269–282.

Makino, H., Tajiri, T., Miyashita, M., Sasajima, K., Anbazhagan, R., Johnston, J. and Gabrielson, E. (2005) Differential expression of TCEAL1 in esophageal cancers by custom cDNA microarray analysis. Diseases of the Esophagus, 18(1), pp. 37–40.

Makridakis, N.M. and Reichardt, J.K.V. (2012) Translesion DNA polymerases and cancer. Frontiers in Genetics, 3(SEP), p. 174.

Malacaria, E., Pugliese, G.M., Honda, M., Marabitti, V., et al. (2019) Rad52 prevents excessive replication fork reversal and protects from nascent strand degradation. Nature Communications, 10(1).

Mao, Z., Bozzella, M., Seluanov, A. and Gorbunova, V. (2008) DNA repair by nonhomologous end joining and homologous recombination during cell cycle in human cells. 7(18), pp. 2902–2906.

Maréchal, A. and Zou, L. (2015) RPA-coated single-stranded DNA as a platform for post-translational modifications in the DNA damage response. Cell Research, 25(1), p. 9.

Maréchal, A., Li, J.M., Ji, X.Y., Wu, C.S., et al. (2014) PRP19 Transforms into a Sensor of RPA-ssDNA after DNA Damage and Drives ATR Activation via a Ubiquitin-Mediated Circuitry. Molecular Cell, 53(2), p. 235.

Maric, M., Maculins, T., De Piccoli, G. and Labib, K. (2014) Cdc48 and a ubiquitin ligase drive disassembly of the CMG helicase at the end of DNA replication. Science (New York, N.Y.), 346(6208), p. 1253596.

Masuda, Y., Mitsuyuki, S., Kanao, R., Hishiki, A., Hashimoto, H. and Masutani, C. (2018) Regulation of HLTF-mediated PCNA polyubiquitination by RFC and PCNA monoubiquitination levels determines choice of damage tolerance pathway. Nucleic Acids Research, 46(21), p. 11340.

Mattera, R., Yien, C.T., Weissman, A.M. and Bonifacino, J.S. (2006) The Rab5 Guanine Nucleotide Exchange Factor Rabex-5 Binds Ubiquitin (Ub) and Functions as a Ub Ligase through an Atypical Ub-interacting Motif and a Zinc Finger Domain. Journal of Biological Chemistry, 281(10), pp. 6874–6883.

Maya-Mendoza, A., Moudry, P., Merchut-Maya, J.M., Lee, M., Strauss, R. and Bartek, J. (2018) High speed of fork progression induces DNA replication stress and genomic instability. Nature 2018 559:7713, 559(7713), pp. 279–284.

Metzger, M.B., Hristova, V.A. and Weissman, A.M. (2012) HECT and RING finger families of E3 ubiquitin ligases at a glance. Journal of Cell Science, 125(3), pp. 531–537.

Mevissen, T.E.T. and Komander, D. (2017) Mechanisms of Deubiquitinase Specificity and Regulation. Annual Review of Biochemistry, 2017 Jun 20;86:159-192.

Meyer, H., Bug, M. and Bremer, S. (2012) Emerging functions of the VCP/p97 AAA-ATPase in the ubiquitin system. Nature Cell Biology 2012 14:2, 14(2), pp. 117–123.

Meyer, H.J. and Rape, M. (2014) Enhanced Protein Degradation by Branched Ubiquitin Chains. Cell, 157(4), pp. 910–921.

Mirsanaye, A.S., Typas, D. and Mailand, N. (2021) Ubiquitylation at Stressed Replication Forks: Mechanisms and Functions. Trends in Cell Biology, 31(7), pp. 584–597.

Moldovan, G.L., Dejsuphong, D., Petalcorin, M.I.R., Hofmann, K., Takeda, S., Boulton, S.J. and D'Andrea, A.D. (2012) Inhibition of homologous recombination by the PCNA-interacting protein PARI. Molecular Cell, 45(1), p. 75.

Moreno, S.P., Bailey, R., Campion, N., Herron, S. and Gambus, A. (2014) Polyubiquitylation drives replisome disassembly at the termination of DNA replication. Science, 346(6208), pp. 477–481.

Moreno S.P., Jones R.M., Poovathumkadavil D., Scaramuzza S., Gambus A. (2019) Mitotic replisome disassembly depends on TRAIP ubiquitin ligase activity. Life Science Alliance. 2(2):e201900390.

Morgan, M.T., Haj-Yahya, M., Ringel, A.E., Bandi, P., Brik, A. and Wolberger, C. (2016) Structural basis for histone H2B deubiquitination by the SAGA DUB module. Science (New York, N.Y.), 351(6274), p. 725.

Motegi, A., Sood, R., Moinova, H., Markowitz, S.D., Liu, P.P. and Myung, K. (2006) Human SHPRH suppresses genomic instability through proliferating cell nuclear antigen polyubiquitination. The Journal of Cell Biology, 175(5), p. 703.

Mou, H., Smith, J.L., Peng, L., Yin, H., et al. (2017) CRISPR/Cas9-mediated genome editing induces exon skipping by alternative splicing or exon deletion. Genome Biology, 18(1), pp. 1–8.

Mourón, S., Rodriguez-Acebes, S., Martínez-Jiménez, M.I., García-Gómez, S., Chocrón, S., Blanco, L. and Méndez, J. (2013) Repriming of DNA synthesis at stalled replication forks by human PrimPol. Nature Structural & Molecular Biology 2013 20:12, 20(12), pp. 1383–1389.

Murai, J., Huang, S.Y.N., Das, B.B., Renaud, A., et al. (2012) Trapping of PARP1 and PARP2 by clinical PARP inhibitors. Cancer Research, 72(21), pp. 5588–5599.

Murai, J., Huang, S.-Y.N., Renaud, A., Zhang, Y., et al. (2014) Stereospecific PARP Trapping by BMN 673 and Comparison with Olaparib and Rucaparib. Molecular Cancer Therapeutics, 13(2), pp. 433–443.

Najafabadi, H.S., Mnaimneh, S., Schmitges, F.W., Garton, M., et al. (2015) C2H2 zinc finger proteins greatly expand the human regulatory lexicon. Nature Biotechnology 2015 33:5, 33(5), pp. 555–562.

Nakabeppu, Y. (2014) Cellular Levels of 8-Oxoguanine in either DNA or the Nucleotide Pool Play Pivotal Roles in Carcinogenesis and Survival of Cancer Cells. International Journal of Molecular Sciences 2014, Vol. 15, Pages 12543-12557, 15(7), pp. 12543–12557.

Nakayasu, E.S., Sydor, M.A., Brown, R.N., Sontag, R.L., et al. (2015) Identification of salmonella typhimurium deubiquitinase ssel substrates by immunoaffinity enrichment and quantitative proteomic analysis. Journal of Proteome Research, 14(9), pp. 4029–4038.

Nathan, J.A., Tae Kim, H., Ting, L., Gygi, S.P. and Goldberg, A.L. (2013) Why do cellular proteins linked to K63-polyubiquitin chains not associate with proteasomes?. The EMBO Journal, 32(4), p. 552.

Navas-Pérez, E., Vicente-García, C., Mirra, S., Burguera, D., et al. (2020) Characterization of an eutherian gene cluster generated after transposon domestication identifies Bex3 as relevant for advanced neurological functions. Genome Biology 2020 21:1, 21(1), pp. 1–27.

Niimi, A., Brown, S., Sabbioneda, S., Kannouche, P.L., et al. (2008) Regulation of proliferating cell nuclear antigen ubiquitination in mammalian cells. Proceedings of the National Academy of Sciences of the United States of America, 105(42), pp. 16125–16130.

Nijman, S.M.B., Huang, T.T., Dirac, A.M.G., Brummelkamp, T.R., Kerkhoven, R.M., D'Andrea, A.D. and Bernards, R. (2005) The Deubiquitinating Enzyme USP1 Regulates the Fanconi Anemia Pathway. Molecular Cell, 17(3), pp. 331–339.

Nishi, R., Wijnhoven, P., Le Sage, C., Tjeertes, J., et al. (2014) Systematic characterization of deubiquitylating enzymes for roles in maintaining genome integrity. Nature Cell Biology 2014 16:10, 16(10), pp. 1016–1026.

Oestergaard, V.H., Langevin, F., Kuiken, H.J., Pace, P., et al. (2007) Deubiquitination of FANCD2 Is Required for DNA Crosslink Repair. Molecular Cell, 28(5), p. 798.

Oh, E., Mark, K.G., Mocciaro, A., Watson, E.R., et al. (2020) Gene expression and cell identity controlled by anaphase-promoting complex. Nature 2020 579:7797, 579(7797), pp. 136–140.

Ohtake, F., Saeki, Y., Ishido, S., Kanno, J. and Tanaka, K. (2016) The K48-K63 Branched Ubiquitin Chain Regulates NF-κB Signaling. Molecular Cell, 64(2), pp. 251–266.

Ohtake, F., Tsuchiya, H., Saeki, Y. and Tanaka, K. (2018) K63 ubiquitylation triggers proteasomal degradation by seeding branched ubiquitin chains. Proceedings of the National Academy of Sciences of the United States of America, 115(7), pp. E1401–E1408.

Orthwein, A., Noordermeer, S.M., Wilson, M.D., Landry, S., et al. (2015) A mechanism for the suppression of homologous recombination in G1 cells. Nature 2015 528:7582, 528(7582), pp. 422–426.

Özkaynak, E., Finley, D. and Varshavsky, A. (1984) The yeast ubiquitin gene: head-to-tail repeats encoding a polyubiquitin precursor protein. Nature 1984 312:5995, 312(5995), pp. 663–666.

Pai, C.C. and Kearsey, S.E. (2017) A Critical Balance: dNTPs and the Maintenance of Genome Stability. Genes 2017; Vol. 8, Page 57, 8(2), p. 57.

Painter, R.B. (1980) A replication model for sister-chromatid exchange. Mutation Research/Fundamental and Molecular Mechanisms of Mutagenesis, 70(3), pp. 337–341.

Paoletti, F., El-Sagheer, A.H., Allard, J., Brown, T., Dushek, O., Esashi, F. (2020) Molecular flexibility of DNA as a key determinant of RAD51 recruitment. EMBO Journal, 39(7):e103002.

Park, J.M., Yang, S.W., Yu, K.R., Ka, S.H., et al. (2014) Modification of PCNA by ISG15 Plays a Crucial Role in Termination of Error-Prone Translesion DNA Synthesis. Molecular Cell, 54(4), pp. 626–638.

Parker, J.L., Bucceri, A., Davies, A.A., Heidrich, K., Windecker, H. and Ulrich, H.D. (2008) SUMO modification of PCNA is controlled by DNA. The EMBO Journal, 27(18), pp. 2422–2431.

Pashkova, N., Gakhar, L., Winistorfer, S.C., Yu, L., Ramaswamy, S. and Piper, R.C. (2010) WD40 Repeat Propellers Define a Ubiquitin-Binding Domain that Regulates Turnover of F Box Proteins. Molecular Cell, 40(3), p. 433.

Passmore, L.A. and Barford, D. (2004) Getting into position: the catalytic mechanisms of protein ubiquitylation. Biochemical Journal, 379(Pt 3), p. 513.

Pei, J., Kim, B.H. and Grishin, N. V. (2008) PROMALS3D: a tool for multiple protein sequence and structure alignments. Nucleic Acids Research, 36(7), p. 2295.

Pellegrini, L. (2012) The Pol α -Primase Complex. Subcellular Biochemistry, 62, pp. 157–169.

Penengo, L., Mapelli, M., Murachelli, A.G., Confalonieri, S., et al. (2006) Crystal Structure of the Ubiquitin Binding Domains of Rabex-5 Reveals Two Modes of Interaction with Ubiquitin. Cell, 124(6), pp. 1183–1195.

Perpiñá, U., Herranz, C., Martín-Ibáñez, R., Boronat, A., et al. (2020) Cell Banking of HEK293T cell line for clinical-grade lentiviral particles manufacturing. Translational Medicine Communications 2020 5:1, 5(1), pp. 1–13.

Perry, M., Biegert, M., Kollala, S.S., Mallard, H., et al. (2021) USP11 mediates repair of DNA–protein cross-links by deubiquitinating SPRTN metalloprotease. Journal of Biological Chemistry, 296, p. 100396.

Pillutla, R.C., Shimamoto, A., Furuichi, Y. and Shatkin, A.J. (1999) Genomic Structure and Chromosomal Localization ofTCEAL1,a Human Gene Encoding the Nuclear Phosphoprotein p21/SIIR. Genomics, 56(2), pp. 217–220.

Pinato, S., Gatti, M., Scandiuzzi, C., Confalonieri, S. and Penengo, L. (2011) UMI, a Novel RNF168 Ubiquitin Binding Domain Involved in the DNA Damage Signaling Pathway. Molecular and Cellular Biology, 31(1), p. 118.

Pinder, J., Salsman, J. and Dellaire, G. (2015) Nuclear domain 'knock-in' screen for the evaluation and identification of small molecule enhancers of CRISPR-based genome editing. Nucleic Acids Research, 43(19), p. 9379.

Pommier, Y. (2006) Topoisomerase I inhibitors: camptothecins and beyond. Nature Reviews Cancer 2006 6:10, 6(10), pp. 789–802.

Pommier, Y. (2009) DNA Topoisomerase I Inhibitors: Chemistry, Biology and Interfacial Inhibition. Chemical Reviews, 109(7), p. 2894.

Pommier, Y., Sun, Y., Huang, S.Y.N. and Nitiss, J.L. (2016) Roles of eukaryotic topoisomerases in transcription, replication and genomic stability. Nature Reviews Molecular Cell Biology, 17(11), p. 703.

Popp, M.W. and Maquat, L.E. (2016) Leveraging Rules of Nonsense-Mediated mRNA Decay for Genome Engineering and Personalized Medicine. Cell, 165(6), pp. 1319–1322.

Prag, G., Misra, S., Jones, E.A., Ghirlando, R., Davies, B.A., Horazdovsky, B.F. and Hurley, J.H. (2003) Mechanism of Ubiquitin Recognition by the CUE Domain of Vps9p. Cell, 113(5), pp. 609–620.

Promonet, A., Padioleau, I., Liu, Y., Sanz, L., et al. (2020) Topoisomerase 1 prevents replication stress at R-loop-enriched transcription termination sites. Nature Communications, 11(1).

Prudden, J., Pebernard, S., Raffa, G., Slavin, D.A., et al. (2007) SUMO-targeted ubiquitin ligases in genome stability. The EMBO Journal, 26(18), p. 4089.

Puertollano, R. and Bonifacino, J.S. (2004) Interactions of GGA3 with the ubiquitin sorting machinery. Nature Cell Biology, 2004 6:3, 6(3), pp. 244–251.

Qi, S.M., Cheng, G., Cheng, X.D., Xu, Z., Xu, B., Zhang, W.D. and Qin, J.J. (2020) Targeting USP7-Mediated Deubiquitination of MDM2/MDMX-p53 Pathway for Cancer Therapy: Are We There Yet?. Frontiers in Cell and Developmental Biology, 8, p. 233.

Radley, E.H., Long, J., Gough, K.C. and Layfield, R. (2019) The 'dark matter' of ubiquitin-mediated processes: opportunities and challenges in the identification of ubiquitin-binding domains. Biochemical Society Transactions, 47(6), pp. 1949–1962.

Raftopoulou, C., Roumelioti, F.M., Dragona, E., Gimelli, S., et al. (2020) Karyotypic Flexibility of the Complex Cancer Genome and the Role of Polyploidization in Maintenance of Structural Integrity of Cancer Chromosomes. Cancers 2020, Vol. 12, Page 591, 12(3), p. 591.

Rahighi, S., Braunstein, I., Ternette, N., Kessler, B., et al. (2016) Selective Binding of AIRAPL Tandem UIMs to Lys48-Linked Tri-Ubiquitin Chains. Structure, 24(3), pp. 412–422.

Ran, F.A., Hsu, P.D., Wright, J., Agarwala, V., Scott, D.A. and Zhang, F. (2013a) Genome engineering using the CRISPR-Cas9 system. Nature Protocols 2013 8:11, 8(11), pp. 2281–2308.

Ran, F.A., Hsu, P.D., Lin, C.Y., Gootenberg, J.S., et al. (2013b) Double nicking by RNA-guided CRISPR cas9 for enhanced genome editing specificity. Cell, 154(6), pp. 1380–1389.

Rape, M. (2017) Ubiquitylation at the crossroads of development and disease. Nature Reviews Molecular Cell Biology 2017 19:1, 19(1), pp. 59–70.

Rattan, R., Narita, K., Chien, J., Maguire, J.L., Shridhar, R., Giri, S., Shridhar, V. TCEAL7, a putative tumor suppressor gene, negatively regulates NF-kappaB pathway. Oncogene. 2010 Mar 4;29(9):1362-73.

Rayner, E., Durin, M.-A., Thomas, R., Moralli, D., et al. (2019) CRISPR-Cas9 Causes Chromosomal Instability and Rearrangements in Cancer Cell Lines, Detectable by Cytogenetic Methods. The CRISPR Journal, 2(6), pp. 406–416.

Renaudin, X. and Rosselli, F. (2020) The FANC/BRCA Pathway Releases Replication Blockades by Eliminating DNA Interstrand Cross-Links. Genes 2020; Vol. 11, Page 585, 11(5), p. 585.

Rennie, M.L., Arkinson, C., Chaugule, V.K., Toth, R. and Walden, H. (2021) Structural basis of FANCD2 deubiquitination by USP1–UAF1. Nature Structural & Molecular Biology 2021 28:4, 28(4), pp. 356–364.

Reyes-Turcu, F.E., Horton, J.R., Mullally, J.E., Heroux, A., Cheng, X. and Wilkinson, K.D. (2006) The Ubiquitin Binding Domain ZnF UBP Recognizes the C-Terminal Diglycine Motif of Unanchored Ubiquitin. Cell, 124(6), pp. 1197–1208.

Reyes-Turcu, F.E., Ventii, K.H. and Wilkinson, K.D. (2009) Regulation and Cellular Roles of Ubiquitin-specific Deubiquitinating Enzymes. Annual Review of Biochemistry, 78, p. 363.

Rivera-Mulia, J.C. and Gilbert, D.M. (2016) Replicating Large Genomes: Divide and Conquer. Molecular Cell, 62(5), pp. 756–765.

Ronau, J.A., Beckmann, J.F. and Hochstrasser, M. (2016) Substrate specificity of the ubiquitin and Ubl proteases. Cell Research, 26(4), p. 441.

Rushworth, L.K., Harle, V., Repiscak, P., Clark, W., et al. (2020) In vivo CRISPR/Cas9 knockout screen: TCEAL1 silencing enhances docetaxel efficacy in prostate cancer. Life Science Alliance, 3(12).

Sahtoe, D.D. and Sixma, T.K. (2015) Layers of DUB regulation. Trends in Biochemical Sciences, 40(8), pp. 456–467.

Sakato, M., Zhou, Y. and Hingorani, M.M. (2012) ATP Binding and Hydrolysis-Driven Rate-Determining Events in the RFC-Catalyzed PCNA Clamp Loading Reaction. Journal of Molecular Biology, 416(2), pp. 176–191.

Saldivar, J.C., Cortez, D. and Cimprich, K.A. (2017) The essential kinase ATR: Ensuring faithful duplication of a challenging genome. Nature Reviews Molecular Cell Biology. Nature Publishing Group, pp. 622–636.

Sale, J.E., Lehmann, A.R. and Woodgate, R. (2012) Y-family DNA polymerases and their role in tolerance of cellular DNA damage. Nature Reviews Molecular Cell Biology 2012 13:3, 13(3), pp. 141–152.

Sale, J.E. (2013) Translesion DNA Synthesis and Mutagenesis in Eukaryotes. Cold Spring Harbor Perspectives in Biology, 5(3).
Sartori, A.A., Lukas, C., Coates, J., Mistrik, M., et al. (2007) Human CtIP promotes DNA end resection. Nature, 450(7169), p. 509.

Sato, Y., Yoshikawa, A., Mimura, H., Yamashita, M., Yamagata, A. and Fukai, S. (2009) Structural basis for specific recognition of Lys 63-linked polyubiquitin chains by tandem UIMs of RAP80. The EMBO Journal, 28(16), pp. 2461–2468.

Saxena, S. and Zou, L. (2022) Hallmarks of DNA replication stress. Molecular Cell, 82(12), pp. 2298–2314.

Schindelin, J., Arganda-Carreras, I., Frise, E., Kaynig, V., et al. (2012) Fiji: an open-source platform for biological-image analysis. Nature Methods, 2012 9:7, 9(7), pp. 676–682.

Scott, D., Oldham, N.J., Strachan, J., Searle, M.S. and Layfield, R. (2015) Ubiquitin-binding domains: Mechanisms of ubiquitin recognition and use as tools to investigate ubiquitin-modified proteomes. Proteomics, 15(5–6), pp. 844–861.

Scully, R., Panday, A., Elango, R. and Willis, N.A. (2019) DNA double-strand break repair-pathway choice in somatic mammalian cells. Nature Reviews Molecular Cell Biology 2019 20:11, 20(11), pp. 698–714.

Sebesta, M., Cooper, C.D.O., Ariza, A., Carnie, C.J., Ahel, D. (2017) Structural insights into the function of ZRANB3 in replication stress response. Nature Communications, 8:15847.

Sekiyama, N., Jee, J., Isogai, S., Akagi, K.I., et al. (2012) NMR analysis of Lys63-linked polyubiquitin recognition by the tandem ubiquitin-interacting motifs of Rap80. Journal of Biomolecular NMR, 52(4), pp. 339–350.

Semlow, D.R. and Walter, J.C. (2021) Mechanisms of Vertebrate DNA Interstrand Cross-Link Repair. Annual Review of Biochemistry. 2021 Jun 20;90:107-135.

Sfeir, A. and Symington, L.S. (2015) Microhomology-mediated end joining: a back-up survival mechanism or dedicated pathway?. Trends in Biochemical Sciences, 40(11), p. 701.

Shah, P., Qiang, L., Yang, S., Soltani, K. and He, Y.Y. (2017) Regulation of XPC deubiquitination by USP11 in repair of UV-induced DNA damage. Oncotarget, 8(57), p. 96522.

Shi, Yuan, Chen, X., Elsasser, S., Stocks, B.B., et al. (2016) Rpn1 provides adjacent receptor sites for substrate binding and deubiquitination by the proteasome. Science, 351(6275).

Sims, A.E., Spiteri, E., Sims, R.J., Arita, A.G., et al. (2007) FANCI is a second monoubiquitinated member of the Fanconi anemia pathway. Nature Structural & Molecular Biology 2007 14:6, 14(6), pp. 564–567.

Sims, J.J., Scavone, F., Cooper, E.M., Kane, L.A., Youle, R.J., Boeke, J.D. and Cohen, R.E. (2012) Polyubiquitin-sensor proteins reveal localization and linkage-type dependence of cellular ubiquitin signaling. Nature Methods, 9(3), p. 303.

Slade, D. (2018) Maneuvers on PCNA Rings during DNA Replication and Repair. Genes, 9(8), p. 416.

Sloper-Mould, K.E., Jemc, J.C., Pickart, C.M. and Hicke, L. (2001) Distinct Functional Surface Regions on Ubiquitin. Journal of Biological Chemistry, 276(32), pp. 30483–30489.

Sollier, J., Stork, C.T., García-Rubio, M.L., Paulsen, R.D., Aguilera, A. and Cimprich, K.A. (2014) Transcription-Coupled Nucleotide Excision Repair Factors Promote R-Loop-Induced Genome Instability. Molecular Cell, 56(6), pp. 777–785.

Somyajit K., Gupta R., Sedlackova H., Neelsen K.J., Ochs F., Rask M.B., Choudhary C., Lukas J. (2017) Redox-sensitive alteration of replisome architecture safeguards genome integrity. Science. 10;358(6364):797-802.

Song, A.X., Zhou, C.J., Guan, X., Sze, K.H. and Hu, H.Y. (2010) Solution structure of the N-terminal domain of DC-UbP/UBTD2 and its interaction with ubiquitin. Protein Science : A Publication of the Protein Society, 19(5), p. 1104.

Sonneville, R., Moreno, S.P., Knebel, A., Johnson, C., Hastie, C.J., Gartner, A., Gambus, A., Labib, K. (2017) CUL-2LRR-1 and UBXN-3 drive replisome disassembly during DNA replication termination and mitosis. Nature Cell Biology, 19(5):468-479.

Sowa, M.E., Bennett, E.J., Gygi, S.P. and Harper, J.W. (2009) Defining the Human Deubiquitinating Enzyme Interaction Landscape. Cell, 138(2), pp. 389–403.

Spiliotopoulos, A., Ferreras, L.B., Densham, R.M., Caulton, S.G., et al. (2019) Discovery of peptide ligands targeting a specific ubiquitin-like domain– binding site in the deubiquitinase USP11. Journal of Biological Chemistry, 294(2), pp. 424–436.

Spratt, D.E., Walden, H. and Shaw, G.S. (2014) RBR E3 ubiquitin ligases: new structures, new insights, new questions. Biochemical Journal, 458(Pt 3), p. 421.

Stepanenko, A.A. and Dmitrenko, V. V. (2015) HEK293 in cell biology and cancer research: phenotype, karyotype, tumorigenicity, and stress-induced genome-phenotype evolution. Gene, 569(2), pp. 182–190.

Stewart, L., Redinbo, M.R., Qiu, X., Hol, W.G.J. and Champoux, J.J. (1998) A model for the mechanism of human topoisomerase I. Science, 279(5356), pp. 1534–1541.

Stinson, B.M. and Loparo, J.J. (2021) Repair of DNA Double-Strand Breaks by the Non-homologous End Joining Pathway. Annual Review of Biochemistry, 90, p. 137.

Sun, Y., Saha, S., Wang, W., Saha, L.K., Huang, S.Y.N. and Pommier, Y. (2020) Excision Repair of Topoisomerase DNA-Protein Crosslinks (TOP-DPC). DNA Repair, 89, p. 102837.

Sundquist, W.I., Schubert, H.L., Kelly, B.N., Hill, G.C., Holton, J.M. and Hill, C.P. (2004) Ubiquitin Recognition by the Human TSG101 Protein. Molecular Cell, 13(6), pp. 783–789.

Swatek, K.N. and Komander, D. (2016) Ubiquitin modifications. Cell Research. Nature Publishing Group, pp. 399–422.

Symington, L.S. (2014) End Resection at Double-Strand Breaks: Mechanism and Regulation. Cold Spring Harbor Perspectives in Biology, 6(8), p. a016436.

Tanaka, S., Nakato, R., Katou, Y., Shirahige, K. and Araki, H. (2011) Origin Association of Sld3, Sld7, and Cdc45 Proteins Is a Key Step for Determination of Origin-Firing Timing. Current Biology, 21(24), pp. 2055–2063.

Tanaka, S., Umemori, T., Hirai, K., Muramatsu, S., Kamimura, Y. and Araki, H. (2006) CDK-dependent phosphorylation of Sld2 and Sld3 initiates DNA replication in budding yeast. Nature 2006 445:7125, 445(7125), pp. 328–332.

Terai, K., Abbas, T., Jazaeri, A.A. and Dutta, A. (2010) CRL4Cdt2 E3 Ubiquitin Ligase Monoubiquitinates PCNA to Promote Translesion DNA Synthesis. Molecular Cell, 37(1), pp. 143–149.

Thangavel, S., Berti, M., Levikova, M., Pinto, C., et al. (2015) DNA2 drives processing and restart of reversed replication forks in human cells. The Journal of Cell Biology, 208(5), p. 545.

Todi, S. V., Winborn, B.J., Scaglione, K.M., Blount, J.R., Travis, S.M. and Paulson, H.L. (2009) Ubiquitination directly enhances activity of the deubiquitinating enzyme ataxin-3. The EMBO Journal, 28(4), pp. 372–382.

Todi, S. V., Scaglione, K.M., Blount, J.R., Basrur, V., et al. (2010) Activity and Cellular Functions of the Deubiquitinating Enzyme and Polyglutamine Disease Protein Ataxin-3 Are Regulated by Ubiquitination at Lysine 117. The Journal of Biological Chemistry, 285(50), p. 39303.

Toledo, L.I., Altmeyer, M., Rask, M.B., Lukas, C., et al. (2013) ATR Prohibits Replication Catastrophe by Preventing Global Exhaustion of RPA. Cell, 155(5), pp. 1088–1103.

Toledo, L., Neelsen, K.J. and Lukas, J. (2017) Replication Catastrophe: When a Checkpoint Fails because of Exhaustion. Molecular Cell, 66(6), pp. 735–749.

Tom, S., Henricksen, L.A. and Bambara, R.A. (2000) Mechanism Whereby Proliferating Cell Nuclear Antigen Stimulates Flap Endonuclease 1. Journal of Biological Chemistry, 275(14), pp. 10498–10505.

Tomasz, M., Lipman, R., Chowdary, D., Pawlak, J., Verdine, G.L. and Nakanishi, K. (1987) Isolation and Structure of a Covalent Cross-Link Adduct Between Mitomycin C and DNA. Science, 235(4793), pp. 1204–1208.

Tracz, M. and Bialek, W. (2021) Beyond K48 and K63: non-canonical protein ubiquitination. Cellular & Molecular Biology Letters 2021 26:1, 26(1), pp. 1–17.

Truong, L.N., Li, Y., Shi, L.Z., Hwang, P.Y.H., et al. (2013) Microhomology-mediated End Joining and Homologous Recombination share the initial end resection step to repair DNA double-strand breaks in mammalian cells. Proceedings of the National Academy of Sciences of the United States of America, 110(19), pp. 7720–7725.

Tsherniak, A., Vazquez, F., Montgomery, P.G., Weir, B.A., et al. (2017) Defining a Cancer Dependency Map. Cell, 170(3), pp. 564-576.e16.

Tsui, C., Raguraj, A. and Pickart, C.M. (2005) Ubiquitin Binding Site of the Ubiquitin E2 Variant (UEV) Protein Mms2 Is Required for DNA Damage Tolerance in the Yeast RAD6 Pathway. Journal of Biological Chemistry, 280(20), pp. 19829–19835.

Tuladhar, R., Yeu, Y., Tyler Piazza, J., Tan, Z., et al. (2019) CRISPR-Cas9-based mutagenesis frequently provokes on-target mRNA misregulation. Nature Communications 2019 10:1, 10(1), pp. 1–10.

Tumini, E. and Aguilera, A. (2021) The Sister-Chromatid Exchange Assay in Human Cells. Methods in Molecular Biology, 2153, pp. 383–393.

Tzelepis, K., Koike-Yusa, H., De Braekeleer, E., Li, Y., et al. (2016) A CRISPR Dropout Screen Identifies Genetic Vulnerabilities and Therapeutic Targets in Acute Myeloid Leukemia. Cell Reports, 17(4), p. 1193.

Ubhi, T. and Brown, G.W. (2019) Exploiting DNA replication stress for cancer treatment. Cancer Research, 79(8), pp. 1730–1739.

Unk, I., Hajdú, I., Fátyol, K., Szakál, B., et al. (2006) Human SHPRH is a ubiquitin ligase for Mms2-Ubc13-dependent polyubiquitylation of proliferating cell nuclear antigen. Proceedings of the National Academy of Sciences of the United States of America, 103(48), pp. 18107–18112.

Unk, I., Hajdú, I., Fátyol, K., Hurwitz, J., et al. (2008) Human HLTF functions as a ubiquitin ligase for proliferating cell nuclear antigen polyubiquitination. Proceedings of the National Academy of Sciences of the United States of America, 105(10), pp. 3768–3773.

van den Boom, J. and Meyer, H. (2018) VCP/p97-Mediated Unfolding as a Principle in Protein Homeostasis and Signaling. Molecular Cell, 69(2), pp. 182–194.

Van Wietmarschen, N. and Lansdorp, P.M. (2016) Bromodeoxyuridine does not contribute to sister chromatid exchange events in normal or Bloom syndrome cells. Nucleic Acids Research, 44(14), pp. 6787–6793.

Varadan, R., Walker, O., Pickart, C. and Fushman, D. (2002) Structural Properties of Polyubiquitin Chains in Solution. Journal of Molecular Biology, 324(4), pp. 637–647.

Varadan, R., Assfalg, M., Raasi, S., Pickart, C. and Fushman, D. (2005) Structural Determinants for Selective Recognition of a Lys48-Linked Polyubiquitin Chain by a UBA Domain. Molecular Cell, 18(6), pp. 687–698.

Vassin, V.M., Anantha, R.W., Sokolova, E., Kanner, S. and Borowiec, J.A. (2009) Human RPA phosphorylation by ATR stimulates DNA synthesis and prevents ssDNA accumulation during DNA-replication stress. Journal of Cell Science, 122(22), p. 4070.

Vignard, J., Mirey, G. and Salles, B. (2013) Ionizing-radiation induced DNA double-strand breaks: A direct and indirect lighting up. Radiotherapy and Oncology, 108(3), pp. 362–369.

Vijay-Kumar, S., Bugg, C.E. and Cook, W.J. (1987) Structure of ubiquitin refined at 1.8Åresolution. Journal of Molecular Biology, 194(3), pp. 531–544.

Vrtis, K.B., Dewar, J.M., Chistol, G., Wu, R.A., Graham, T.G.W. and Walter, J.C. (2021) Single-strand DNA breaks cause replisome disassembly. Molecular Cell, 81(6), pp. 1309-1318.e6.

Vujanovic, M., Krietsch, J., Raso, M.C., Terraneo, N., et al. (2017) Replication Fork Slowing and Reversal upon DNA Damage Require PCNA Polyubiquitination and ZRANB3 DNA Translocase Activity. Molecular Cell, 67(5), pp. 882-890.e5.

Wagner, S., Carpentier, I., Rogov, V., Kreike, M., et al. (2008) Ubiquitin binding mediates the NF-κB inhibitory potential of ABIN proteins. Oncogene, 2008 27:26, 27(26), pp. 3739–3745.

Wang, J.C. (2002) Cellular roles of DNA topoisomerases: a molecular perspective. Nature Reviews Molecular Cell Biology 2002 3:6, 3(6), pp. 430–440.

Wang, B., Alam, S.L., Meyer, H.H., Payne, M., Stemmler, T.L., Davis, D.R. and Sundquist, W.I. (2003) Structure and Ubiquitin Interactions of the Conserved Zinc Finger Domain of Npl4. The Journal of Biological Chemistry, 278(22), p. 20225.

Wang, Y., Liu, J., Huang, B., Xu, Y.-M., et al. (2015) Mechanism of alternative splicing and its regulation. Biomedical Reports, 3(2), p. 152.

Wang, R., Wang, S., Dhar, A., Peralta, C. and Pavletich, N.P. (2020) DNA clamp function of the mono-ubiquitinated Fanconi Anemia ID complex. Nature, 580(7802), p. 278.

Wang, Y., Zhang, H., Zhong, H. and Xue, Z. (2021) Protein domain identification methods and online resources. Computational and Structural Biotechnology Journal, 19, pp. 1145–1153.

Wasserman, M.R., Schauer, G.D., O'Donnell, M.E. and Liu, S. (2019) Replication Fork Activation Is Enabled by a Single-Stranded DNA Gate in CMG Helicase. Cell, 178(3), p. 600.

Watanabe, K., Tateishi, S., Kawasuji, M., Tsurimoto, T., Inoue, H. and Yamaizumi, M. (2004) Rad18 guides polη to replication stalling sites through physical interaction and PCNA monoubiquitination. The EMBO Journal, 23(19), pp. 3886–3896.

Wertz, I.E., O'Rourke, K.M., Zhou, H., Eby, M., et al. (2004) De-ubiquitination and ubiquitin ligase domains of A20 downregulate NF-κB signalling. Nature, 2004 430:7000, 430(7000), pp. 694–699.

Whitfield, M.L., Sherlock, G., Saldanha, A.J., Murray, J.I., et al. (2002) Identification of Genes Periodically Expressed in the Human Cell Cycle and Their Expression in Tumors. Molecular Biology of the Cell, 13(6), pp. 1977–2000.

Wiltshire, T.D., Lovejoy, C.A., Wang, T., Xia, F., O'Connor, M.J. and Cortez, D. (2010) Sensitivity to poly(ADP-ribose) polymerase (PARP) inhibition identifies ubiquitin-specific peptidase 11 (USP11) as a regulator of DNA double-strand break repair. Journal of Biological Chemistry, 285(19), pp. 14565–14571.

Wold, M.S. (1997) Replication protein A: a heterotrimeric, single-stranded DNA-binding protein required for eukaryotic DNA metabolism. Annual Review of Biochemistry, 1997;66:61-92.

Wu, X., Liu, S., Sagum, C., Chen, J., et al. (2019) Crosstalk between Lys63- and Lys11-polyubiquitin signaling at DNA damage sites is driven by Cezanne. Genes & development, 33(23–24), pp. 1702–1717.

Wu R.A., Semlow D.R., Kamimae-Lanning A.N., Kochenova O.V., Chistol G., Hodskinson M.R., Amunugama R., Sparks J.L., Wang M., Deng L., Mimoso C.A., Low E., Patel K.J., Walter J.C. (2019) TRAIP is a master regulator of DNA interstrand crosslink repair. Nature. 567(7747):267-272.

Xia, B., Amador, G., Viswanatha, R., Zirin, J., Mohr, S.E. and Perrimon, N. (2020) CRISPR-based engineering of gene knockout cells by homology-directed insertion in polyploid Drosophila S2R+ cells. Nature Protocols, 15(10), p. 3478.

Yang, W. and Woodgate, R. (2007) What a difference a decade makes: Insights into translesion DNA synthesis. Proceedings of the National Academy of Sciences of the United States of America, 104(40), p. 15591.

Yata, K., Lloyd, J., Maslen, S., Bleuyard, J.Y., Skehel, M., Smerdon, S.J., Esashi, F. (2012) Plk1 and CK2 act in concert to regulate Rad51 during DNA double strand break repair. Molecular Cell, 45(3):371-83.

Yau, R. and Rape, M. (2016) The increasing complexity of the ubiquitin code. Nature Cell Biology. Nature Publishing Group, pp. 579–586.

Yau, R.G., Doerner, K., Castellanos, E.R., Haakonsen, D.L., et al. (2017) Assembly and Function of Heterotypic Ubiquitin Chains in Cell-Cycle and Protein Quality Control. Cell, 171(4), pp. 918-933.e20.

Yazinski, S.A. and Zou, L. (2016) Functions, Regulation, and Therapeutic Implications of the ATR Checkpoint Pathway. Annual Review of Genetics. 2016 Nov 23;50:155-173.

Ye, Y., Akutsu, M., Reyes-Turcu, F., Enchev, R.I., Wilkinson, K.D. and Komander, D. (2011) Polyubiquitin binding and cross-reactivity in the USP domain deubiquitinase USP21. EMBO reports, 12(4), pp. 350–357.

Ye, Y., Meyer, H.H. and Rapoport, T.A. (2003) Function of the p97–Ufd1–Npl4 complex in retrotranslocation from the ER to the cytosol dual recognition of nonubiquitinated polypeptide segments and polyubiquitin chains. Journal of Cell Biology, 162(1), pp. 71–84.

Yeeles, J.T.P., Deegan, T.D., Janska, A., Early, A. and Diffley, J.F.X. (2015) Regulated eukaryotic DNA replication origin firing with purified proteins. Nature 2015 519:7544, 519(7544), pp. 431–435.

Yeeles, J.T.P., Janska, A., Early, A. and Diffley, J.F.X. (2017) How the Eukaryotic Replisome Achieves Rapid and Efficient DNA Replication. Molecular Cell, 65(1), p. 105.

Yeh, C.H. and Shatkin, A.J. (1994a) A HeLa-cell-encoded p21 is homologous to transcription elongation factor SII. Gene, 143(2), pp. 285–287.

Yeh, C.H. and Shatkin, A.J. (1994b) Down-regulation of Rous sarcoma virus long terminal repeat promoter activity by a HeLa cell basic protein. Proceedings of the National Academy of Sciences, 91(23), pp. 11002–11006.

Yeh, C.D., Richardson, C.D. and Corn, J.E. (2019) Advances in genome editing through control of DNA repair pathways. Nature Cell Biology 2019 21:12, 21(12), pp. 1468–1478.

Yekezare, M., Gó mez-González, B. and Diffley, J.F.X. (2013) Controlling DNA replication origins in response to DNA damage – inhibit globally, activate locally. Journal of Cell Science, 126(6), pp. 1297–1306.

Yoshikawa, A., Sato, Y., Yamashita, M., Mimura, H., Yamagata, A. and Fukai, S. (2009) Crystal structure of the NEMO ubiquitin-binding domain in complex with Lys 63-linked di-ubiquitin. FEBS Letters, 583(20), pp. 3317–3322.

Yu, M., Liu, K., Mao, Z., Luo, J., Gu, W. and Zhao, W. (2016) USP11 Is a Negative Regulator to γH2AX Ubiquitylation by RNF8/RNF168. Journal of Biological Chemistry, 291(2), pp. 959–967.

Yuan, J., Luo, K., Zhang, L., Cheville, J.C. and Lou, Z. (2010) USP10 Regulates p53 Localization and Stability by Deubiquitinating p53. Cell, 140(3), p. 384.

Zegerman, P. and Diffley, J.F.X. (2006) Phosphorylation of Sld2 and Sld3 by cyclin-dependent kinases promotes DNA replication in budding yeast. Nature 2006 445:7125, 445(7125), pp. 281–285.

Zellweger, R., Dalcher, D., Mutreja, K., Berti, M., et al. (2015) Rad51-mediated replication fork reversal is a global response to genotoxic treatments in human cells. The Journal of Cell Biology, 208(5), p. 563.

Zeman, M.K. and Cimprich, K.A. (2014) Causes and consequences of replication stress. Nature Cell Biology. NIH Public Access, pp. 2–9.

Zhang, S., Chea, J., Meng, X., Zhou, Y., Lee, E.Y.C. and Lee, M.Y.W.T. (2008) PCNA is ubiquitinated by RNF8. https://doi.org/10.4161/cc.7.21.6949, 7(21), pp. 3399–3404.

Zhang, N., Wang, Q., Ehlinger, A., Randles, L., et al. (2009) Structure of the S5a:K48-linked diubiquitin complex and its interactions with Rpn13. Molecular Cell, 35(3), p. 280.

Zhang J., Dewar J.M., Budzowska M., Motnenko A., Cohn M.A., Walter J.C. (2015) DNA interstrand cross-link repair requires replication-fork convergence. Nature Structural & Molecular Biology. 22(3):242-7.

Zhang, T., Zhou, Z., Yang, H. and Wang, W. (2022) MRE11-RAD50-NBS1-CtIP: one key nuclease ensemble functions in the maintenance of genome stability. Genome Instability & Disease 2022 3:3, 3(3), pp. 123–135.

Zheng, N. and Shabek, N. (2017) Ubiquitin Ligases: Structure, Function, and Regulation. Annual Review of Biochemistry, 2017 Jun 20;86:129-157.

Zheng, W., Zhou, X., Wuyun, Q., Pearce, R., Li, Y. and Zhang, Y. (2020) FUpred: detecting protein domains through deep-learning-based contact map prediction. Bioinformatics, 36(12), pp. 3749–3757.

Zhou, J., Xu, Y., Lin, S., Guo, Y., et al. (2018) iUUCD 2.0: an update with rich annotations for ubiquitin and ubiquitin-like conjugations. Nucleic Acids Research, 46(D1), pp. D447–D453.

Zhu, X., Ménard, R. and Sulea, T. (2007) High incidence of ubiquitin-like domains in human ubiquitin-specific proteases. Proteins, 69(1), p. 1.

Zou, L. and Elledge, S.J. (2003) Sensing DNA damage through ATRIP recognition of RPA-ssDNA complexes. Science, 300(5625), pp. 1542–1548.